بِسْمِ اللّٰهِ الرَّحْمٰنِ الرَّحِيْمِ

In the Name of God, the Compassionate, the Merciful

And we want to bestow our favours on those who were oppressed on earth, and make them leaders of mankind and make them the inheritors. (Quran, The Story, 28:5)

TRANSFER COEFFICIENTS OVER INCLINED TUBE BANKS

By

HOSSEIN NOIE BAGHBAN

Thesis submitted for the degree

of

Doctor of Philosophy

Department of Chemical Engineering

The University of Aston in Birmingham

June 1987

The University of Aston in Birmingham

TRANSFER COEFFICIENTS OVER INCLINED TUBE BANKS

HOSSIEN NOIE BAGHBAN PH.D 1987

THESIS SUMMARY

The thesis presents experimental results for shell–side transfer coefficients and pressure drops across four different tube banks, using small–scale models, with yawed tubes, as found in many types of heat exchangers, boilers and nuclear reactors. The tube banks investigated have a staggered tube layout on a rotated square pitch, with a 1.25 pitch–to–diameter ratio. The angle of attack was varied between 45^{o} and 90^{o}. An extensive range of Reynolds number, i.e. 0.5 to 12 600, covering so–called laminar, transition and turbulent flows, was investigated.

A diffusion-controlled electrochemical mass transfer technique has been employed to measure mass transfer coefficients. The heat transfer coefficients may be then readily obtained from the mass transfer values by applying the well-established Chilton–Colburn analogy.

The results for the normal tube bank, which forms the base case for the study on inclined tube banks, show close agreement with previous work.

The transfer coefficients and pressure drops of the inclined tube banks are compared with results from the ideal normal tube bank to examine the effect of inclination angle on heat transfer and pressure drop variations.

The variation of the transfer coefficients row–by–row and the entrance and exit effects have also been investigated.

An auxiliary investigation has been carried out on the role of natural convection.

A preliminary correlation of transfer coefficients and pressure drops against the variation in the yaw angle has been attempted.

The results are discussed in the light of the few existing theoretical treatments and experimental data for these situations, and recommendations made for future work.

KEY WORDS IDEAL NORMAL TUBE BANKS INCLINED TUBE BANKS
TRANSFER COEFFICIENTS PRESSURE DROPS
ELECTROCHEMICAL TECHNIQUE

DEDICATED TO MY WIFE

ACKNOWLEGEMENTS

In recognition of the help and advice received the author wishes to extend his sincere thanks to:

The Government of The Islamic Republic of Iran for the financial support provided throughout this project.

Dr JD Jenkins for his valuable help, moral support and supervision and his patient review of the draft thesis.

The staff of the Department for their assistance and their careful construction of equipments.

My parents for providing all possible moral support, and also to my wife for her patience, understanding and encouragement throughout the course of this work.

Finally, above all I may give glory unto God and remember him always that he is surely watching over us, and easing my task for me, and freeing my tongue from its impediment that men may understand my speech.

LIST OF CONTENTS

APPENDICES

LIST OF TABLES

LIST OF FIGURES

CHAPTER ONE

INTRODUCTION

Investigation of fluid flow and heat transfer in tube banks is still of great practical interest due to their wide spread use in many types of industrial equipment. The simplest case of combined fluid–flow and heat transfer occurs in axial flow, typically inside the tubes of heat exchangers. The more complex situation of transverse flow across arrays of tubes is related to conditions found on the shell–side of heat exchangers, reboilers and condensers: it is also encountered in nuclear reactors. Often transverse flow is at an angle to the tube bank, i.e. we have inclined flow; and in reality many flows in shell–and–tube heat exchangers with baffles, coiled–tube heat exchangers, multistart helical heat exchangers and high temperature gas cooled reactors, are of this type. It is therefore surprising that, as revealed by the literature survey reported below, so little experimental evidence is available for such situations.

Tube banks are of two general orientations; which is used depends on whether good heat transfer characteristics or good pressure drop characteristics are most important. Frequently–used tube bundle arrangements include in–line and staggered arrangements as illustrated in Figure 2.2. For minimum pressure drop, typically an in–line arrangement would be used; for maximum heat transfer, a staggered arrangement.

Tube–bundle geometry is characterized by the transverse pitch, P_t, and the longitudinal pitch, P_l, between the tube centres; the diagonal pitch, P_d, between the centres of the tubes in the diagonal row is sometimes used for the staggered

arrangement. To define the Reynolds number for flow through the tube bank, the flow velocity is based on the minimum area available for flow, whether the minimum area occurs between tubes in a transverse row or between tubes considered in a zig–zag row across the tube bank.

As already noted, tube banks are often employed in process equipment; the classical example is the shell–and–tube heat exchanger used in almost every branch of industry for the transfer of heat from one fluid to another. The simplest form of industrial shell–and–tube heat exchanger is the T.E.M.A."E"–type shell, fitted with segmental baffles as illustrated in Figure 1.1 (Standards of the Tubular Exchanger Manufacturer's Association (1978)).

There are a number of reasons for the wide–spread use of this type of exchanger. Flow across banks of tubes is, from both physical and constructional considerations, one of the most effective means of achieving heat transfer. The repeated expansion and separation of the boundary layer on the down–stream side of the tubes causes strong eddying producing a high degree of turbulence, which, in turn, leads to high transfer coefficients since fluid elements are quickly brought to the heat transfer surfaces and then quickly removed.

The baffled shell–and–tube heat exchanger utilises flow across tube banks in a configuration which is sturdy enough for industrial use and which provides a large heat transfer surface–area to volume ratio.

Because of the wide–spread use of shell–and–tube heat exchangers, the high capital investment required and the significant costs of maintenance and renewal, proper

initial design is an important economic consideration. A complete thermal and hydraulic design of a shell–and–tube heat exchanger, or indeed heat transfer equipment generally, requires accurate information concerning the following:

1) Heat transfer coefficient data for clean surfaces for both inside and outside the tubes.
2) Fluid fouling characteristics.
3) The temperature driving force (a Log–Mean Temperature Difference [LMTD] is commonly used).
4) Pressure drop data, again for both sides.

The conditions of flow for fluids on the shell–side of industrial heat exchangers are complex and involve a large number of variables. Some of the more important of these variables are as follows.

1) Tube arrangement [(a) equilateral triangle, (b) rotated square, and (c) in–line square].
2) Tube diameter.
3) Tube pitch (centre–line distance between tubes).
4) Tube length.
5) Number of tube rows.
6) Fluid flow rates.
7) Physical properties of the fluids.
8) Shell diameter.
9) Baffle specifications [(a) type,(b) size of cutdown, (c) baffle spacing,and (d) baffle thickness].
10) Internal leakage paths [(a) tube to baffle, (b) baffle to shell, and (c) tube bundle to shell].

The bundle geometrical parameters affect each of the flow elements in a different way. The effect of varying geometries can be illustrated by the fact that increasing the baffle spacing reduces the pressure drop at the expense of reduced heat transfer coefficients. Hence changes in geometry may improve one performance index at the expense of the other.

In spite of the complex flow arrangement, the heat transfer coefficient and pressure drop have, in the past, been obtained from dimensionless empirical charts of the performance indices against flow rate expressed as Reynolds number.

As the tube bundle in a shell–and–tube heat exchanger consists of rows of cylinders, investigation of fluid flow in the shell–side of a shell–and–tube heat exchanger is superficially comparable to flow in a rectangular tube bank. More specifically, a rectangular unit is very similar geometrically to the cross–flow zone in the centre of a cylindrical heat exchanger.

The arrangement of segmentally baffled shell–and–tube heat exchangers as shown in Figure 1.1 makes the flow patterns extremely complex and destroys the ideal case of purely normal flow. While the flow through the baffle window is predominantly parallel to the tubes, the flow between the baffles is neither uniform nor, in fact, normal to the tubes. Baffle space variations affect the angle of flow across the tube bundle and so are relevant to this work. The fluid streams on the shell–side of baffled shell and tube heat exchangers are shown in Figure 1.2, which has been taken from Tinker [1951].

This work is concerned with the investigation of heat and mass transfer

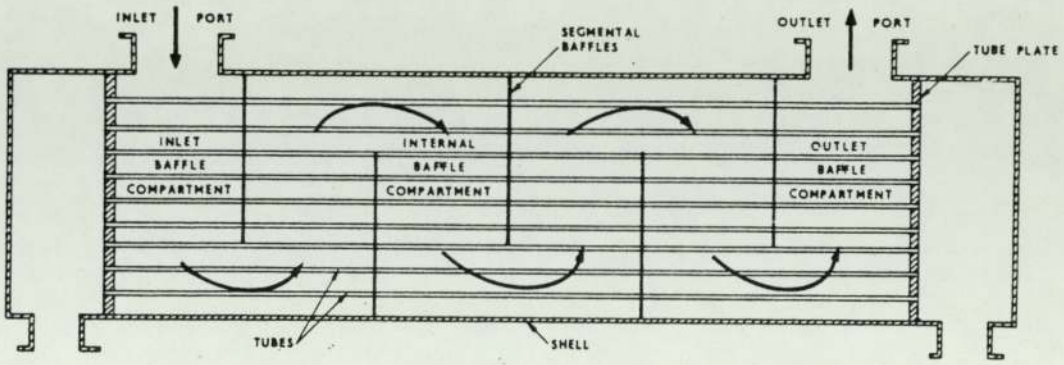

Fig. 1.1 Segmentally baffled–shell–and tube heat exchanger with single pass shell (Mackley [1973])

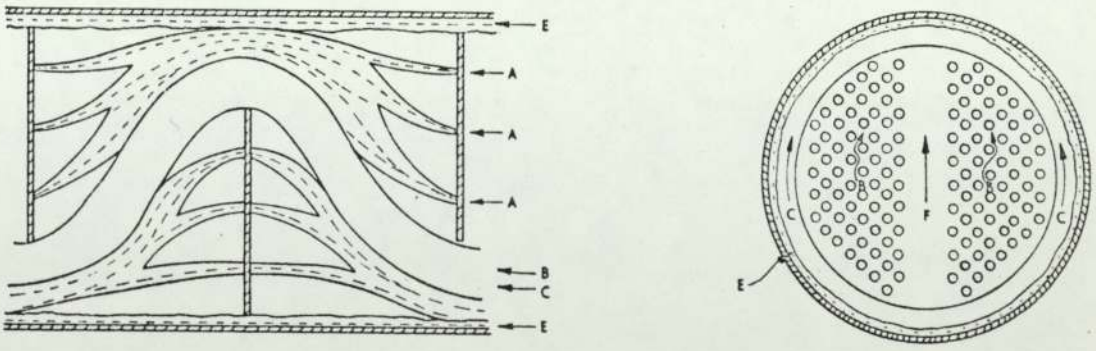

Fig. 1.2 Illustration of the shell–side fluid streams, stream A represents the leakage stream through the annular spaces between tubes and baffles holes, stream B the cross flow stream through the transfer surface between successive baffle windows, stream C the bundle by–pass stream and stream E the leakage stream passing through the shell–to–baffle clearance (Tinker [1951])

CHAPTER TWO

LITERATURE SURVEY

2.1 INTRODUCTION

The characteristics of rectangular tube–banks in cross–flow provide a simple basis for the study of heat transfer and pressure drop in more complex tube bundle geometries such as those encountered in baffled shell–and–tube heat exchangers. Heat transfer to or from a bank (or bundle) and pressure drop characteristics of tube bundles have numerous applications in the design of heat exchangers and industrial heat transfer equipment, such as steam generation in a boiler or air cooling in the coil of an air conditioner.

The geometric arrangement is shown schematically in Figure 2.1. Typically, one fluid moves over the tubes, while a second fluid, at a different temperature, passes through the tubes.

Rectangular tube banks may be classified into:

1)*Ideal tube–banks*, in which the tube arrangement is geometrically regular throughout the bank and the bank is effectively laterally infinite, i.e. all flow channels through the bank have the same size and shape. Laterally infinite tube banks are closely approximated experimentally by using half tubes at the side walls, the remaining wall effect being negligible.

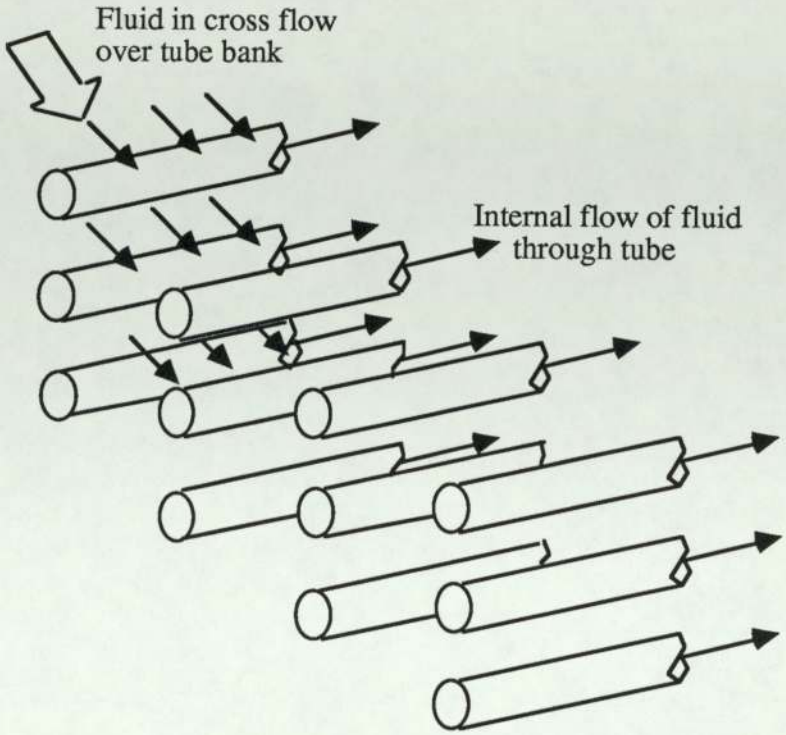

Fig. 2.1 Schematic of a tube bank in cross flow

2)*Uniform tube–banks with by–pass streams*, in which the tube arrangement is geometrically regular, but in which a clearance exists between the outer row of tubes and the wall. This arrangement is the one usually encountered in commercial exchangers, which sometimes also have similar longitudinal channels through the centre of the tube array. Sealing strips are often used to block the by–pass stream.

3)*Non–uniform tube–banks*, in which there is no geometrical unit cell layout of the tubes. This arrangement is used in some commercial exchangers to eliminate some of the problems arising from excessive by–passing between tube bank and shell.

In this work we are specifically interested in the convective heat transfer coefficients and pressure drop associated with cross and inclined flow over ideal tube banks.

A bank of tubes (also refered to as a rod bundle, tube assembly, tube array or tube arrangement) is geometrically defined by the way the tubes are arranged (Fig. 2.2), i.e. "in–line" or "staggered" and the transverse, S_t, and longitudinal, S_l, pitch to diameter ratios, i.e.

$$S_t = P_t/D \qquad [2.1]$$

$$S_l = P_l/D \qquad [2.2]$$

where P_t is transverse pitch and P_l is longitudinal pitch as shown in Figure 2.2.

The staggered tube bundle generally provides a higher heat transfer rate for the same mass flow rate. However, the in–line arrangement provides less resistance to flow and is preferable when pressure drop across the tube bundle must be minimized.

The following three kinds of arrangements (Fig. 2.2a, b, c) are very often encountered.

i) *Square in–line*, i.e. an in–line arrangement as (Fig. 2.2a), for which

$$P_t = P_l \qquad [2.3]$$

ii) *Rotated square*, i.e. a staggered arrangement in which groups of three adjacent tubes form a right–angled triangle. The diagonal pitch, P_d, between the centres of the tubes in the diagonal row, a dimension which is sometimes used for the staggered arrangement, is defined as (Fig. 2.2b)

$$P_d = [\, (P_l/2)^2 + (P_t/2)^2 \,]^{1/2} \qquad [2.4]$$

iii) *Equilateral–triangular*, i.e. a staggered arrangement in which each group of three adjacent tubes form an equilateral triangle. The diagonal pitch of this arrangement is defined as in (ii) (Fig. 2.2c).

To define the Reynolds number for flow through the tube bank, the flow velocity is based on the minimum area available for flow, whether the minimum area occurs between the tube in a transverse row or in an alternate diagonal zig–zag path along the direction of a tube row normal to the flow. Then the Reynolds number for flow across a tube bank is defined as

$$Re = \frac{DG_{max}}{\mu} \qquad [2.5]$$

where G_{max}, $= \rho V_{max}$ = maximum mass flow velocity, is the mass flow rate per unit area where the velocity is maximum, and D is the outside diameter of the tubes. ρ is the density and V_{max} the maximum velocity based on the minimum area available for fluid flow.

The maximum flow velocity, V_{max}, for the in–line arrangement shown in Figure 2.2a is determined from

$$V_{max} = V_s \frac{P_t}{P_t - D} = V_s \frac{P_t/D}{P_t/D - 1} \qquad [2.6]$$

where V_s is the superficial velocity based on flow inside the heat exchanger shell without the tubes. Clearly, for the in–line arrangement, $P_t - D$ gives the minimum free–flow area between the adjacent tubes in a transverse row per unit length of the tube.

For the staggered arrangement show in Figure 2.2b the minimum free–flow area may occur between adjacent tubes either in a transverse row or in a diagonal row. In the former case, V_{max} is determined as given above; in the latter case, it is determined from

$$V_{max} = V_s \frac{P_t}{2(P_d - D)} = 1/2\ V_s \frac{P_t/D}{P_d/D - 1} \qquad [2.7]$$

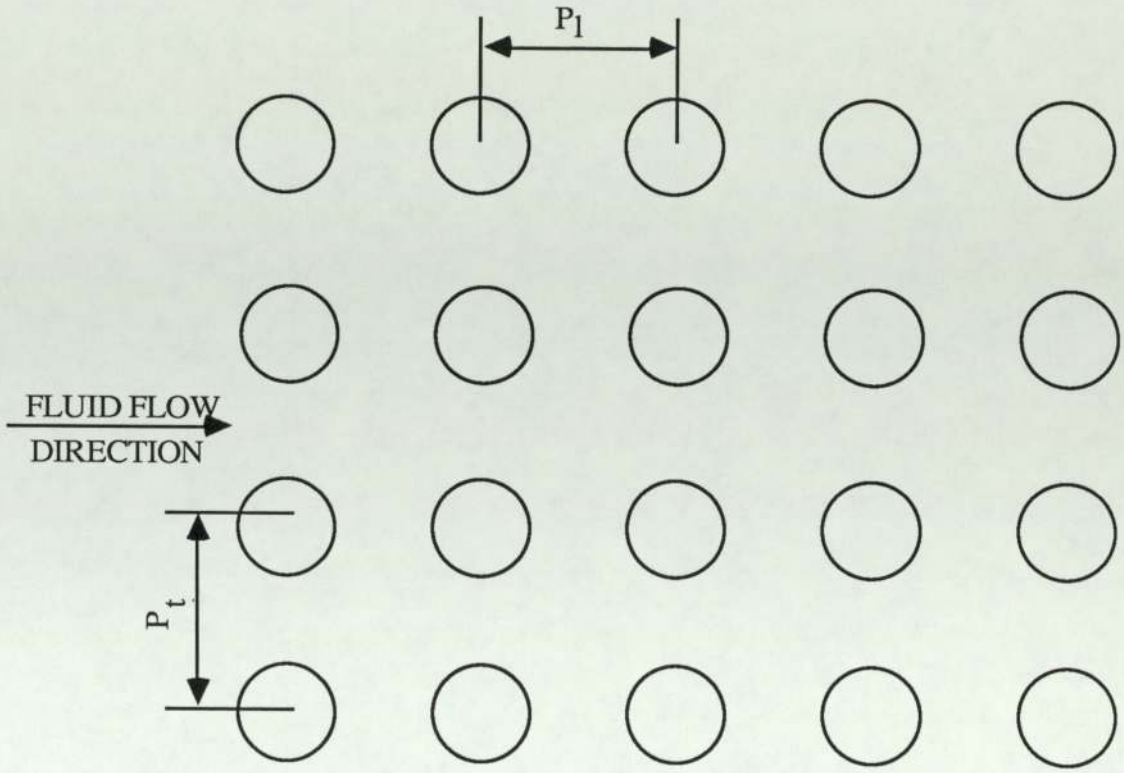

Fig. 2.2a Square in–line arrangement

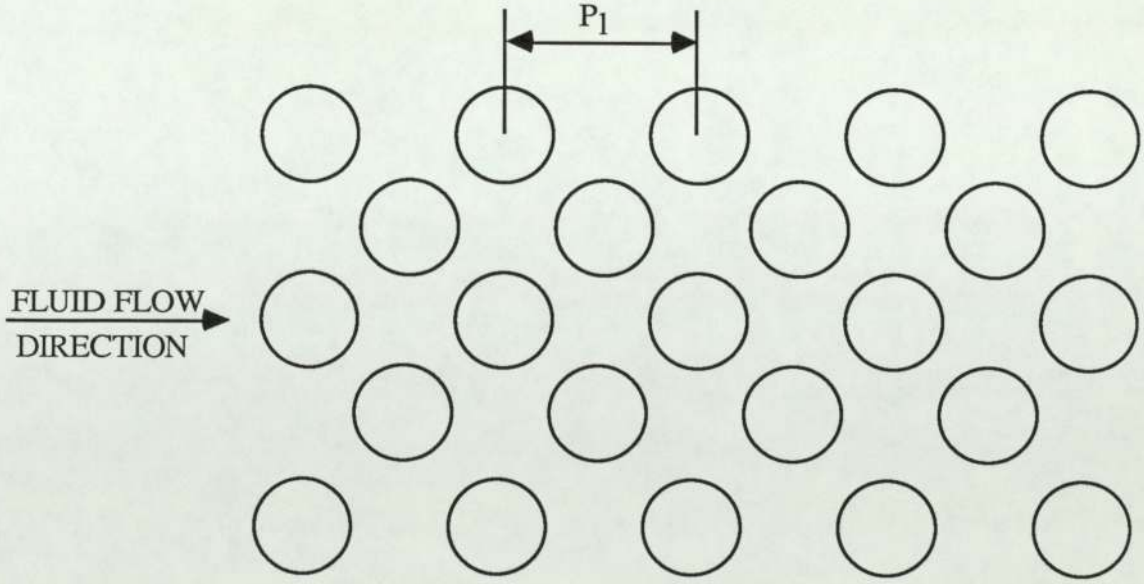

Fig. 2.2b Rotated square staggered arrangement

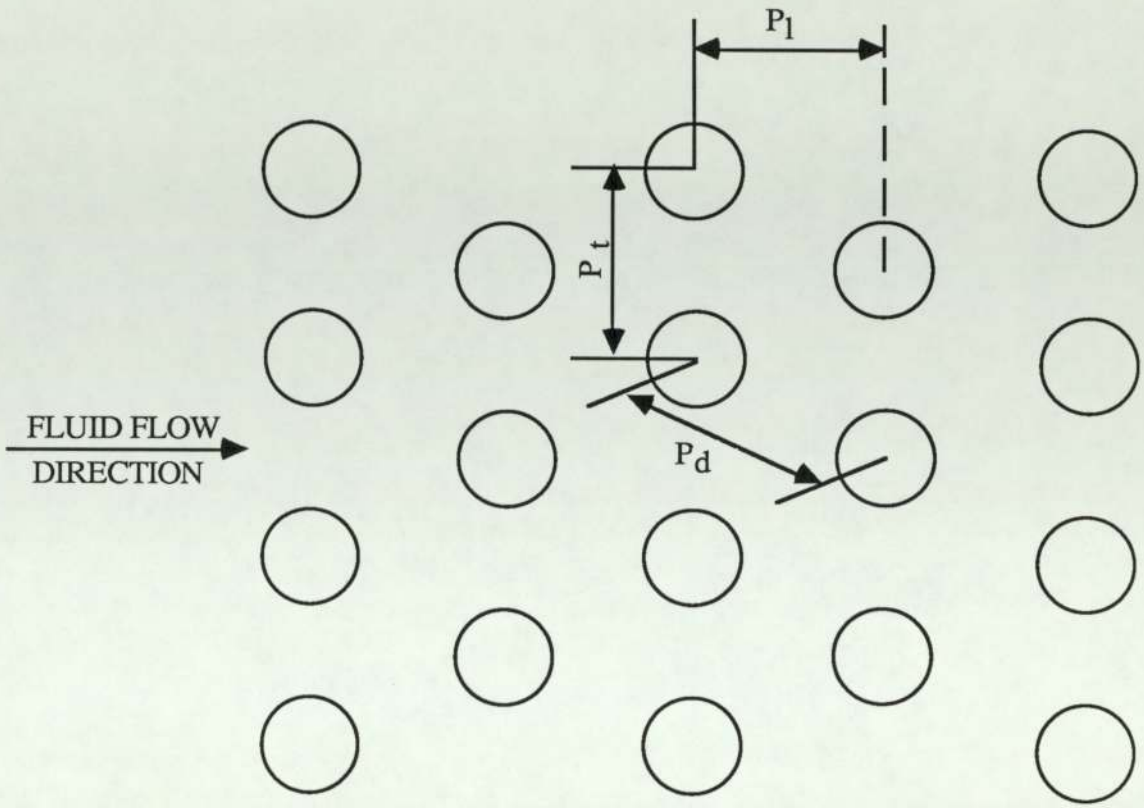

Fig. 2.2c Equilaterial triangular staggered arrangement

2.2 HEAT TRANSFER AND PRESSURE DROP ACROSS TUBE BANKS

Investigations of fluid flow and heat transfer in a variety of tube banks have been carried out using gaseous and liquid transfer media. These two transfer media are considered separately below.

In studying heat transfer in fluids flowing normal to banks of tubes, it has been usual to use air as the transfer medium under uniform wind–tunnel conditions. Two

notable examples are the investigations of Pierson [1937] and Huge [1937], whose extensive data were correlated by Grimison [1937]. All of this work, presented in 1937, was concerned with air flow at high Reynolds number. In all, 22 staggered and 16 in–line tube arrangements, 10 rows deep, were studied by these investigators over the Reynolds number range from $2x10^3$ to $4x10^4$. The correlation is summarized by McAdams [1954]. Kays, London and Lo [1954] also used air as the fluid flowing normal to the tube banks and extended the range of Reynolds number to the range of laminar flow. More recently the heat transfer and pressure drop associated with staggered and in–line tube bundles have been investigated at high Reynolds number by Achenbach [1977] using air as fluid.

Pierson [1937] tested thirty eight arrangements of tubes, differing in centre–to–centre spacing both in the direction of flow and transversely. The spacing, for both in–line and staggered tube rows, varied from the closest practicable to three tube diameters. Each bank (with two exceptions) comprised ninety tubes, arranged in ten rows of nine tubes transverse to the air stream.

Pierson demonstrated that both convective heat transfer and the flow resistance of tube banks vary markedly with changes in tube arrangements, and no simple statement of the variation was possible. He also found that the rate of change of these characteristics with changes in the Reynolds number was characteristic of the tube arrangement. He expressed the friction factor as exponential functions of Reynolds number, i.e. Re^n, where n varied from 0.2 to about –0.3.

Huge [1937] used nine tube arrangements with tubes of both 12.7 mm diameter and 17.5 mm diameter, the transverse P/D ratio range from 1.25 to 2 and longitudinal

P/D ratio range from 1.25 to 3. The tube banks had ten rows in the direction of the flow, both in–line and staggered, and were ten tubes wide with the exception of one case which was eight tubes wide. In addition, three arrangements of tubes of 50.8 mm diameter were used in banks of ten rows deep and from nine to fifteen tubes wide. Huge showed that for values of the Reynolds number in the range of commercial practice, the Nusselt number varied as the 0.61 power of the Reynolds number. The friction factor was not so consistently related to the Reynolds number but the relationships varied with the tube arrangement.

Kays et al. [1954] obtained heat transfer and flow friction data for flow normal to tube bundles for the Reynolds range, 500 to 20 000 (based on tube diameter). They tested six staggered tube patterns and one in–line arrangement. Tentative correlations were presented for the staggered arrangements allowing interpolation of the test results to obtain design data partially covering a transverse P/D ratio range from 1.25 to 2.50, and a longitudinal P/D ratio range from 0.75 to 1.50.

Achenbach [1977] measured the heat transfer and pressure drop of smooth–tube staggered and in–line tube bundles in the range of Reynolds number $4x10^4<Re<7x10^6$. He found that the heat transfer and pressure drop of staggered and in–line tube bundles show a close similarity to the corresponding quantities for a single circular cylinder in cross flow. At the critical Reynolds number, which was defined to be $Re_{crit} = 4.5x10^5$, the pressure drop and heat transfer changed their dependence on the Reynolds number. He also studied the effect of surface roughness on the pressure drop and heat transfer.

The situation with liquid as the transfer medium has been investigated by Omohundro, Bergelin and Colburn [1949], Bergelin, Davis and Hull [1949], Bergelin,

Brown, Hull and Sullivan [1950] and Bergelin, Brown and Doberstein [1952] who studied a number of tube banks, using a light spindle oil as the heat transfer medium and reaching an upper Reynolds number of about $1x10^4$. Dwyer and associates [1954 and 1956] studied heat transfer in water flowing at Reynolds numbers up to $1.2x10^6$ across a staggered arrangement of tubes.

In the first paper by Omohundro, Bergelin and Colburn [1949] measurements of overall pressure drop and heat transfer coefficient were reported for a bank of seventy tubes arranged in ten rows in equilateral triangular fashion of P/D = 1.25, for a range of Reynolds number from 1 to 1000. Average heat transfer coefficients were obtained for a rectangular tube bank, seven (9.5 mm diameter) tubes wide by ten rows deep. These data and those of subsequent investigations were all correlated in the j–factor form originally employed by Colburn [1933].

Measurements of the same quantities in the same Reynolds number region have been reported by Bergelin, Davis and Hull [1949] but here the tube arrangements considered were extended to in–line square and staggered square arrays of P/D = 1.25.

In the paper by Bergelin, Brown, Hull and Sullivan [1950] the results of the two previous papers, together with an additional account of the overall pressure drop and heat transfer coefficient behaviour for in–line square, staggered square and equilateral triangular arrangements of P/D ratio equal to 1.25 and 1.50 were presented for Reynolds numbers up to 1000.

In the last paper of the series, by Bergelin, Brown and Doberstein [1952], the investigations were extended to the range of Reynolds numbers 100 to 10 000.

Staggered and in–line square and equilateral triangular tube arrangements were again studied at two pitch–to–diameter ratios. For the square patterns, while the data for the staggered and in–line orientations were coincident at Reynolds numbers above about 4000, at lower Reynolds numbers the data diverged with the in–line arrangement being inferior to the staggered case. There was evidence, however, that the data converged again for Reynolds numbers less than 100.

The friction factor results of Bergelin and co–workers for five tube banks are plotted in Figure 2.3, where $f_G(\mu/\mu_w)^{0.14}$ is plotted versus Re, the Reynolds number based on D and G_{max} (see above). The heat transfer results of Bergelin and co–workers for five tube banks are shown in Figure 2.4, where $j_h(\mu/\mu_w)^{0.14}$ is plotted against Re. j_h is the heat transfer j–factor defined by

$$j_h = h(C_p G_{max})^{-1} Pr^{2/3} \qquad [2.8]$$

Dwyer et al. [1954 and 1956] obtained heat transfer coefficients at high Reynolds number for cross–flow for high temperature, high pressure water flow through a tube bank consisting of 200 tubes, 10 wide and 20 deep. The tubes were 20.57 mm OD and spaced on equilateral triangular centres, 32.51 mm apart. Most of these data were obtained in the Reynolds number range $2x10^5$ to $1.2x10^6$.

Overall pressure drop and heat transfer coefficient measurements within a Reynolds number range of 600 to 40 000 have been reported by Jones and Monroe [1958] and Gram, Machey and Monroe [1958] in two companion papers. Ten–row in–line tube arrangements covering an extensive range of $S_t x S_l$ were considered and correlations for the effect of tube bank geometry were proposed.

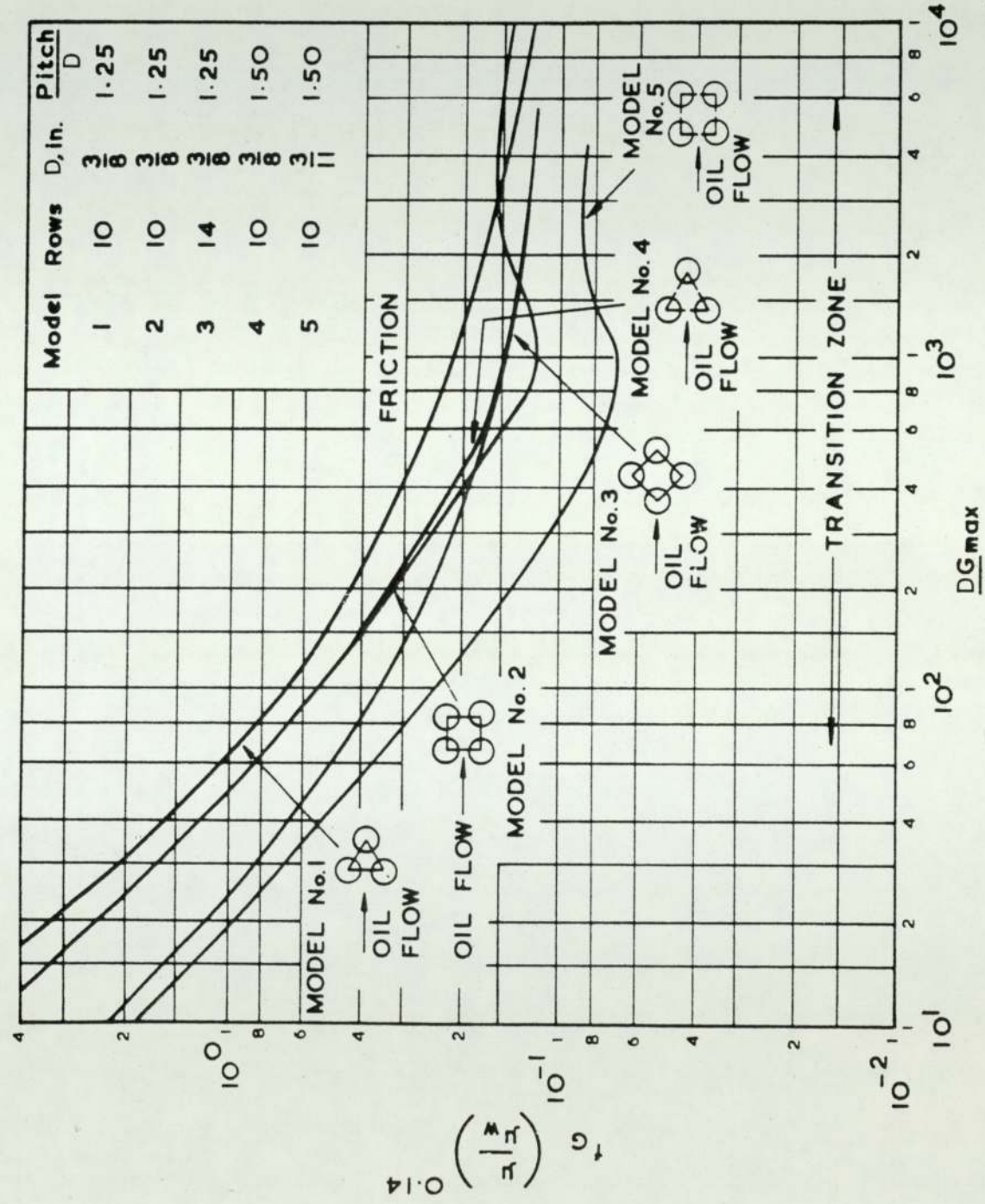

Fig 2.3 Smoothed curves of friction factors for five tube banks for transition zone (Bergelin et al. [1952])

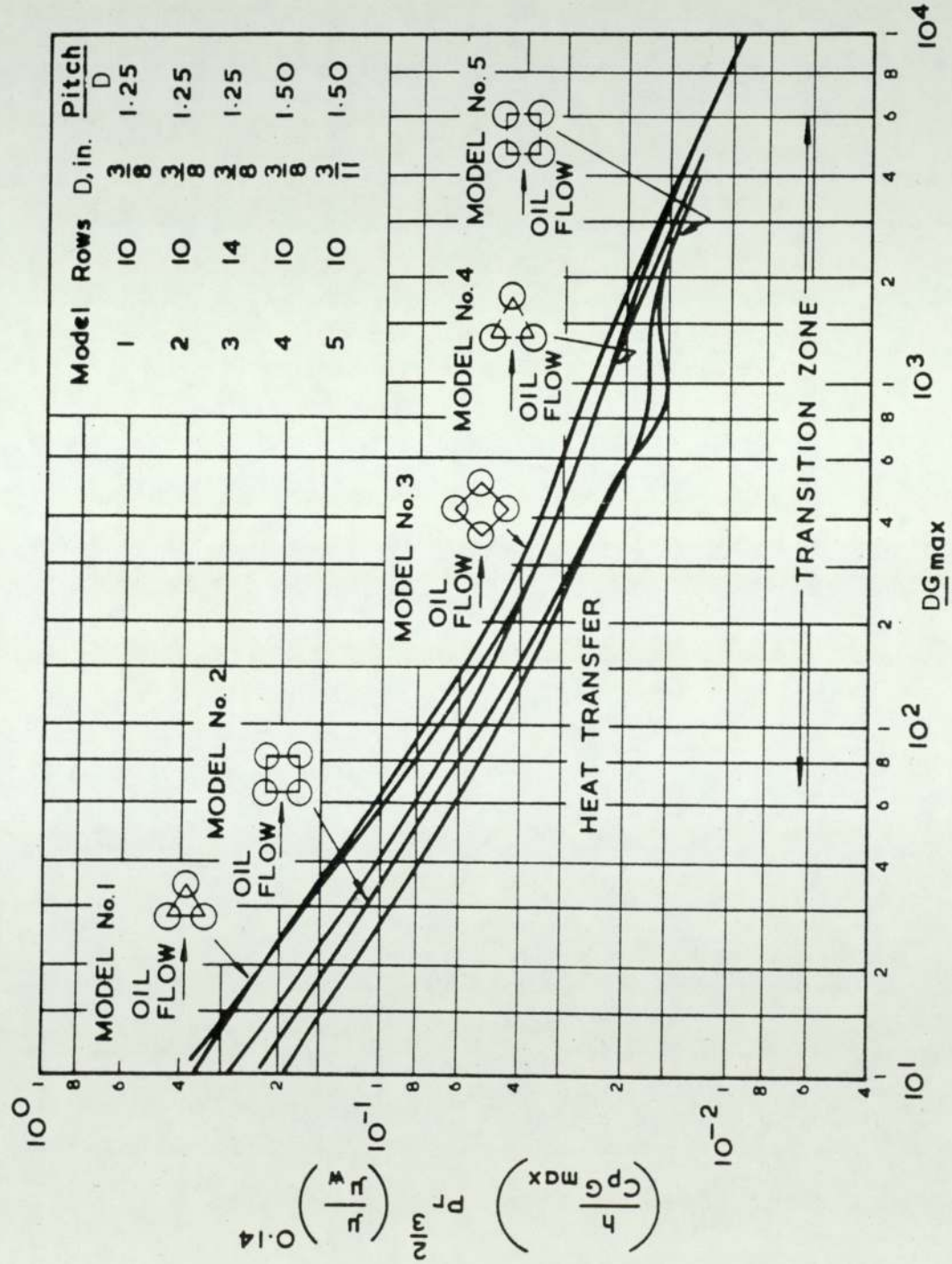

Fig 2.4 Smoothed curves of heat transfer factors for five tube banks for transition zone (Bergelin et al. [1952])

Experimental measurements over a Reynolds number range from $5x10^3$ to $2x10^6$ have been reported by Hammecks and Scholz [1967]. These workers determined overall pressure drop and heat transfer coefficients for three bundles of bare tubes which only differed in the tube arrangements, having the same transverse and longitudinal pitches. The three arrangements with nine rows were parallel in–line, parallel staggered and crossed in–line. The pitch to diameter ratios were 2.06 and 1.38 for the transverse pitch and the longitudinal pitch respectively. They considered that the change from a laminar boundary layer to a turbulent one accounted for the sharp change of slope in their plot of pressure drop coefficient and heat transfer coefficient against Reynolds number.

2.3 HEAT TRANSFER AND PRESSURE DROP ACROSS INCLINED TUBE BANKS

Compared to flow normal to a tube bank, inclined flow has received very little attention thus far. In these cases, where experimental studies exist, the data refer to very special flow situations. There are only a few published data on inclined tube bundles. However, a number of studies on a single cylinder (i.e. yawed) tube have been carried out (Kazakevitch [1954], Williams and Griskey [1975] and Kraabel et al. [1982]). These were largely concerned with point–to–point variations around the tube, which could be explained in terms of the changes in the nature of the flow past the cylinders. However, in a tube bank these variations would be damped by the presence of adjacent cylinders. In any case, the measured effect of yaw–angle differs among these three investigations.

An early study was that of Ornatski [1940] who investigated the heat transfer for banks of tubes in a stream of air impinging at angle of 15 to 90 degrees to the axes of the tubes. A range of Reynolds number from 5000 to 15 000 was covered for $P_l = P_t = 2D$. For banks of more than about 5 rows the results were expressed as

$$Nu = CRe^{0.6} \qquad [2.9]$$

The constant C for the different angles of impact are shown in Table 2.1. Ornatski found that the heat transfer in the first row of the in–line banks was about 30 per cent less than the average for the subsequent rows.

Table 2.1

Constants, C, in Ornatski's equation [2.9] for Nusselt number for oblique flow of air

φ	90^o	80^o	70^o	60^o	45^o	30^o	15^o
C	0.29	0.29	0.28	0.27	0.24	0.20	0.12

There are a few theoretical studies for the case of three–dimensional flow over a inclined bank of tubes.

For a uniformly–inclined fully–developed flow the Engineering Science Data Unit publication 74040 [1974] suggests ways for calculating the overall pressure drop in a tube bank. ESDU [1974] suggests that, for Reynolds numbers less than 50 and inclination angles greater than 30^o, the pressure drop in the direction of the inclined flow can be considered as independent of the inclination and equal to the pressure drop in the

transverse direction. Here the Reynolds number is defined in terms of the mean velocity of the incident flow and the tube diameter, while the inclination angle is the angle between the uniformly inclined flow and the tube axes. This suggestion is based on a theoretical study of cross flow past elliptical tubes, presented by Masliyah [1973].

Butterworth [1978] presented a model for predicting multidimensional flow in tube bundles which treated the heterogeneous system of tubes and fluid as a homogeneous system with averaged flow properties. He also used, in another paper [1978], a similar approach to derive an equation for heat transport during three–dimensional flow in tube bundles. The general heat transfer equation included convection, dissipation, conduction and source terms.

The prediction of heat transfer in tube banks under conditions of turbulent fully–developed flow inclined to the axes of the tubes has recently been investigated by Antonopoulos [1985]. His investigation also included the limiting cases of purely axial ($\varphi=0^{o}$) and purely transverse flow ($\varphi=90^{o}$). He found that at a fixed Re_h (the Reynolds number based on the hydraulic diameter, i.e. $Re_h=\rho V D_h/\mu$) of the inclined flow, the average Nusselt number (Nu_h), based on D_h, increases with yaw angle φ. The maximum value was obtained for purely transverse flow and the minimum for purely axial flow.

The predicted average values of $Nu_h/Pr^{0.36}$ as a function of the axial Reynolds number, Re_a, for various values of the transverse Reynolds number, Re_c, as a parameter

for fully–developed inclined flow are shown in Figure 2.5. These results relate to a staggered arrangement of P_t x P_l = 2.42 x 1.64. The inclination angles θ are marked at various locations along the curves (Antonopoulos [1985]).

2.4 VARIATION IN HEAT TRANSFER FROM ROW TO ROW IN TUBE BANKS

In tube banks the interaction due to the surrounding tubes causes a marked deviation from flow around a single cylinder (Polhausen [1921], Ulsamer [1932] and Hilpert [1933]). Data for the variation of heat transfer from row to row in tube banks have been given by Griffiths and Awbery [1933], Pierson [1937], Thomson, Scott, Laird and Holden [1951], Snyder [1953], Kays, London and Lo [1954], Sheehan et al. [1954], Kays and London [1964], Welch and Fairchild [1964]. The majority of these authors show the heat transfer increasing from row to row from the first row inwards and levelling off after 3 to 10 rows depending on the tube bank arrangement.

Griffiths and Awbery [1933] determined local heat transfer coefficients in a ten rows deep staggered tube bundle. The bundle was constructed from steel tubes 47.5 mm in diameter, set at equal longitudinal and transverse pitches of 2.0. The results obtained showed a 61% increase in the value of the heat transfer coefficient up to the third row, after which it remained relatively constant.

One of the most complete treatments of the subject of convective heat transfer within tube banks is that of Pierson [1937]. In his test series he investigated a total of thirty eight different tube bank configurations, each tube bank containing ninety tubes,

arranged in rows of nine and transverse to the incoming air stream. The variation in Nusselt number from row to row was plotted as the ratio:

$$\frac{\text{h for bank n rows deep}}{\text{h for bank 10 rows deep}} \qquad (n = 1, 2, ..., 10)$$

versus Reynolds number, for several tube configurations. The results showed an increase in h for the first three to four rows, after which it remained relatively constant. The data give no indication, however, of the relationship between a ten–rows–deep bank and deeper banks.

Bergelin, Colburn and Hull [1950] found that for a tube bank of up to ten rows deep, the mean heat transfer coefficient of the tube bank varied inversely as $N_t^{0.18}$, where N_t is the number of the tube rows.

A ten–row deep staggered tube bank with equal longitudinal and transverse P/D ratios of 1.80 was used by Snyder [1953]. The bank was built from 30.75 mm diameter brass tubes, each tube being approximately 225 mm long. As shown in Figure 2.6 the local Nusselt number increased up to the third row, decreased at the fifth row and then remained relatively constant until the tenth row. The average values of Nusselt number are plotted in Figure 2.7. This variation occurred over the range of Reynolds number studied, $8x10^3$ to $2x10^4$. Data are also presented as Nusselt number/Reynolds number plots for each row in Figure 2.8. It was found that the constant C in the general equation $Nu=CRe^m$ decreased for the first three rows and then increased, whereas the value of the exponent increased and then decreased (see Table 2.2). The results were compared with the correlation of Grimison [1937].

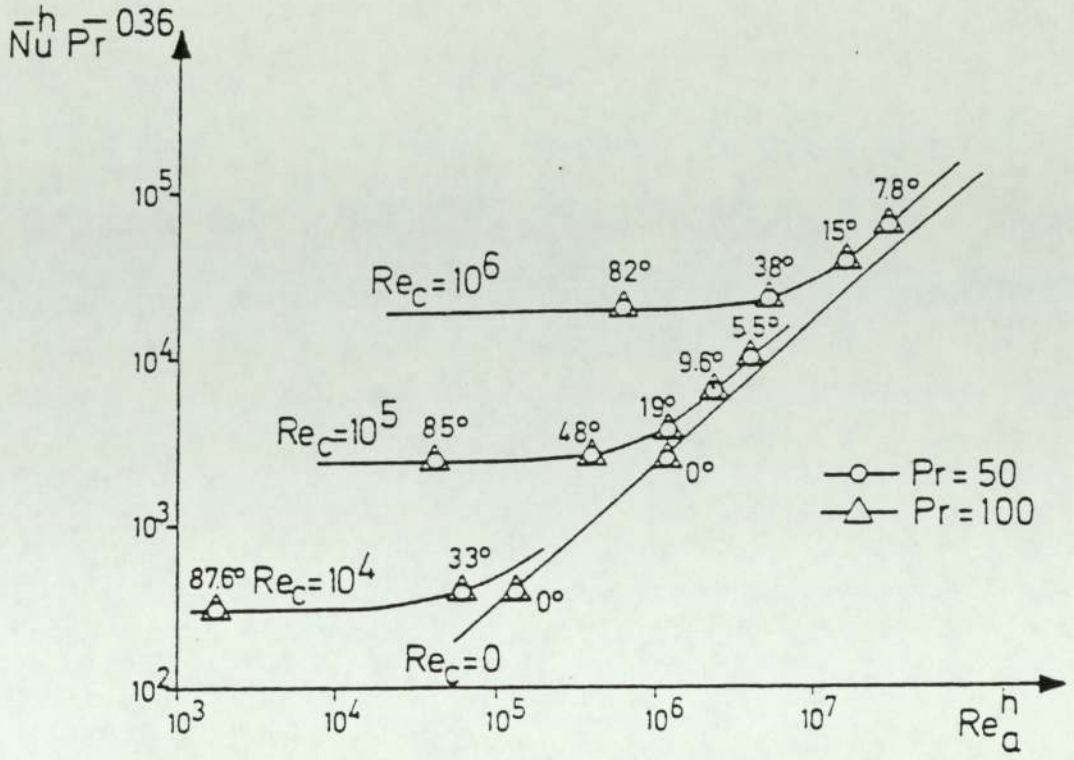

Fig. 2.5 Predicted $Nu_h/Pr^{0.36}$ as a function of the axial Reynolds number Re_a with the transverse Reynolds number Re_c as a parameter for fully–developed inclined flow through a staggered arrangement of P_t x P_l = 2.42 x 1.64 (Antonopoulos [1985])

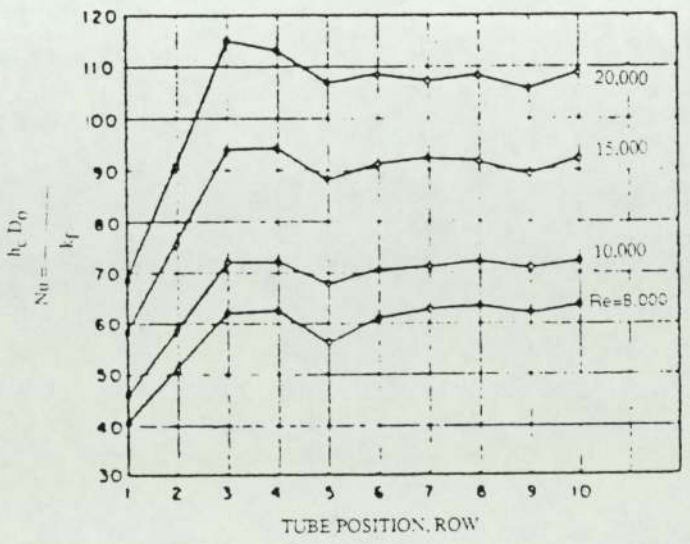

Fig. 2.6 Local Nusselt number as a function of tube position with Reynolds number as a parameter (Snyder [1953])

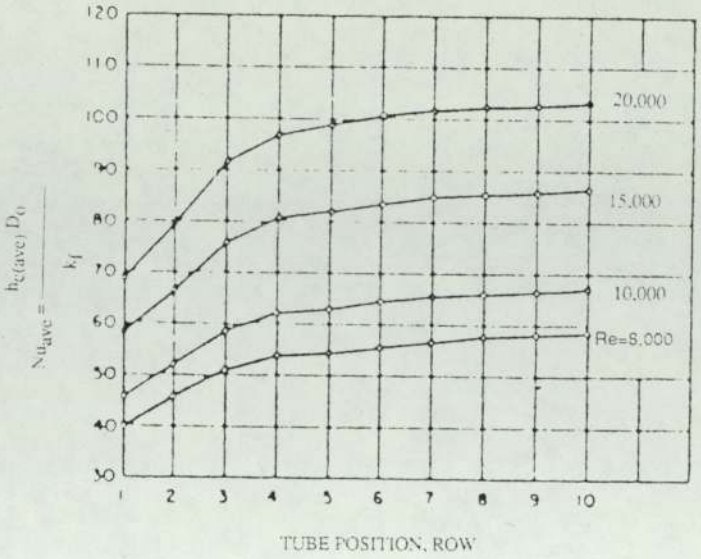

Fig. 2.7 Average Nusselt number versus tube position with Reynolds number as a parameter (Snyder [1953])

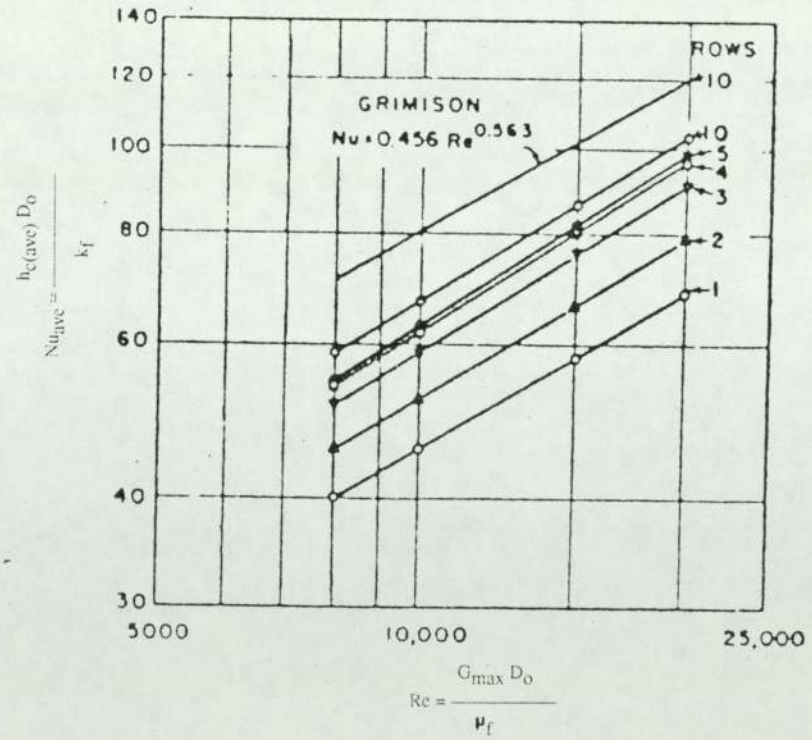

Fig. 2.8 Correlation of Nu_{av} versus Reynolds number for a ten–row tube bank (Snyder [1953])

Table 2.2
Values of m and C in the correlation equation $Nu = CRe^m$ for transverse rows in a ten–row tube bank (Snyder [1953])

Row	1	2	3	4	5	6	7	8	9	10
m	0.588	0.608	0.638	0.640	0.654	0.640	0.625	0.624	0.622	0.620
C	0.200	0.190	0.162	0.169	0.150	0.178	0.207	0.213	0.216	0.223

McAdams, in 1954, reported that in staggered tube bundle arrangements the coefficients in the first row were approximately 0.63 times the mean coefficient of an infinite number of rows, and a ten–row tube bank had a mean coefficient of an infinite tube bank. The higher coefficients at the rear rows of tube banks were attributed to increased turbulence caused by the presence of the tubes in front of them.

Kays, London and Lo [1954] used a transient technique to determine the row–to–row coefficient variation. The tube banks tested were constructed of 244 mm long, 9.375 mm diameter aluminium tubes, covering a longitudinal P/D ratio range of 1.00 to 1.50 and a transverse P/D ratio of 1.25 to 2.00. Tests were conducted for both longitudinal flow and transverse flow, and the transverse variation was found to be less than 1% for a Reynolds number lower than 10^4. The row–to–row heat transfer coefficient variation, plotted in Figure 2.9 as h_{ROD}/h versus row number, indicates that the coefficient is lower nearer the bank entrance than in the interior, over the range of Reynolds number tested. This behaviour was found to vary somewhat with the Reynolds number, but Kays et al. [1954] concluded that this effect was minimal and could be neglected. However, to provide a more useful result for most exchanger design work where the overall correction is less than 10 per cent, the data of Figure 2.9 were averaged by the full line, and the integrated results are presented in Figure 2.10.

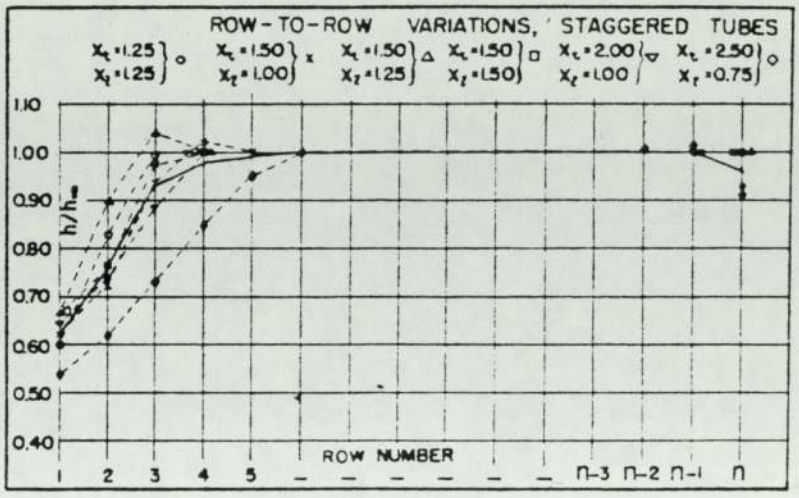

Fig. 2.9 Row–to–row variation of normalised heat transfer coefficient (Kays et al. [1954])

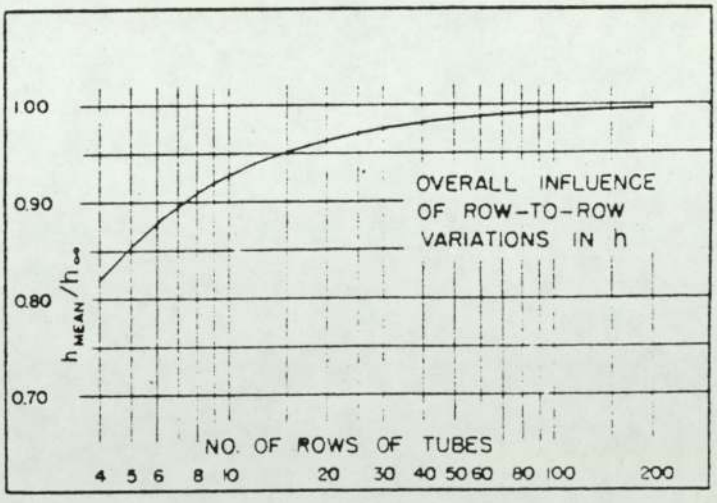

Fig.2.10 Influence of row–to–row variations on overall normalised heat transfer coefficient (Kays et al. [1954])

Kays et al. [1954] found that for tube bundles having less than 10 transverse rows in the direction of flow, there was some reduction in the heat transfer coefficient. Based on the results of their experiments, the heat transfer coefficient, h_N, for $N<10$ could be determined by utilizing the following relationship

$$h_N = C_1 h_{N\geq 10} \qquad \text{for } 1\leq N\leq 10 \qquad [2.10]$$

Table 2.3 lists the values of the correction factor C_1 for both in–line and staggered tube arrangements, with N varying from 1 to 9. The results depend only slightly on the Reynolds number.

Table 2.3

Correction factor C_1 for equation [2.10]

Row No.	1	2	3	4	5	6	7	8	9
In–line	0.64	0.80	0.87	0.90	0.92	0.94	0.96	0.98	0.99
Staggered	0.68	0.75	0.83	0.89	0.92	0.95	0.97	0.98	0.99

The results of Kays and London [1964] show a 5% variation as the rows are increased from 15 to 200.

In the investigations carried out by Welch and Fairchild [1964], electrically heated air was passed over a ten row deep tube bank constructed from 12.5 mm diameter, 300 mm long brass tubes. Water under forced circulation was used to cool the tubes, and the row–to–row heat transfer coefficient determined from mass and

temperature balances. Tube bank configurations tested covered those with longitudinal pitches of 1.5 to 6.0, and transverse pitches of 1.0 to 2.0. The results were presented as h_{ROD}/h versus Reynolds number, and the effect of tube bank configurations on individual row heat transfer at constant Reynolds number was also shown.

From the above review, tentative conclusions may be drawn, the local coefficient within the tube bank appears to increase for the first few rows, after which it remains relatively constant until the last row, where a decrease in value is observed.

2.5 CORRELATIONS FOR HEAT TRANSFER IN TUBE BANKS

The heat transfer characteristics of a tube in a bank are determined mainly by flow velocity, physical properties of the fluid, heat flux intensity, heat flux direction, and the arrangement of the tubes.

Dimensional analysis (e.g. Coulson and Richardson [1977]) shows that the general equation for heat transfer is

$$hD/k = \Psi[(\rho VD/\mu), (C_p\mu/k), (\beta g\Delta TD^3\rho^2/\mu)] \qquad [2.11]$$

or

$$Nu = \Psi[Re, Pr, Gr] \qquad [2.12]$$

where C_p = specific heat at bulk temperature

ΔT = temperature difference

D = tube outside diameter

g = acceleration of gravity

h = heat transfer coefficient

k = thermal conductivity

V = velocity of fluid

ρ = fluid density at bulk temperature

μ = fluid viscosity at bulk temperature

β = coefficient of cubical expansion

For conditions in which only natural convection occurs the velocity is dependent solely on the buoyancy effects, represented by the Grashof number (Gr), and the Reynolds group (Re) can be omitted. Thus

$$Nu = f(Pr, Gr) \qquad [2.13]$$

Again, when forced convection occurs the effects of natural convection are usually negligible and the Grashof number may be omitted. Thus

$$Nu = f(Pr, Re) \qquad [2.14]$$

Experiment shows that heat transfer by forced convection for flow normal to tube banks may be represented by an equation of the form

$$Nu = CRe^{m} Pr^{n} \qquad [2.15].$$

where the Reynolds number is based on the tube outside diameter and a characteristic flow area. The constants have been evaluated in several investigations, and slight variations have been proposed by some workers, but often the power on the Reynolds number is recommended as 0.6 for ideal tube banks and that on the Prandtl number as 0.33. C is a constant which depends on the tube arrangement.

Numerous investigations into cross–flow heat transfer in tube banks have studied the effects of such geometrical variables as tube arrangement, tube diameter and spacing and have derived corresponding experimentally–based values for the constants in equation [2.15].

One of the first correlations for heat transfer to staggered smooth tube banks in cross–flow was given by Colburn [1933]. The existing data for the flow of gases normal to staggered tube banks were plotted as the dimensionless group $(Nu/Pr^{0.33})$ against Reynolds number. The characteristic dimension was the tube diameter and the velocity was determined from the minimum free area for flow. Between Reynolds numbers of 2000 to 32 000 the curve was well represented by the equation:

$$Nu = 0.33Pr^{0.33}Re_{max}{}^{0.6} \qquad [2.16]$$

or

$$j_h = 0.33Re_{max}{}^{0.4} \qquad [2.17]$$

where

$$j_h = NuPr^{0.33}/Re \qquad [2.18]$$

The equations are for ten or more rows of tubes. For in–line arrangements, Colburn [1933] derived a similar equation with the value of the constant 0.33 reduced to 0.26, showing inferior coefficients compared with the staggered arrangement.

Sieder and Tate [1936] modified equation [2.16] to include changes in fluid viscosity between the bulk of the fluid and the tube surface. For viscous liquids there will be a marked difference at any cross–section between the viscosity of the fluid adjacent to the surface and the value at the axis (in tubular flow) or at the bulk temperature of the fluid. They multiplied the right hand side of equation [2.16] by the ratio $(\mu/\mu_w)^{0.14}$. Thus

$$Nu = 0.33Pr^{0.33}Re_{max}{}^{0.6}(\mu/\mu_w)^{0.14} \qquad [2.19]$$

Grimison [1937] correlated the extensive data of Huge [1937] and Pierson [1937] in the Reynolds number range 2000 to 40 000, for both staggered and in–line arrangements with air (the Prandtl number usually has a value of about 0.74 for gases), for tube bundles having 10 or more transverse rows in the direction of flow with an expression of the form

$$Nu = bRe_{max}{}^{n} \qquad [2.20]$$

where G_{max} is based on the minimum area available for fluid flow. (The minimum area for flow may lie along the horizontal plane through the tube centre–lines, or along the zig–zag path through the centre–lines of nearest neighbours.)

This expression has been generalized to fluids other than air by including the Prandtl number effect in the form

$$Nu = 1.13bRe^{n} Pr^{0.33} \qquad [2.21]$$

The values of b and n for different tube arrangements have been tabulated. These values are reproduced in Table 2.4.

Table 2.4

Constants b and n in the correlation of Nusselt number against Reynolds number equation [2.20] (Grimison [1937])

Arrangement	P_l/D	P_t/D = 1.25		1.50		2.0		3.0	
		b	n	b	n	b	n	b	n
Staggered	0.6	...	...	...	...	...	...	0.213	0.636
	0.9	...	...	...	...	0.446	0.571	0.401	0.581
	1.0	...	...	0.497	0.588	...	...	...	...
	1.125	...	...	...	...	0.478	0.565	0.518	0.560
	1.250	0.518	0.556	0.505	0.554	0.519	0.556	0.522	0.562
	1.50	0.451	0.568	0.460	0.562	0.452	0.568	0.488	0.568
	2.0	0.404	0.572	0.416	0.568	0.482	0.556	0.449	0.570
	3.0	0.310	0.592	0.356	0.580	0.440	0.562	0.421	0.574
In–line	1.25	0.348	0.592	0.275	0.608	0.100	0.704	0.063	0.752
	1.50	0.367	0.586	0.250	0.620	0.101	0.702	0.067	0.744
	2.0	0.418	0.570	0.299	0.602	0.229	0.632	0.198	0.648
	3.0	0.290	0.601	0.357	0.584	0.374	0.581	0.286	0.608

Experimental evidence shows that neither the Colburn nor the Grimison correlations can be extrapolated above a Reynolds number of 70 000. Sheehan, Schomer and Dwyer [1954] found that in a tube bank of equilateral triangular pitch, the Colburn curve fitted well for water as the test fluid up to a Reynolds number of 70 000, where the heat transfer coefficient was proportional to $Re^{0.6}$. For Reynolds numbers between 70 000 and 10^6 the value of the Reynolds number exponent rose to 0.8,

i.e. $$Nu = 0.33Re^{0.8}Pr^{0.33}(\mu/\mu_w)^{0.14} \qquad [2.22]$$

Brauer [1961] has reported heat transfer data for smooth circular, profiled, and oval tubes in cross–flow. For oval tubes with the major axis in the direction of flow the mean heat transfer for the three staggered arrangements tested was represented by the equation

$$Nu = 0.236Re_h^{0.62}Pr^{0.33} \qquad [2.23]$$

with the Reynolds number based on an equivalent hydraulic diameter D_h,

where $$D_h = 4A_s/S_p \qquad [2.24]$$

with A_s = Area available for flow

S_p = Perimeter of the tube

Stasiulevicius [1963] investigated heat transfer in a staggered bank of tubes with a single tube in the bank heated electrically. The range of Reynolds number covered in this work was from 10^4 to $1.5x10^6$. A change in the exponent of the Reynolds number was noted at $2x10^5$ from 0.6 to 0.8–0.9. Similar results were reported by Stasiulevicius and Samoshka [1963], for different arrangements of staggered banks the index of the Nusselt number–Reynolds number relationship changed from 0.6 to 0.78–0.93 for values of Reynolds number from $1.6x10^5$ to $2x10^5$.

Kays and London [1964] have correlated the staggered bank data of Kays,

London and Lo [1954] by an equation of the form

$$StPr^{0.67} = C_h Re'_v{}^{-0.4} \qquad [2.25]$$

where Re'_v is based on a modified volumetric equivalent diameter. Values of C_h are given by Kays and London in terms of the transverse and longitudinal pitch to tube diameter ratios.

A study of heat transfer in cross flow across tube banks using water as cross–flow fluid has been reported by Zukauskas et al. [1968]. Only one tube was heated in the bundle and this was placed in the 6th row of the 10 transverse rows. Values of the exponent of the Reynolds number were tabulated and ranged from 0.6 to 0.74 for Reynolds numbers from $2x10^4$ to $2x10^6$.

Zukauskas [1972] reviewed the work of various investigators and proposed the following correlation for the heat transfer coefficient for flow across tube bundles

$$Nu = C_2 Re^m Pr^{0.36} (Pr/Pr_w)^n \qquad [2.26]$$

where Pr_w is the Prandtl number evaluated at the wall temperature, and n = 0 for gases, and = 0.25 for liquids, valid for $0.7<Pr<500$ and $N\geq20$, here N is the number of tube rows. For liquids, the physical properties are evaluated at the bulk temperature, since the viscosity correction term is included through the Prandtl number ratio. For gases, the properties are evaluated at the film temperature and the viscosity correction term $(Pr/Pr_w)^n$ is omitted.

The coefficient C_2 and the exponent m were determined by correlating the experimental data for air, water, and oil reported by numerous investigators. Table 2.5 lists the recommended values of C_2 and m of equation [2.26].

Table 2.5

Constant C_2 and exponent m of equation [2.26] (Zukauskas [1972])

Geometry	Re	C_2	m	Remarks
In–line	10 to 10^2	0.8	0.40	
	10^2 to 10^3	Large and moderate longitudinal pitch, can be regarded as a single tube		
	10^3 to $2x10^5$	0.27	0.63	
	$2x10^5$ to 10^6	0.21	0.84	
Staggered	10 to 10^2	0.9	0.40	
	10^2 to 10^3	About 20 percent higher than that for single tube		
	10^3 to $2x10^5$	$0.35(P_t/P_l)^{0.2}$	0.60	$P_t/P_l<2$
	10^3 to $2x10^5$	0.40	0.60	$P_t/P_l>2$
	$2x10^5$ to 10^6	0.022	0.84	

Equation [2.26] correlates the experimental data very well for tube bundles having 20 or more rows in the direction of flow. For bundles having less than 20 rows, the Nusselt number can be found from

$$Nu_N = C_3 Nu_{N\geq 20} \qquad [2.27]$$

where the correction factor C_3 is given in Figure 2.11 for both in–line and staggered tube arrangements.

Whitaker [1972] proposed a new general form of correlation of heat transfer for packed beds and compact (void fraction less than 0.65) staggered tube bundles. The Nusselt number for a wide range of packing materials and tube arrangements was thus expressed for Re>50 by the equation

$$Nu = (0.5Re^{1/2} + 0.2Re^{2/3})Pr^{1/3}(\mu/\mu_w)^{0.14} \qquad [2.28]$$

He compared the above correlation with a wide range of experimental data (Bergelin, Colburn and Hull [1950], Bergelin et al. [1958], Kays et al. [1954] and Pierson [1937]) as shown in Figure 2.12.

Whitaker also plotted the data for in–line tube bank arrangements of several investigators (Bergelin et al. [1950], Edwards et al. [1956] and Fairchild et al. [1961]) and compared them with the correlation used for staggered tube bundles. As shown in Figure 2.13, he found that the correlation failed and hence he concluded that the effect of S_l and S_t must be included in any correlation for heat transfer in in–line tube bundles.

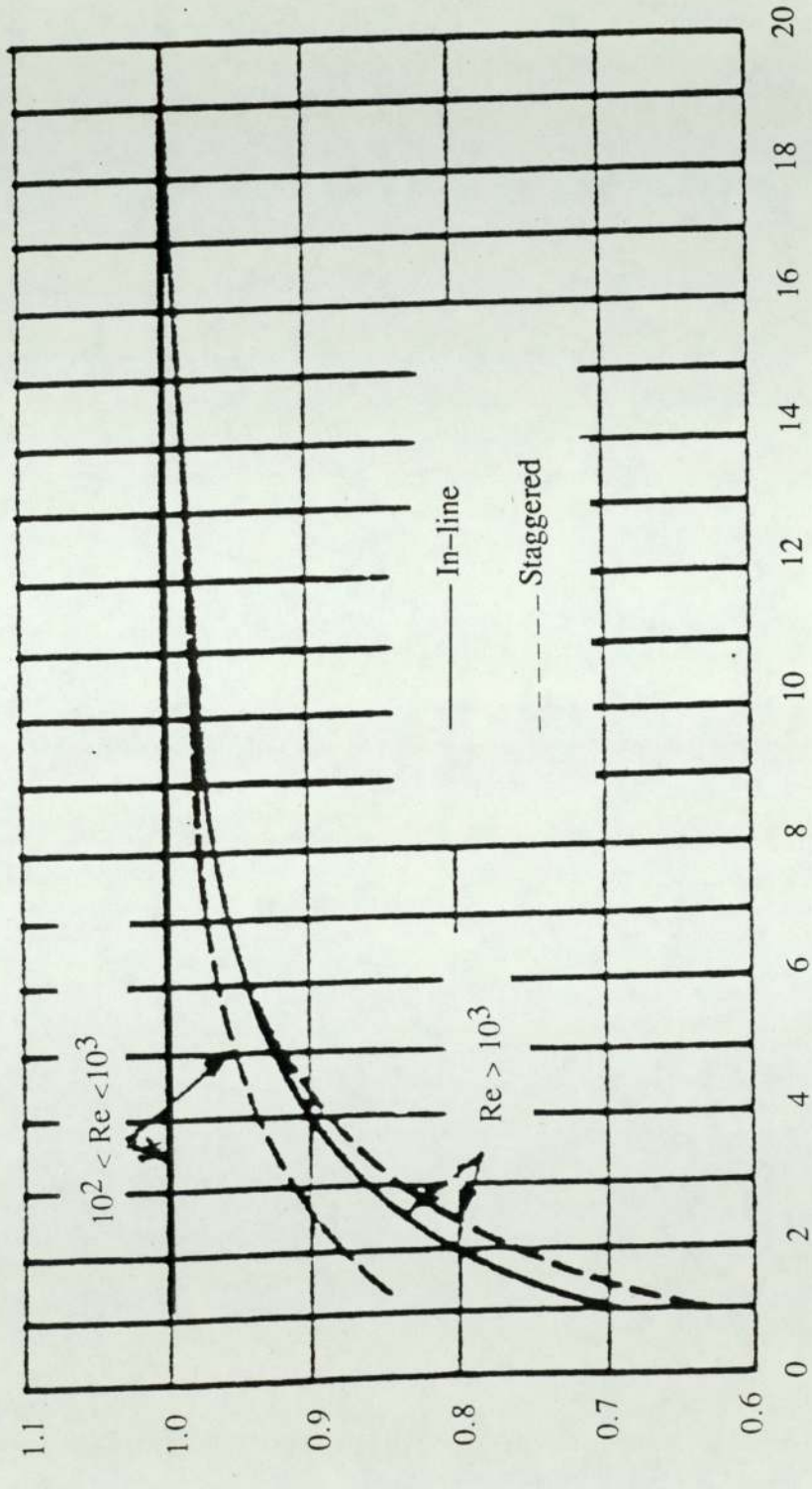

Fig. 2.11 Correction factor C_3 in equation [2.27] (Zukauskas [1972])

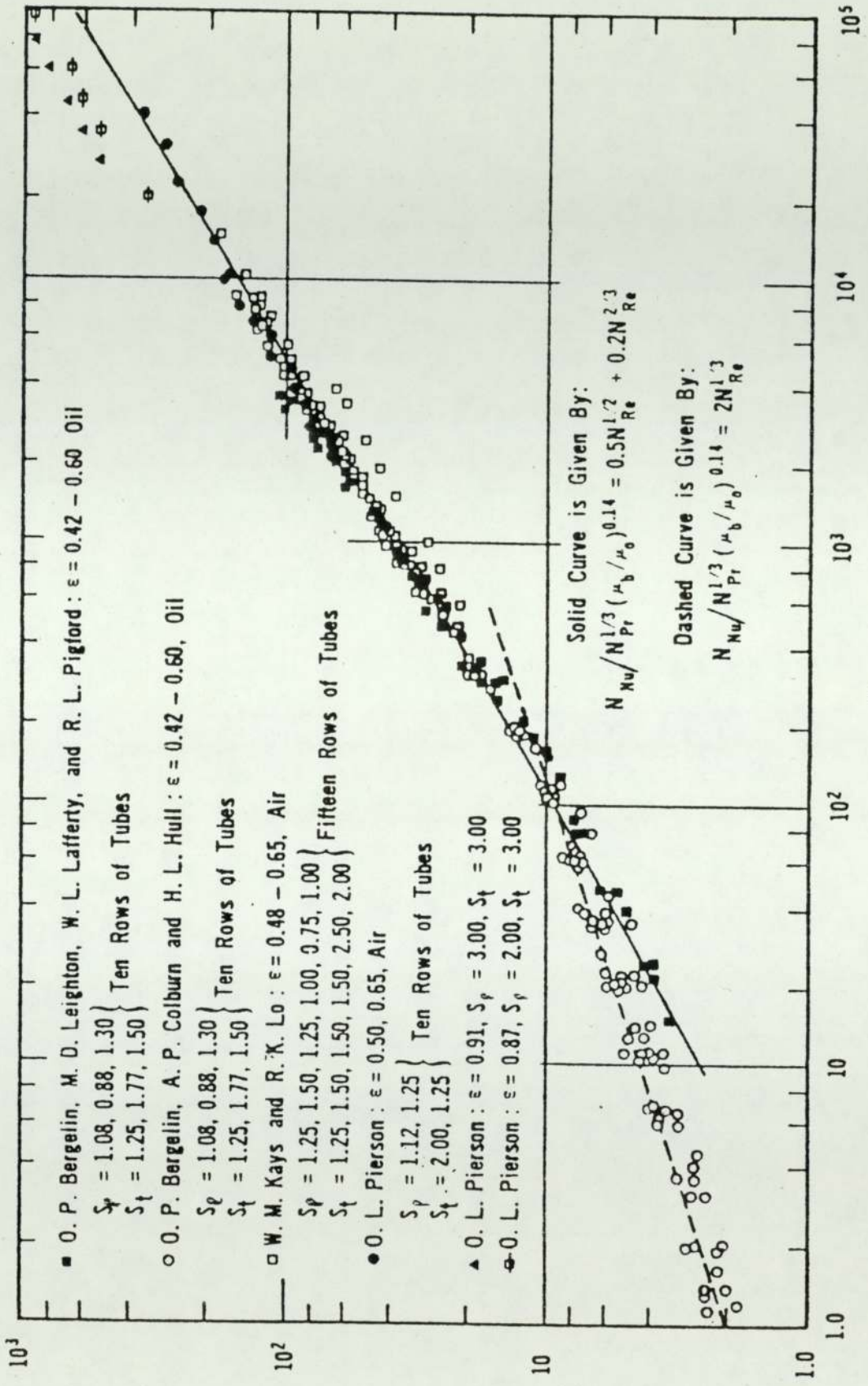

Fig. 2.12 Heat transfer to fluids flowing past staggered tube banks (Whitaker [1972])

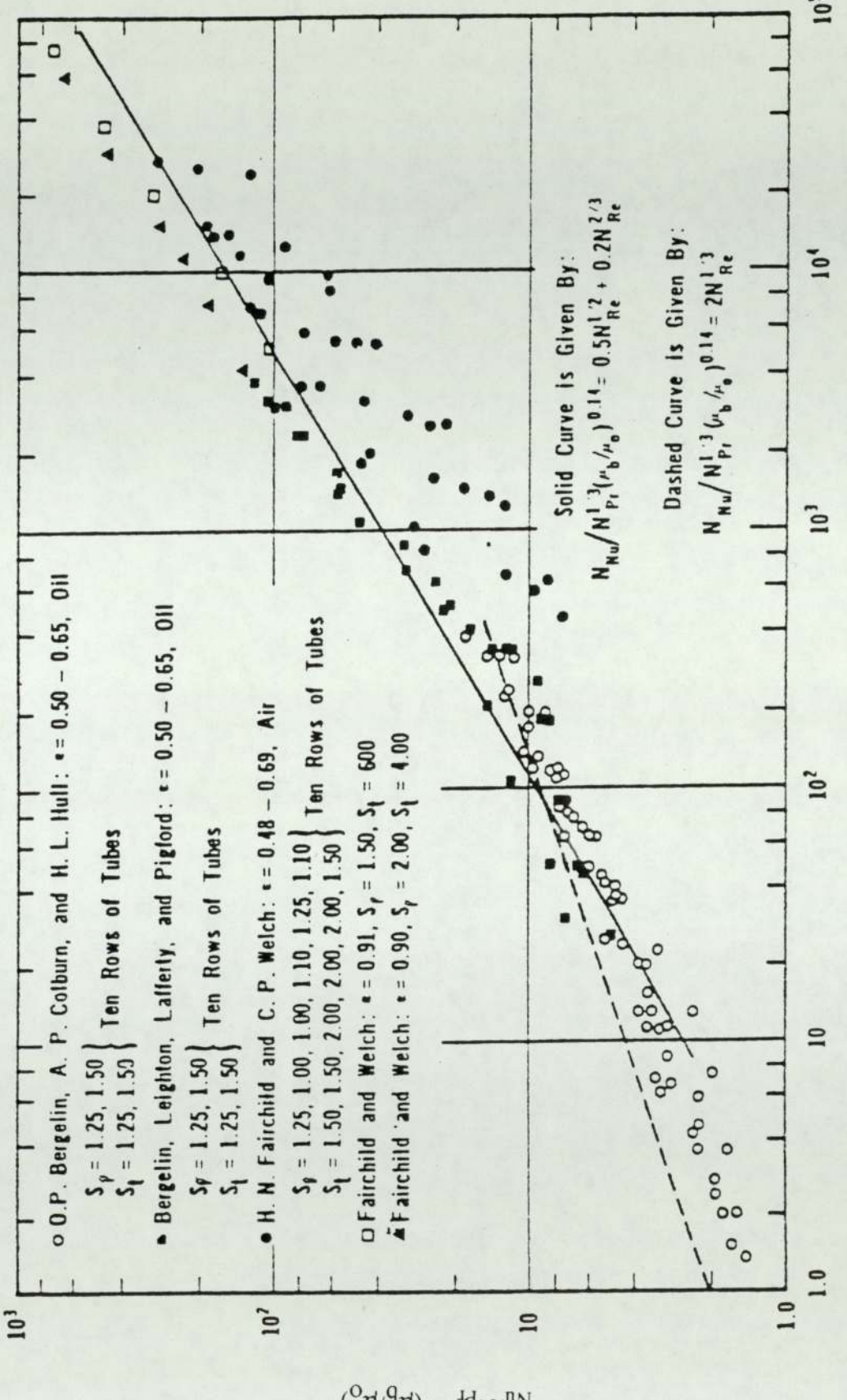

Fig. 2.13 Heat transfer to fluids flowing past in-line tube banks (Whitaker [1972])

The Engineering Science Data Unit (ESDU) publication 73031 [1973] presented a similar correlation for the flow of a constant property fluid in the Reynolds number range of 10 to $2x10^6$. The equation is

$$Nu = aRe^m Pr^{0.34} F_n \qquad [2.29]$$

The values of a and m are shown in Table 2.6 for staggered and in–line tube arrangements for the Reynolds number ranges given.

Table 2.6

The equation constant and exponent value of the ESDU correlation (ESDU [1973])

Range of Re	in–line		staggered	
	a	m	a	m
10 to $2x10^2$	0.742	0.431	1.309	0.360
$2x10^2$ to $2x10^5$	0.211	0.651	0.273	0.635
$2x10^5$ to $2x10^6$	0.116	0.700	0.124	0.700

The factor F_n corrects for the number of tube rows crossed and is used to account for turbulence generated due to the fluid flow through the bundle. This factor was determined from experimental data.

The variations of Nusselt number with respect to Reynolds number covering gases and liquids are shown in Figures 2.14 and 2.15 for staggered tube arrangements.

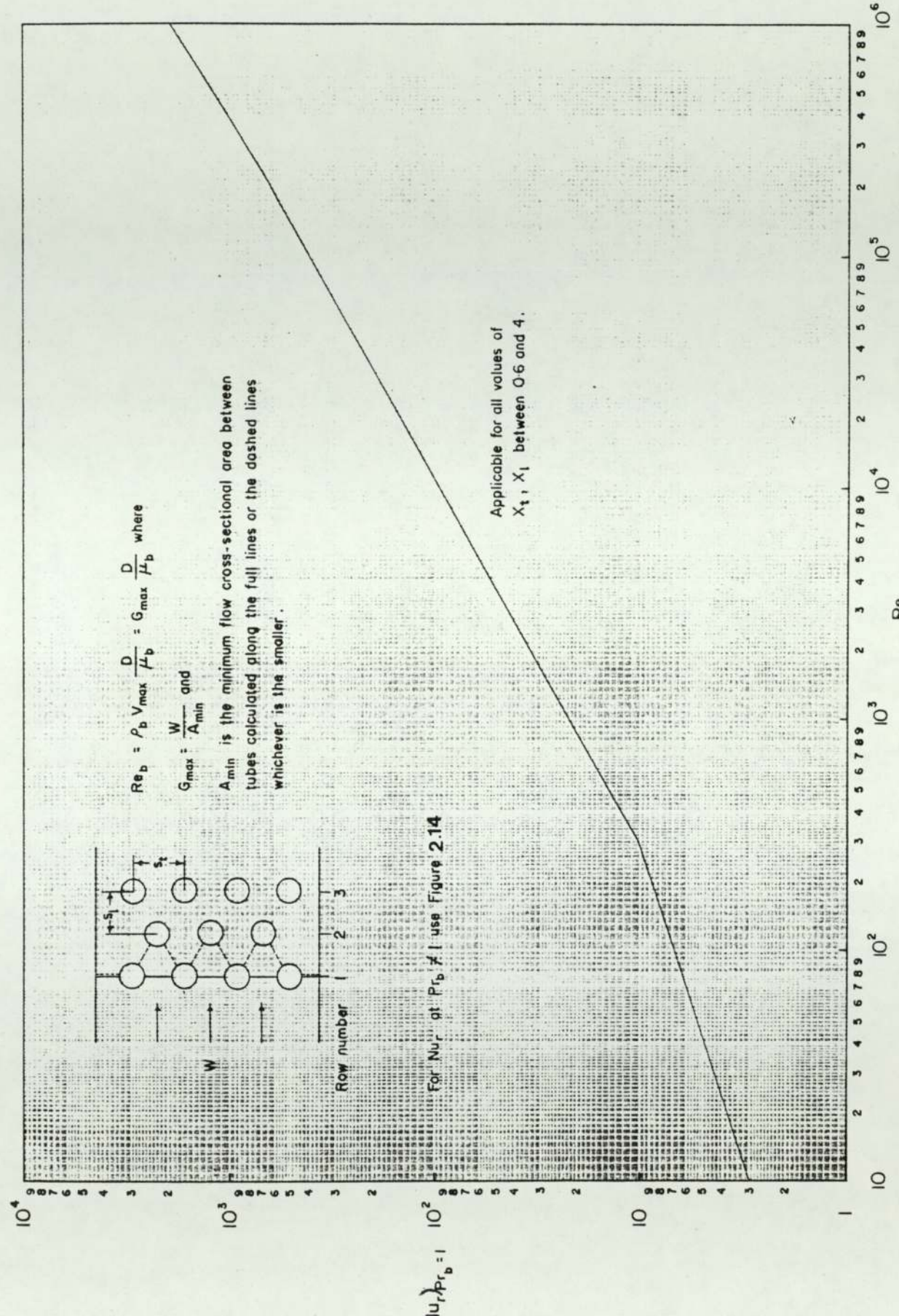

Fig. 2.14 Nusselt number for the reference conditions and $Pr_b = 1$. Staggered tube banks (ESDU [1973])

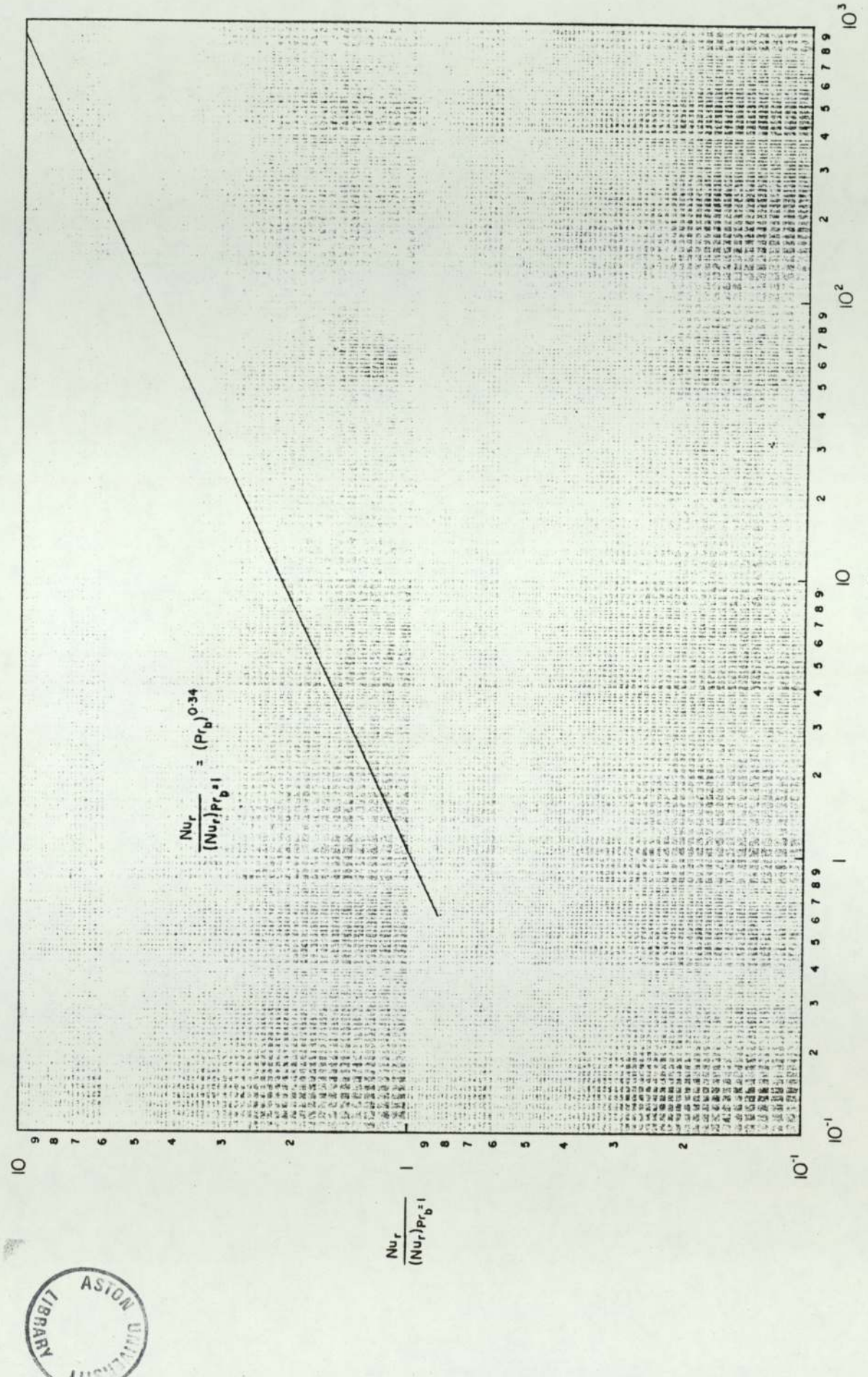

Fig. 2.15 Effect of Pr_b on values of $(Nu)_{Pr=1}$ for both in–line and staggered tube banks (ESDU [1973])

However, the agreement between corresponding data sets has been poor. This has been discussed in detail by Boucher and Lapple [1948]. They reviewed the data of seventeen different investigations.

Several definitions of friction factor, f, have been used in the correlation of pressure drop data for tube banks. Three of them, defined by Grimison [1937], Chilton and Genereaus [1933] and Kays et al. [1964], are set out in equations [2.30], [2.31] and [2.32] respectively.

$$f_G = \{\Delta P/N'\}\{g_c\rho/2G_{max}^2\} \qquad [2.30]$$

$$f_{CG} = \{\Delta P/NL\}\{g_c\rho/2G_{max}^2\}\{D_v/P_l\} \qquad [2.31]$$

$$f_{KL} = \{\Delta P/NL\}\{g_c\rho/2G_{max}^2\}\{D'_v/P_l\} \qquad [2.32]$$

Here g_c is a conversion factor required for non–coherent systems of units, traditionally called the gravitional constant, and is therefore equal to 1.0 for SI units, ρ is the density of the fluid, G_{max} is the maximum mass velocity which for in–line tube banks is based on the minimum cross–sectional area transverse to flow. For staggered tube banks, G_{max} is based on either the minimum area transverse to flow, or on the minimum flow area on the diagonals joining the centres of nearest neighbour tubes of adjacent transverse rows, depending on which flow area is the smallest.

In the definition of friction factor used by Grimison [1937], N' is the number of major restrictions encountered in the flow through the bank. For in–line banks and

staggered banks when G_{max} is based on the minimum transverse flow area, N' becomes equal to NL (the number of transverse rows). For staggered banks when G_{max} is based on the diagonal flow area, N' is equal to (NL – 1).

In the definition of friction factor presented by Kays and London [1964] and Chilton et al. [1933] D_v and D'_v are the volumetric equivalent diameter and modified volumetric equivalent diameter respectively which are defined as

$$D_v = \frac{4 \text{ x free volume in tube bank}}{\text{exposed suface area of tubes}} \qquad [2.33]$$

$$D'_v = \frac{4 \text{ x minimum area of flow x NL x } P_t}{\text{heat transfer area in exchanger}} \qquad [2.34]$$

Zukauskas [1972] recently correlated the pressure drop due to fluid friction for flow across tube bundles by

$$f_Z = \{\Delta P/N\}\{2\rho/G_{max}{}^2\}\{1/Z\} \qquad [2.35]$$

where f_Z = friction factor

N = number of tube rows in direction of flow

Z = correction factor for effects of tube bundle configuration (Z=1 for square and equilateral triangle tube arrangements)

Figures 2.16 and 2.17 show the friction factor, f, for an in–line arrangement with square tube array and a staggered arrangement with equilateral triangular tube array respectively. In these figures $X_T(=S_T/D)$, $X_L(=S_L/D)$, and $X_D(=S_D/D)$ denote, respectively, the dimensionless transverse pitch, longitudinal pitch, and diagonal pitch. The correction factor Z is plotted on the insert in these figures. For tube arrangements with $S_T \neq S_L$ or $S_T \neq S_D$, appropriate correction factors should be obtained from these figures and included in the pressure drop expression, equation [2.35].

More recently Butterworth [1979] evaluated the pressure drop in the simple form

$$\Delta P = \mu L V_s / K \qquad [2.36]$$

where V_s is the superficial velocity, K is the permeability and ΔP is the pressure drop over the depth L in the flow direction.

The equation [2.36] was derived from the following equation

$$V = -(K/\mu)(dP/dx) \qquad [2.37]$$

where μ is dynamic viscosity and x the distance in the flow direction.

The equation [2.37] was employed by Butterworth [1977 and 1978] while studying multidimensional shell–side flow, relating velocity to pressure gradient. He also used the term "flow conductivity" for K instead of permeability, since the

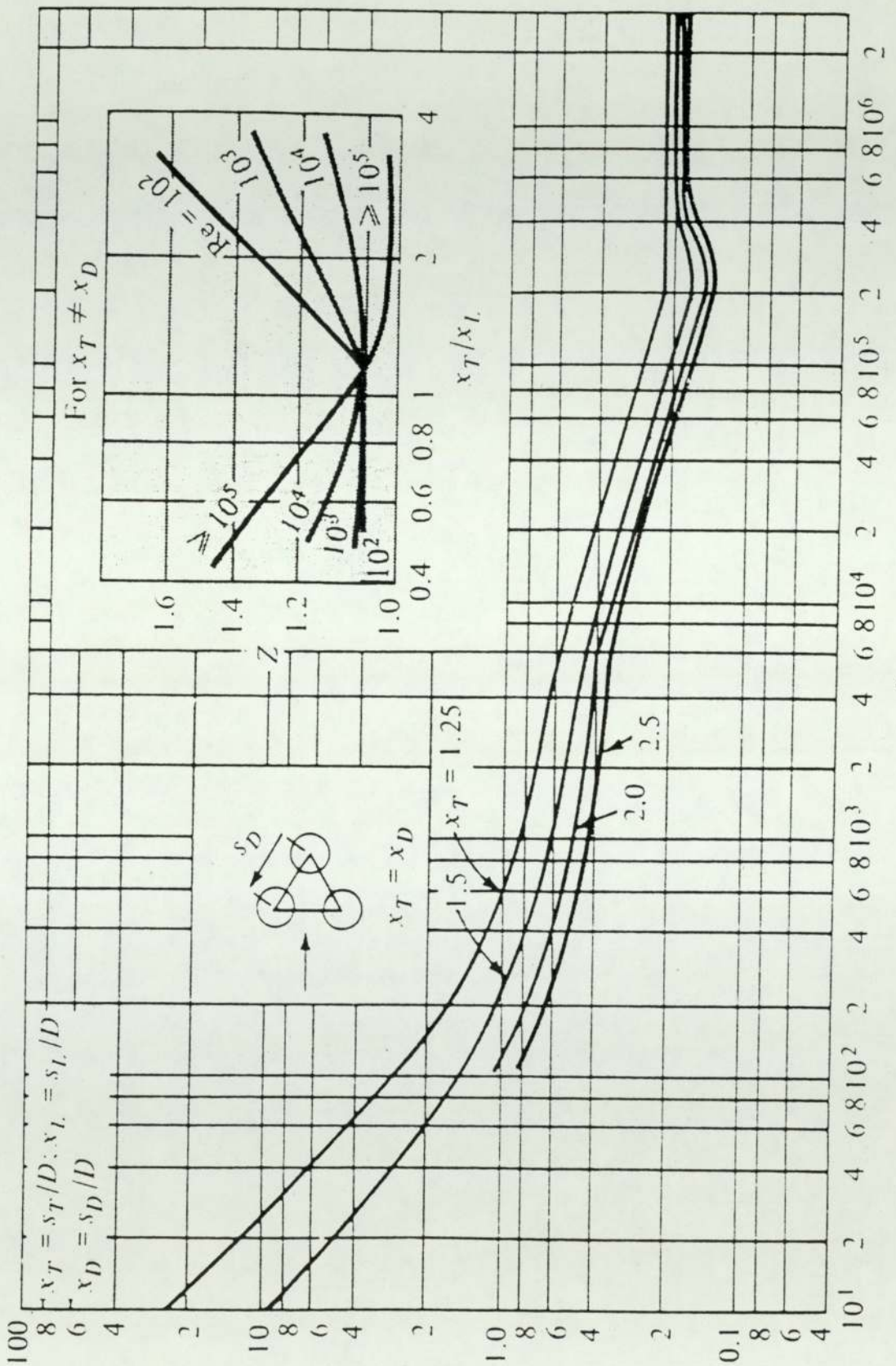

Fig. 2.16 Friction factor, f, and the correction factor, Z, for use in equation [2.35] for in–line tube arrangement (Whitaker [1972])

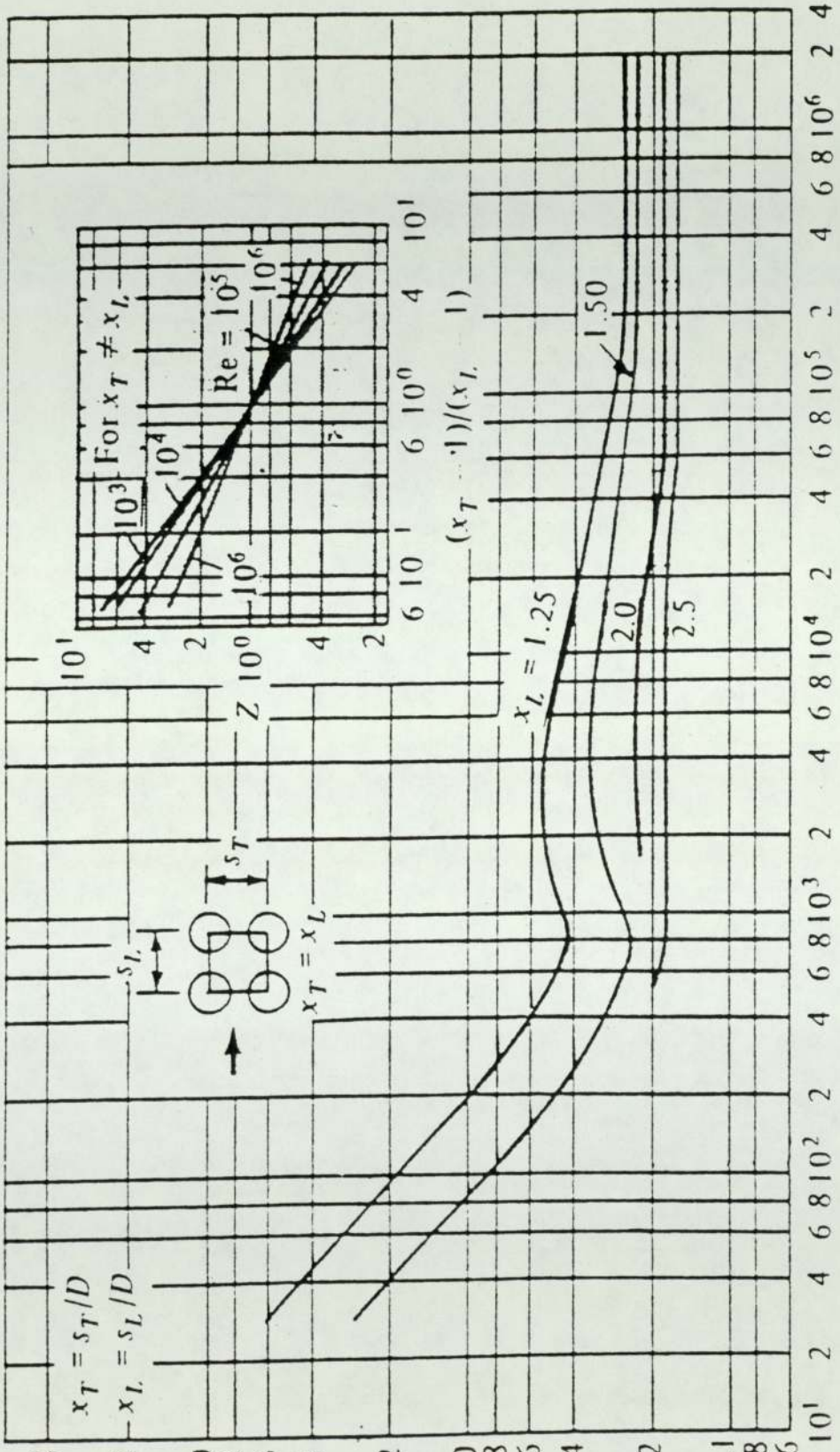

Fig. 2.17 Friction factor, f, and the correction factor, Z, for use in equation [2.35] for staggered tube arrangement (Whitaker [1972])

permeability is usually regarded as independent of V_S, whereas in practical shell–side flow problems K varies strongly with V_S. K is given by

$$\frac{1}{K^2} = \frac{1}{K_L{}^2} + \frac{1}{K_H{}^2} \qquad [2.38]$$

where K_L and K_H are flow conductivities at low and high flow (or Reynolds numbers) respectively. The values of K_L and K_H are obtained from the equations below.

For square or rotated square arrays

$$K_L = 4.23x10^{-3}DD_v{}^3/P^2 \qquad [2.39]$$

$$K_H = 8.19(P - D)^3Re^{-0.912}/D_v \qquad [2.40]$$

where D_v is tube volumetric equivalent diameter, i.e.

$$D_V = (4P^2 - \pi D^2)/\pi D \qquad [2.41]$$

For triangular or rotated triangular arrays

$$K_L = 6.8x10^{-3}DD_v{}^3/P^2 \qquad [2.42]$$

$$K_H = 1.11(P - D)^3 Re^{-0.733}/D_v \qquad [2.43]$$

$$D_v = (2x3^{0.5}P^2 - \pi D^2)/\pi D \qquad [2.44]$$

Many equations have been given for predicting friction factors for flow across banks of tubes, although some authors have preferred to give only a graphical presentation of results.

Chilton and Generaux [1933] recommended the following equation for laminar flow across banks of tubes,

$$f_{CG} = 26.5/Re_v \qquad [2.45]$$

where Re_v the is the Reynolds number based on the volumetric equivalent diameter D_v, i.e.

$$Re_v = \rho V D_v/\mu \qquad [2.46].$$

The following equations have proposed by Chilton et al. [1933] for turbulent flow across tube banks.

For in–line arrangements

$$f_G = 0.33Re_c^{-0.2} \qquad [2.47]$$

For staggered arrangements

$$f_G = 0.75 Re_c^{-0.2} \qquad [2.48]$$

where $$Re_c = G_{max} D_c / \mu \qquad [2.49],$$

and $D_c = (P_t - D)$ = the clearance between tubes in a transverse row.

In his classical paper Grimison [1937] attempted to correlate tha data of Huge [1937] and Pierson [1937] with considerable success. Friction factor plots were presented graphically at fixed values of Re in terms of the transverse and longitudinal pitch ratio S_t and S_l. Later Jakob [1938] reanalysed the data and obtained the following equations.

For in–line arrangements

$$f_G = Re^{-0.15} \left\{ 0.044 + \frac{0.08 S_l}{(S_t - 1)^{[0.43 + 1.13/S_l]}} \right\} \qquad [2.50]$$

For staggered arrangements

$$f_G = Re^{-0.16} \left\{ 0.25 + \frac{0.1175}{(S_t - 1)^{1.08}} \right\} \qquad [2.51]$$

For both arrangements 5000<Re<40 000.

The pressure drop ΔP for flow across a bank of N tube rows in the direction of flow can be calculated according to Jakob [1938] from

$$\Delta P = \{f_G G_{max}^2 N/2.09x10^8 \rho\}(\mu/\mu_w)^{0.14} \qquad [2.52]$$

Kays and London [1964] have correlated the staggered tube bank friction data of Kays, London and Lo [1954] by mean of the equation

$$f = C_f Re^{-0.18} \qquad [2.53]$$

where C_f is given as a function of S_t and S_l.

The correlation method used in this work was selected from among these approaches; the method chosen is that of Grimison [1937], this being the simplest in form and that used by Bergelin et al. [1952], since their model was virtually identical to the normal flow tube bank model used here, thus facilitating comparison of the two sets of experimental data. Measurement of friction factor data was not the thrust of this project but comparison demonstrates whether or not the flow situations are similar and thus whether or not the heat and mass transfer data can be compared.

2.7 MASS TRANSFER TECHNIQUE APPLICATIONS

The diffusion controlled electrochemical method has found successful application in a variety of convective heat and mass transfer investigations (Mizushina [1971] and Wragg [1977]). In the following sections a brief review of various mass transfer studies is given.

2.7.1 NATURAL CONVECTION

In natural convection studies, many geometries have been investigated. Wilke, Eisenberg and Tobias [1953] used the cathodic reduction of Cu^{++} ions to copper from acidic copper sulphate solutions for studying mass transfer by free convection to vertical plates. The results obtained were in the laminar regime (i.e. $3x10^6<GrSc<4x10^8$) and the correlating equation was

$$Sh = 0.677(GrSc)^{0.25} \qquad [2.54]$$

Equation [2.54] is in good agreement with the data obtained by Wagner [1949] using the same technique and also with data obtained by experiments on solid dissolution.

Fouad and Ibl [1960] extended the work on vertical plates into the turbulent region, again using the copper deposition technique, and correlated the data in the range $4x10^{13}<GrSc<10^{15}$ by the equation

$$Sh = 0.31(GrSc)^{0.28} \qquad [2.55]$$

Fenech and Tobias [1960] have correlated data obtained on horizontal plates in the range $10^3<GrSc<1.4x10^{13}$ by the equation

$$Sh = 0.19(GrSc)^{0.33} \qquad [2.56]$$

The limiting currents were measured in an unstirred cell at horizontal cathodes facing upward. Electrolyte compositions varied from 0.01 to 0.7M $CuSO_4$ in 1.5M H_2SO_4. The authors considered that their results showed the boundary layer to be turbulent, as in the analogous heat transfer mode.

Electrochemical free convection mass transfer experiments on single horizontal cylinders were reported by Schutz [1963] who was able to correlate his findings in the laminar region by the dimensionless equation

$$Sh = 0.53(GrSc)^{0.25} \qquad [2.57]$$

This equation is in exact agreement with established heat transfer correlations for single horizontal cylinders (McAdams [1954]) which may be expressed as

$$Nu = 0.53(GrPr)^{0.25} \qquad [2.58]$$

Equation [2.58] is valid in the range $10^3<GrPr<10^9$.

Fouad and Gouda [1964] studied natural convection conditions at vertical nickel electrodes by observations of the limiting current density of the cathodic process for electrodes of different heights using the ferro–ferricyanide redox system. In the range

$9x10^9<GrSc<4.57x10^{11}$ the results were correlated by the equation

$$Nu = 0.45(GrSc)^{0.25} \qquad [2.59],$$

and in the range $4.57x10^{11}<GrSc<10^{14}$ the data were represented by the relationship

$$Nu = 0.15(GrSc)^{0.29} \qquad [2.60]$$

Smith and Wragg [1974] studied free convection mass transfer at vertical arrays of horizontal cylinders. The limiting current was measured by the electrolysis of copper sulphate solution containing 1.5M sulphuric acid as swamping electrolyte. All single cylinder results were in good agreement with the results of Schutz [1963], the correlating equation for single cylinders was

$$Sh = 0.56(GrSc)^{0.25} \qquad [2.61]$$

2.7.2 FORCED CONVECTION

The electrochemical method has been used for both laminar and turbulent forced convection situations.

Lin, Denton, Gaskill and Putnam [1951] studied a number of redox systems in connection with mass transfer from a wall of an annulus to a liquid in laminar and turbulent flow. They found that the reduction of ferricyanide has the highest reaction rate constant. The Schmidt number was varied from 300 to 3000 and Reynolds number

from 260 to 30 000. The data in the laminar region (10^4<ReScD/L<10^6) were correlated by the equation:

$$Sh = 1.62(ReScD/L)^{0.33} \qquad [2.62]$$

In later work, Ross and Wragg [1965] investigated the effects of electrode length and annulus geometry. The electrochemical system used in this instance was cathodic deposition of copper from acidified copper sulphate solutions on to copper cathodes. The correlating equation for the laminar region was:

$$Sh = 1.76(ReScD/L)^{0.33} \qquad [2.63]$$

Equation [2.63] was later modified by Ross and Wragg [1968] in a recorrelation of the same data using improved values of diffusivity to

$$Sh = 1.94(ReScD/L)^{0.33} \qquad [2.64]$$

Hubbard and Lightfoot [1966] investigated flow in a rectangular channel using the diffusion–controlled reaction of potassium ferricyanide at a nickel cathode in the presence of a large excess of sodium hydroxide. Observations were made at Schmidt numbers from 1700 to 30 000 and Reynolds numbers from 7000 to 60 000 by varying temperature, caustic concentration and flow rate.

Mizushina [1971] used the same electrochemical reaction as Hubbard and Lightfoot and varied the Schmidt number between 3000 to 80 000. This work confirmed the finding of Hubbard et al. [1966] that Sherwood number varies with the

1/3 power of the Schmidt number and about the 0.9 power of the Reynolds number.

Hegge Zijnen [1958] measured heat transfer from horizontal wires and cylinder to air in the case of a vibrating wire and of wires and cylinders of various diameters in smooth and in turbulent air flows of known intensity and scale of tubulence. The Reynolds number range was from 60 to 25 800. Hegge Zijnen obtained the correlation by compiling the results of many investigators, mainly on heat transfer. He obtained the overall correlation

$$Sh = 0.38Sc^{0.2} + (0.56Re^{0.5} + 0.001Re)Sc^{0.33} \quad [2.65]$$

Equation [2.65] predicts $Sh/Sc^{1/3}$ values which are slightly higher than the data of Dobry and Finn [1956].

Grassman, Ibl and Trub [1961] compared their electrochemical data for transverse flow past a cylinder for the Reynolds number range between 120 to 12 000 and a Schmidt number of 2780, with correlations produced by various investigators utilising other techniques, with not very good agreement, their results were higher than those predicted by equation [2.65] (see below).

Vogtlander and Bakker [1963] concluded that gauzes and single wires behave in a similar manner. Their mass transfer data in the Reynolds number range between 5 and 100 were in good agreement with the correlation given by Hegge Zijnen [1958]. They accounted for the higher Grassman et al. [1961] results by observing that in that work the diameter of the test cylinder was large compared with the diameter of the tube it was mounted in, and consequently acceleration of flow took place past the test cylinder.

Mandelbaum and Bohm [1973] measured mass transfer cofficients for packed beds of Raschig rings at low Reynolds number in the range 0.0346 to 29.7. Mandelbaum recognised the existence of free convection at low Reynolds number and demonstrated that the dimensionless parameters which characterize the combined action of both forced and free convection are $Re/Gr^{1/2}$ and $Sh/(ScGr)^{1/4}$. They found that bouyancy forces play a significant role at lower than 0.1 for values of $Re/Gr^{1/2}$ for both aiding and opposing flow. Use of these observations is made below.

CHAPTER THREE

BACKGROUND OF WORK

In this chapter two aspects which are relevant to later discussion of the experimental results are considered. First, the flow patterns around single tubes and tube banks are discussed. Second, the differential equations governing flow and heat transfer, i.e. the continuity, momentum and energy equations are set out and the latest solution method of these equations for the fully–developed turbulent case considered in brief.

3.1 FLOW PATTERNS FOR FLOW AROUND SINGLE TUBES AND TUBE BANKS

Flow past a single tube in a bank of tubes may be compared to flow past a single cylinder in an infinite fluid. In this latter case a boundary layer forms on the forward portion of the cylinder and ultimately separates from its surface, producing, at high enough Reynolds number, a turbulent wake behind the cylinder. In Figure 3.1 (Knudsen and Katz [1958]) a cross–section of a cylinder with fluid flowing past it is shown.

The effect of turbulence on a typical flow pattern is indicated by the set of photographs in Figure 3.2 (Prandtl and Tietjens [1934]). These were taken at intervals after the initiation of transverse flow over a cylinder, that is, the initial velocity was zero.

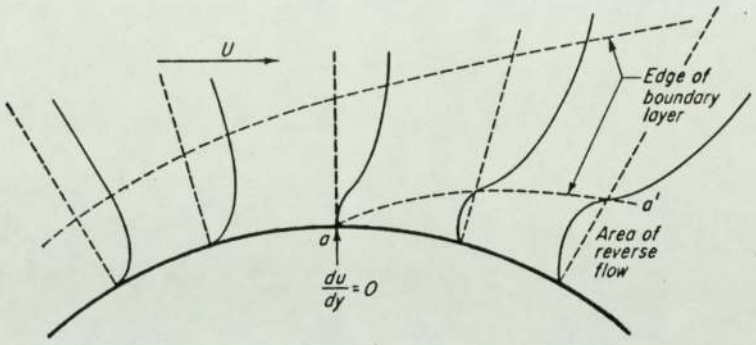

Fig. 3.1 Schematic sketch of a boundary layer on a circular cylinder (Knudsen and Katz [1958]

The types of flow that may occur are also illustrated in Figures 3.3 (a), (b) (Whitaker [1976]) for various ranges of the Reynolds number. The flow over the front half of the cylinder will be a boundary–layer type of flow, and may be handled by the standard boundary layer analysis. When the Reynolds number is large the flow over the rear of the cylinder is more complex.

However, the pattern of flow around a tube in a bank is much influenced by the presence of the surrounding tubes. In a contraction between adjacent tubes of a transverse row, the pressure gradient changes, and this causes a corresponding change of thickness and velocity distribution in the boundary layer and of the flow pattern to the rear of the tube.

The two most common tube–bank arrangements are the staggered and in–line arrangements, both can be described through the relative transverse spacing, $S_l = P_l/D$, and the longitudinal, $S_t = P_t/D$ (see Fig. 2.2).

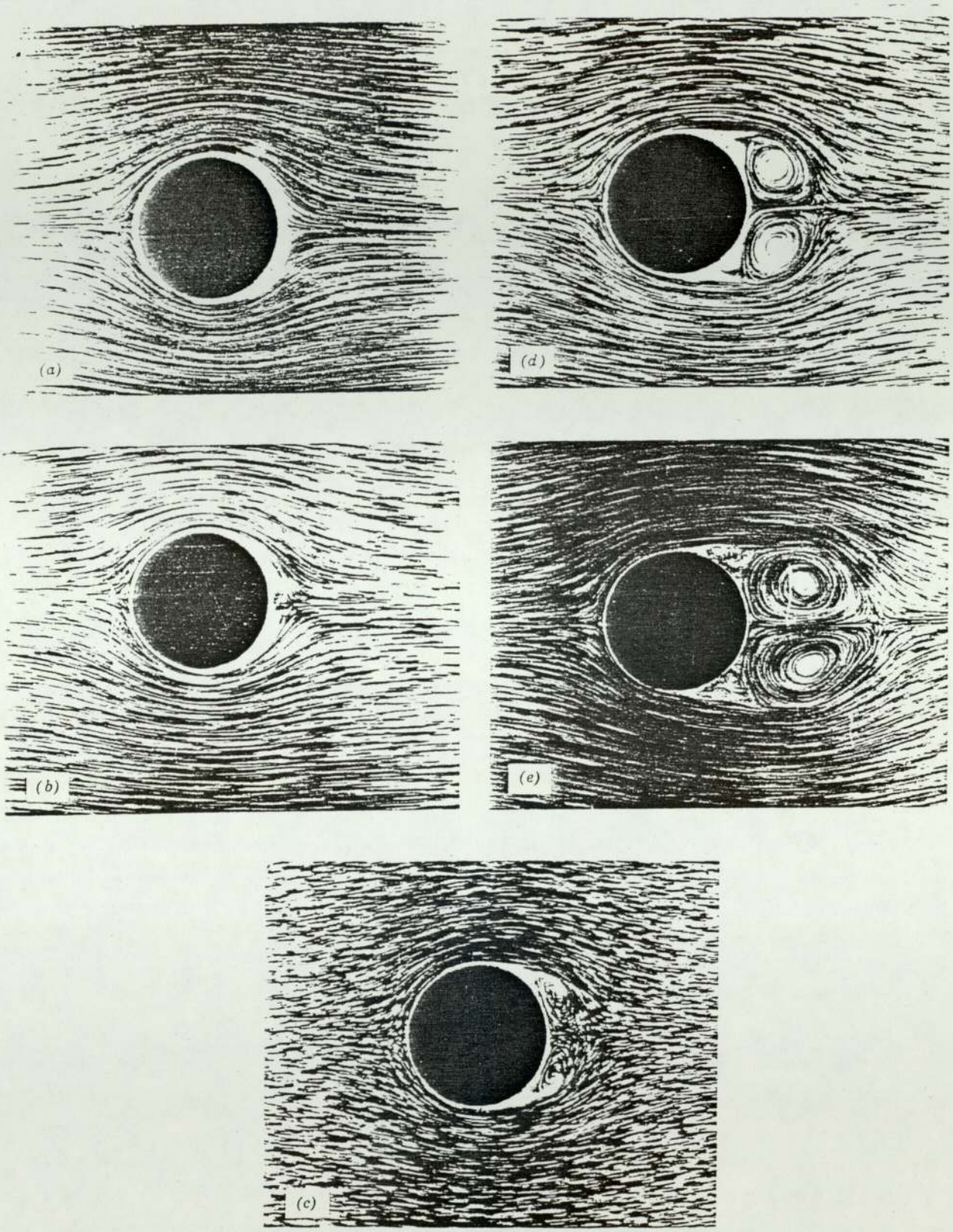

Fig. 3.2 Flow patterns showing the development of turbulence at a series of five intervals of time after the initiation of flow across a circular cylinder. The first picture was taken just as the flow began, the last after fully developed turbulent flow was estalished (Prandtl and Tietjens [1934])

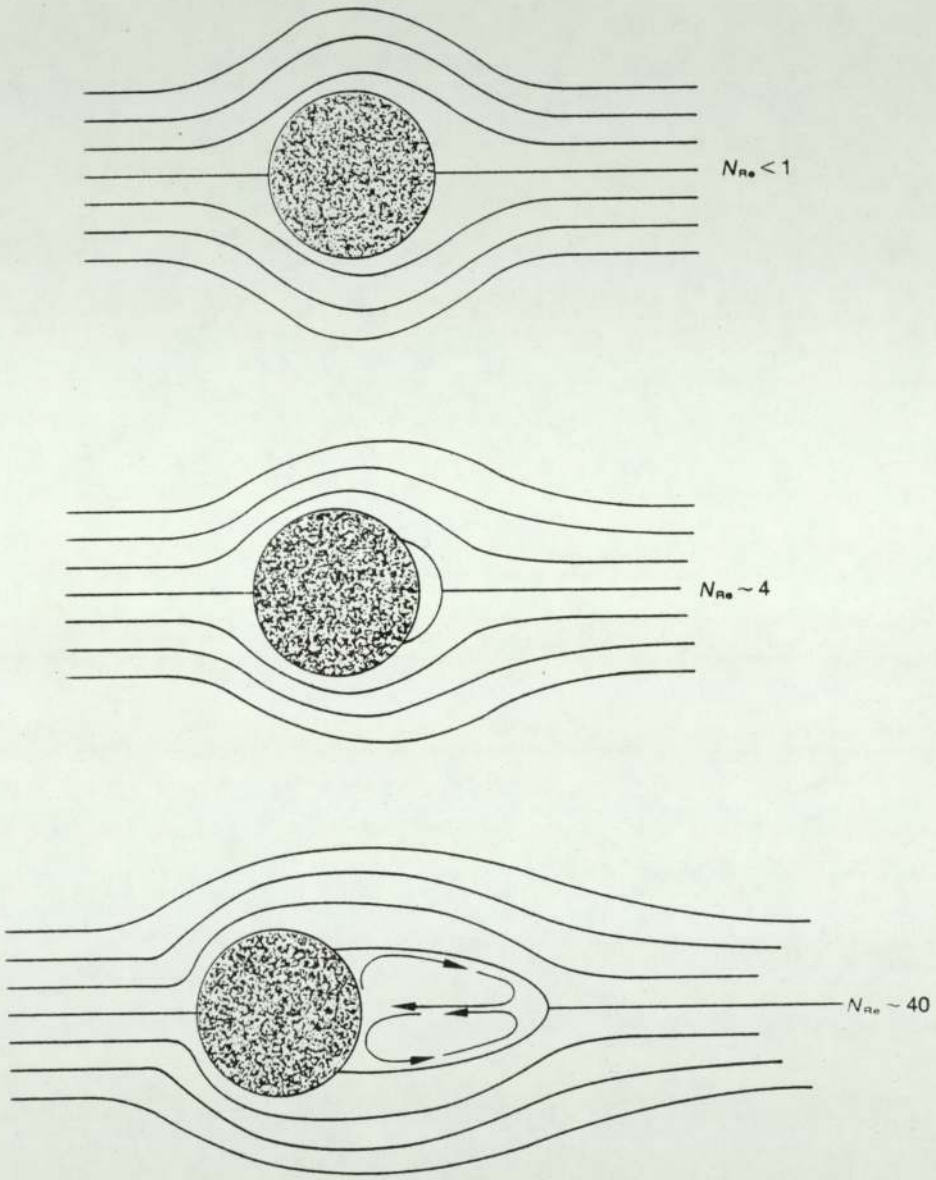

Fig. 3.3a Flow field around a cylinder (Whitaker [1976])

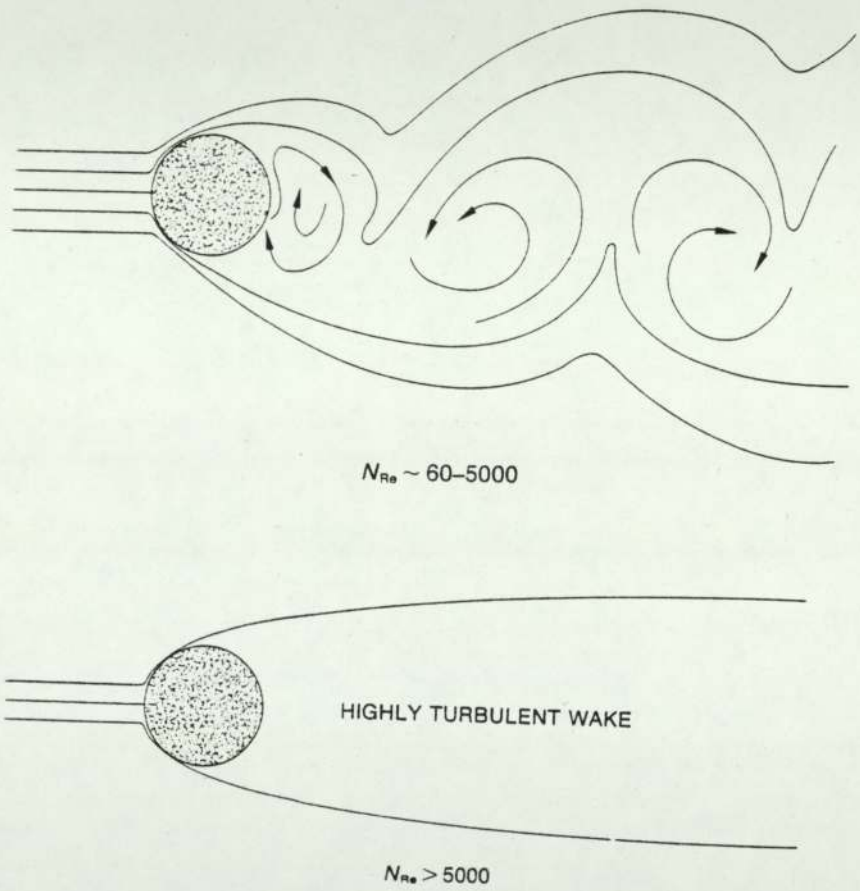

Fig. 3.3b Flow field around a cylinder (Whitaker [1976])

In banks of both arrangements, flow around a tube in the first row is similar to the flow around a single tube, but the flow pattern in subsequent rows is different (Zukauskas [1972]).

Wallis [1934] studied visually the flow of fluids perpendicular to tube banks by observing the motion of fine aluminum powder placed on the surface of water flowing perpendicular to the tubes. The axes of the tubes were vertical. After a number of trials, Wallis was able to obtain some good photographs of the patterns which occured as the water flowed through the tube bank.

He studied four different in–line tube arrangements with the transverse P/D ratio range from 1.5 to 2.0 and longitudinal P/D ratio range from 1.8 to 3.4, and three different staggered arrangements with P/D ratio from 1.5 to 2.6 and from 1.0 to 1.3 for the transverse pitch and the longitudinal pitch respectively. He also studied one staggered arrangement in which the tubes were elliptical in section with 2.0 and 2.1 transverse and longitudinal pitch ratio.

In Figure 3.4 (a), (b), (c), and (d) the flow patterns observed by Wallis are shown for the staggered tube arrangements which are relevant to this work. When the tubes are widely spaced, a turbulent wake occurs behind each tube and extends nearly up to the next tube, which is two transverse rows away. However, a boundary layer is formed on the forward part of each tube in the bundle, and separation of this boundary layer takes place. For the closely spaced staggered arrangements the turbulent wake behind each tube is considerably reduced. With these spacings the tubes are placed so that they are not in the turbulent wake of the tubes immediately upstream, with the result that energy dissipation is likely to be reduced. The only place where there is a large

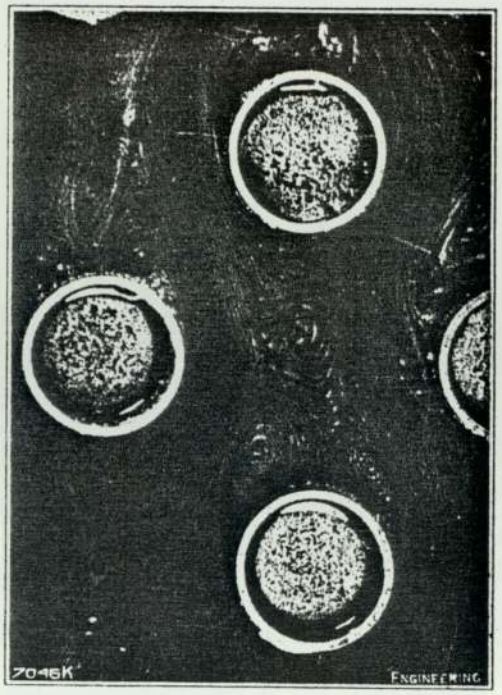

Fig. 3.4a Flow Through Widely Spaced Staggered Nest
2.6 Diameters by 1.3 Diameters

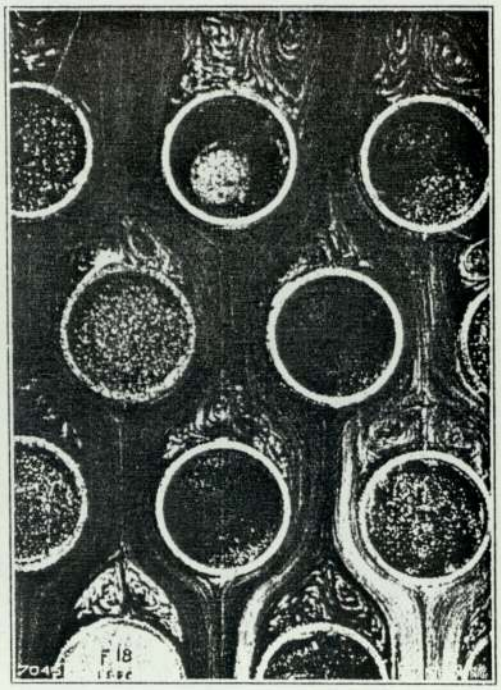

Fig 3.4b Staggered Nest with Reduced Transverse Pitch
1.5 Diameters by 1.3 Diameters

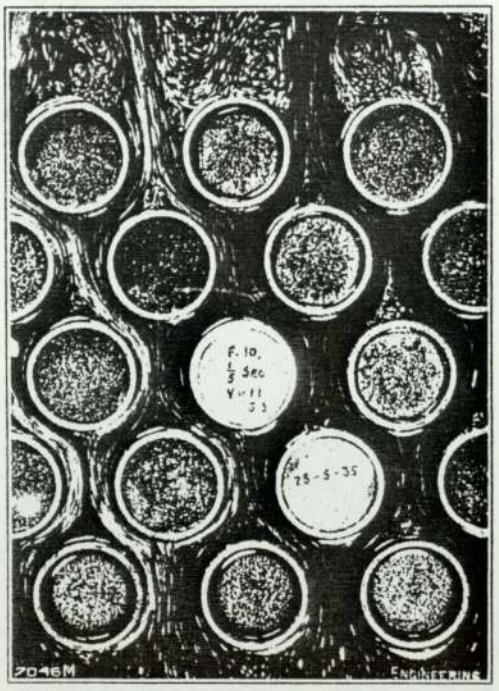

Fig 3.4c Effect of Close Longitudinal Pitching
1.5 Diameters by 1.0 Diameter.

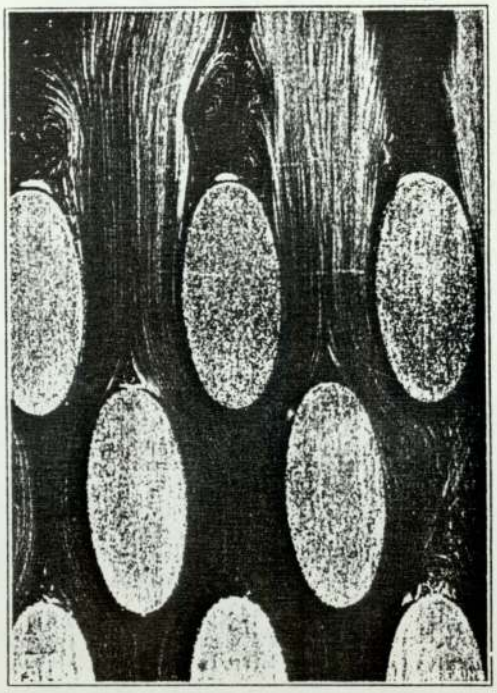

Fig 3.4d Elliptical Tubes. (Wallis [1934])

turbulent wake is behind the last transverse row of tubes.

The variations in flow can be related to the row–by–row variation in transfer coefficients obtained in both previous work on tube banks and in this work, and this point is returned to below.

3.2 THE EQUATIONS OF CONSERVATION

As already noted, in designing a shell–and–tube heat exchanger two important factors upon which a designer needs to have accurate information are heat transfer coefficients and friction factors for both the inside and outside of the tubes.

One way of providing the information required is to build a scale model of the tube bank under consideration, and to determine experimentally correlations of the variation of heat transfer coefficients and friction factors with Reynolds number.

The alternative to experimental measurement is to develop a theoretical model for predicting the information the designer requires. In order to perform these tasks the theoretical method will have to solve the equations governing mass, momentum and heat transfer.

The flow of fluid and the transfer of heat within a tube bank or around a cylinder are all governed by certain basically simple laws. These laws are the conservation of mass, momentum and energy, and can be expressed mathematically as partial differential equations.

These equations are then solved within the flow domain under consideration, which is usually either the area around a single cylinder or the area occupied by fluid within the symmetry unit of a tube bank (Fig. 3.5).

In the following section the mass, momentum and energy equations and their solutions are described in brief.

3.2.1 THE CONTINUITY EQUATION FOR THREE DIMENSIONAL FLOW

The continuity equation is the mathematical expression of the law of conservation of mass. This equation is developed by writing a mass balance over a cubical element of space having dimensions dx, dy, dz through which the fluid is flowing. The equation is usually written as

$$\nabla.\rho\mathbf{V} = -\partial\rho/\partial t \qquad [3.1]$$

in which $\nabla.\rho\mathbf{V}$ is the divergence of $\rho\mathbf{V}$, and the operator $\nabla = \partial/\partial x + \partial/\partial y + \partial/\partial z$. Equation [3.1] is the general continuity equation for three–dimensional flow. It is a mathematical expression of the law of conservation of mass and involves no assumptions; it describes the rate of change of density at a fixed point resulting from the changes in the mass velocity vector $\rho\mathbf{V}$. For the steady–state flow of an incompressible fluid the density is constant, and the continuity equation becomes

$$\nabla.\mathbf{V} = 0 \qquad [3.2]$$

3.3.2 THE MOMENTUM EQUATIONS, THE NAVIER–STOKES EQUATION

Every particle of fluid at rest or in steady or accelerated motion obeys Newton's second of motion, which states that the time rate of change of momentum is equal to the external forces.

The momentum equations for fluid flow are a mathematical expression of Newton's second law applied to moving masses of fluid. The derivation of the equations involves determining the inertial force of the flowing fluid in each coordinate direction and equating it to external forces acting on the fluid. The three main external forces which may act on the fluid are field forces (gravity forces), normal forces (pressure), and shear or tangential forces (caused by the resistance of the fluid to deformation).

By writing the momentum balance over a volume element dxdydz, the general equation of motion is obtained. The Navier–Stokes equation is a combination of the simple form of the momentum equation with constant ρ and μ, and the equation of continuity $\nabla.\mathbf{V} = 0$.

$$\rho\left(\frac{\partial V}{\partial t} + V_x\frac{\partial V}{\partial x} + V_y\frac{\partial V}{\partial y} + V_z\frac{\partial V}{\partial z}\right) = -\nabla P + \mu\nabla^2\mathbf{V} + \rho g \quad [3.3]$$

where the operator ∇^2 is the Laplacian operator, P is the pressure of fluid, and g is the gravity vector.

3.2.3 THE ENERGY EQUATION FOR THREE–DIMENSIONAL FLOW

When flow is nonisothermal, the temperature of the fluid is a dependent variable which is a function of x, y, z, and t. Just as the continuity equation is a mathematical expression of the law of conservation of mass and gives the velocity distribution in space, the energy equation is a mathematical expression for the law of conservation of energy and gives the temperature distribution in space.

The energy equation, in the absence of heat sources and ignoring radiation effects, is

$$\rho C_p(\partial T/\partial t + V.\nabla T) = k\nabla^2 T \qquad [3.4]$$

3.2.4 SOLUTION OF THE CONSERVATION EQUATIONS

As mentioned before, the flow pattern and the thermal map of a shell–and–tube heat exchanger may be obtained either through actual testing of a scale model or by using an analytical prediction method. With the advent of powerful digital computers and advances in the development of computational fluid mechanics, it has become possible to solve the conservation equations of mass, momentum, and energy for both the shell–side and tube–side fluids numerically.

For laminar flow the time–dependent equations of conservation can be solved numerically using existing numerical techniques without major difficulty. But it is the usual practice for turbulent flows to work with the time–averaged equations of conservation. The equations of conservation in the time–averaged form for constant

density are expressed as (Hinze [1959]).

$$\partial/\partial x_i(\rho V_j) = 0 \qquad [3.5]$$

$$\partial/\partial x_j(\rho V_j V_i) = \partial/\partial x_i[-\overline{\rho v_i' v_j'} - P\gamma_{ij} + \mu(\partial V_i/\partial x_j + \partial V_j/\partial x_i - e_{ij}\gamma_{ij})] \qquad [3.6]$$

$$\partial/\partial x_j(\rho V_j h) = \partial/\partial x_j(-\overline{\rho v_j' h'} + \partial T/\partial x_j) \qquad [3.7]$$

where V_i, V_j = instantaneous velocity in the direction x_i, x_j respectively,

P = local pressure,

h = total specific enthalpy,

T = local temperature,

$e_{ij} = \partial V_i/\partial x_j + \partial V_j/\partial x_i$ = rate of strain tensor,

γ_{ij} = Kronecker delta,

ρ = fluid density,

μ = fluid viscosity,

K = thermal conductivity, and the overbars indicating mean values have been omitted for all variables for simplicity.

The Reynolds stresses $\overline{\rho v_i' v_j'}$ and the turbulent heat flux $\overline{\rho v_j' h'}$, which represent the transfer of momentum and energy by the turbulent motion appear in the time–averaged equations of momentum and energy. Because of the introduction of these

unknowns, additional equations, comprising a "turbulence model", are required to enable the closure of the equation set. A survey of the turbulence models as well as a description of an appropriate model (k-ε tubulence model Launder and Spalding [1972]) is given by Antonopoulos [1985].

Antonopoulos [1984 and 1985] in his publications presented the heat transfer and hydrodynamic aspects of a computational study concerning turbulent flow and heat transfer in banks of tubes. His paper [1985] is concerned with the prediction of heat transfer in banks of tubes under conditions of turbulent fully–developed flow inclined to the axes of the tubes, including the limiting cases of purely axial and purely transverse flow.

One of the novel points in his method is that the differential equations governing flow and heat transfer, i.e. the continuity, momentum and energy equations, were expressed in terms of general curvilinear–orthogonal coordinates ζ, η in the passage cross–section and a rectilinear coordinate ξ in the axial direction, as shown in Figure 3.6. The solution method is a finite–difference one. The effects of tubulence were simulated by the "k-ε turbulence model" (Launder et al. [1972]) noted above. This formulation allows any selected solution domain, as for example those shown in the cross–sectional view of Figure 3.5 or in the enlarged isometric view of Figure 3.6, to be mapped by grids which conform to its shape. A typical curvilinear–orthogonal grid, which is computer–generated (Antonopoulos [1979]) by a numerical procedure described in Antonopoulos [1979], is shown in Figure 3.7. This grid arrangement possesses the advantages that grid lines are aligned with the flow thus reducing

numerical diffusion and that all boundaries of the solution domain are grid lines, so that imposition of the boundary conditions is straightforward and accurate.

The relevance of Antonopoulos's work to this study is clear, but any detailed description of his techniques, equations and numerical methods is outside the scope of this thesis. Close study of his plots shows that his results are for Reynolds numbers well above the values reached in this work, therefore direct comparison is not possible. However, the plots of heat transfer and fluid flow show that his results are asymptotic to pure cross flow results and to pure axial results and these facts are used as guidance in the data correlation described below.

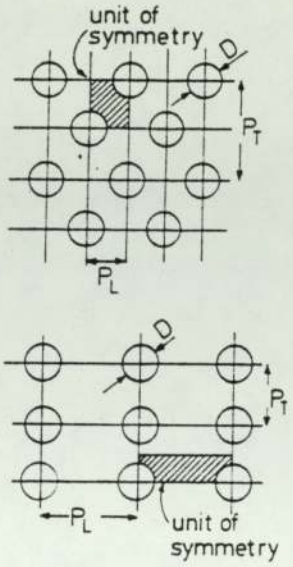

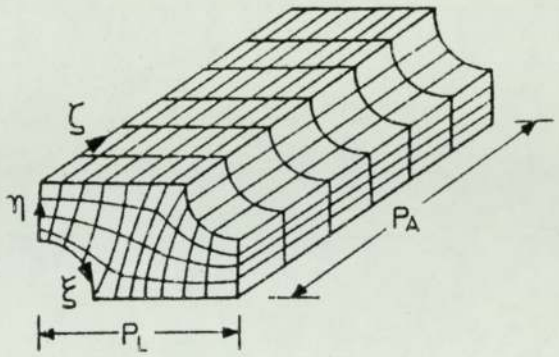

Fig. 3.6 Typical solution domain mapped with curvilinear–orthogonal computational mesh (Antonopoulos [1985])

Fig. 3.5 Unit of symmetry (solution domain) of staggered and in–line tube banks in cross–sectional view (Antonopoulos [1985])

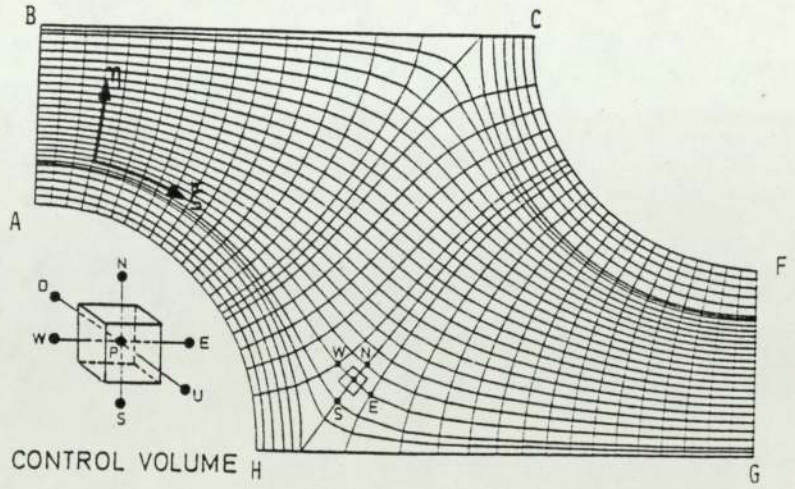

Fig. 3.7 Typical computational mesh (cross–sectional view) with indication of control volume (Antonopoulos [1985])

CHAPTER FOUR

THE ANALOGY BETWEEN HEAT AND MASS TRANSFER

4.1 INTRODUCTION

The analogies between momentum, heat and mass transfer have been the concern of many investigators, whose objective was to derive expressions for heat and mass transfer coefficients using fluid friction data and to calculate heat transfer coefficients from experimental data on mass transfer, and vice versa. The differential equations governing convective heat, mass and momentum transfer in steady flow and in the absence of chemical reaction and internal generation of heat, simplify in their vector form to

for heat transfer $$V\nabla T = k/\rho C_p \nabla^2 T \qquad [4.1]$$

for mass transfer $$V\nabla C = D_v \nabla^2 C \qquad [4.2]$$

for momentum transfer $$V\nabla V = \eta \nabla^2 V \qquad [4.3]$$

where $k/\rho C_p$, D_v and η are heat, mass and momentum diffusivities respectively.

From the solution of equation [4.1] and [4.2] under dynamically similar conditions, various forms of heat and mass analogy have been proposed. Since their complete analytical solution is generally impossible, the analogies so formed are of semi–empirical form.

One such semi–empirical analogy, which Mackley [1973], Prowse [1977], and Nibber [1981] have chosen for their work, and is retained for the present work, was proposed by Chilton and Colburn [1934].

4.2 THE CHILTON–COLBURN ANALOGY

The analogy between the two transport phenomena (i.e heat and momentum transfer) in a turbulent fluid was first proposed by Reynolds [1874]. Reynolds ignored the existence of the laminar sub–layer close to the surface and assumed that the fluid was turbulent right up to the solid surface. Under such conditions the following relationship holds

$$St = \frac{h}{\rho V C_p} = \frac{\tau}{\rho V^2} \qquad [4.4]$$

This expression is only valid when the Prandtl number of the fluid is close to unity.

By assuming the existence of a laminar sub–layer, Taylor [1916] and Prandtl [1928] did further theoretical work on the relationship and modified the simple Reynolds analogy. In their treatment they assumed that the simple Reynolds analogy was applicable to the transfer of heat and momentum from the main stream to the edge of the laminar sub–layer. In this region outside the laminar sub–layer, molecular diffusion processes were assumed to be negligible and the turbulent eddy diffusivities for momentum and heat were assumed to be of equal magnitude. Transfer through the laminar sub–layer was then presumed to be attributable solely to molecular diffusion in

the complete absence of eddy diffusion. Taylor and Prandtl both modified equation [4.4] to give

$$St = \frac{h}{\rho V C_p} = \frac{\tau}{\rho V^2} / [1 + \alpha(Pr - 1)] \qquad [4.5]$$

The quantity α is the ratio of the velocity of the edge of the laminar sub–layer to the stream velocity. For the case of Pr=1, the relationship simplifies to the Reynolds analogy.

Sherwood [1940] developed a corresponding expression for the analogy between mass and momentum transfer, as given below

$$\frac{K_m}{V} = \frac{\tau}{\rho V^2} / [1 + \alpha(Sc - 1)] \qquad [4.6]$$

These expressions are derived by making the assumption that there is an abrupt transition from turbulent to laminar flow at the boundary of the laminar sub–layer. This neglects the existence of an intermediate buffer zone.

The terms $[1 + \alpha(Pr - 1)]$ in equation [4.5] and $[1 + \alpha(Sc - 1)]$ in equation [4.6] are correction factors, which have been introduced into the simple Reynolds analogy. However, the correction factor approaches unity under certain conditions and the Reynolds analogy is closely followed. These conditions are as follows.

1) For systems for which the Prandtl and Schmidt numbers are approximately equal, the

correction factors for heat and mass transfer are approximately equal and the simple Reynolds analogy will be followed closely. Also, for gases Prandtl and Schmidt numbers are approximately unity and hence the correction factors are unity.

2) Under highly turbulent conditions, the laminar sub–layer is extremely thin and the velocity of the edge of the laminar sub–layer will be small. In these conditions, the quantity, α, will be effectively zero and the correction factor will again be unity.

For turbulent flow in pipes, Colburn [1933] found that heat transfer data when correlated in terms of j–factors, showed approximately the same characteristics as a friction factor correlation. He represented the heat–momentum relationship by the expression

$$j_h = \frac{h}{\rho V C_p} Pr^{0.67} = \frac{\tau}{\rho V^2} = 0.023 Re^{-0.2} \qquad [4.7]$$

or

$$j_h = (Nu/RePr)Pr^{0.67} = 0.023 Re^{-0.2} \qquad [4.8]$$

or

$$Nu/Pr^{0.33} = 0.023 Re^{0.8} \qquad [4.9]$$

Comparing equation [4.7] with that of the Prandtl–Taylor analogy shows that $Pr^{0.67}$ replaces the term $[1 + \alpha(Pr - 1)]$ as the correction factor in the Reynolds analogy.

Later, Chilton and Colburn [1934] extended the above principle to the analogy between heat and mass transfer by defining a mass transfer j–factor, j_m, as

$$j_m = \frac{k_m}{V} Sc^{0.67} = 0.023Re^{-0.17} \qquad [4.10]$$

or $$j_m = (Sh/ReSc)Sc^{0.67} = 0.023Re^{-0.17} \qquad [4.11]$$

or $$Sh/Sc^{0.33} = 0.023Re^{0.83} \qquad [4.12]$$

By comparing equation [4.7] and [4.10]:

$$j_m = \frac{k_m}{V} Sc^{0.67} = j_h \qquad [4.13]$$

Chilton et al. showed from experimental data that this empirical analogy applied not only for turbulent flow in pipes, but also for flow across tubes and across plane surfaces.

In recent years, this analogy has been successfully applied to flow across gauzes by Vogtlander et al. [1963], across tube banks by Mackley [1973], and in furnace ducts by Lucas [1971] and Lucas et al. [1975]. One of the striking examples of the analogy working well is that described by Tagg, Patrick and Wragg [1979]. These workers by using the Chilton–Colburn analogy found that the data for peak mass transfer rate at the wall downstream of a sudden enlargement were shown to be correlated together with independently–obtained heat transfer data by the equation

$$Sh/Sc^{0.33} = 0.27Re^{0.67} \qquad [4.14]$$

Both dynamic similarity and similarity of boundary conditions are required by the analogy. The use of the Reynolds number fulfils the first condition. The second condition implies that the type of boundary condition is the same in both cases. In the redox electrochemical technique, the boundary condition is essentially one of constant composition at the wall, analogous to a constant wall temperature in the heat transfer case. However, Lucas [1970] in his studies of rapid heating furnaces, showed that the analogy still held for the case of a uniform heat flux system being modelled by such an electrochemical method, a comparison being made between an electrically–heated model and the two mass transfer techniques employed.

After 1945 the number of theoretical studies of turbulent heat and momentum transfer increased rapidly. Some notable investigations are those of Seban et al. [1951] and Lyon [1951].

The exponent on the property number in equation [4.7] and [4.13] has been verified by Jenkins et al. [1976] to be 0.67 for an adequate description of mass and heat transfer processes.

CHAPTER FIVE

THE ELECTROCHEMICAL MASS TRANSFER TECHNIQUE

5.1 INTRODUCTION

A mass transfer system was used as early as 1921 by Thoma to model heat transfer from rectangular tube banks. An ammonia–air mixture was passed over tube banks fabricated from filter paper and soaked in a known quantity of phosphoric acid. The amount of ammonia absorbed was determined by titration and, since the ammonia concentration at the tube surface was effectively zero, the transfer coefficient could be calculated.

The electrochemical method of modelling mass transfer between a liquid and a solid surface by measuring the transfer rate of certain ions in aqueous solutions to an electrode has been developed during the past 30 years. The measured quantity is the electrical current produced by the transfer of certain reacting ions to electrodes forming part of the surface being studied. Various systems have been suggested, but the one most frequently applied in practice is an aqueous solution of the redox couple potassium ferri– and ferrocyanide with an added non–reacting electrolyte, usually sodium hydroxide. This technique has been widely used and is the technique chosen for this work.

The diffusion–controlled electrode reaction was recognised as a powerful tool

to study transport phenomena in liquids after the work of Levich [1947] and Agar [1947]. This was followed by a systematic study of the transfer rate of ions and other reacting species in electrochemical reactions by Lin et al. [1951], who measured the transfer rate for several kinds of mixtures and determined mass transfer coefficients in both laminar and turbulent flow. Since then the diffusion controlled electrochemical technique has been utilised in a variety of convective heat and mass transfer studies.

Wragg [1977] reviewed the basic principles of the limiting diffusion current technique and illustrated its application in many areas of chemical engineering; 139 literature references were cited. A comprehensive review of many applications has been published by Mizushina [1971], together with the use of well–known analogies between the various transport phenomena. The technique was applied to the study of flow in pipes by Shaw et al. [1963], Grassman et al. [1961], Hubbard et al. [1966] and Berger et al. [1983], pipe flow at abrupt expansions by Costello [1969], Tagg et al. [1979], flow in annuli by Lin et al. [1951], Bazan et al. [1964], Ross and Wragg [1965], flow over cylinders by Dobry et al. [1956], Grassman et al. [1961] and Vogtlander et al. [1963], flow through packed and fluidised beds by King et al. [1967], Hicks et al. [1968] and Jolls et al. [1969], mass transfer in semi–cylindrical hollows by Aggarwal and Talbot [1978], mass transfer in fluidized bed by Walker and Wragg [1980], simulation of heat transfer in a partially blocked nine pin sub–channel by Patrick et al. [1984], and modelling of free convection in heat transfer by Patrick and Wragg [1985].

Mackley [1973] developed the technique for the study of heat transfer on the shell–side of shell and tube heat exchangers, employing the Chilton–Colburn analogy. The technique has also been used by Prowse [1977] and Nibber [1981] to measure heat transfer in shell–and–tube heat exchangers.

5.2 THE POTASSIUM FERRI–FERROCYANIDE SYSTEM

The electrochemical system used in the experiments was the well known aqueous solution of potassium ferri– and ferrocyanide. The solution consisted of equimolar concentrations of potassium ferri– and ferrocyanides with a large excess of sodium hydroxide as the inert electrolyte.

The electrolyte flows past the nickel surface under investigation, which was connected to the negative pole of a direct current power supply and hence became the cathode. Another nickel electrode, connected as an anode to the positive terminal of the power supply, was also installed in the flow circuit. The precise shape of the anode was not important, as long as its surface area was bigger than that of the cathode. Initially it was thought that the precise location of the anode was not important. In practice it was found that at low Reynolds number the location of the anode was indeed not significant but at high Reynolds number, obtaining the limiting current was not easy and this difficulty may have reduced the accuracy of the experimental results. This problem was solved during the second set of experiments by putting the anodes as close as possible to the cathodes. This made it easier to obtain good plateaux in the current versus applied potential plots at high Reynolds number.

The principal electrochemical reactions of this redox system are

	Standard Electrode Potential	
$Fe(CN)_6^{3-} + e \longrightarrow Fe(CN)_6^{4-}$	0.356V	[5.9]

Ferricyanide reduction at the cathode

$$Fe(CN)_6^{4-} \longrightarrow Fe(CN)_6^{3-} + e \qquad 0.356V \qquad [5.10]$$

Ferrocyanide oxidation at the anode

Because the reaction at the cathode is the reverse of the anode reaction, the current passing between the anode and cathode through the medium does not change the overall concentration of the solution.

Two other reactions are feasible

Standard Electrode Potential

$$2H^+ + 2e \longrightarrow H_2 \qquad 0.00V \qquad [5.11]$$

at the cathode

$$2OH^- \longrightarrow H_2O + 1/2\,O_2 + 2e \qquad 0.401V \qquad [5.12]$$

at the anode

Which reaction occurs depends in part on the equilibrium electrode potential, and on the value of the applied potential and this has to be increased above the equilibrium electrode potential to cause the reaction to proceed.

5.3 THEORY OF THE ELECTROCHEMICAL TECHNIQUE

It has been known for many years that, under certain circumstances, the current passing through an electrolytic cell is independent of the applied voltage, but is a

function of the mass transfer rates, (see Wagner [1949] and Einsenberg et al. [1953]). This situation is represented by the extreme right hand portion of the curve in Figure 5.1. Then it is possible to measure mass transfer coefficients by measuring current, as pointed out by Ibl [1955]. For this purpose a mixture of two electrolytes is used (Wagner [1949] and Eisenberg et al. [1953]): one, providing the active anions or cations, is in low concentration and its anions and cations together have a low potential of discharge, the other, sometimes called the indifferent or supporting electrolyte, is present in high concentration and its anions and cations together have a higher potential of discharge. When an electrical potential, lying between the upper and lower potentials of discharge, is applied between two electrodes in aqueous solution, the anions and cations of the supporting electrolyte can not be discharged at the electrodes. Therefore they do not contribute to the Faradaic current. Instead a reduction of the active electrolyte ions occurs at the cathode and an oxidation at the anode, therefore a current flows through the circuit, proportional to the number of ions reacting at the electrodes in unit time.

The electrochemical process can be seen as a heterogeneous chemical reaction in that ions move from the bulk of the electrolyte to the surface of the electrode where chemical and physical changes occur.

The rate of the reaction and hence current flow is at first determined by the applied potential. This dependence is expressed by the Tafel equation, as shown in Figure 5.1.

$$Y = A + B\log I \qquad [5.1]$$

where Y is the overpotential, A and B are constants and I is the current density. The

above situation holds only as long as the rate–controlling step in the process is the rate of reaction [5.2] (i.e. chemical polarisation).

$$M^{n+} + ne \longrightarrow M \qquad [5.2]$$

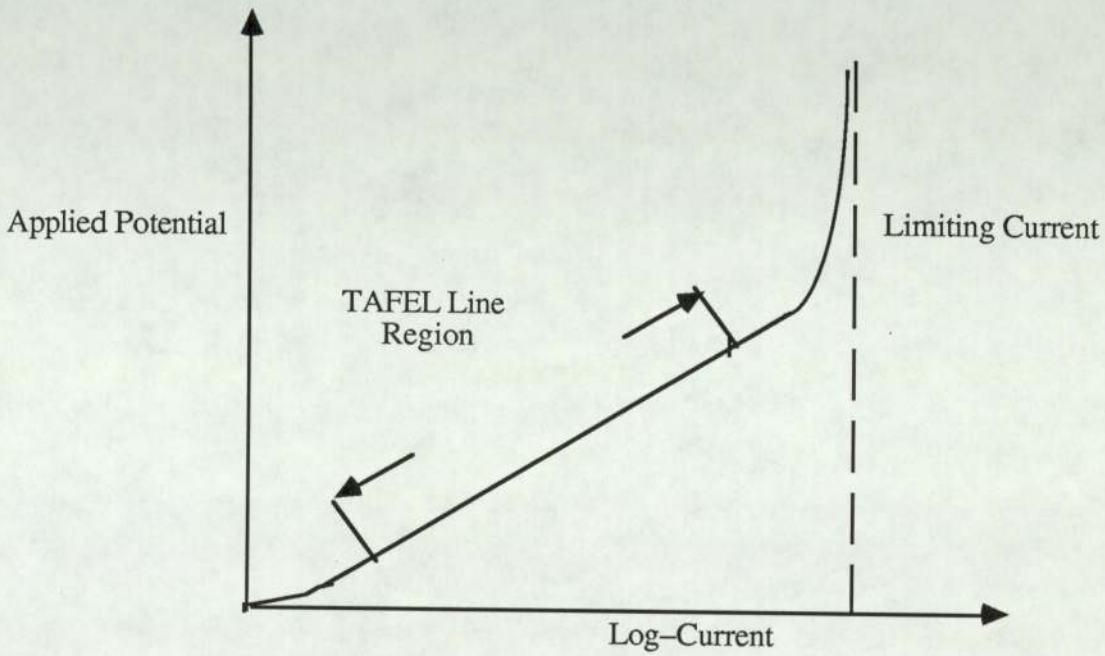

Fig. 5.1 Plot of potential versus the logarithm of current

At a high applied potential this rate is fast and the controlling step then becomes the rate of mass transfer of the ions to the electrode surface to replace those that have been removed by the electrode reaction. This limiting situation is commonly referred to as one in which concentration polarisation exists as this condition is associated with a decrease in concentration of the active species in the immediate vicinity of the electrode.

In measuring the rates of mass transfer by the use of electrochemical reactions it is convenient to make the chemical polarisation negligible because the mass transfer coefficients are more easily obtained from limiting current measurements when the concentration at the liquid–solid interface can be assumed to be virtually zero.

The movement of the ions, and hence flow of the current to the cathode, is brought about in three ways, which are (i) migration due to the potential field, (ii) diffusion due to the concentration gradient, and (iii) convection by fluid flow.

With the addition of a large excess of indifferent electrolyte, such as sodium hydroxide (whose decomposition potential is above that of the redox reaction), to the solution, the effect of migration due to the potential field can be neglected, (Sutey and Knudsen [1967]).

In the case of both laminar and turbulent forced convection the diffusion is confined to the laminar boundary layer and thus the bulk convection contribution is negligible in comparison with the diffusional process in the mass transfer diffusion layer. The concentration gradient is confined to within the laminar velocity boundary layer and the bulk concentration may be considered to be uniform. The transport mechanisms in terms of the electrochemical system used in this work are shown in Figure 5.2.

For the case of steady and unidirectional mass transfer in the y–direction perpendicular to the surface of the electrode, the rate of transfer of a reacting ionic species, i, may be represented by:

$$N_i = -n_i\gamma_i C_i(1 + \varepsilon_\psi/D_i)\partial\psi/\partial y - D_i\,(1 + \varepsilon_D/D_i)\,\partial C_i/\partial y + VC_i \qquad [5.3]$$

where $\gamma_i = D_iF/RT$ = ionic mobility of species i

ψ = electrical potential

ε_ψ = eddy diffusivity for electrical potential

ε_D = eddy diffusivity for mass

C_i = bulk concentration of species i

D_i = diffusion coefficient of species i

F = Faraday's constant

R = universal gas constant

n_i = valency of reacting species i

V = velocity in y–direction

The terms on the right hand side of equation [5.3] represent the contributions of migration, diffusion and convection respectively. The last term for convection vanishes in the redox process because there is no net bulk flow in the y–direction.

The indifferent ions compensate for any potential gradients produced by heterogeneity in the reacting ions concentrations, particularly in the region close to the electrode surface. Thus the electric potential gradient, $\partial\psi/\partial y$, will be approximately zero and the migration term may be neglected. Thus in equation [5.3] only the diffusion term remains, and

$$N_i = -(D_i + \varepsilon_D)\partial C_i/\partial y \qquad [5.4]$$

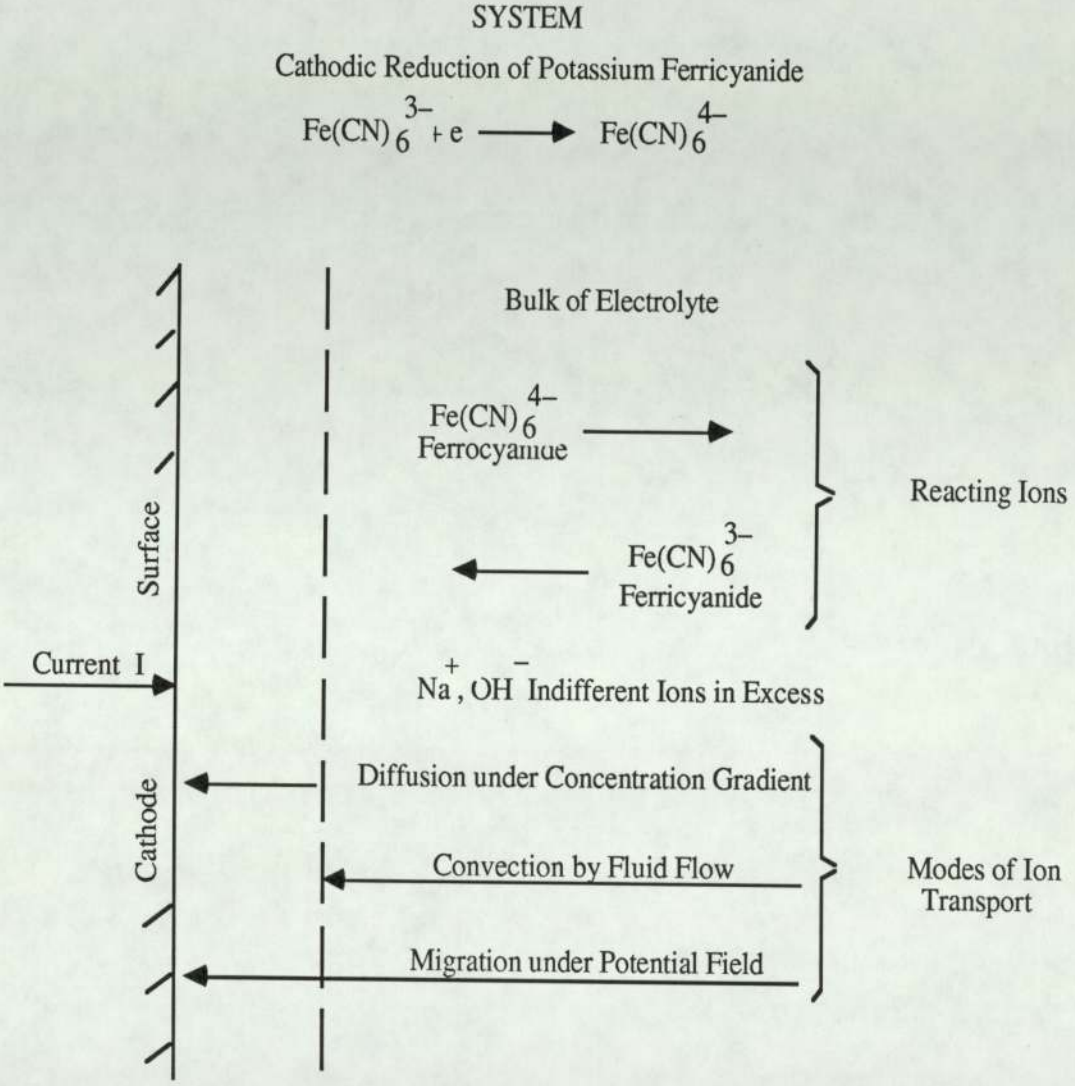

Fig. 5.2 Mechanism of diffusion controlled electrochemical technique (After Mackley [1973])
The broken line represents the edge of the concentration boundary layer.

The rate of mass transfer may alternatively be expressed in terms of a mass transfer coefficient, k_m, defined by

$$N_i = k_m(C_b - C_s) \qquad [5.5]$$

where C_b and C_s are concentrations of the transferring species in the fluid bulk and at the electrode surface respectively.

The current density [I] measured in the circuit can be converted to the rate of transfer of ferricyanide ions by

$$N_i = I/nF \qquad [5.6]$$

where F and n are Faraday's constant (equal to 96 487 coulombs/mol) and the reaction valency respectively.

Hence by substituting equation [5.6] into equation [5.5] the corresponding mass transfer coefficient over the cathode surface in terms of current density is

$$k_m = \frac{I/nF}{C_b - C_s} \qquad [5.7]$$

In this case, I, being associated with pure diffusion mass transfer is termed the "diffusion current density".

The maximum rate of mass transfer or "limiting current density" can be seen from equation [5.7] to exist when C_s is zero.

Figure 5.3 shows the well–known discharge characteristic which is obtained when a potential difference is applied between two electrodes. It can be seen that the curve is divided into three regions. Initially, as the potential on the electrode is gradually increased, the current increases until the surface concentration of ferricyanide ions becomes negligibly small. On increasing the potential further, the current reaches a stable value (the limiting current), signifying the electrolyte reaction to be diffusion controlled with the surface concentration of the ferricyanide ions very nearly zero. Here the current becomes independent of voltage and the plateau of the current–voltage–curve is reached. Further rise in the potential causes electrolysis of water, with a dramatic increase in the current. Therefore a simple test was needed prior to any experiment to check that the electrochemical reaction was diffusion controlled and not reaction controlled.

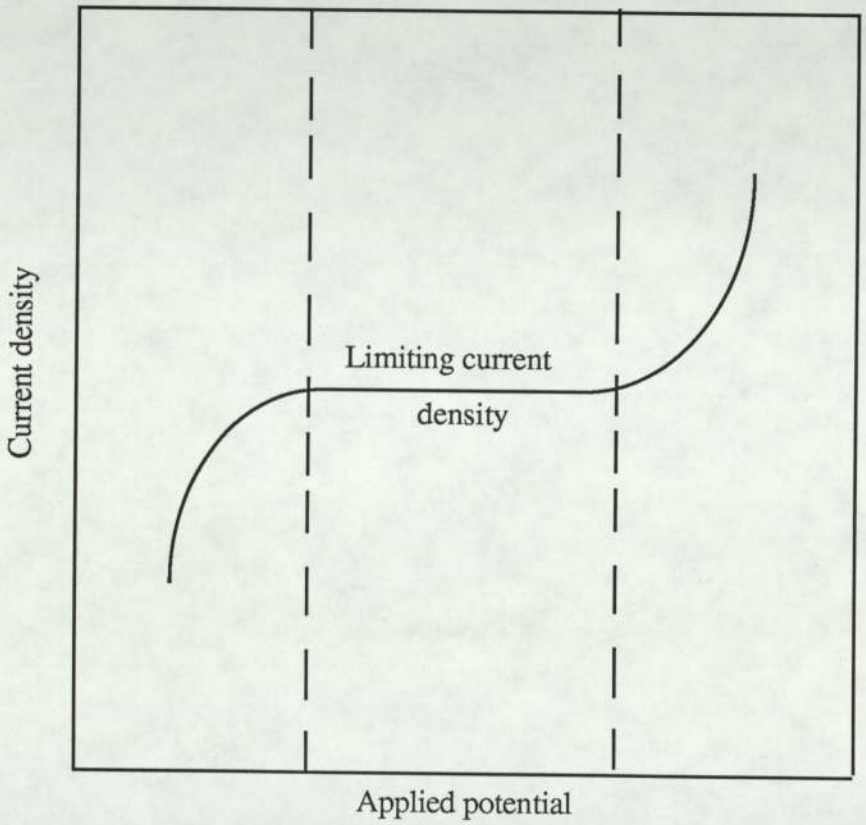

Fig. 5.3 Discharge characteristic

To obtain reliable results it should always be checked by experiment that, for a certain range of voltage, the current through the electrolyte is independent of voltage. Thus with the knowledge of the bulk concentration of the reacting species C_b, which is measured by titration (see Appendix 5), mass transfer coefficients are obtained directly from the limiting current I_L, using equation [5.8]

$$k_m = \frac{I_L}{nFC_bS} \qquad [5.8].$$

As the diffusion rate of ions is made to increase, e.g. by increasing the flow rate, under the same conditions of electrolysis, the value of the limiting current is increased and finally the flat portion of the polarization curves disappears above a certain upper limit of the flow rate as shown in Figure 5.4. In such a situation the chemical polarization becomes significant, as the reacting ions can not be removed from the electrode surface at the higher diffusion rates. Hence, the surface concentration is no longer approximately zero and equation [5.8] is no longer valid. Since the diffusivity is approximately a linear function of temperature, while the reaction rate varies exponentially with temperature, the critical flow rate can often be modified simply by changing the operating temperature.

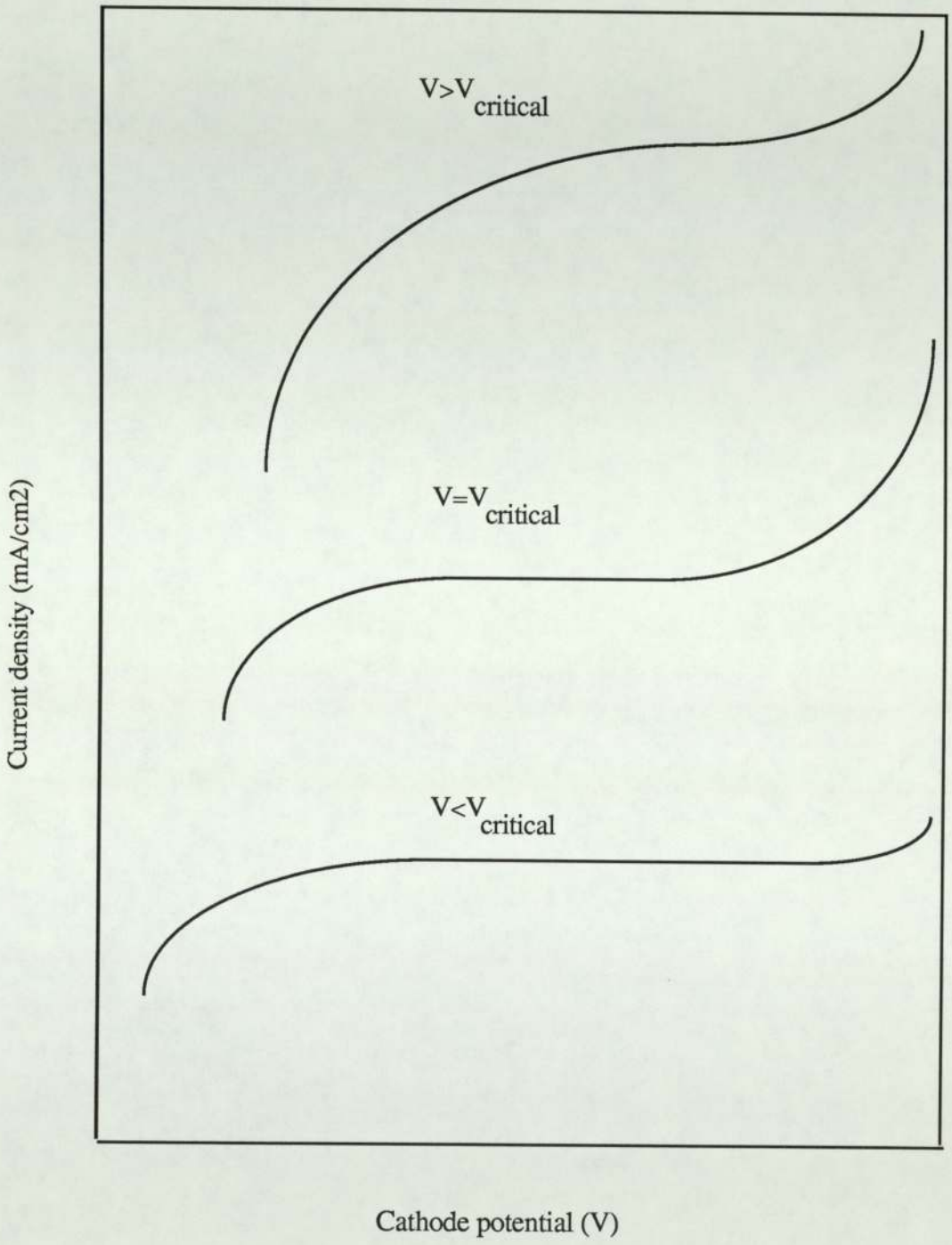

Fig. 5.4 Current–potential curves showing critical flow rate

5.4 ADVANTAGES AND DISADVANTAGES OF THE METHOD

The advantages of the potassium ferri– and ferrocyanide system over other methods are numerous. Some are as follows.

1) An accuracy of about 1%, generally not achievable in heat transfer measurements, may be attained.

2) The method allows measurements of not only the average value but also the local values of mass transfer rate.

3) The electrodes are physically unaltered during the electrochemical process.

4) The fabrication of a model of the system being studied is easier and hence models of complex geometry can be studied.

5) Chemical polarisation is usually negligible, even at high mass transfer rates, because of the high speed of the electrochemical reactions. This leads to the system having a high critical velocity (typically 4.26 m/s (Eisenberg et al. [1954])).

6) As this is a redox system, where the reaction at the electrodes are complementary, the bulk concentration of the reacting ions remain constant. Competing electrochemical reactions can be avoided if the discharge potential range for the limiting current is not exceeded.

7) The surface roughness of polished nickel electrodes is low.

8) The concentration of the chemicals in the system can be determined easily and accurately by volumetric titration.

Although the theory of the technique is relatively simple and has many advantages, in practice various problems arise, especially if measurements are to be accurate and cover the widest possible range of flow conditions. For some of these difficulties, Berger et al. [1983] have given explanations and offer guide lines on how they can be overcome. These problems are discussed below.

Effect of Temperature. The strong dependence of the diffusion coefficient on temperature makes accurate temperature control necessary. Berger et al. [1983] showed that for a $3^{o}C$ rise in temperature, the limiting current can change by as much as 20%. This implies that, if the error in the limiting current is not to exceed 1%, temperature control should be accurate to $\pm 0.2^{o}C$ at least.

Elimination of Migration. As mentioned previously, sodium hydroxide is used as a indifferent electrolyte to reduce the migration current of the reacting species of ions by increasing the solution conductivity, so reducing all potential gradients therein and making the contribution of migration negligible. Too high a concentration of NaOH can affect the electrodes and other components of the rig. Also the high concentration increases the Schmidt number . Therefore, the higher the Schmidt number the thinner will be the concentration boundary layer and the smaller become the protrusions and roughness which will affect the transfer process on the surface. Berger et al. [1983] found that the optimum quantity of NaOH for equimolar 0.005–0.01M ferri– and ferrocynanide solution is 0.5–1M, which reduces the migration current to 1% of the total current.

Effect of Adverse Conditions. Certain precautions are necessary when using the ferri– and ferrocyanide system, due to the relative instability of the ions when in solution. The electrolyte is sensitive to sunlight and dissolved oxygen, especially at temperatures above 60°C. Photochemical decomposition of ferri– and more significantly of ferrocyanide resulting in the formation of hydrogen cyanide and hydroxide ions, takes place according to the equations shown below.

$$[Fe(CN)_6]^{4-} + H_2O \underset{\text{Dark}}{\overset{\text{Light}}{\rightleftharpoons}} \{[Fe(CN)_5].H_2O\}^{3-} + CN^- \quad [5.13]$$

$$CN^- + H_2O \rightleftharpoons HCN + OH^- \quad [5.14]$$

These reactions were proposed by Koltholf and Pearson [1931].

The hydrogen cyanide contaminates the solution and poisons the electrode surface. Therefore the solution should not be exposed to light at any point in the apparatus and any transparent part of the rig must be covered with opaque material such as aluminium foil.

The effects of oxygen on the solution and electrodes are complex and much uncertainty exists concerning the real effects of oxygen on measurements. A possible simultaneous reaction involving oxygen at the cathode is

$$O_2 + 2H_2O + 4e \longrightarrow 4OH^- \quad [5.15]$$

as suggested by Aggarwal and Talbot [1979]. Also, the presence of oxygen may lead to oxide films on electrodes or, more likely, to oxidation of ferrocyanide. As in earlier work (e.g. Mackley [1973]), the solutions are stripped of oxygen by bubbling nitrogen through them (see below).

5.5 PREPARATION OF ELECTRODES

The electrode surfaces need a cleaning on the microscopic level and removal of any oxide film prior to the experimental run (see Appendix 1). This is done by cathodically activating the electrode, which involves electrolysis of water using a current density of 0.1 mA/mm^2. Hydrogen is evolved at the cathode and oxygen at the anode (Mackley [1973]).

5.6 PREPARATION OF SOLUTION

The bulk of solution should be isolated from exposure to air at all times. Nitrogen is usually used to saturate the solution and drive off any oxygen before adding the ferri– and ferrocyanide to the solution and a positive nitrogen atmosphere is always maintained in the main tank to prevent reabsorption of oxygen. Nitrogen bubbled through the tank before the solution is used, helps to maintain a high degree of nitrogen saturation.

If electrolyte is left on the test section and exposed to air, the cyanide

decomposes, and if this occurs on an electrode it poisons the electrode. If the test section is then simply cleaned with acid and then degreased before activating (as some users of this technique claim as sufficient), the surface contamination on the electrode remains and a lower limiting current is obtained. It is therefore desirable to remove the test section from the rig immediately after a set of experiments and thoroughly rinse it with clean water.

CHAPTER SIX

EXPERIMENTAL APPARATUS

6.1 INTRODUCTION

The electrolyte solution, [$Fe(CN)_6K_4$, $Fe(CN)_6K_3$, NaOH], constituting the shell–side fluid, was circulated through the tube bank models. Measurements of mass transfer coefficients on the shell–side of the tubes were made using the electrochemical technique previously described (Chapter 5). A tube side fluid is not necessary because of the nature of the technique.

A series of readings were made in two sets of experiments for a characteristic Reynolds number range from 0.5 to 12 600, corresponding to electrolyte flow rates in the range of 1.5×10^{-3} to 48.1 dm^3/min.

One run with four readings for flow normal to the tube bank at zero Reynolds number (no imposed flow natural convection alone) was carried out to find the value of $Sh/(ScGr)^{0.25}$ (see Section 8.4.2.3).

Two runs were done to measure the overall pressure drop across the tube banks for each model in a Reynolds number range from 70 to 6 300.

6.2 MATERIALS OF CONSTRUCTION

Due to the presence of sodium hydroxide in the electrolyte solution, the solution is very corrosive, so it is necessary to make the models of materials which are resistant to the corrosive attack of the solution.

Literature studies revealed that the materials of construction most commonly used with this redox electrochemical system were glass, perspex, stainless steel, and neoprene rubber. Compatibility charts indicated that both polyvinyl chloride (PVC) and polypropylene were unaffected by sodium hydroxide solutions.

For this reason perspex was used for the entire material of the body of the tube bank models, and the tube material was nickel. QVF glassware was used in the construction of the flow circuit.

The end of the tubes (see Figure 6.8) and the space between the walls of the duct leading the wires out of the test section were filled with "Araldite" which is impermeable to NaOH. Nichrome wires with PTFE sleeving and thermocouple wires which have good resistance against sodium hydroxide were used.

Two stainless steel circulating pumps were chosen to avoid any corrosion.

6.3 THE ELECTROLYTE FLOW CIRCUIT

The experimental flow circuit is illustrated diagrammatically in Figure 6.1, and a

photograph of the rig is shown in Figure 6.2. The rig consists of a storage tank for the electrolyte solution (S), two stainless steel centrifugal pumps (P), five rotameters (R), four models (M), a thermometer (T), connecting lines of QVF glassware and valves (V).

The electrolyte solution was drawn from a storage tank and delivered by two stainless steel pumps to the tube bank models. The solution was then returned to the tank thus completing the flow circuit. QVF glass pipes of 38 mm ID nominal bore were used.

The storage tank, or reservoir, consisted of two 305 mm nominal bore QVF glass sections providing a storage capacity of approximately 70 litres. The top of the tank was sealed with a 6.5 mm thick perspex plate in order to maintain a positive nitrogen pressure and also keep other materials (e.g. dust) out of the system.

In order to obtain results under identical conditions and so giving a better comparison between the models, the output from the rotameters was connected to four vertical pipes. Each of the four models were installed in the top of each of these. A bundle of hard PVC tubes, 300 mm long, were inserted into the bottom of the vertical pipes to act as flow straighteners. The flow reducer on top of each pipe then converted the developed profile into a near–uniform velocity profile (see Fig. 6.3).

To control the temperature of the solution, a stainless steel helical cooling coil supplied with mains water was located inside the tank. The rate of flow of water inside the coil was controlled by using a Rotameter 7S size (flowrate up to 5 dm^3/min). The tank was provided with a gas–venting valve and an electrolyte–filling point.

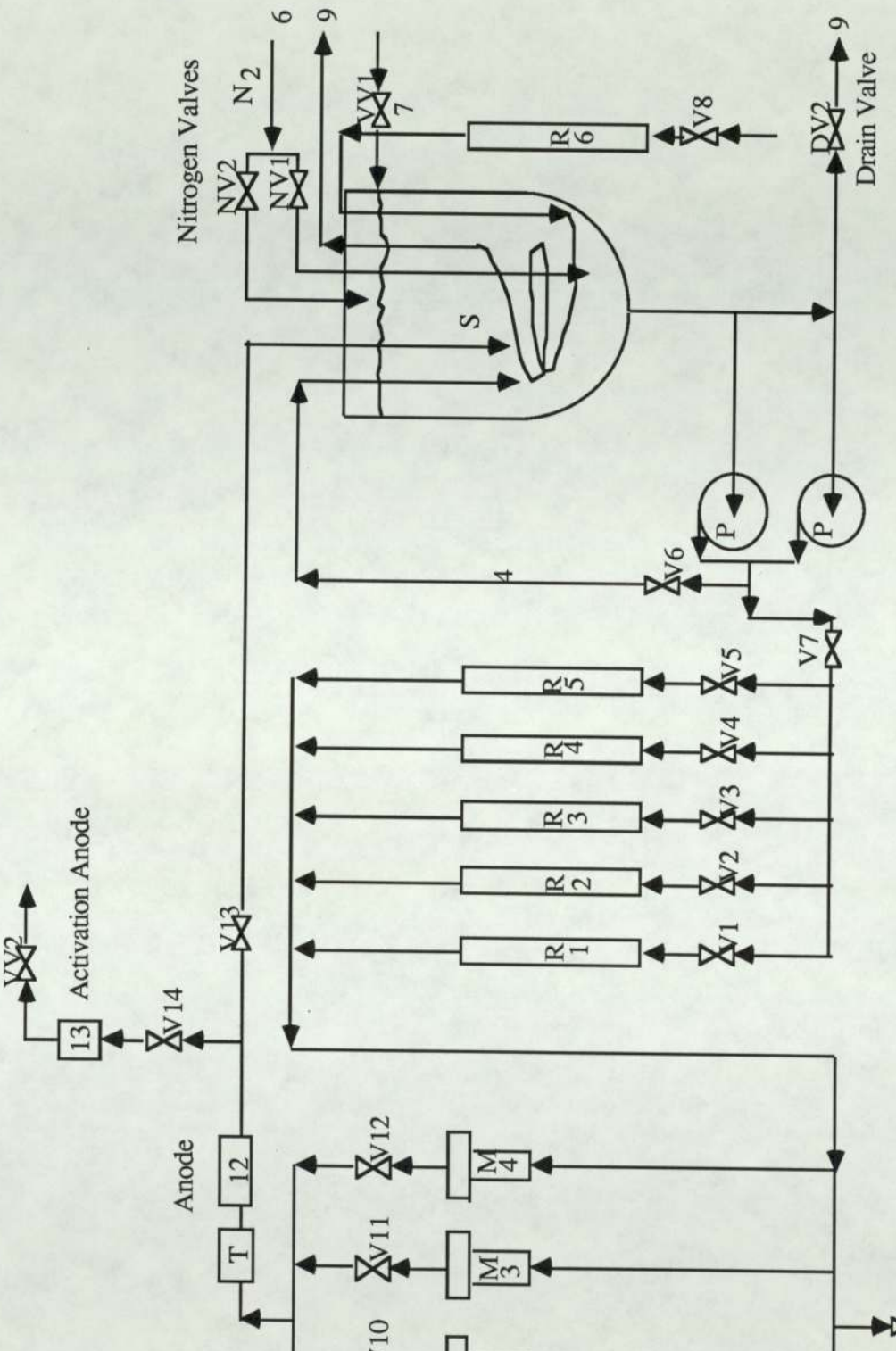

Fig. 6.1 Flow circuit

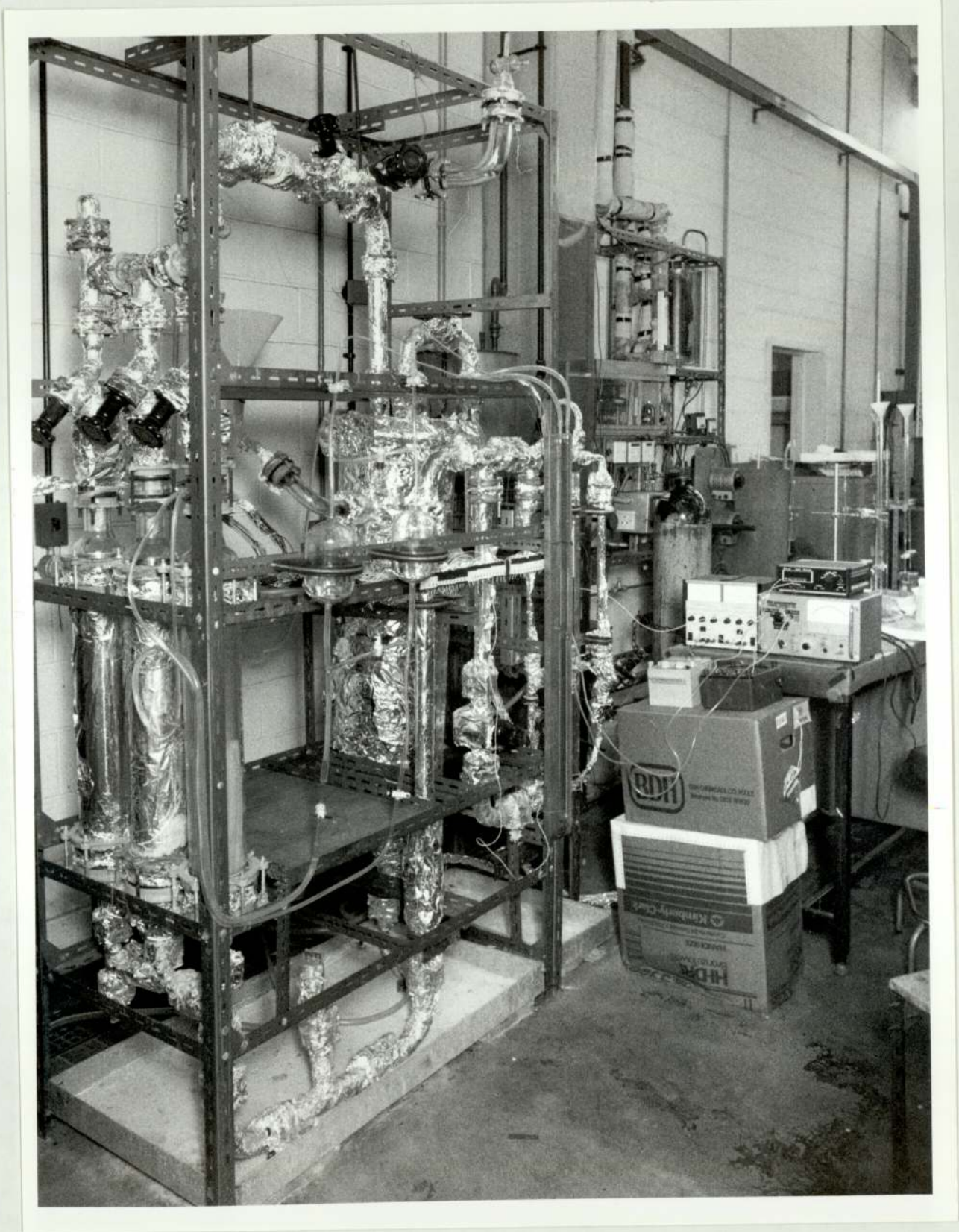

Fig. 6.2 Photograph of rig

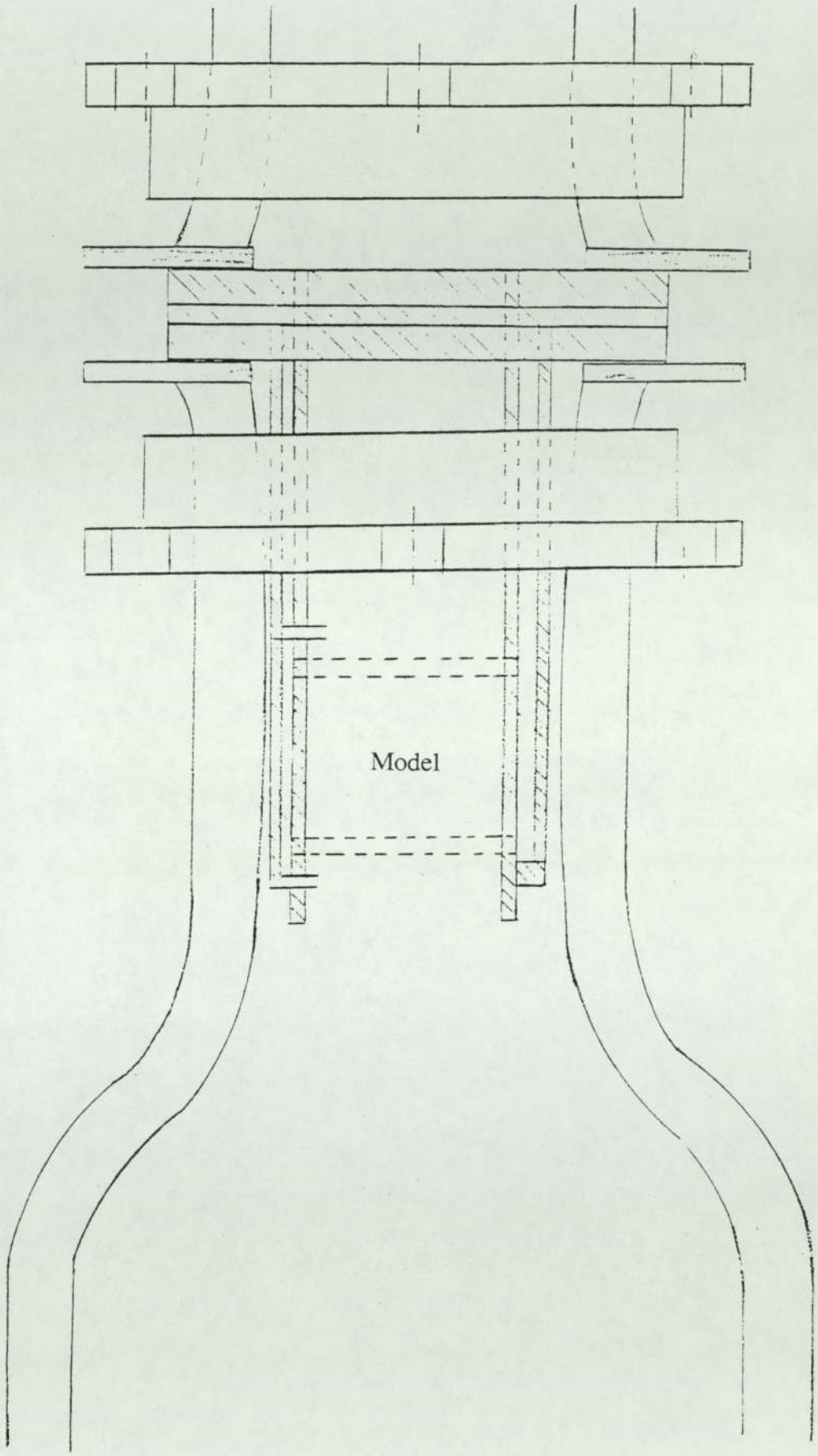

Fig. 6.3 Schemtic of first model location inside top of vertical tube

The top plate (perspex) had two holes (approximately 20 mm in diameter) to accept the return pipe and the by–pass pipe, and holes for passing the cooling coil feed water lines and the nitrogen purge line.

The by–pass line (4) was of flexible PVC tubing with a screw clip to adjust the flow. The pipes entering the storage tank were long enough to dip into the solution and hence gas entrainment was avoided. This provided bubble–free flow and ensured proper functioning of the electrodes i.e. without disturbances due to gas bubbles. All openings around the pipes in the top plate were sealed with "Araldite".

Two stainless steel centrifugal pumps with a maximum capacity of about 40 dm^3/min were used. These two pumps were fitted in parallel as shown in Figure 6.1. Each pump ran at only one speed and therefore the by–pass line was incorporated in the pump's delivery line to prevent overload at low flow rates. The pumps were connected to the rig with flexible PVC tubes to avoid vibrational problems.

The flow rate was measured through five different rotameters arranged in parallel. Four of them were the Metric 7S, 14S, 24S and 47S sizes produced by the Rotameter Manufacturing Company. Stainless steel floats were used. Flowrates up to 1, 5, 20, 100 dm^3/min respectively could be measured. The fifth one (the smallest one) had a glass float and gave accurate metering from $2x10^{-3}$ to $5.5x10^{-3}$ dm^3/min and was used for very low flowrates. These flowmeters were calibrated by using both analytical and experimental methods, as shown in Appendix 3.

Even with two pumps in parallel, each of 40 dm^3/min capacity, the maximum volumetric flow rate obtained was about 48 dm^3/min corresponding to a Reynolds

number of 12 600.

A thermometer–well was incorporated in the pipe work at a point just upstream of the exchanger model. The temperature of the electrolyte solution was measured using a mercury in glass thermometer and an electronic thermometer (Comark) to an estimated accuracy better than $\pm 0.2^{o}C$.

A vent pipe was located at the highest point in the pipe work to allow the complete removal of gas from the system.

As shown in Figures 6.7 (a), (b), (c), and (d), the angle of attack (yaw angle) to the fluid flow was 90^{o} for Model 1 (i.e. flow normal to the tubes), 70^{o} for Model 2, 57.5^{o} for Model 3 and 45^{o} for Model 4.

Samples of electrolyte were obtained from a bleed line located on the thermometer–well.

The activation anode was located inside an "L" shaped tube with a valve on either end (see Section 6.5).

In order to protect the electrolyte solution from the adverse effects of sunlight as explained in Section 5.4, all the glass pipes and ancillaries were covered with aluminium foil. Removable covers over the rotameter scales allowed inspection for the flow rate to be read when this was required.

6.4 TUBE BANK MODELS

The three inclined tube banks models with angles of attack of 70^{o}, 57.5^{o} and 45^{o} are shown photographically in Figures 6.4. Photographs of the tube banks are presented in Figure 6.5 (a), (b), and (c). A drawing of the first model is given in Figure 6.6. Cross–sections are depicted in Figures 6.7 (a), (b), (c), and (d).

The first model is geometrically similar to the Model 3 unit used in the heat transfer research work of Bergelin et al. [1949 and 1957] at the University of Delaware.

The tube size, spacing arrangement, and the other dimensions except the angle between the flow and the tubes are the same in all four models. The first model was installed with the tubes horizontal. The electrolyte solution flowed upwards through the tube bank, as drawn in Figure 6.7. The essential dimensions of the four models are given in Table 6.1.

Table 6.1

Dimensions and constants	
outside tube diameter	3 mm
tube arrangement	staggered square
tube pitch	3.75 mm
pitch/outside diameter ratio	1.25
clearance between tubes	0.75 mm
number of exposed tubes per row	5 or 6
number tube rows	12
total number of exposed tubes	66

Fig. 6.4 Photographs of the inclined tube bank models

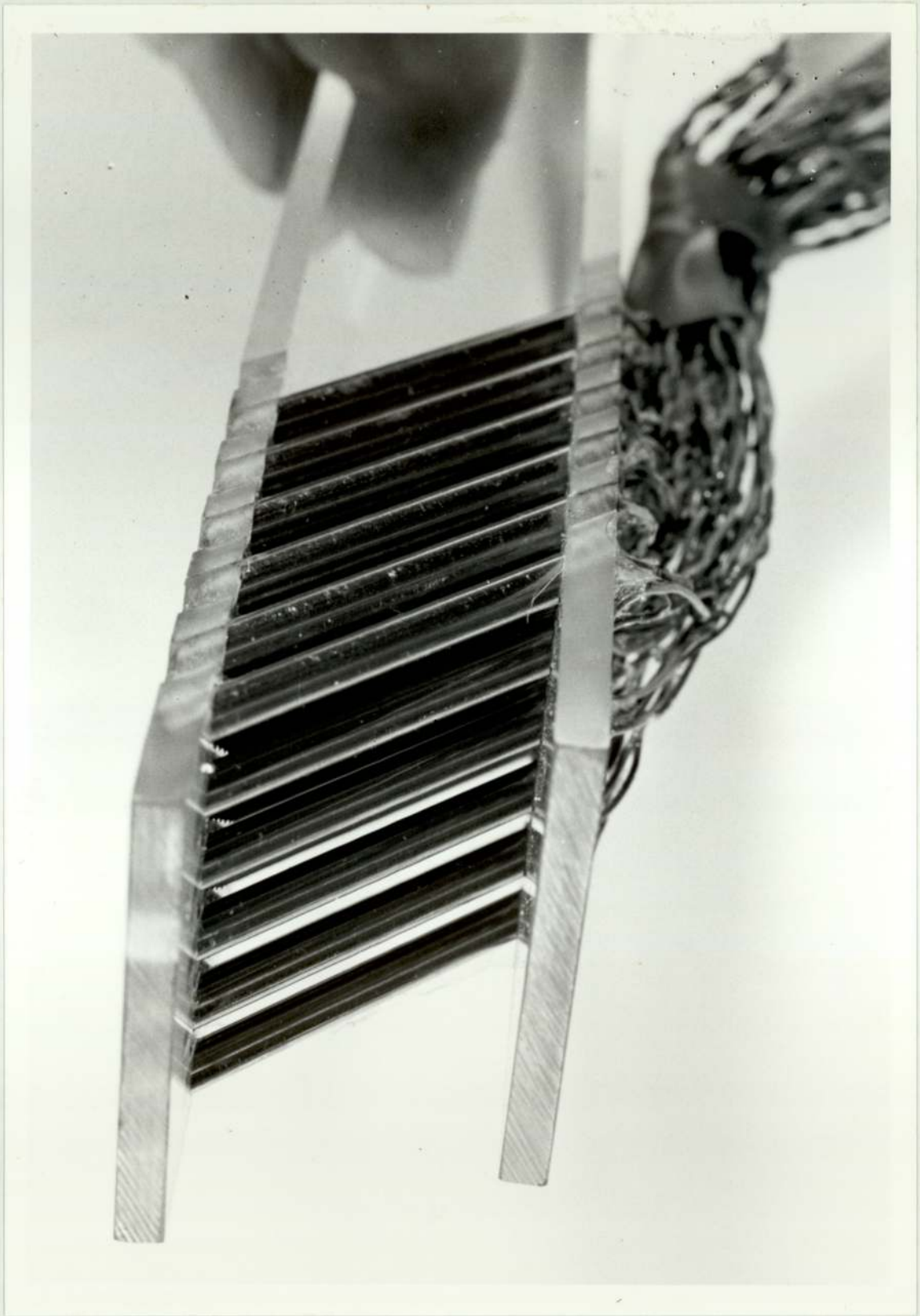

Fig. 6.5a Photograph of the inclined tube bank (φ=57.5^{O})

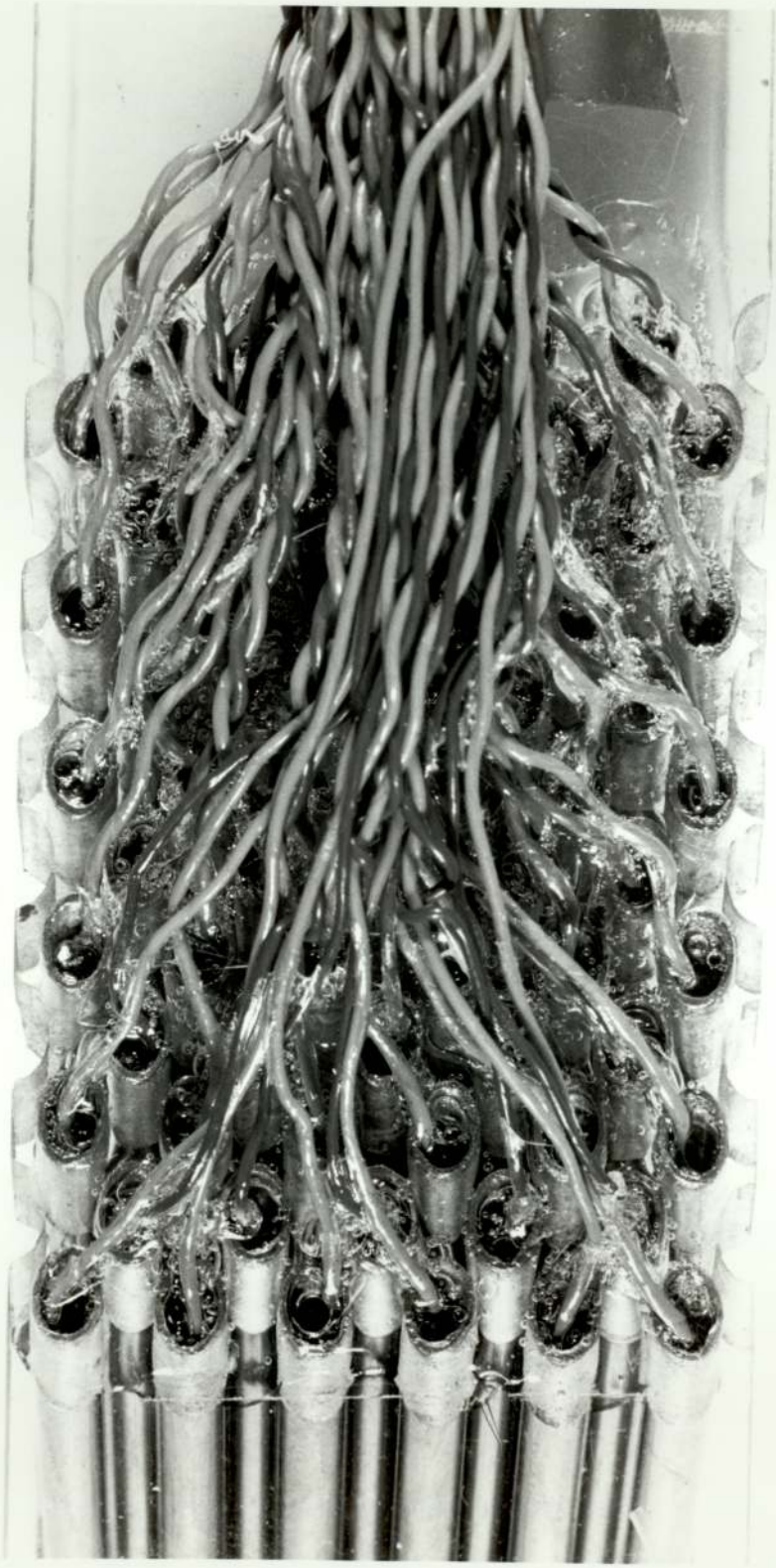

Fig. 6.5b Photograph of the inclined tube bank (φ=57.5^{O})

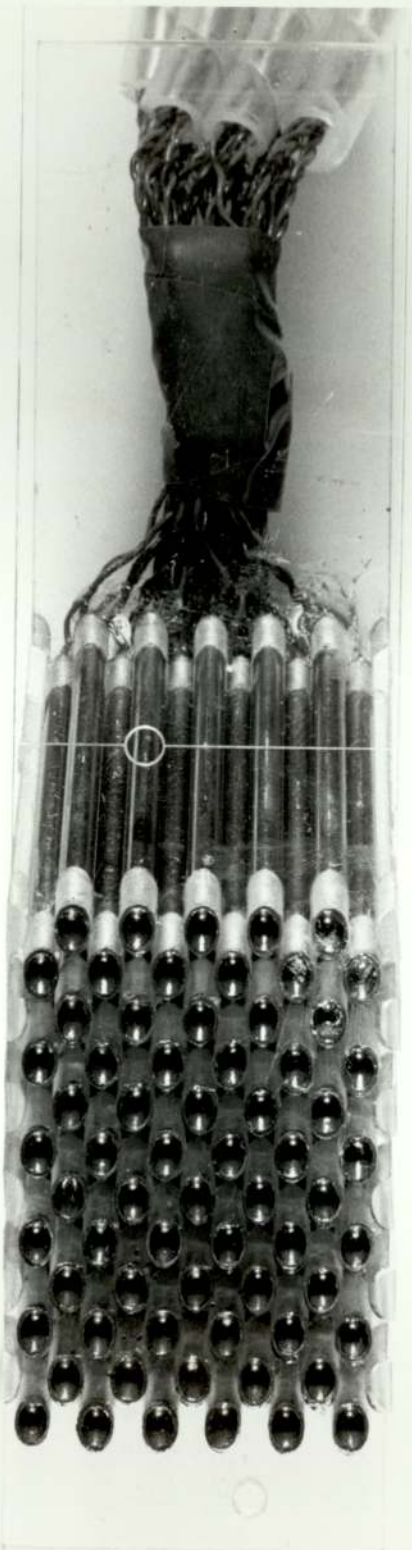

Fig. 6.5c Photograph of the inclined tube bank (φ=57.5^{o})

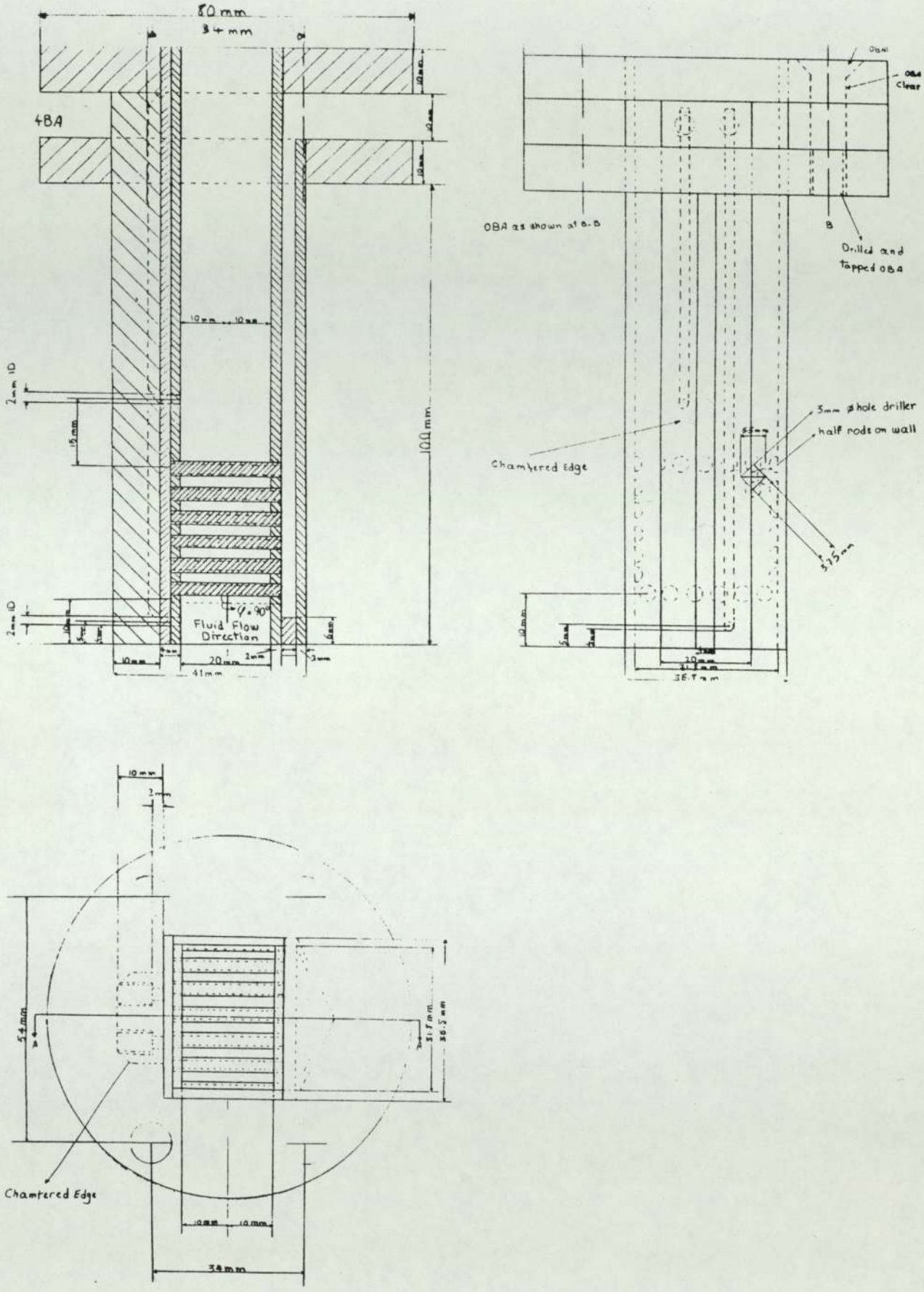

Fig. 6.6 Full drawing of first model

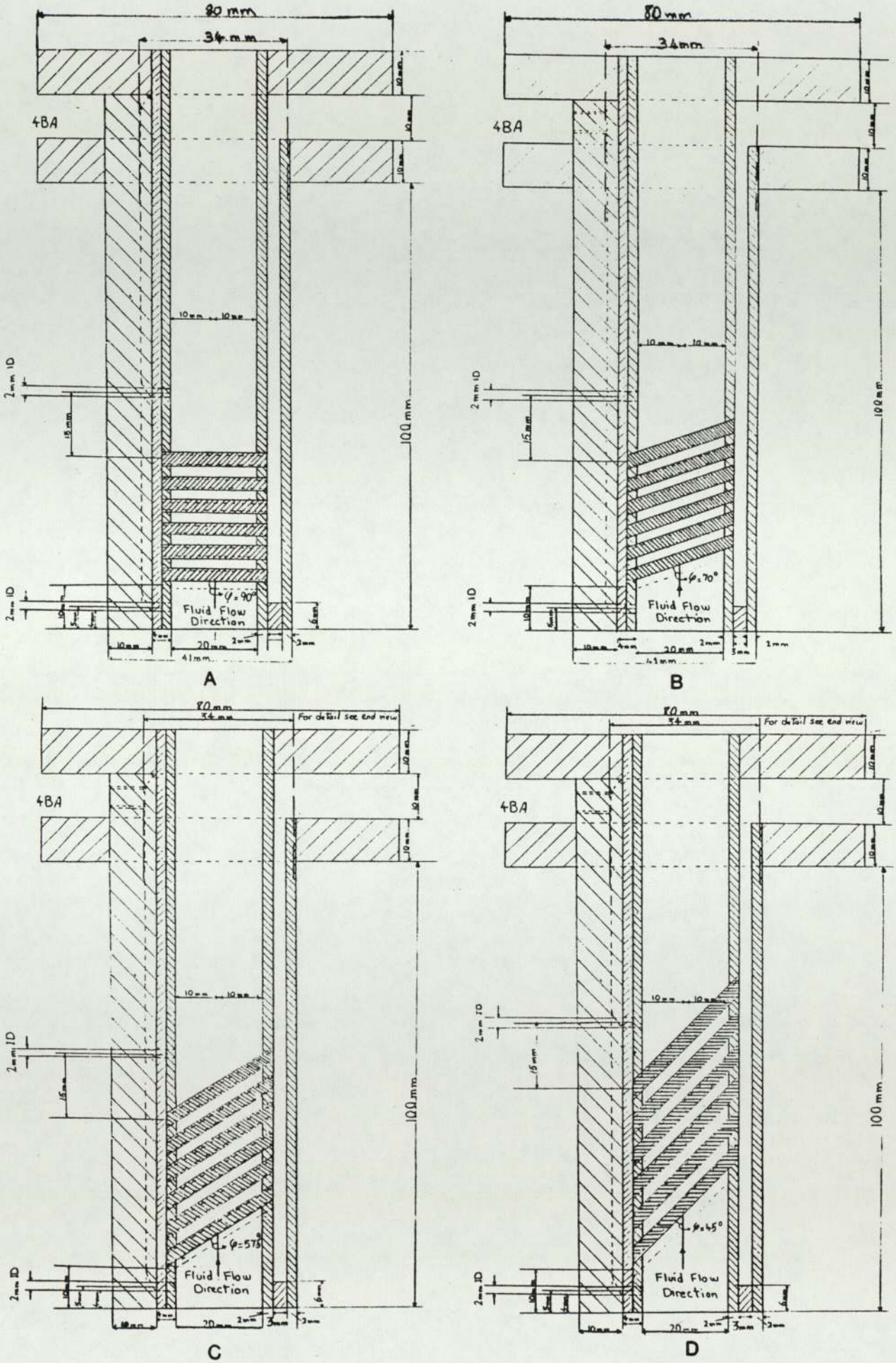

Fig. 6.7 Cross section drawing of four models

Each model consists of a rectangular perspex shell containing sixty–six 3 mm OD nickel tubes arranged in twelve rows, with alternatively five and six tubes in a row. The exposed length of the tubes were 20 mm, 21.28 mm, 23.71 mm and 28.28 mm respectively for the four models. In order to obtain uniform flow distribution and to eliminate bundle bypassing twelve 3 mm OD perspex half–rods were mounted on the walls of the model.

In order to join the various parts of the models together a special perspex monomer (methyl methacrylate) was used. This adhesive was applied in liquid form and polymerized under ultraviolet light. Sodium hydroxide rapidly corrodes solder and unwanted metal ions will go into solution, affecting the results of the experiment. Because of the high penetration rate of sodium hydroxide, all small cracks and joints had perspex momomer applied to them to help to seal them in order to keep sodium hydroxide solution away from the vulnerable joints.

As shown schematically in Figure 6.8, the tubes were filled with a low melting point solder (Wood's metal, melting point 70^{o}C), leaving a gap of about 2 mm at either end of the tubes. These end gaps were sealed with liquid "Araldite" to stop the caustic solution penetrating to the solder.

Nichrome wires with PTFE sleeving were inserted into each tube of Model 1 during the process of filling them with Wood's metal. Due to leakage through the gaps between the wires and the PTFE sleeving, chrome thermocouple wire was used for the remaining models.

6.5 CONSTRUCTION OF ANODES AND CATHODES

The nickel tubes were used as cathodes. Since local transfer coefficients were required, the tubes had to be electrically isolated from each other, so that each tube could be used on its own as a cathode.

Five cylindrical nickel sheets with areas larger than the total area of the cathodes were located inside the return pipes to act as anodes. Four of them were fitted in just after the models to keep the distances between the anodes and the cathodes as short as possible, and these were used in the second set of experiments. The reason for having a very short distance is discussed in Section 7.4. As for the cathodes, a Nichrome wire was used to connect these anodes into the circuit. The dimensions of each anode were 120x60 mm, providing a net surface area of 144 mm^2. This brought all the cathodes to a common limiting voltage range enabling a specific voltage to be used where all the electrodes were at their limiting current values.

An additional anode was used as an activation anode by placing another nickel strip inside an "L" shaped tube after the main anode and before the tank down–stream from the flow.

The "L" shaped tube had an internal diameter of 20 mm with a valve on either end. When using the activation process the upper valve was left fully open so that the oxygen generated could escape and not interfere with the main flow in the system. The lower valve was only partially open in order to allow an area sufficient for the current to pass (see Figure 6.1).

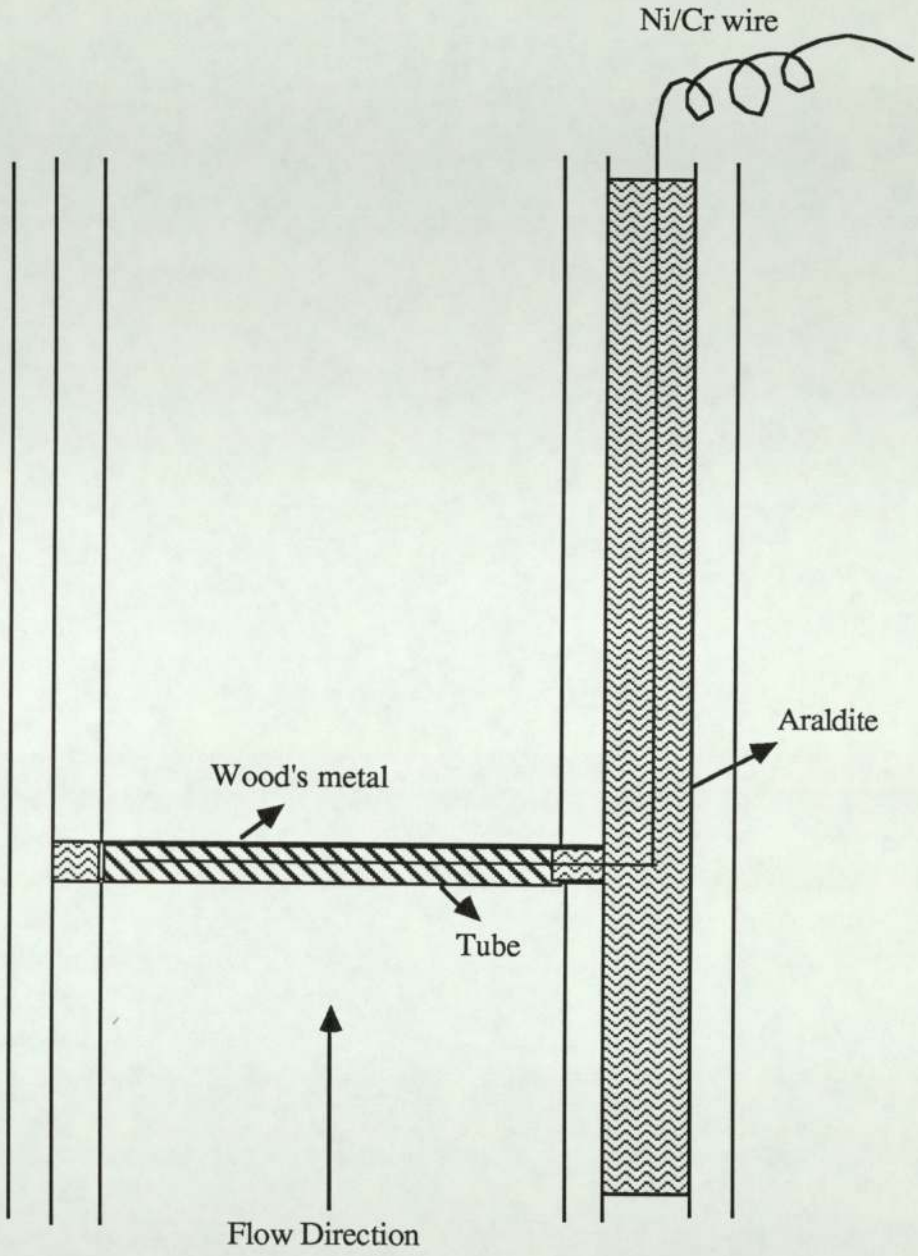

Fig. 6.8 Schematic drawing of first model with one tube

6.6 TEMPERATURE MEASUREMENT

As already noted, the temperature of the circulating electrolyte solution for the first experiment was measured by a mercury thermometer which had been calibrated as illustrated in Section 7.2, and in the second set of runs by an electronic thermometer (Comark).

6.7 ELECTRICAL INSTRUMENTATION

The two basic elements required in the electrical circuit are

1) A source of constant potential, which can be varied and which does not change when a current is drawn from it.
2) A current measuring device.

A flow diagram of the electrical circuit employed in making limiting current measurements is depicted in Figure 6.9. A variable power supply of stabilized DC voltage enables external potentials of up to 30 volts to be applied across the electrodes.

The positive terminal of the power supply was connected to the anodes, while the negative was connected to a digital ammeter to measure current passing through the electrolyte and the wire from the ammeter was connected to the cathode (the tubes inside the model).

The potential was supplied to each row separately and the limiting currents read

with an accuracy of ±0.01 mA. In the electrode activation process the electrical supply was disconnected from the main anodes and was connected to the activation anode. The activation process was also carried out on each tube row. A multi–range voltmeter (AVO meter) was used to monitor the potential difference between anode and cathode.

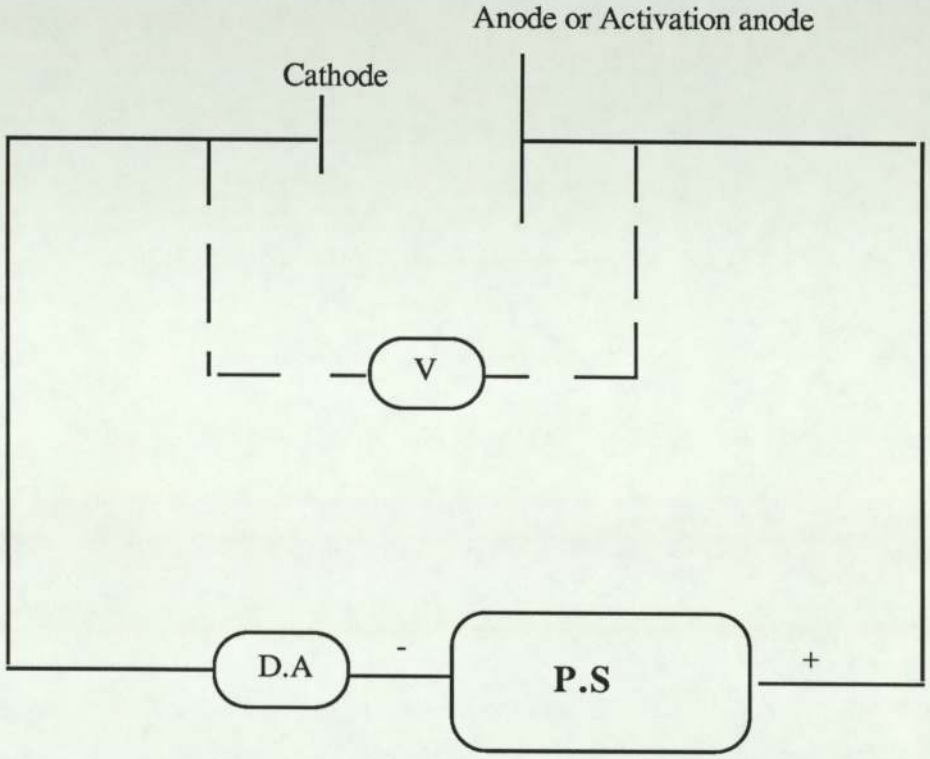

Fig.6.9 Flow diagram of the electrical instrumentation circuit

6.8 PRESSURE INSTRUMENTATION

To measure the pressure drop across the tube bundle two holes were drilled before and after each tube bank on one wall of each of the models. The distances between the centre of the holes to the centre–lines of the lower row and the upper row were 5 mm and 15 mm respectively. A back cover with two channels was fixed with adhesive to the wall on the model, in order to provide a connection between the pressure tappings and the two perspex outlet tubes.

The pressure drops were measured by connecting these two perspex tubes to two glass vessels with an internal diameter of 80 mm, as illustrated in Figure 6.10.

These glass vessels were partly filled by water and converted the liquid pressure into a pneumatic pressure. This pressure was transmitted from the top of the vessels via a 6.3 mm internal diameter pneumatic line to the pressure measuring instruments. The instruments used included a U–tube manometer and an electronic micromanometer. Differential pressure drops of less than 100 mm H_2O were measured by the electronic micromanometer.

The pressures and levels on these vessels and manometer was equalised by opening valves V1 and V2 in Figure 6.10.

The advantages of this system are many. But a major disadvantage of this system is that a high response time is needed due to the system sensitivity.

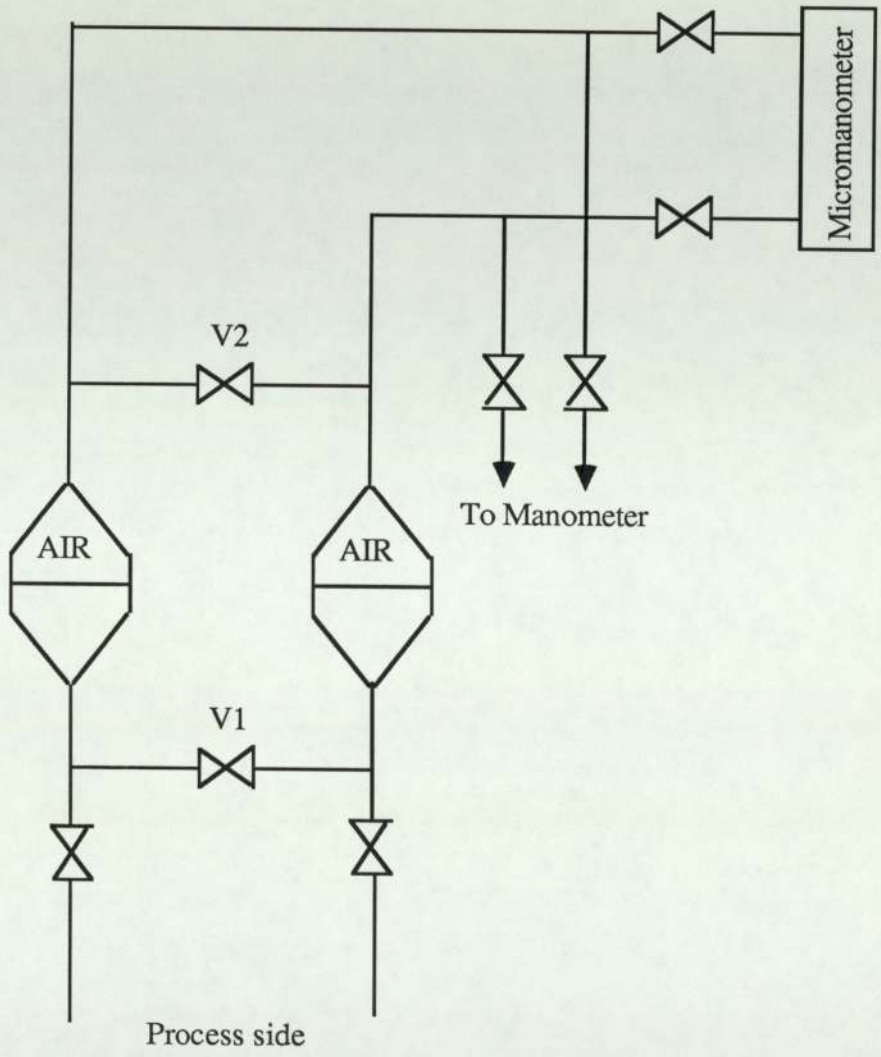

Fig. 6.10 Pressure instrumentation diagram

6.9 EFFECT OF SUNLIGHT

As discussed in Chapter 5 previously, solutions containing ferrocyanide and ferricyanide ions decompose in sunlight, this being more significant for the latter ion. Therefore all the glass pipes, tank and ancillaries were covered with aluminium foil.

CHAPTER SEVEN

EXPERIMENTAL PROCEDURE

The following sections describe the features of the experimental procedure leading up to and including the experimental runs.

7.1 CALIBRATION OF ROTAMETERS

Five variable area flow meters were used (GPE MeteRate, Rotameters metric 7S, 14S, 24S and 47S sizes). Some previous users of the electrochemical technique, e.g. Mackley [1973] and Prowse [1977], used water for the calibration runs and applied the resulting curve to determine the electrolyte flow. The physical properties, especially viscosity, of the two fluids would effect the accuracy of the flow rate. A better technique was needed to increase the accuracy of the flowmeters. A direct calibration using electrolyte solution was used to calibrate the GPE MeteRate. The direct calibration was hazardous for very high flow rates. Therefore Rotameters Metric 7S, 14S, 24S and 47S were calibrated indirectly using the Rotameter Manufacturing Company technique; the calibration for the Metric 7S rotameter was checked by a direct calibration. This is discussed in more detail in Appendix 3.

7.2 CALIBRATION OF THERMOMETER

As mentioned in Section 5.4 the temperature should be measured accurately to ± 0.2 K at least in order to measure the limiting current with an accuracy of $\pm 1\%$. A

calibration chart for the thermometer used is shown in Figure 7.1. This had been calibrated against a NPL–certificated platinum resistance thermometer (Jenkins [1983]).

7.3 PREPARATION OF ELECTROLYTE SOLUTION

The electrolyte comprised a molar aqueous solution of sodium hydroxide and a 0.01 molar mixture of potassium ferrocyanide and potassium ferricyanide. The volume of solution needed was approximately 70 litres. The procedure adopted in making up this solution is discussed in Appendix 4.

7.4 ELECTRODE ACTIVATION

The electrode surface required careful and thorough cleaning giving removal of any oxide film prior to the experiment so as to reduce error in the limiting current due to chemical polarization. This was done by cathodically activating the electrode, which involved electrolysis of water. Hydrogen was evolved at the cathode and oxygen at the anode.

Some workers such as Eisenberg et al. [1956], Sutey et al. [1967], Mackley [1973], Prowse [1977], Nibber [1981] and Berger et al. [1983] have used the activation process prior to their experiments whereas some workers e.g. Hubbard et al. [1966] and Aggarwal and Talbot [1979] have found the activation process was unnecessary. A fuller discussion is given in Appendix 1.

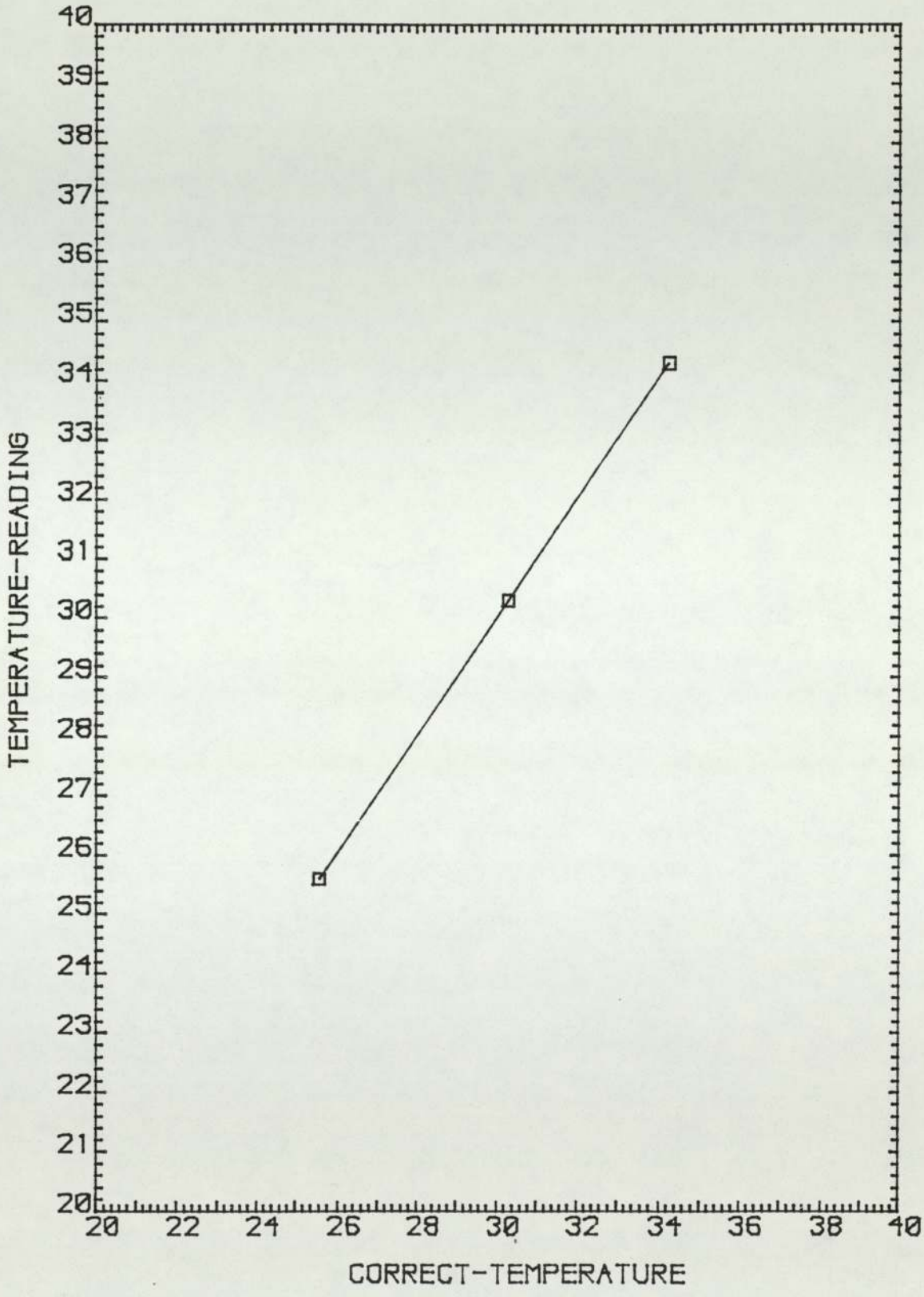

Fig. 7.1 Calibration of Thermometer

In the present work a current density of about 0.1 mA/mm^2 for about 20 minutes was used for the activation process. Mackley [1973] found that satisfactory results were obtained by using this current density.

In previous work the surfaces of the cathodes were polished by emery cloth before the activation process. In this study because of the small size of the models such polishing was impossible after the models had been assembled, therefore the tube banks were rinsed in 10% hydrochloric acid for around 15 minutes and then washed with distilled water before replacing the models in the flow circuit.

Before starting the experiments, it was expected that the activation process could be done for all the tubes at once, by using a current of 1.3 A (the total surface area of the tubes was 1243.44 mm^2). However it was found that the maximum current flowing through the system did not go above 0.334 A, and this was not sufficient for the required activation process.

Thus the activation process was carried out for each row individually by supplying about 0.3 A. The following procedure was used in the first set of runs.

All drain valves were closed. The flow through the exchanger model was adjusted to about 25 dm^3/min. The positive terminal of the power supply was connected to the activation anode which was located inside the "L" shaped tube with two valves on either end (see Fig. 6.1).

The upper valve, i.e. VV2, was fully left open during the activation process, so that the oxygen generated could escape and not interfere with the main flow in the system. The lower valve, i.e. V14, was only partially open in order to allow current to pass.

The negative terminal of the power supply was connected to a digital ammeter to measure the current passing through the cell and the wire from the ammeter was connected to each row in turn. Each row was separately activated for about 10 minutes using an activation current of 0.3 A for the first set of experiments.

During the activation process a steady purge of nitrogen was passed through the electrolyte in the reservoir to remove hydrogen produced as a result of electrolysis.

At the end of the activation period the voltage was interrupted and the valves V14 and VV2 were closed. Then the potassium salts were added to the sodium hydroxide solution and the rig was ready for operation.

The above procedure was carried out in the first set of experiments. As discussed before two sets of experiments were carried out for each model. Some useful points were found in the second set of experiments.

The first, which was related to the activation process, was the maximum current that could be passed between cathodes (the whole tube bank) and the activation anode. The maximum current that could be supplied was approximately 0.3 A in the first set of experiments. But in the second set of experiments, by changing the position of the activation anode closer to the cathode this current increased up to nearly 1.0 A. This

means that by decreasing the distance between activation anode and cathode the current increases because the ohmic resistance decreases.

7.5 EXPERIMENTAL RUNS

The electrolyte solution was allowed to circulate at a high flow rate for about 30 minutes to ensure that it was homogenous. At the same time the water through the cooling coils was adjusted in order to stabilize the fluid temperature. A sample of electrolyte was taken and the concentration of ferricyanide was determined immediately as set out in Appendix 5.

The flow rate through the exchanger model was measured and set at the desired value. The electrolyte solution was allowed to circulate at this rate to stabilize the temperature. This period was usually of the order of 10 minutes. The nitrogen purge through NV1 was stopped as it affected both the flow rate and pressure drop, the latter quite significantly, while the NV2 nitrogen purge valve was left open to maintain nitrogen pressure inside the storage tank (see Figure 6.1).

The source of DC potential (a stabilized power supply) was connected across the operation anode and the first row of the tube bank as cathode. The power was switched on. The applied potential was gradually increased by increments (0.1–0.2 volts). The current initially increased until a stable value was reached, i.e. a limiting current. The value of this limiting current across the plateau region was read from the digital ammeter and recorded. All the experiments were carried out under these conditions.

Every care was taken in order to avoid increasing the voltage beyond this limit since it would cause electrolysis of water, the oxygen evolved would adversely affect the electrolyte.

The limiting current was measured in a similar way for each row of the tube bank at the same flow rate. The temperature and flow rate were randomly checked. The investigations were then extended to other flow rates.

On completion of a series of experimental runs, a sample of electrolyte solution was taken to check the concentration of ferricyanide.

The pumps were switched off and the cooling water line was shut off. The power supply was switched off. Nitrogen pressure was maintained in the solution tank through NV1.

Ten runs for the normal tube bank and six runs for each inclined tube bank model, with 6 to 14 readings were carried out to measure mass transfer coefficients. All runs formed two sets of experiments. In the first experiments eight runs for the normal tube bank (Model 1) and four runs for the inclined tube banks (Models 2–4) were carried out, whereas two runs were done in the second set of experiments for each model. In the second set of experiments, as noted before, in addition to the existing anode another four anodes were located as close as possible to the cathodes. As already noted, it was found that the plateaux were obtained very easily and with a very short response time.

The pressure drop was measured in separate runs using water as fluid. Due to limitation of the capacities of the manometers, the pressure measuring equipment was

limited to a minimum flowrate of approximately 0.27 dm^3/min and to a maximum flowrate of approximately 24 dm^3/min corresponding to a range of shell–side characteristic Reynolds number of 70 to 6 300. The pressure drops less than 100 mm H_2O were measured by micromanometer and above that value by U–tube manometer.

CHAPTER EIGHT

SHELL–SIDE INVESTIGATION IN IDEAL NORMAL TUBE BANKS

8.1 SCOPE OF EXPERIMENTAL WORK

As mentioned above, two sets of experiments were carried out. A total of ten runs was made, with between 6 to 14 readings each. The first eight runs, the first data set, covered the characteristic Reynolds number range 0.5–5100, and the last two runs, the second data set, the range 1.0–11 000. The experimental data are tabulated in Appendix 8, specimen calculations for the data are shown in Appendix 7. The Reynolds number for flow through the tube bank is defined as

$$Re = DG_{max}/\mu \qquad [8.1]$$

where D is the outside diameter of the tube, and is the characteristic length, $G_{max}=\rho V_{max}$, where V_{max} is the maximum velocity is based on the diagonal minimum area available for fluid flow (see Fig. 8.1).

The relation between V_{max} and the velocity in the empty channel, V_s (i.e. the superficial velocity), is

$$V_{max} = V_s \frac{P_t}{2(P_d - D)} \qquad [8.2]$$

where P_t and P_d are the transverse and diagonal Pitch (see Fig. 2.2).

The following were derived for each data point, using a computer program.

Re	Reynolds number
Sc	Schmidt number
Gr	Grashof number
Sh	Sherwood number for each row
Sh_{av}	Average Sherwood number for whole tube bank
$Sh/Sc^{1/3}$	Mass transfer dimensionless group for each row
$(Sh/Sc^{1/3})_{av}$	Average $Sh/Sc^{1/3}$ for whole tube bank
$(Sh/Sc^{1/3})_{mean}$	Mean $Sh/Sc^{1/3}$ for rows 5-10
$(Sh/Sc^{1/3})_{rel}$	Relative $Sh/Sc^{1/3}$ of each row with respect to the $(Sh/Sc^{1/3})_{mean}$
$Re/Gr^{1/2}$	Dimensionless parameter of Mandelbaum et al. [1973]
$Sh/(ScGr)^{1/4}$	Dimensionless parameter of Mandelbaum et al. [1973]

The liquid pressure drop across the tube banks was transmitted to the electronic micromanometer and a U–tube manometer by connecting the pressure tapping points to two glass vessels partly filled by water, as described in section 6.8. The overall pressure drops across the tube banks were measured for the Reynolds number range 70–6300 in two runs.

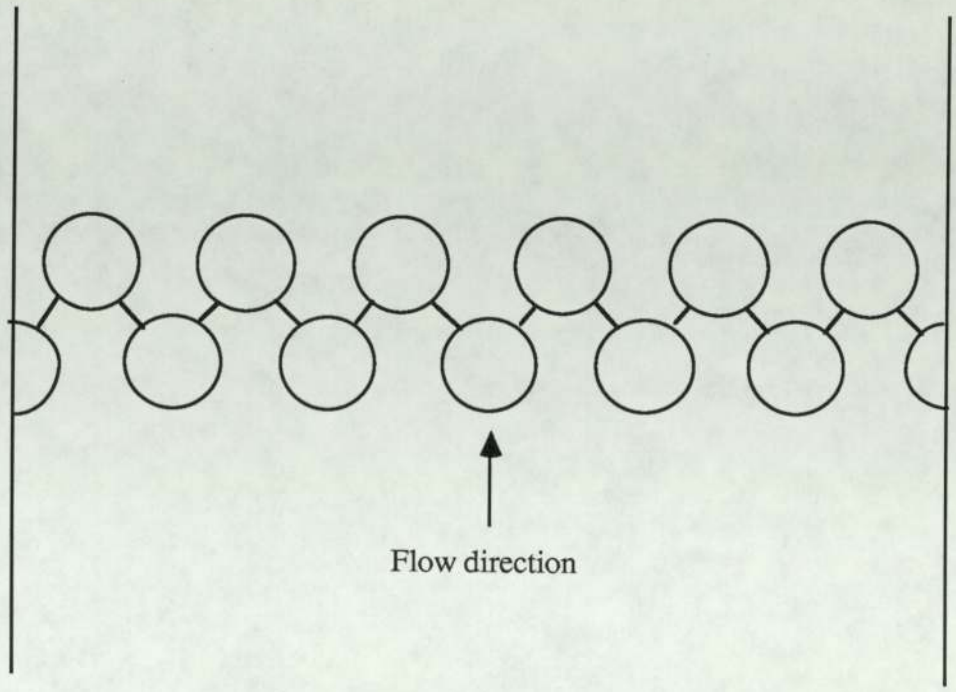

Fig. 8.1 Minimum flow cross section area

8.2 THE PHYSICAL PROPERTIES OF THE ELECTROLYTE

The physical properties (density, ρ, viscosity, μ, diffusivity, D_v, thermal conductivity, k, and specific heat, C_p) of the electrolyte solution of composition 0.01M ferrocyanide, 0.01M ferricyanide and 1.0M sodium hydroxide were obtained for the temperature range 0^oC to 35^oC from references {Washburn [1929], Thorpe and Whitely [1937], Landolt et al. [1950], Eisenberg et al. [1956], Pascal [1956–64] Bazan et al. [1965], Tsederberg [1965], Mandelbaum et al. [1973], Berger et al. [1977] and Weast [1983–84]}.

The Schmidt number, Sc, Prandtl number, Pr, and kinematic viscosity, η, at $20^{o}C$, $25^{o}C$ and $30^{o}C$ were calculated and compared with those obtained from the interpolation formula of Mackley [1973]. Good agreement was observed, and it was decided to use the Mackley formula to obtain the physical properties and dimensionless groups of the electrolyte. The details are given in Appendix 6.

8.3 CORRELATION OF SHELL–SIDE DATA

The design of shell–side tube exchangers requires a knowledge of the shell–side transfer coefficients and pressure drop with respect to the fluid–flow rate.

Shell–side transfer coefficients have been correlated by previous workers. The correlations were listed by Nibber [1981], who used the fact that the transfer coefficient can be made dimensionless by using either $Nu/Pr^{1/3}$ or the Chilton–Colburn j–factor.

Colburn [1933] had correlated the average transfer coefficients and Reynolds numbers for flow across ideal tube banks as

$$Nu/Pr^{1/3} = Re^{b} \qquad [8.3],$$

commonly referred to the Nusselt form (Bergelin et al. [1950]).

The transfer coefficients in the direct heat transfer studies at Delaware University, and mass transfer work by Williams [1962], Mackley [1973] and Prowse[1977] were all expressed mainly in terms of the j–factor. But Nibber [1981]

used $Nu/Pr^{1/3}$ as the dimensionless group to express heat transfer and the analogous $Sh/Sc^{1/3}$ for mass transfer and these replaced the j–factor as the term correlated against the Reynolds number. The relationship between these two dimensionless groups is simple allowing the j–factor data to be converted by equation (8.4).

$$(Sh/Sc^{1/3}) \text{ or } (Nu/Pr^{1/3}) = j_{m \text{ or } h}\, Re \qquad [8.4]$$

The Nusselt approach is adopted in this work.

The friction factor is the dimensionless group used here to express pressure drop. As discussed in Section 2.6, in the correlation of pressure drop data for tube banks, several definitions of friction factor have been used. The correlation used in this work was defined by Grimison [1937] and used by Bergelin and co–workers and is

$$f = \frac{2\Delta P \rho g_c}{4G_{max}{}^2 N'} \qquad [8.5]$$

where N' is the number of major restrictions encountered in the flow through the bank. For the staggered banks, when the minimum flow area is based on the diagonal joining the centres of the nearest neighbour tubes in adjacent transverse rows, N' is equal to NL–1 , where NL is the number of transverse rows.

8.4 DISCUSSION OF EXPERIMENTAL RESULTS

8.4.1 GENERAL

As already stated, mass transfer measurements were made on a staggered ideal tube bank, containing sixty–six 3 mm OD nickel tubes in twelve rows. These investigations were carried out for electrolyte flow rates in the range of 1.5×10^{-3} to 42 litres per minute, corresponding to Reynolds numbers in the range 0.5 to 11 000.

Mass transfer coefficients for each row in turn and thus for the whole tube bank have been calculated. For comparison, mass transfer coefficients are expressed in the form $Sh/Sc^{1/3}$, and heat transfer coefficients in the form $Nu/Pr^{1/3}$, and correlated against the characteristic Reynolds number, based on the diagonal minimum flow area (see Fig. 8.1).

The logarithm of the average $Sh/Sc^{1/3}$ is plotted against the logarithm of the Re for eight runs (i.e. the first set of experimental results) in Figure 8.2 and for runs 1.9 and 1.10 (the second set of experimental results) in Figure 8.8.

The data from this work are compared with those of Bergelin et al. [1950 and 1957], for a virtually identical heat exchanger model (Figs. 8.3, 8.10). Both data–sets are also compared with the ESDU correlation in Figures 8.4 and 8.11.

The role of natural convection was investigated using data obtained in this work and those of Bergelin, Colburn and Hull [1950] (Figs. 8.6–8.7 and 8.12)

The mass transfer data were analysed in the form of individual, relative row values of the dimensionless group ($Sh/Sc^{1/3}$) for the tube bank and are compared to each other. Row–by–row variation and also entrance and exit effects are set out in Figures 8.13–8.16.

As already noted, the pressure drop across the tube banks have been investigated in the Reynolds number range of 70–6300 (Fig. 8.17). The pressure drop data are compared with the data of Bergelin et al. [1950] in Figure 8.18.

8.4.2 AVERAGE TRANSFER COEFFICIENTS FOR NORMAL TUBE BANK IN THE REYNOLDS NUMBER RANGE 0.5–5100

The constant bulk and surface concentrations of the reacting ions in the electrochemical system give a situation analogous to the limiting case of truely isothermal conditions in heat transfer. For such systems it is perfectly justifiable to derive average transfer coefficients from local values by an unweighted averaging procedure. Thus tube bank average dimensionless groups were calculated from all the individual row values using a simple arithmetical average.

The average mass transfer coefficients in the form of the dimensionless group $Sh/Sc^{1/3}$ were plotted against a characteristic Reynolds number. The correlation between transfer coefficients and Reynolds numbers are shown in the logarithmic plots for all runs in Figure 8.2, i.e. the first data set. The internal consistency of the eight runs is good.

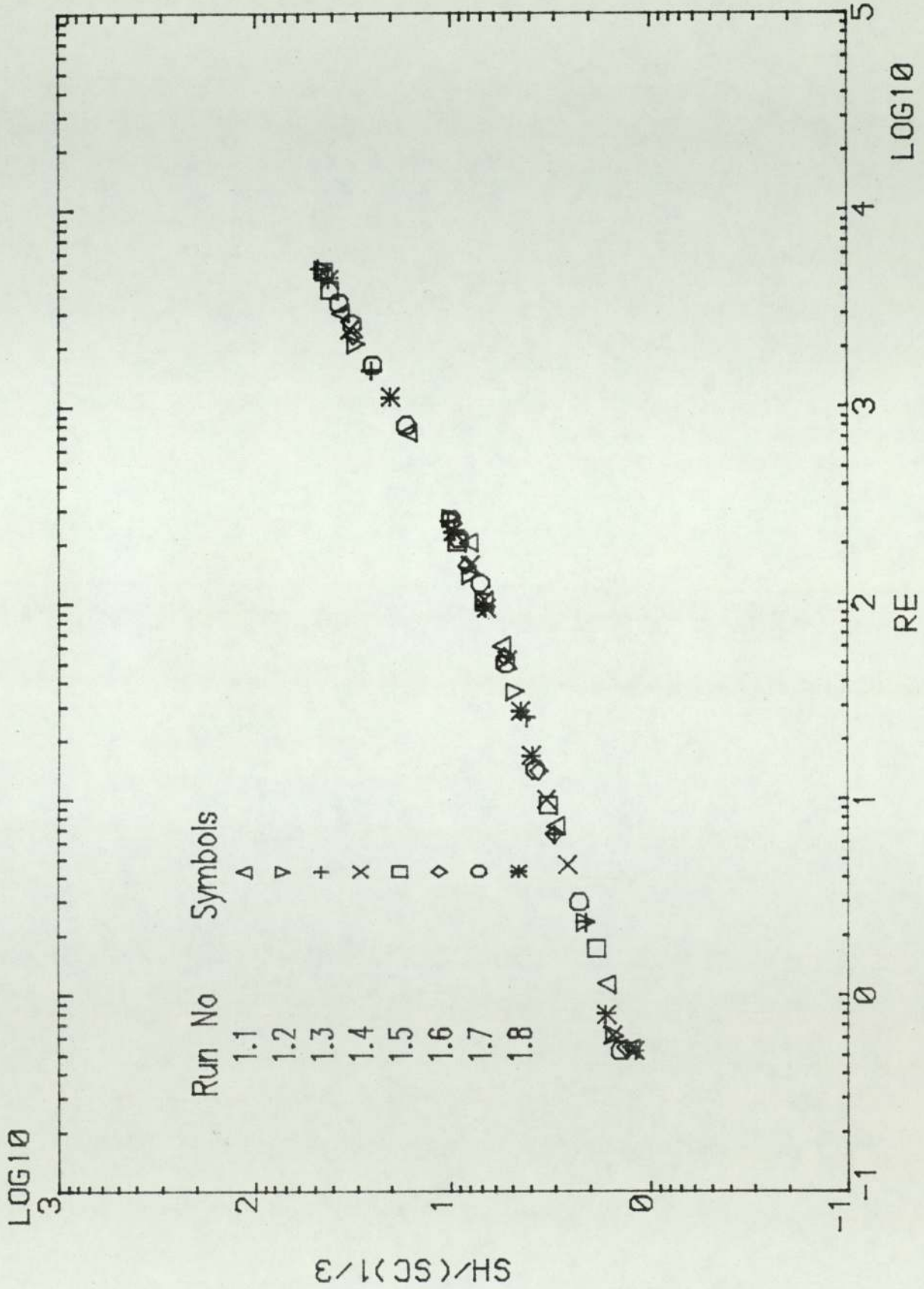

Fig. 8.2 Results of the first data set as Sh/(Sc)1/3 versus Re

8.4.2.1 COMPARISON OF THE FIRST SET OF EXPERIMENTAL RESULTS WITH BERGELIN'S DATA

Data of this work are compared with those of Bergelin, Colburn and Hull [1950] and Bergelin, Leighton, Lafferty and Pigford [1957], obtained in heat transfer studies at the University of Delaware. Bergelin used a similar tube bank model with the same tube arrangement but on a larger scale. Comparison with both the heating and cooling results of Bergelin et al. [1950] show good agreement across the whole Reynolds number range of that work, which was between 1.44 to 560. The comparisons with the results of the cooling runs and the heating runs of Bergelin et al. [1957] shows good agreement at low Reynolds numbers but the agreement becomes poorer at higher flow rates. The comparison with all the data of Bergelin and co–workers is shown in Figure 8.3.

8.4.2.2 COMPARISON OF THE FIRST SET OF EXPERIMENTAL RESULTS WITH THE ESDU CORRELATION

The results of the first set of experiment are also compared with the EDSU correlation [1973] in Figure 8.4. It can be seen again the agreement at higher Reynolds numbers is not exact.

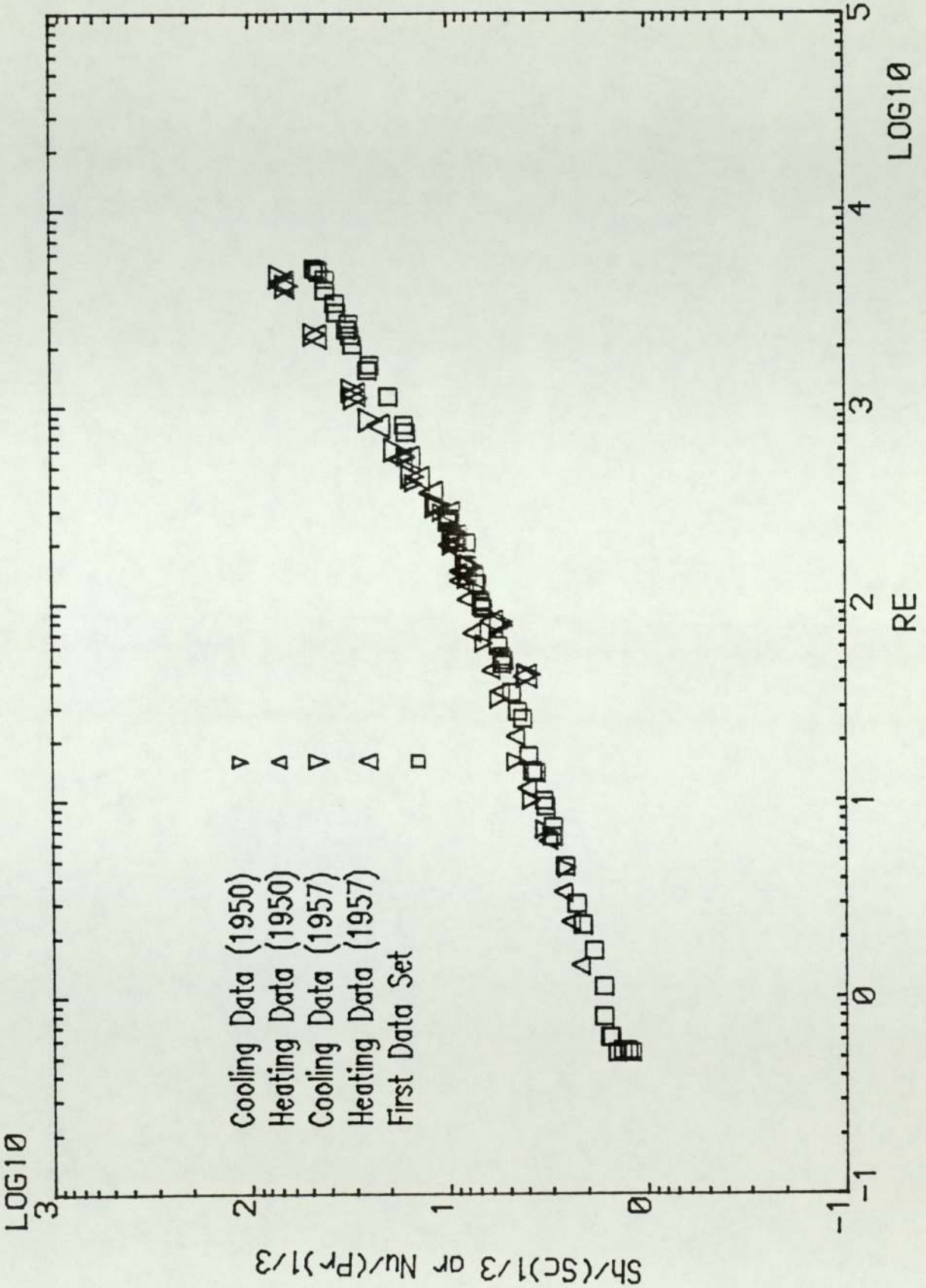

Fig. 8.3 Comparison of First data set with the Bergelin data

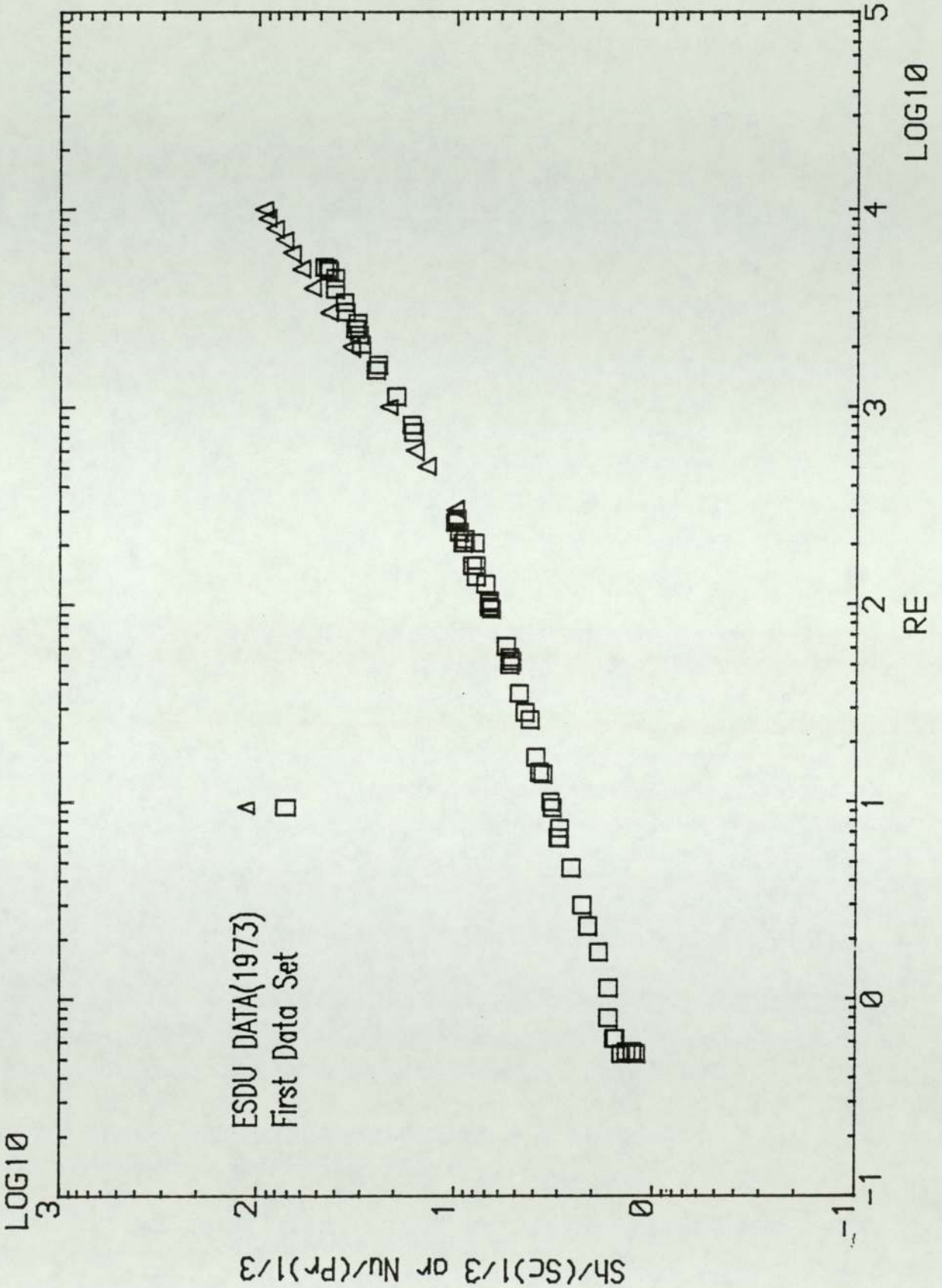

Fig. 8.4 Comparison of First data set with ESDU correlation

8.4.2.3 ROLE OF NATURAL CONVECTION

Natural convection in heat transfer is produced by fluid motion brought about solely by differences of density created by temperature gradients. In the case of mass transfer an analogous situation exists where natural convective mass transfer is produced by density differences due to concentration gradients. Mackley [1973] and Nibber [1981] both found a discrepancy at low Reynolds numbers between j_h and j_m factors. They postulated that perhaps natural convection played a part here, but had different effects for heat transfer as compared to mass transfer, thus creating the disagreement.

Therefore in the present work the role of natural convection at low Reynolds number was investigated, using the method of analysis of Mandelbaum et al. [1973]. They had investigated the role of natural convection at low Reynolds number in packed beds, and developed a method of analysis using the dimensionless parameters $Sh/(ScGr)^{0.25}$ and $Re/Gr^{0.5}$, to investigate the relationship between natural and forced convection. Buoyancy forces play a significant role at values of $Re/Gr^{0.5}$ lower than 0.1 for both aiding and opposing flows. The correlation of mass transfer data of Mandelbaum's work for aiding flow is shown in Figure 8.5, it can be seen that there is a horizontal portion at low Reynolds numbers where natural convection is dominant.

A similar plot for the results of this work is given in Figure 8.6, and shows no horizontal portion at low Reynolds numbers, i.e. natural convection is not important. The lowest value of $Sh/(ScGr)^{0.25}$ is 0.94 on this plot and its value at zero Reynolds number (no flow and therefore natural convection takes place) is 0.6 which is lower than the value of $Sh/(ScGr)^{0.25}$ at the lowest experimental Reynolds number, i.e. there is no horizontal line evident in the experimental region.

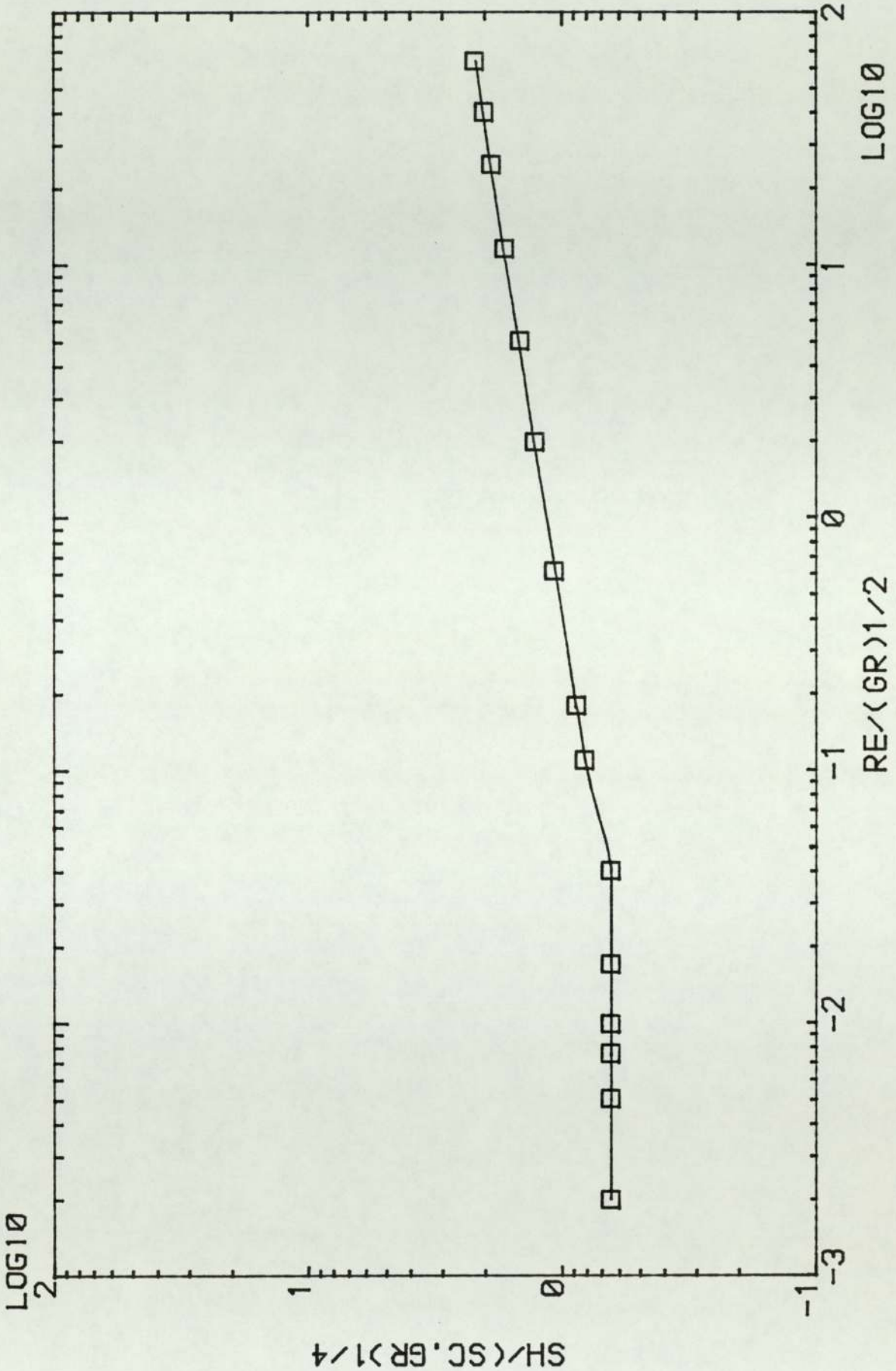

Fig. 8.5 Mass transfer results of Mandelbaum [1973]

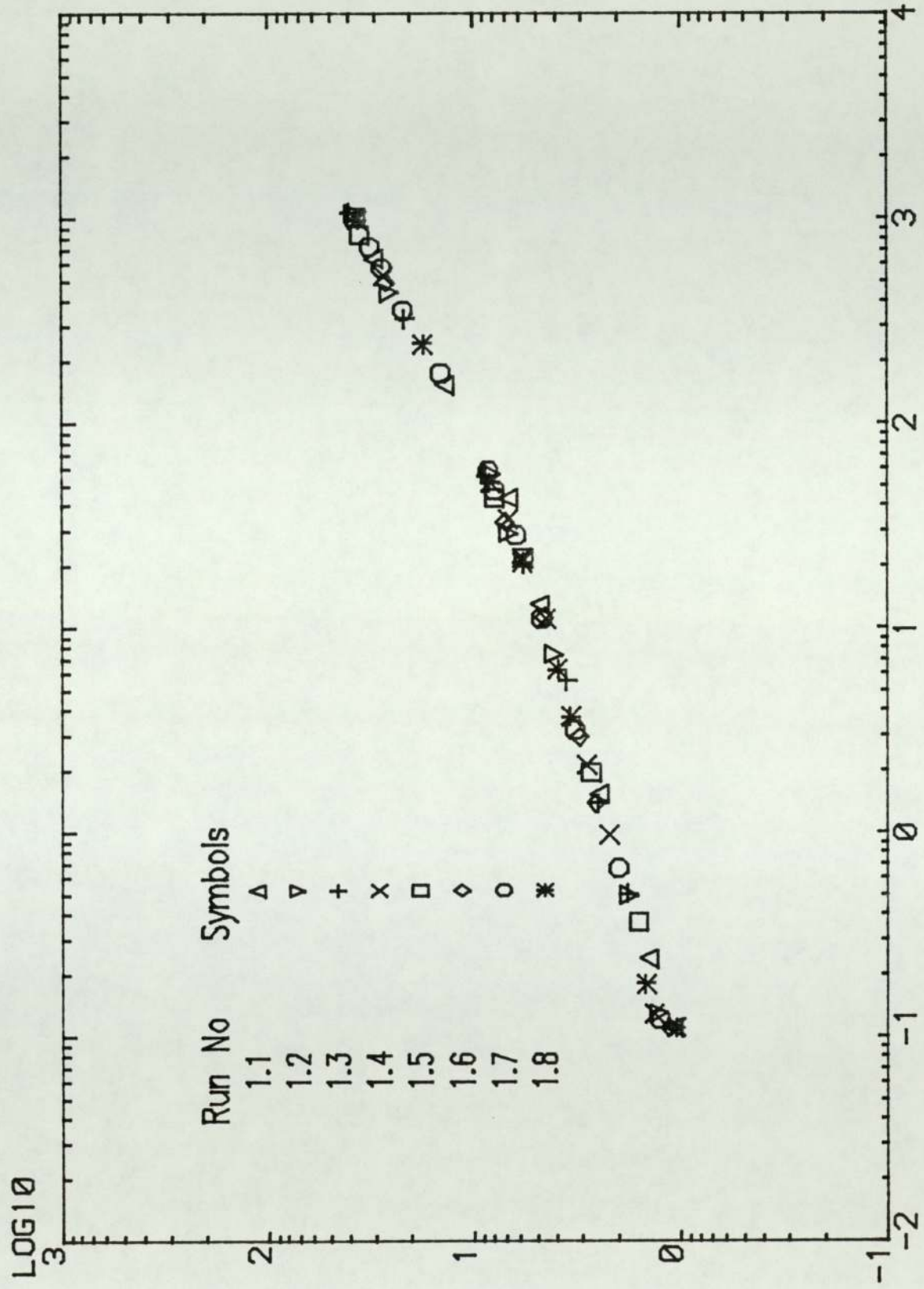

Fig. 8.6 Test for role of natural convection of First data set

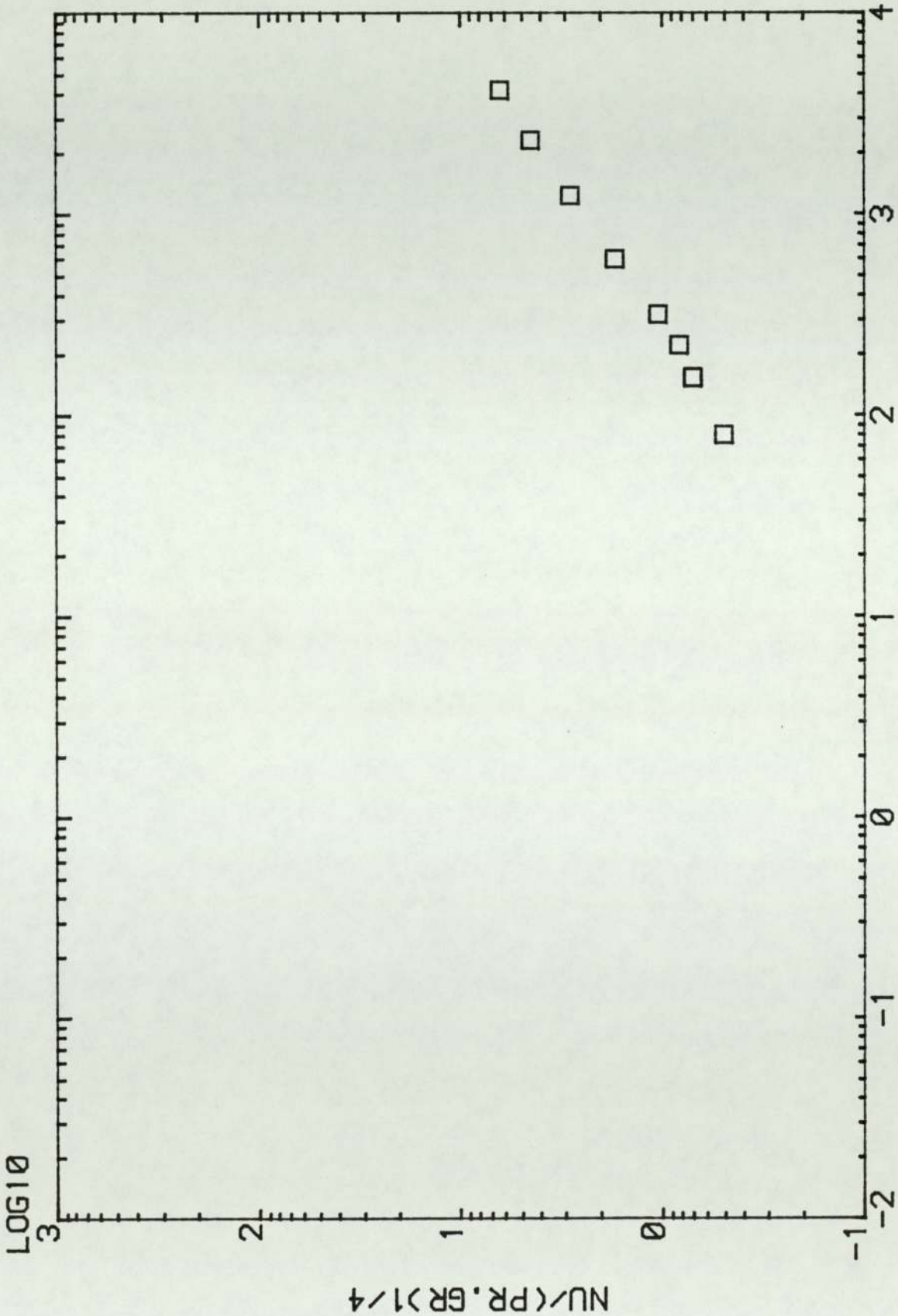

Fig. 8.7 Test for role of natural convection for the Bergelin data

Bergelin et al. [1950] commented that natural convection was not important in their heat transfer situation, and an analysis of their data using the Mandelbaum technique is given in Figure 8.7 and confirms their statement.

Comparison of the mass transfer data obtained here with those of Bergelin and co–workers shows no discrepancy at low Reynolds numbers in contrast to the results of Mackley and Nibber, and confirms the results of this analysis.

8.4.3 AVERAGE TRANSFER COEFFICENTS FOR NORMAL TUBE BANK IN THE REYNOLDS NUMBER RANGE 1.0–11 000

In the second set two runs were carried out. The average values of the mass transfer dimensionless group ($Sh/Sc^{1/3}$) for the whole tube bank have been calculated for the range of Reynolds number 1.0–11 000. The log–log graph of these groups versus Reynolds number for the second set of experimental results (run numbers 1.9 and 1.10) are plotted in Figure 8.8. The agreement between the two runs is good. The close agreement demonstrates the consistency of data obtained using this electrochemical technique.

8.4.3.1 COMPARISON OF THE SECOND EXPERIMENTAL RESULTS

The second set of experimental results are compared with the first set, Bergelin's data and the ESDU correlation in the following section.

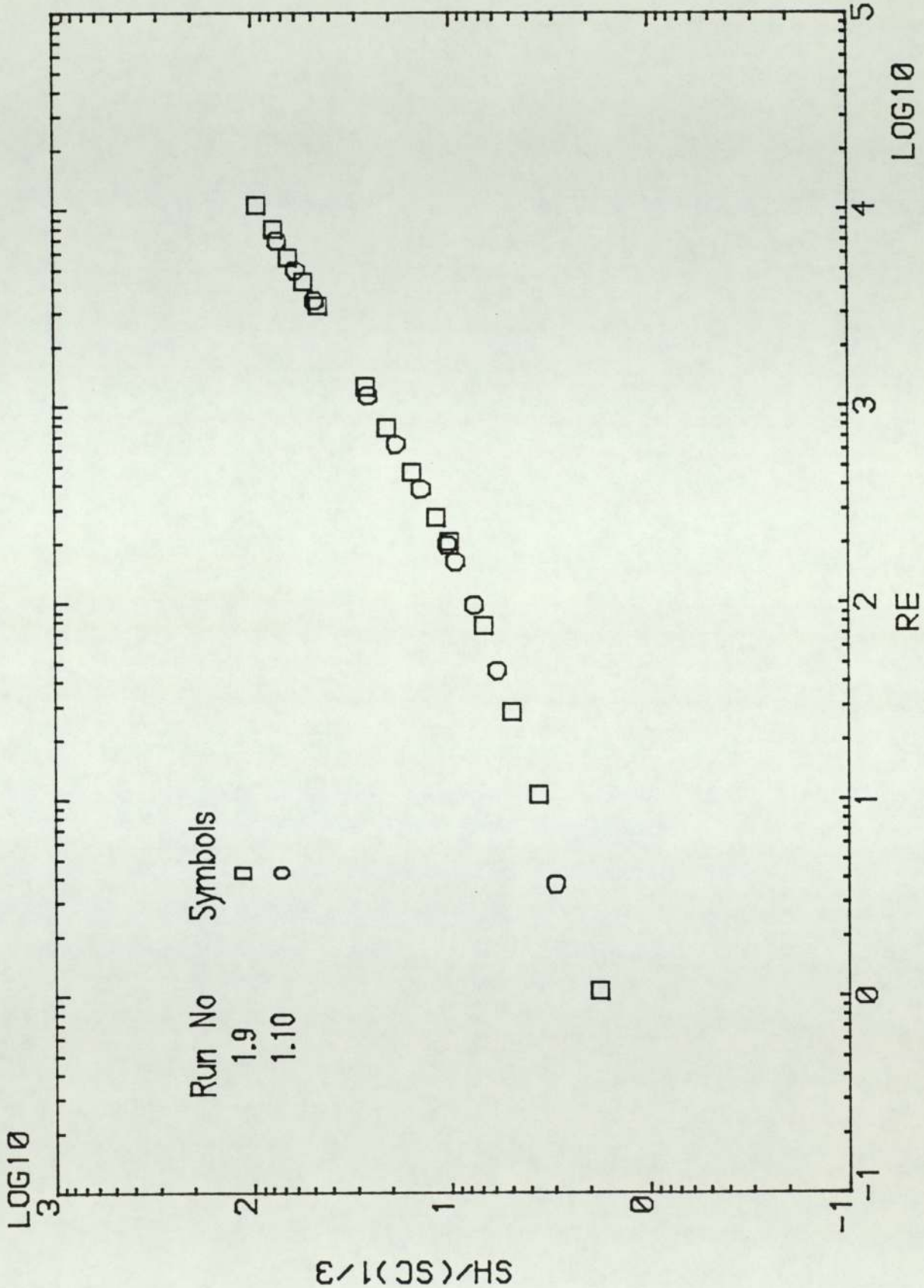

Fig. 8.8 Results of the second data set as Sh/(Sc)1/3 versus Re

8.4.3.1.1 COMPARISON WITH THE FIRST EXPERIMENTAL RESULTS

The results of runs 1.9 and 1.10 were compared with those of the first experimental results, runs 1.1–1.8,. The comparison is shown in Figure 8.9. The agreement between the two results at low Reynolds number is good but as the Reynolds number increases the agreement becomes poorer.

8.4.3.1.2 COMPARISON WITH BERGELIN'S RESULTS

The second set of results are compared with the data of Bergelin et al. [1950 and 1957] in Figure 8.10. In addition to good agreement at low Reynolds numbers, there is good agreement at high Reynolds numbers as well, unlike the first set of results, which show poor agreement at high Reynolds number. The maximum difference is about 15% between the two curves at the high Reynolds numbers. However this difference is within the combined experimental error for each set of runs.

8.4.3.1.3 COMPARISON WITH THE ESDU CORREALTION

The second set of results are compared with the ESDU [1973] correlation in Figure 8.11, and the agreement over all the Reynolds number range is good, especially at high Reynolds number.

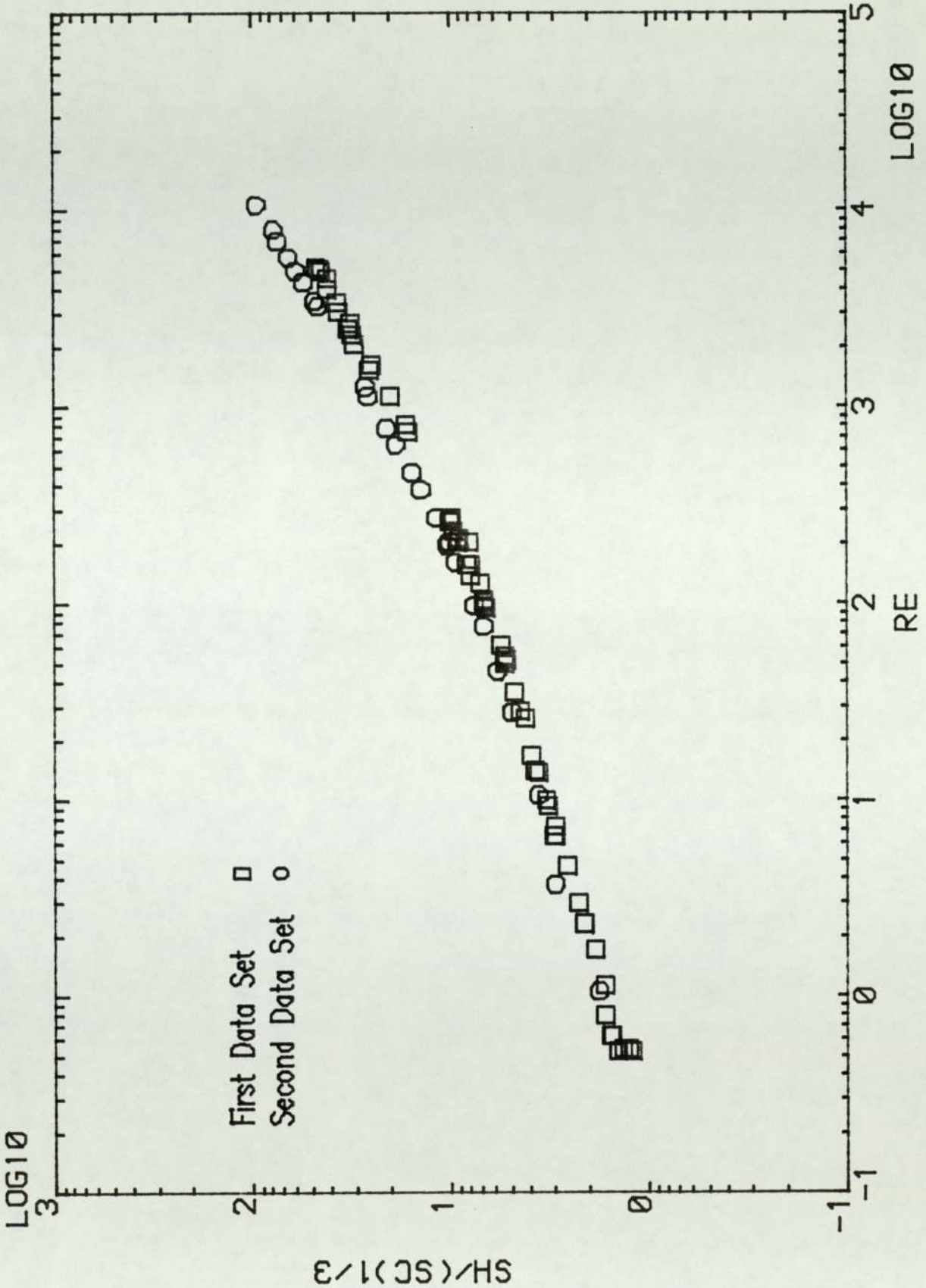

Fig. 8.9 Comparison of First and second data sets

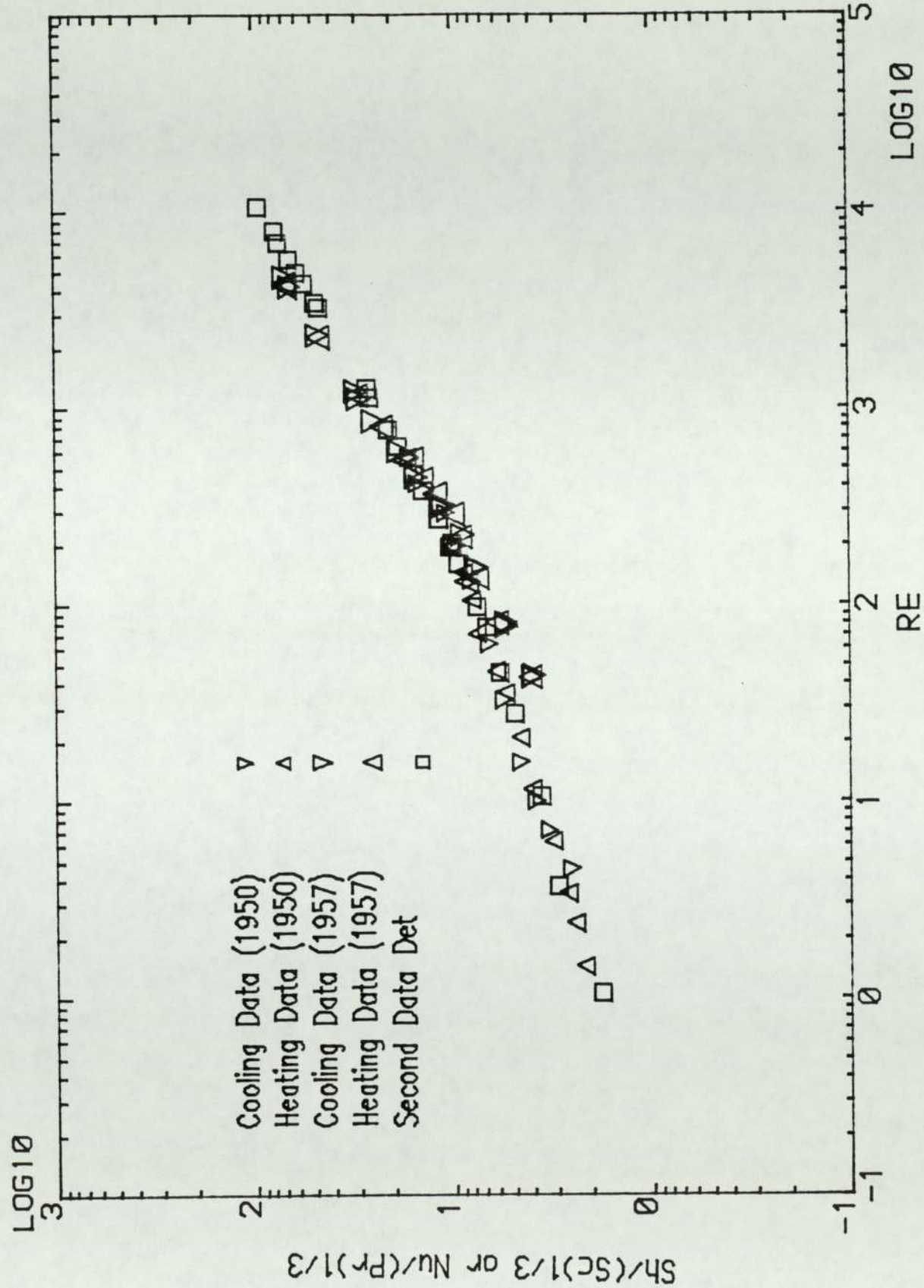

Fig. 8.10 Comparison of second data set with the Bergelin data

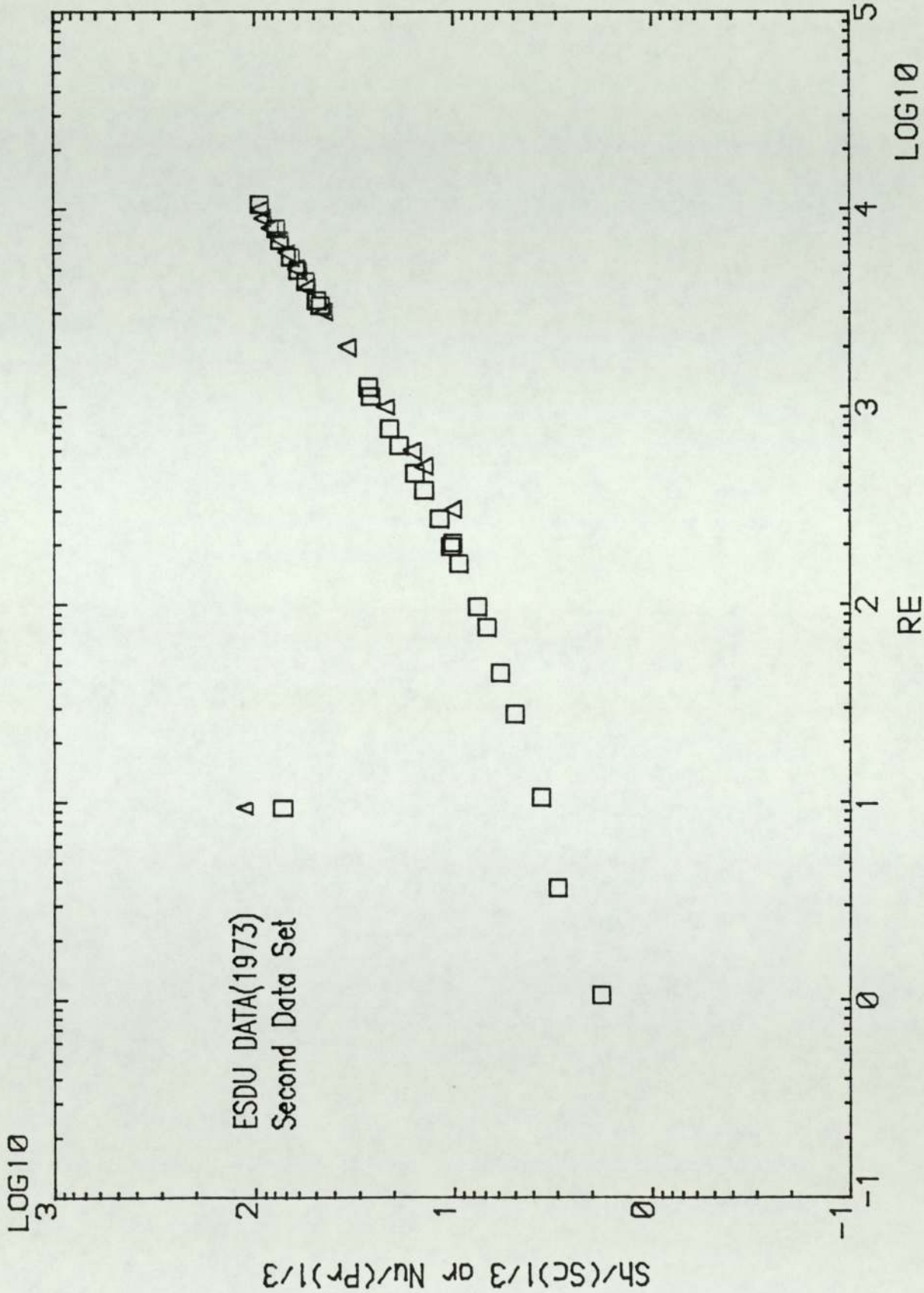

Fig. 8.11 Comparison of second data set with ESDU correlation

The better agreement obtained in the second set of results with the data of previous workers is attributed to changes in both the construction of the rig and in the activation procedures.

As discussed in Chapter 6 the anodes were placed closer to the cathodes, and there was no difficulty in obtaining the plateaux, especially at high Reynolds numbers. It was therefore easier to obtain the limiting currents and more accurate results were obtained.

The surfaces of the cathodes, i.e. the tube bank, were cleaned more effectively . Tube bundles were washed with 10% HCl solution before starting the experiment and the period of the activation process was longer than in the first experiment, i.e. 20 minutes as opposed to 10 minutes.

Accordingly, the second set of experimental results are regarded as being more accurate and reliable and therefore will be used in subsequent data analysis.

8.4.3.2 ROLE OF NATURAL CONVECTION

For these results the role of natural convection was investigated as before. Again as shown in Figure 8.12 there is no horizontal line at low Reynolds numbers, therefore natural convection is not important .

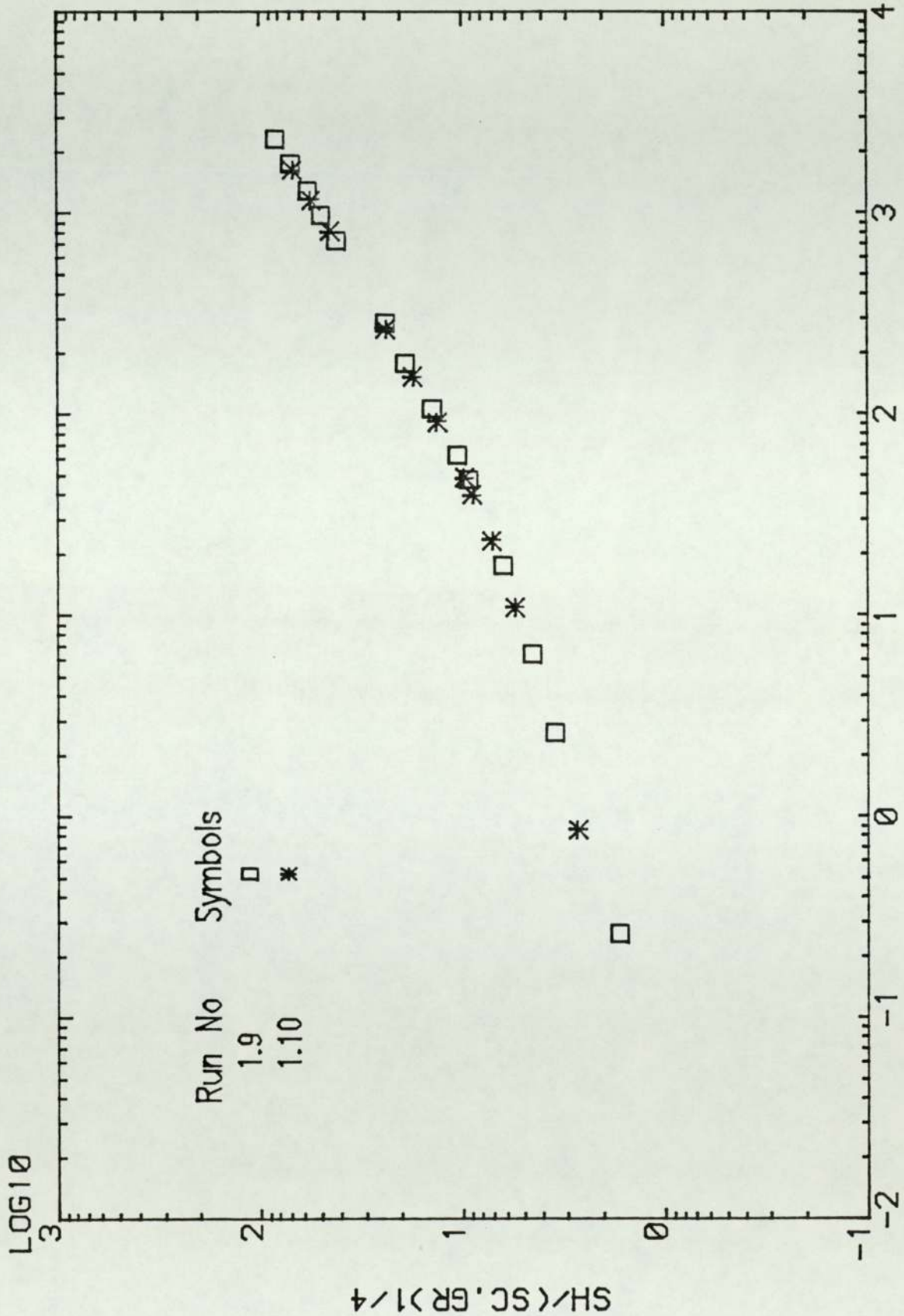

Fig. 8.12 Test for role of natural convection of second data set

8.4.4 VARIATION IN TRANSFER COEFFICIENTS FROM ROW TO ROW

Previous workers, as discussed in Chapter 2, have shown an increase in heat transfer over the first three rows, reaching steady values after row 3. These results compare well with the work shown here where the transfer coefficient increases over the first three rows, and remains constant until row 11 or 12 depending on the Reynolds number. The last row, i.e. row 12, shows a considerable decrease.

The individual row dimensionless mass transfer rates ($Sh/Sc^{1/3}$) were studied in order to provide an insight into row–to–row variations.

Since the transfer coefficients of rows 3 to 11 are almost identical, to show the differences better, the variation of transfer coefficients of rows (run 1.9) 1, 2, 3, 6 and 12 against Reynolds number are shown in Figure 8.13. These results are plotted in Figure 8.14 by changing the origin. The origin was changed to a new position with a displacement of 17% on the co–ordinate for each row to provide a clear representation of the results.

The entrance and exit effects on transfer coefficients of staggered normal tube banks have been investigated for runs 1.9 and 1.10 over the range of Reynolds numbers used. The variation of mass transfer dimensionless group, $Sh/Sc^{1/3}$, with respect to row number is shown in Figure 8.15 for the Reynolds number range $1.0<Re<1000$ and in Figure 8.16 for $1000<Re<11\,000$ for constant Reynolds numbers.

The transfer coefficients of each row at constant Reynolds number and also the

ratio of the transfer coefficients expressed as $Sh/Sc^{1/3}$ for a given tube row to the mean $Sh/Sc^{1/3}$, i.e. $(Sh/Sc^{1/3})_{rel}$ are tabulated in Appendix 8. The mean value of $Sh/Sc^{1/3}$ were calculated for rows 5–10 using a simple arithmetical average since the results from these rows are unaffected by the entrance and exit conditions.

As can be seen the variation in mass transfer coefficients over the first three rows is greater for higher Reynolds numbers. The ratio of transfer coefficients ($(Sh/Sc^{1/3})_{rel}$) for the first row was shown to vary between 56% to 85% for the range of Reynolds numbers 1.0–11 000. The difference in $Sh/Sc^{1/3}$ between the first row and subsequent rows is to be expected as the flow becomes more turbulent inside the tube banks (Section 3.2).

The last row, i.e. row 12, shows a decrease of approximately 14% across the whole range of Reynolds numbers, i.e. the exit effect at the last row seems to be independent of the Reynolds number, but at Reynolds numbers greater than 1000 the 11th row shows a slight decrease.

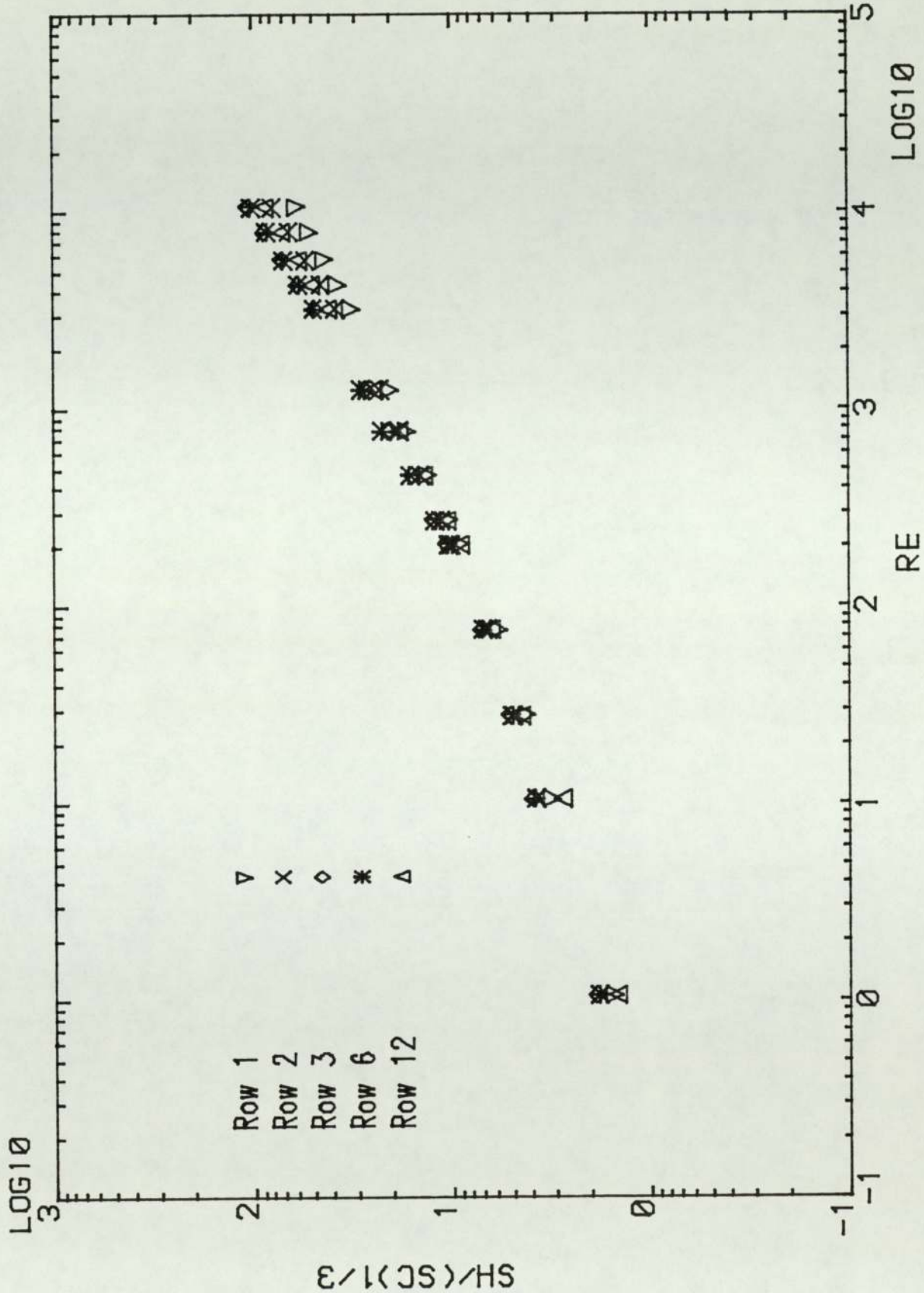

Fig. 8.13 Row-by-Row varaition of transfer coefficients For Model 1

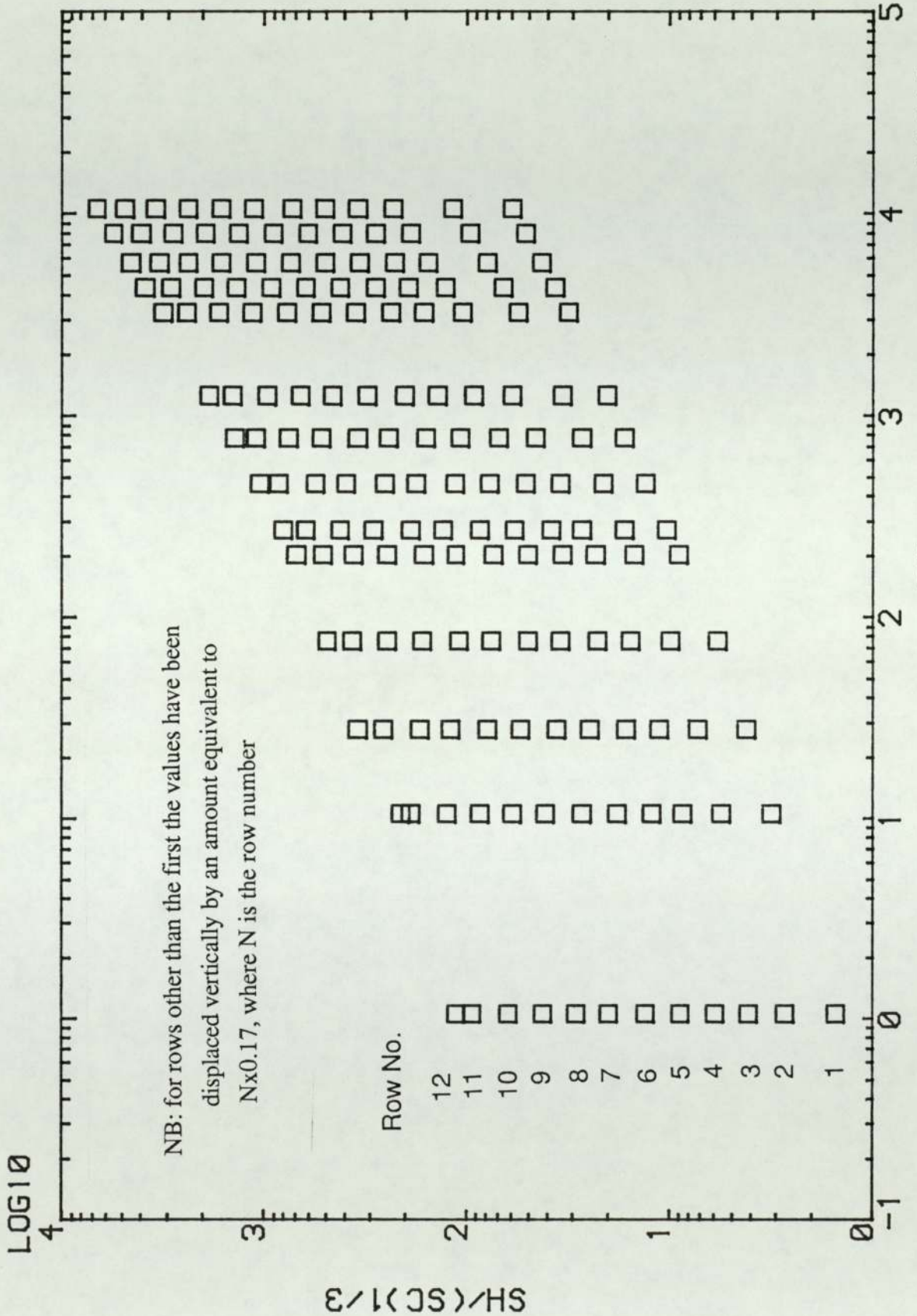

Fig. 8.14 Schematic representation of row-by-row variations by successive displacement of Sh/(Sc)1/3 values

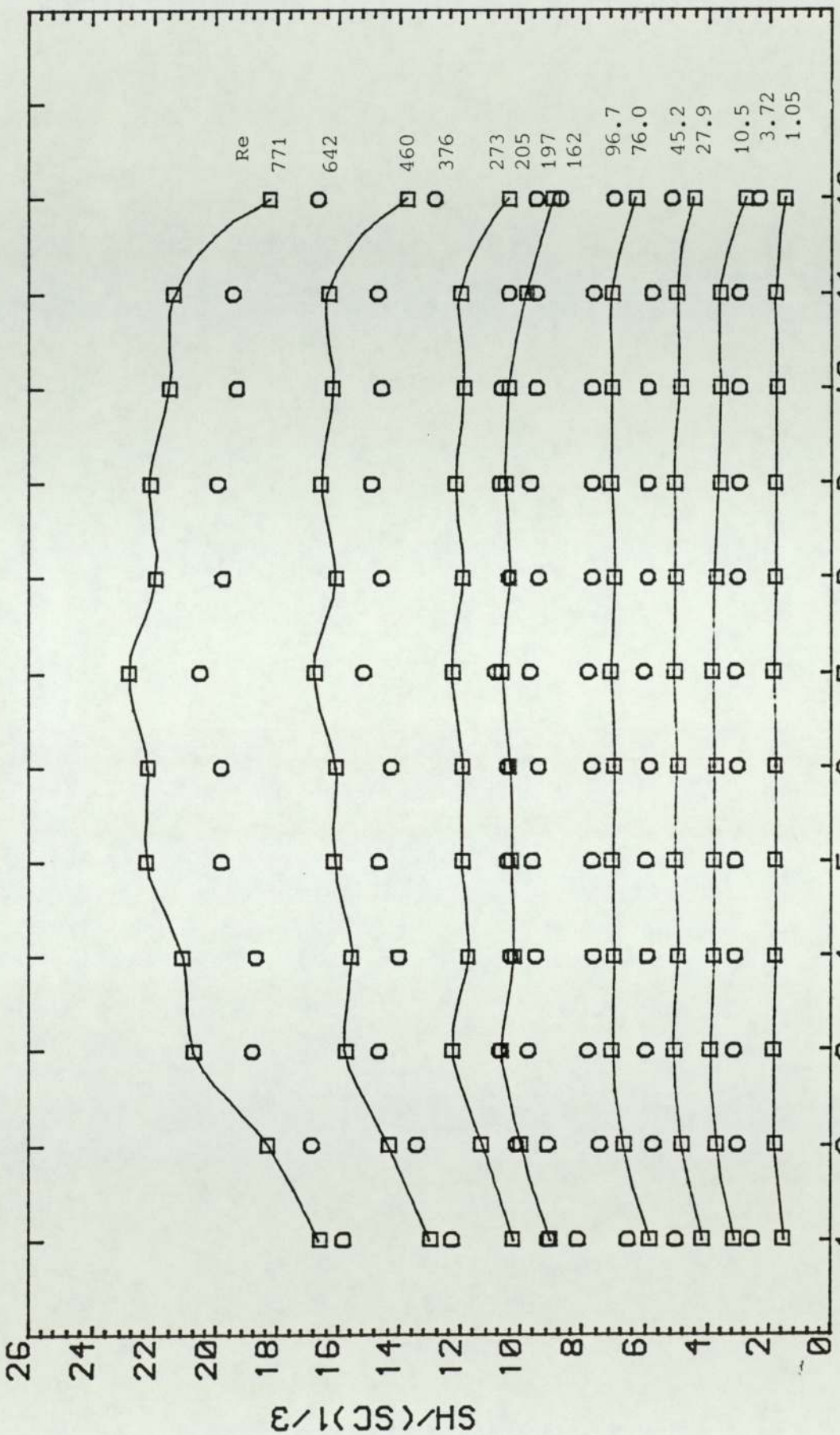

Fig. 8.15 Row-by-row variation of transfer rate $1.0 < Re < 1000$

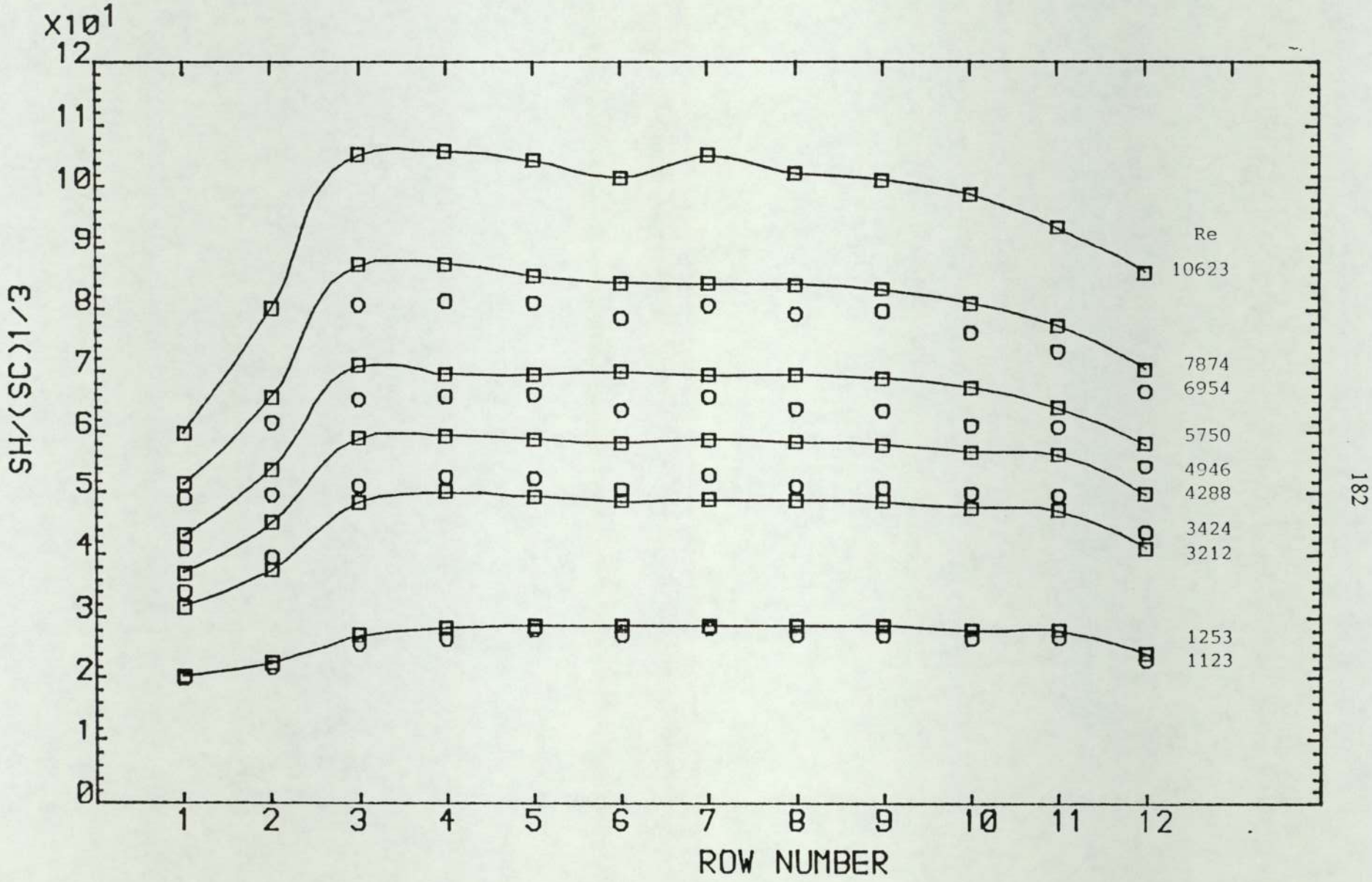

Fig. 8.16 Row-by-row variation of transfer rate 1000<Re<10 600

8.4.5 PRESSURE DROP ACROSS IDEAL NORMAL TUBE BANKS

The pressure drop data are presented as a logarithmic plot of friction factor, f, versus Reynolds number in Figure 8.17 for runs P1.1 and P1.2 for the Reynolds numbers range 70–6300. It can be seen that f and Re can be correlated by two straight lines. In laminar flow ($Re \leq 200$) $f = 10Re^{-1}$ and in the transient and turbulent flow regions, $f = 0.32Re^{-0.176}$. The results are compared with the cooling and heating data of Bergelin, Colburn and Hull [1950] in Figure 8.18. It can be seen that in spite of the difference in size between the models there is good agreement, especially since the model used in this study was so much smaller than the Bergelin model. The good agreement obtained shows that very similar hydrodynamic conditions held in the two programmes of work.

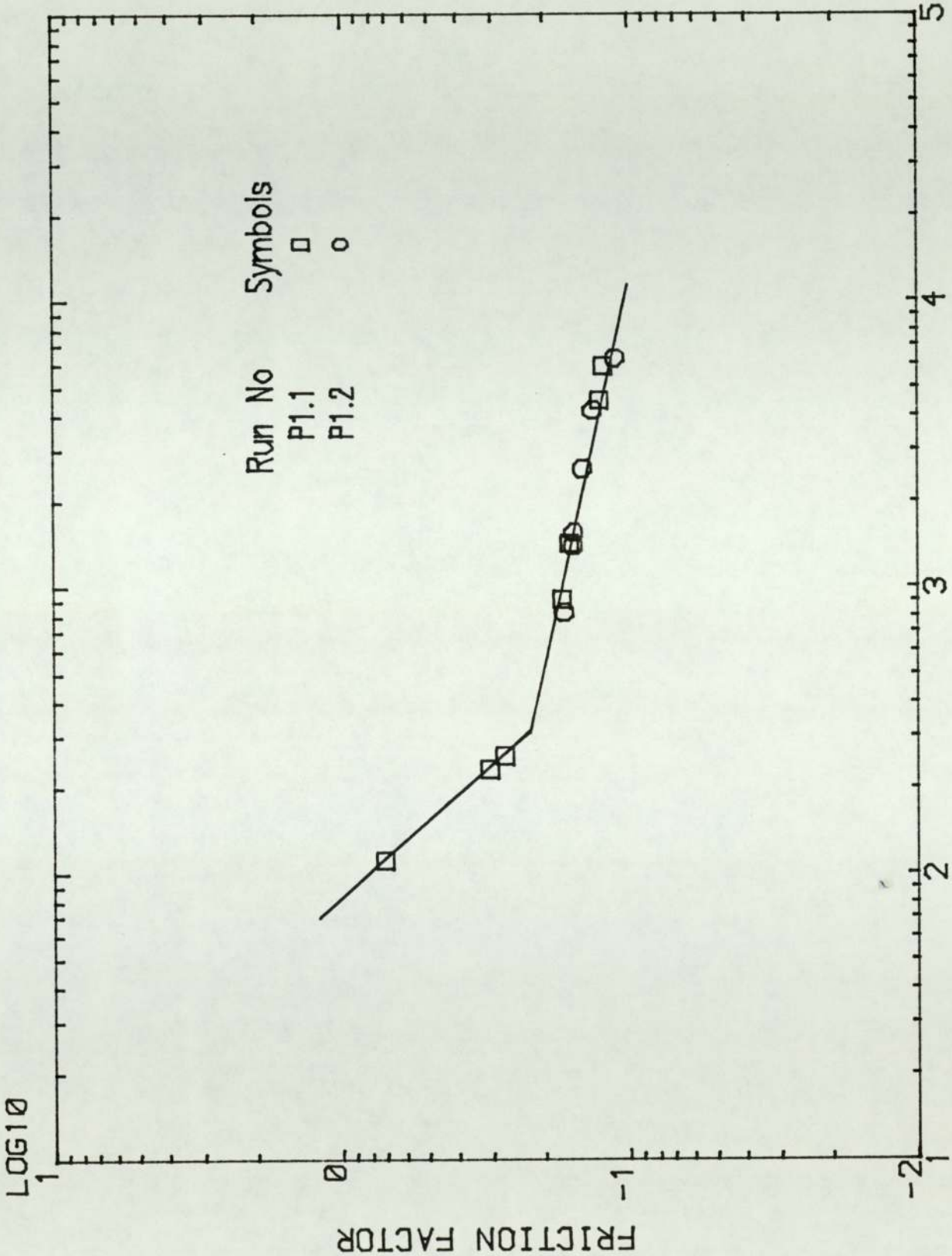

Fig. 8.17 Pressure drop results For Model 1

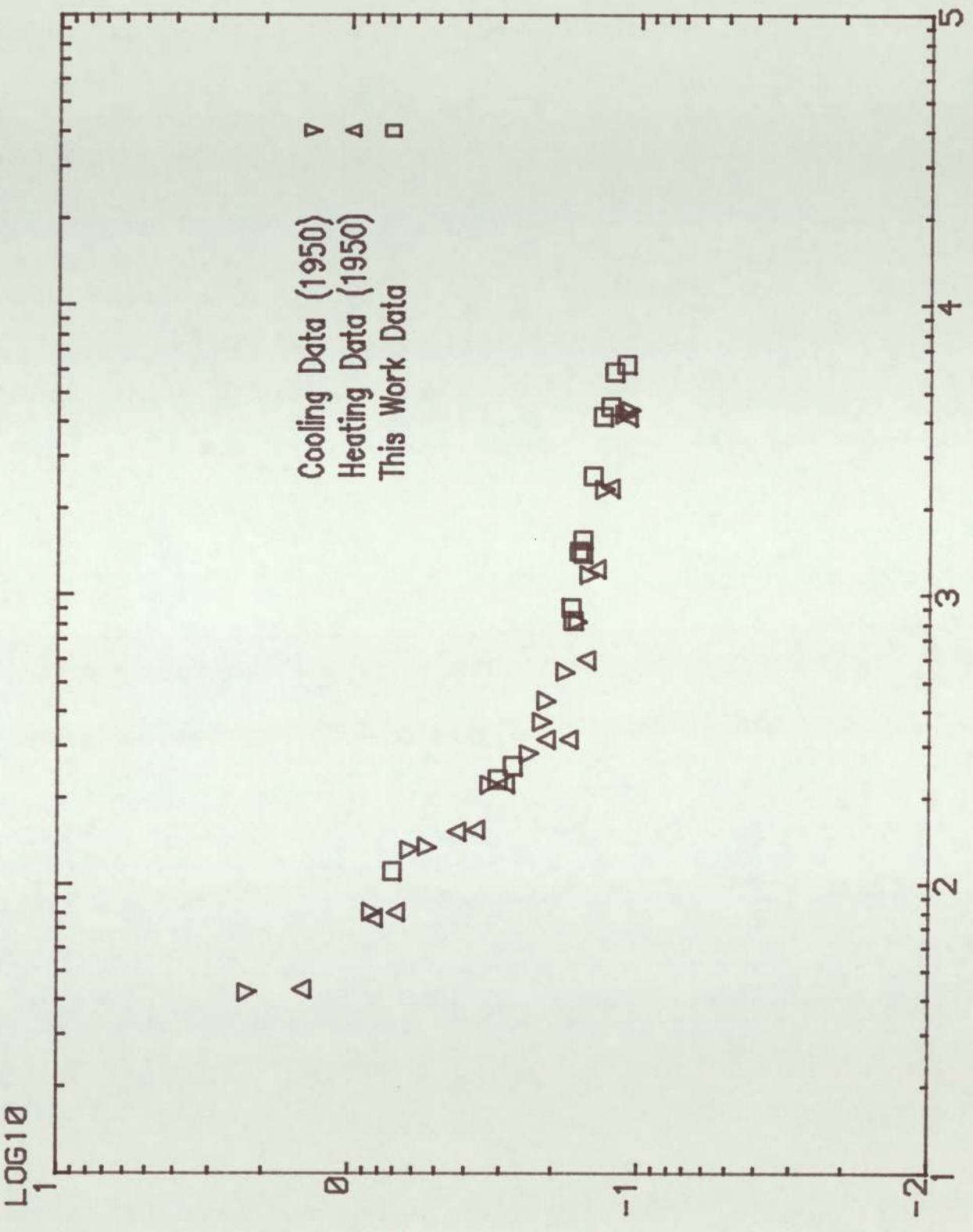

Fig. 8.18 Comparison of pressure drop results with the Bergelin data

8.5 CONCLUSIONS

A number of points arise from the work covered in this chapter.

1. Transfer coefficient measurements have been made in a single piece of work over a wider Reynolds number range than in earlier work, notably that of Bergelin and co–workers, and show a smoother variation with Reynolds number than the two separate Bergelin studies. The corresponding friction factor measurements are in close agreement. This work forms the base case for the subsequent study on inclined tube banks.

2. An auxiliary point is the confirmation of the need for careful electrode preparation, and in particular of an adequate activation period.

3. The studies on the effect of natural convection using the method of analysis of Mandelbaum et al. [1973] showed that natural convection is not important at low Reynolds numbers, thus confirming the earlier view of Bergelin et al. [1950] and removing the queries raised by Mackley [1973] and Nibber [1981].

4. The row–by–row results are in good agreement with those of previous workers. Again the data obtained here cover a wider range of Reynolds numbers than previous investigations and found the following.

i) There is an increase in transfer coefficients over the first three rows, since turbulence created by the first few rows of the tubes causes an increase in the transfer coefficients on inner rows, although the transfer coefficients become more or less

constant after the first three rows until the 11th or 12th row depending on Reynolds number.

ii) The entrance effect on the transfer coefficients was shown to be greater at higher Reynolds numbers. It seems that at higher Reynolds numbers, the turbulence created by the first few rows of tubes is greater.

iii) The small variation of exit effects with Reynolds number is shown in that the ratio of 12th row transfer coefficients to the mean coefficient is virtually the same for all Reynolds numbers. But at Reynolds numbers greater than 1000 the 11th row shows a slight decrease in the equivalent ratio.

CHAPTER NINE

SHELL–SIDE INVESTIGATION IN INCLINED TUBE BANKS

9.1 INTRODUCTION

In this chapter the experimental results from three inclined tube banks are discussed and compared with those of the normal tube bank. The results have been obtained on staggered tube banks in the Reynolds number range $1.0<Re<12\ 600$. The yaw angle was varied between $45^{o}\leq\varphi\leq90^{o}$ to examine the influence of inclination angle on transfer coefficients in and pressure drop across all four tube banks. The row–by–row variation and entrance and exit effects are observed.

9.2 SCOPE OF EXPERIMENTAL WORK

Three models (Models 2, 3 and 4) were used. The Model 2 tube bundle was virtually identical with the Model 1 nomal rectangular tube bundle already described, except that it was so constructed that the tubes were at 20^{o} to the horizontal. For Models 3 and 4 the angle was 32.5^{o} and 45^{o} respectively. The angle of attack (yaw angle) to the fluid flow was therefore 70^{o} for Model 2, 57.5^{o} for Model 3 and 45^{o} for Model 4 (see Fig. 6.7).

Each model consisted of a rectangular perspex box containing sixty–six 3 mm OD nickel tubes, with exposed lengths of 21.28 mm, 23.71 mm and 28.28 mm arranged in twelve rows. The arrangement of tubes was staggered with a rotated square pitch, with a P/D ratio of 1.25.

Six runs with 9 to 14 readings each were carried out on each model to measure mass transfer coefficients. The first four runs formed a first set of runs, and covered the Reynolds number range from 2 to 5500. The last two runs formed a second set and covered the range of Reynolds number 1.0 to 12 600. All the parameters set out in Section 8.1 were calculated from each data point for each inclined tube bank. The methods of calculation for the data are given in Appendix 7, with the data being tabulated in Appendix 8.

The characteristic area used for the Reynolds number for the inclined tube banks is the minimum free area of flow found by projection to the horizontal plane, i.e. it is identical to that for the normal tube bundle. This is the same choice of characteristic area used by Ornatski [1940] and Antonopoulos [1985]. Thus the Reynolds number for flow through the inclined tube bank is defined as

$$Re = DG_{max}/\mu \qquad [9.1]$$

where $G_{max} = \rho V_{max}$ = maximum mass flow velocity, i.e. the mass flow rate per unit area projected on the horizontal plane where the velocity is maximum, D is the outside diameter of the tube, ρ is the density of the fluid, and V_{max} is the maximum velocity based on the minimum area available for fluid flow. V_{max} is related to the velocity in

the empty channel, V_s (i.e. the superficial velocity) by

$$V_{max} = V_s \frac{P_t}{2(P_d - D)} \qquad [9.2]$$

where P_t is the transverse pitch and P_d is the diagonal pitch (see Fig. 2.2).

The overall pressure drops across the models were measured for the Reynolds number range 200 <Re<6300 in two runs.

As discussed in Section 8.3 the mass transfer data were expressed in the form of the dimensionless group $Sh/Sc^{1/3}$, and pressure drop in the form of the friction factor $f=2\Delta P\rho g_c/4G_{max}{}^2N'$.

The tube diameter was chosen as the characteristic length in the Reynolds number as well as in the Sherwood number, Sh.

9.3 DISCUSSION OF EXPERIMENTAL RESULTS

9.3.1 GENERAL

In the discussion of the experimental results, transfer coefficients for inclined tube banks and their comparison with those for the ideal normal tube bank are treated first, pressure drop next.

The variation of mass transfer coefficient (in the form $Sh/Sc^{1/3}$) with Reynolds

number for the first and second set of experimental results is shown in Figures 9.1, 9.2 and 9.3 for Models (2), (3) and (4) respectively.

The comparison of data from the three inclined tube banks with data from the normal tube bank is made in Section 9.3.3, and results are given in Figures 9.4–9.6.

The role of natural convection for inclined tube banks is investigated in Section 9.3.4 using, as above, the method of analysis of Mandelbaum et al. [1973] (see Figs. 9.7–9.9).

The transfer coefficients of individual rows with respect to Reynolds number are presented in Figures 9.10–9.15. The row–by–row variation of individual row results expressed as dimensionless group ($Sh/Sc^{1/3}$) against row number for constant values of Reynolds number were studied to provide an insight into the entrance and exit effects for inclined tube banks (Figs. 9.16–9.21).

The overall pressure drop across the three inclined tube banks are set out for Reynolds numbers of 200 to 6300 in Figures 9.22–9.24, and compared with the pressure drop for the ideal normal tube bank in Figures 9.25–9.27.

9.3.2 AVERAGE TRANSFER COEFFICIENTS OF INCLINED TUBE BANKS

As mentioned before two sets of experiments were carried out for each inclined tube bank. Mass transfer coefficients for each row were obtained in turn. Thus, as

discussed in Section 8.4.3 the average transfer coefficients were calculated from all the individual row values using a simple arithmetic mean. The mass transfer coefficients were re–expressed in the form of the dimensionless group $Sh/Sc^{1/3}$, as before, and were plotted against the characteristic Reynolds number for each run in the set of experiment.

The experimental variations of transfer coefficients with Reynolds number for the first and second experiment for Model 2 ($\varphi = 70^{o}$) are shown on a logarthmic plot in Figure 9.1, for Model 3 ($\varphi = 52.5^{o}$) in Figure 9.2, and for Model 4 ($\varphi = 45^{o}$) in Figure 9.3. Although there is a good agreement between the first set of experimental results (run numbers 1–4) and the second set (run numbers 5–6) at low Reynolds number for all the inclined models, as Reynolds number increases the agreement gets worse, and there is a marked deviation at higher Reynolds numbers. A similar comparison for the two data sets for all the inclined tube banks shows the same features (the ideal normal tube bank was discussed in Section 8.4.3.1.1).

Following the reasons discussed in Section 8.4.3.1.3 (better agreement between the second set of results of normal tube bank and those of previous workers) the second experimental results are regarded as more accurate and more reliable, and therefore will be used in subsequent data analysis.

As shown in Figures 9.1, 9.2 and 9.3 the agreement between the two runs (second data set) on each model is good, hence again demonstrating the consistency of the data obtained when using the electrochemical technique.

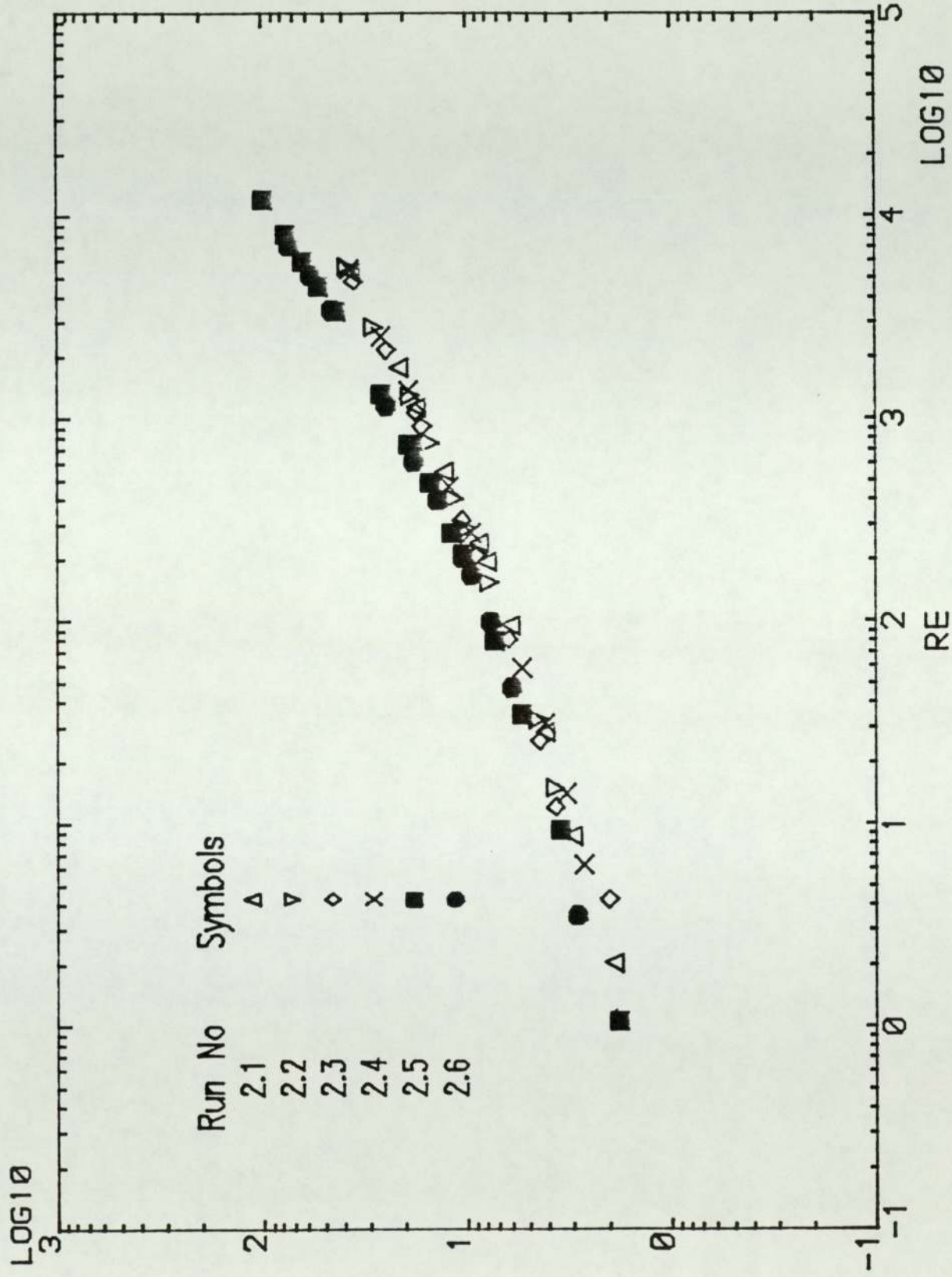

Fig. 9.1 Comparison of First and second data set of Model 2 (φ=70°)

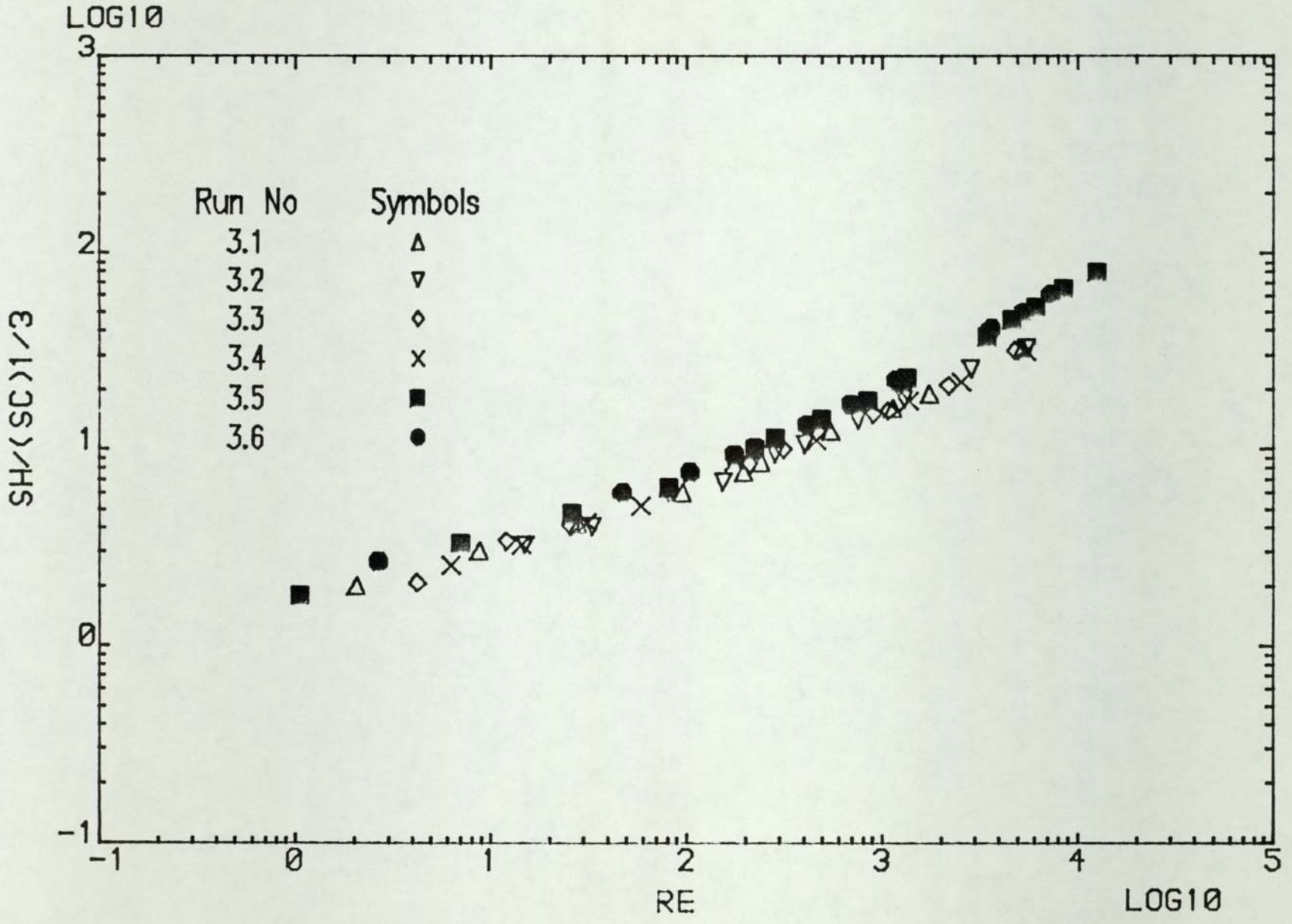

Fig. 9.2 Comparison of First and second data set of Model 3 (φ=57.5^{0})

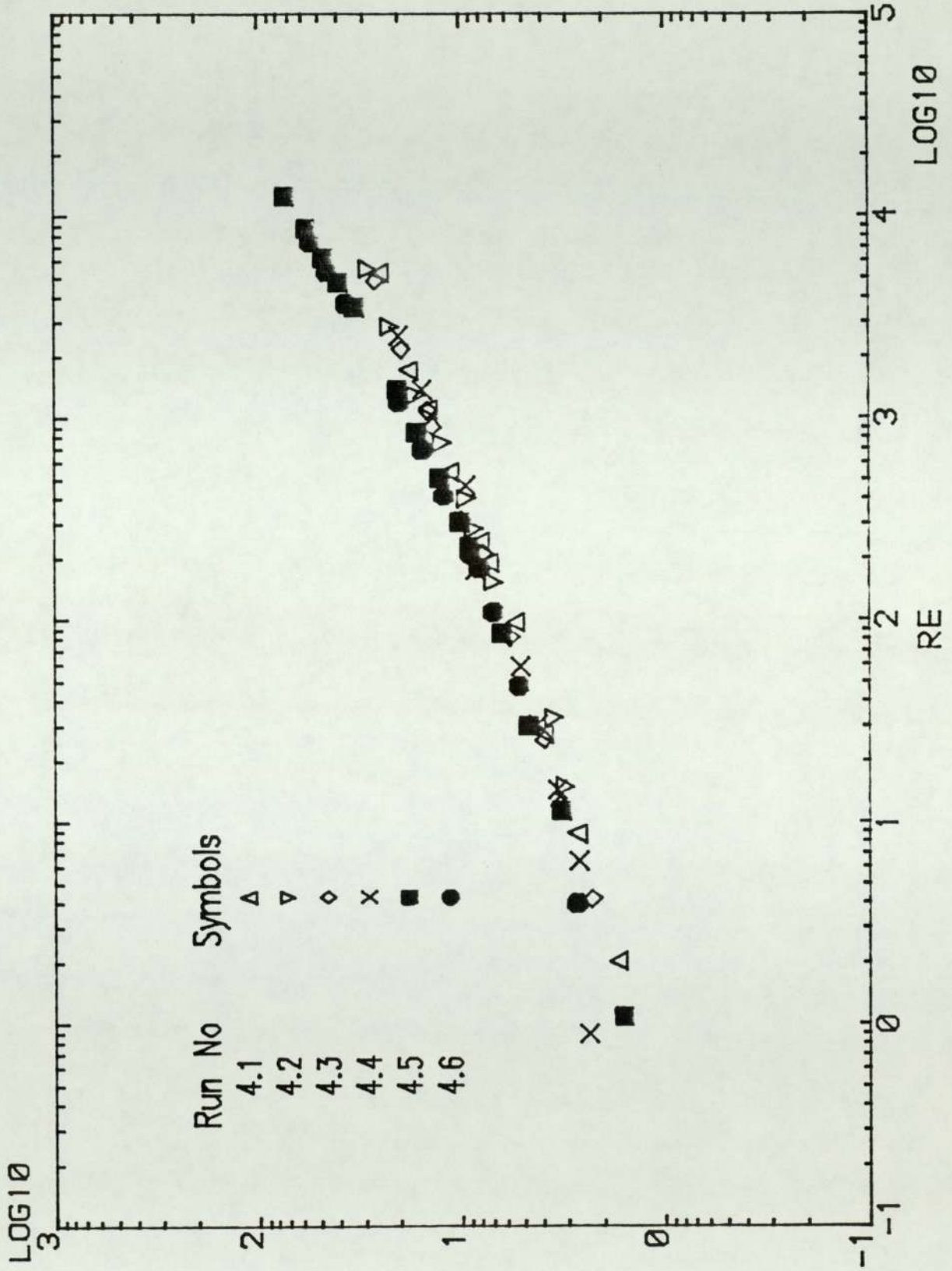

Fig. 9.3 Comparison of First and second data set of Model 1 (φ=45^{o})

9.3.3 COMPARISON WITH IDEAL NORMAL TUBE BANK DATA

To examine the effect of inclined flow on heat and mass transfer, the results from the second data set for the three inclined tube banks (Models 2, 3 and 4) are compared in the following sections with those for the ideal normal tube bank.

As discussed before, the second set of experimental results for the inclined tube bank (run numbers 2.5 and 2.6) and for the normal tube bank (run numbers 1.9 and 1.10) have been used in the comparisons. These results are plotted in Figure 9.4 and show the transfer coefficient (expressed as $Sh/Sc^{1/3}$) versus Reynolds number. It can be seen that the difference between the transfer coefficients for the inclined tube bank and for the normal tube bank at Reynolds number less than 200 is insignificantly small (within ±2%). The results for the inclined tube bank deviate from the normal tube bank results beyond a Reynolds number of 200. The difference between experimental results increases to 5% as the Reynolds number increases to 1300. The difference is relatively constant for the range of Reynolds number $3000<Re<12\ 600$ to about 5±1%, the inclined tube bank results being lower.

In Figure 9.5 the transfer coefficient of first and third models ($\varphi = 52.5^{o}$) are both depicted, again for the two second sets of experimental data. It is apparent that the variation of transfer coefficients are similar at Reynolds numbers lower than 50 (within ±2%). The difference is dependent on flow rate and increases to about 16% as the Reynolds number increases from 50 to 1300. The difference between the two sets of results is constant in the Reynolds number range 3000 to 12600 and is about 21±2%.

A similar comparison to those above is shown in Figure 9.6 for Model 4 ($\varphi = 45^{o}$). The results for Model 4 differ from those of Models 2 and 3 in that the differences between the data start at the lowest Reynolds number value measured (Re = 1.05) by 10% and the difference increases with increasing Reynolds number so that at Re = 1300, it is about 25%, and remains constant beyond 3000 up to Re = 12 600 (the highest Reynolds number measured in this work) at 30±2%.

The above comparisons indicate three important features characteristic of inclined tube banks.

i) The differences between the transfer coefficients of Models 2 and 1 for Reynolds number less than 200 and between the transfer coefficients of Models 3 and 1 for Re<50 are negligible, whereas Model 4 ($\varphi = 45^{o}$) shows a lowering of 10% in transfer coefficient as compared to those of the ideal normal tube bank ($\varphi = 90^{o}$). Therefore as the yaw angle decreases the effect of inclination on transfer coefficient starts at lower Reynolds numbers.

ii) The comparison of all three inclined tube banks with the normal tube bank shows a similar behaviour in the range 50<Re<1300, i.e. the data diverge as the Reynolds number increases.

iii) The differences between the data for each of the inclined tube banks and data for the ideal normal tube bank remain constant for the range 3000<Re<12 600, i.e. the differences between the experimental results for inclined and normal tube banks were

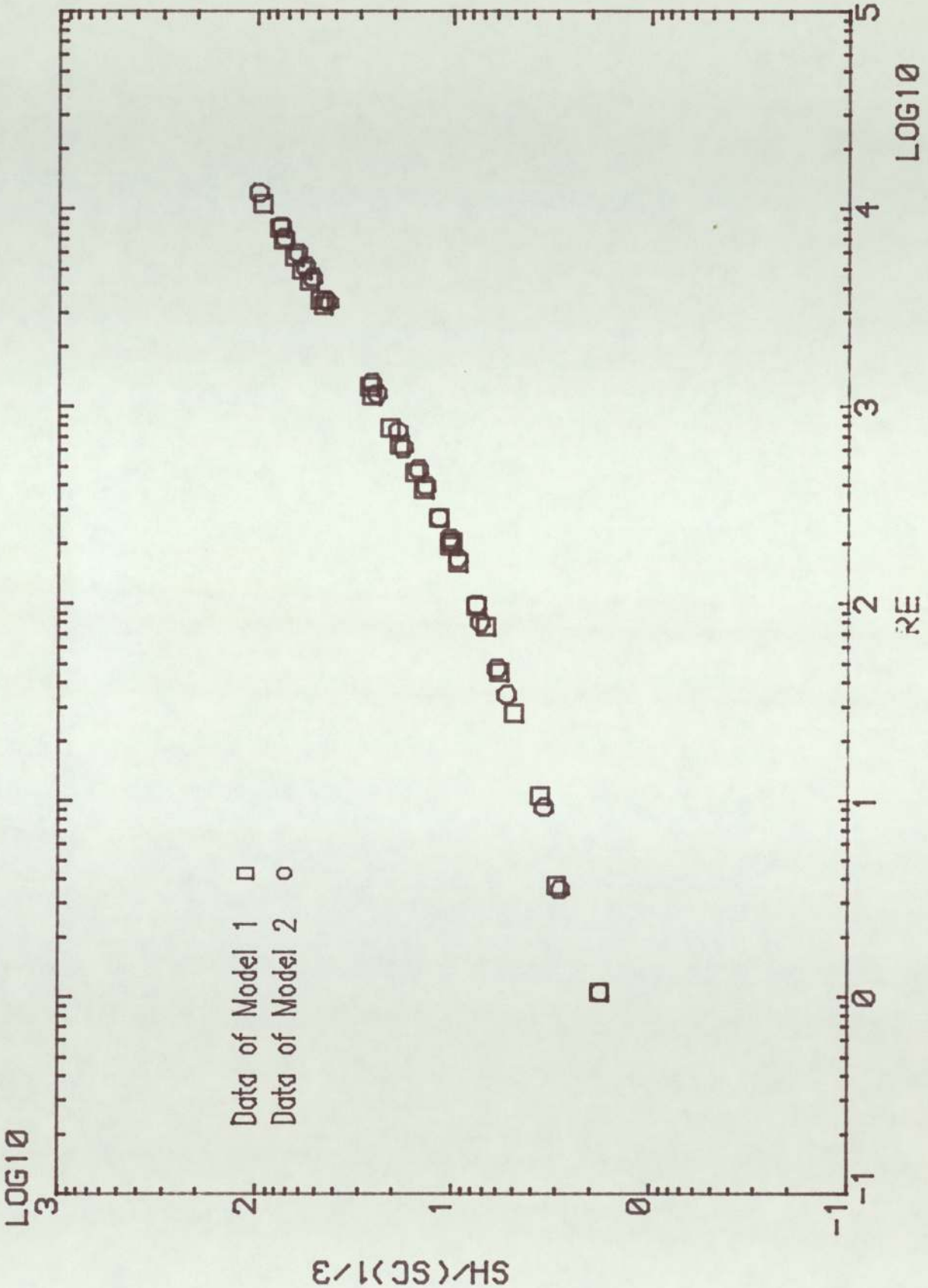

Fig. 9.4 Comparison of data From Model 2 with those From Model 1

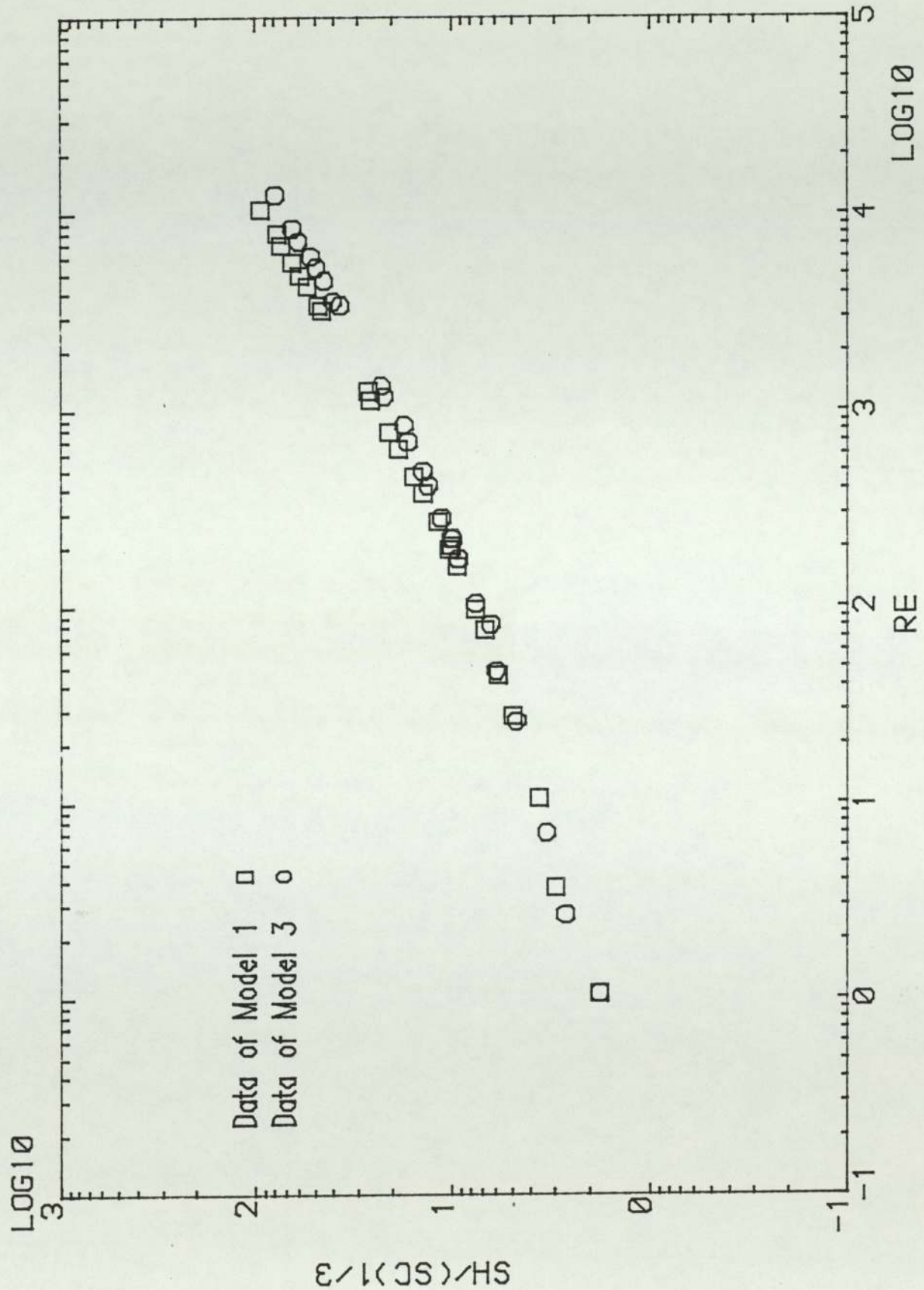

Fig. 9.5 Comparison of data From Model 3 with those From Model 1

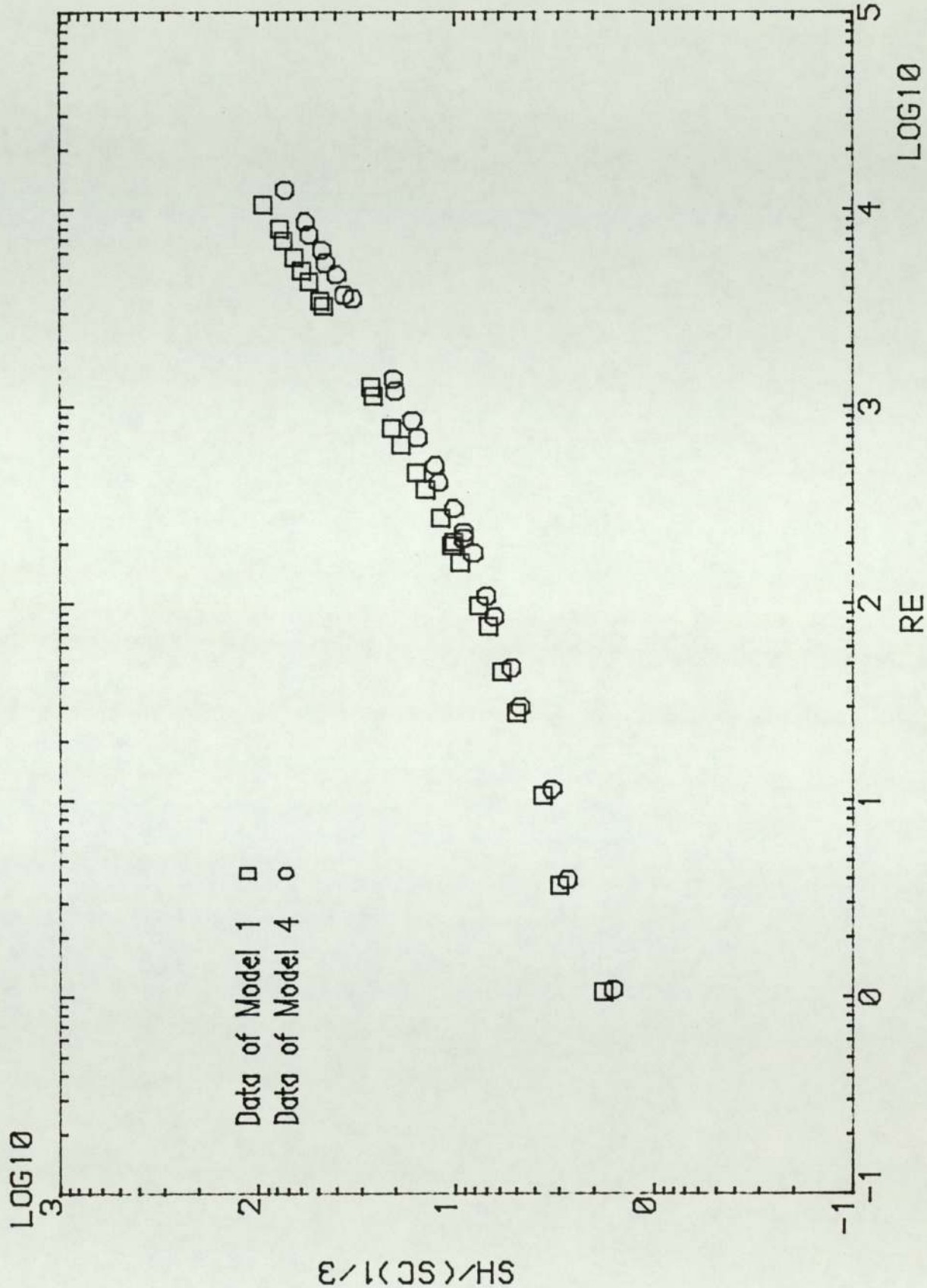

Fig. 9.6 Comparison of data from Model 4 with those from Model 1

independent of Reynolds number in this region. But these differences increase with decrease of yaw angle, therefore the heat and mass transfer decrease as the yaw angle decreases.

9.3.4 ROLE OF NATURAL CONVECTION

The role of natural convection at low Reynolds number has been investigated for these three models, using the analysis of Mandelbaum et al. [1973]. Appropriate graphs are shown in Figures 9.7–9.9. As discussed in Section 8.4.2.3, since there is no straight horizontal portion at low Reynolds numbers, it follows that natural convection is not important for inclined tube banks, a conclusion similar to that for the normal tube bank.

9.3.5 VARIATION IN TRANSFER COEFFICIENTS FROM ROW TO ROW

The transfer coefficients for inclined tube banks have been studied row–by–row. Since the transfer coefficients of the interior rows are identical, therefore to get a better understanding of row–by–row variation of transfer coefficient the results for rows 1, 2, 3, 6, 12 are plotted in Figures 9.10–9.12.

To provide a clear representation of all the results the ordinate scale in Figures 9.13–9.15 is displaced by 17% for each row. As can be seen the differences (or spacings) between the rows are uniform over the investigated Reynolds number range except those for the first, second, third and last rows, which differ. As before, plotting the data on a row–by–row basis makes the situation clearer (Figs. 9.16–9.21).

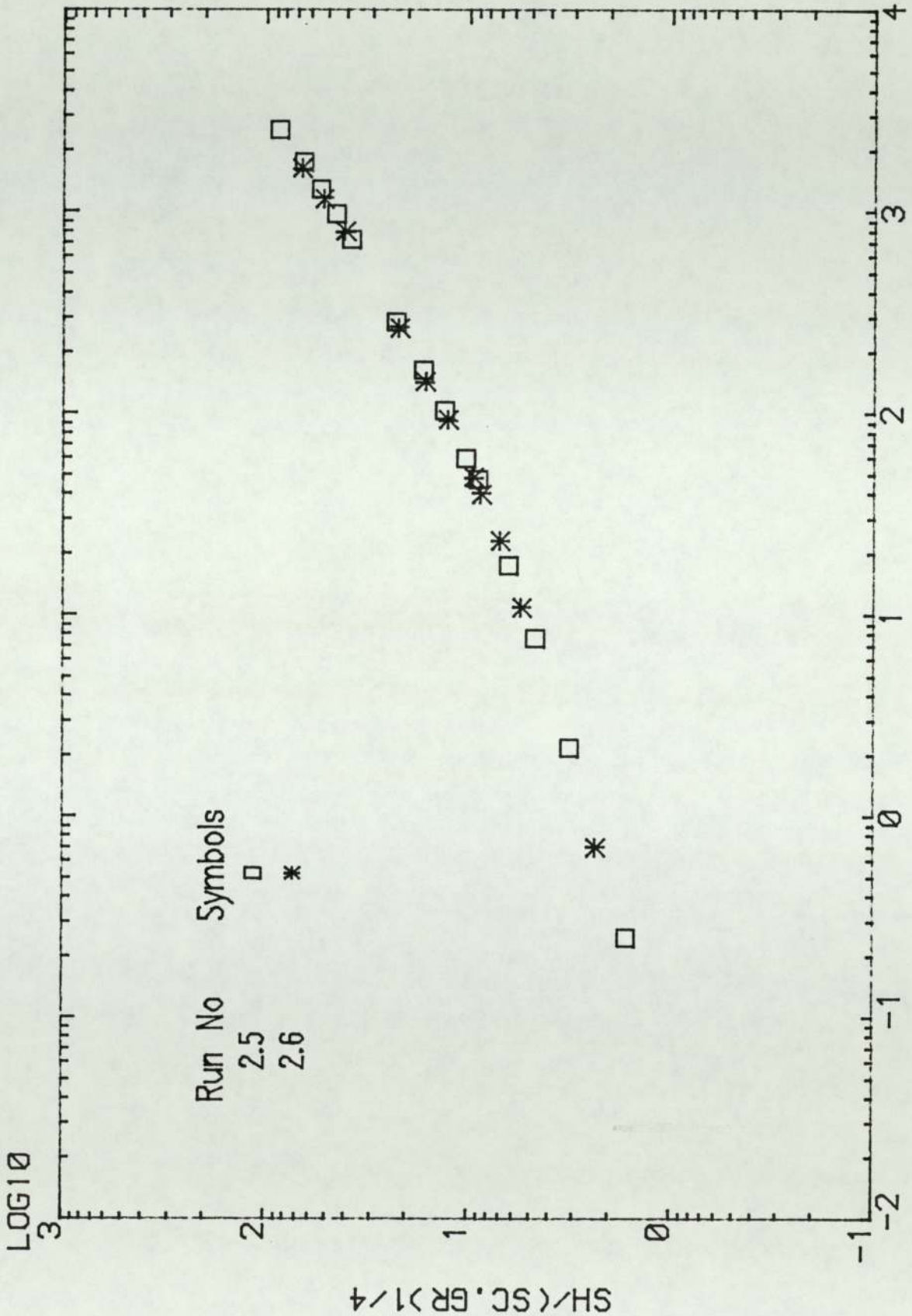

Fig. 9.7 Test for role of natural convection for Model 2

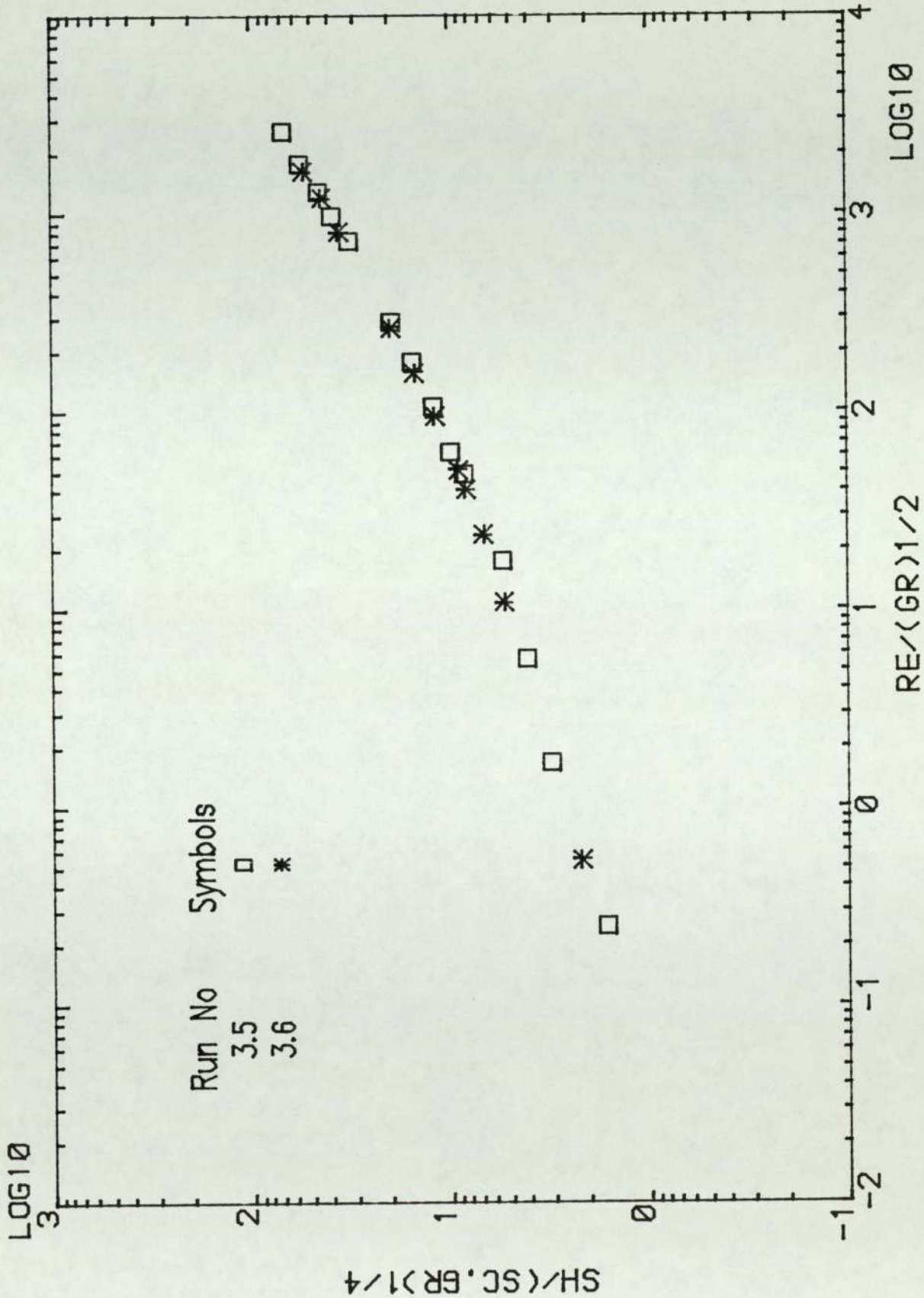

Fig. 9.8 Test for role of natural convection for Model 3

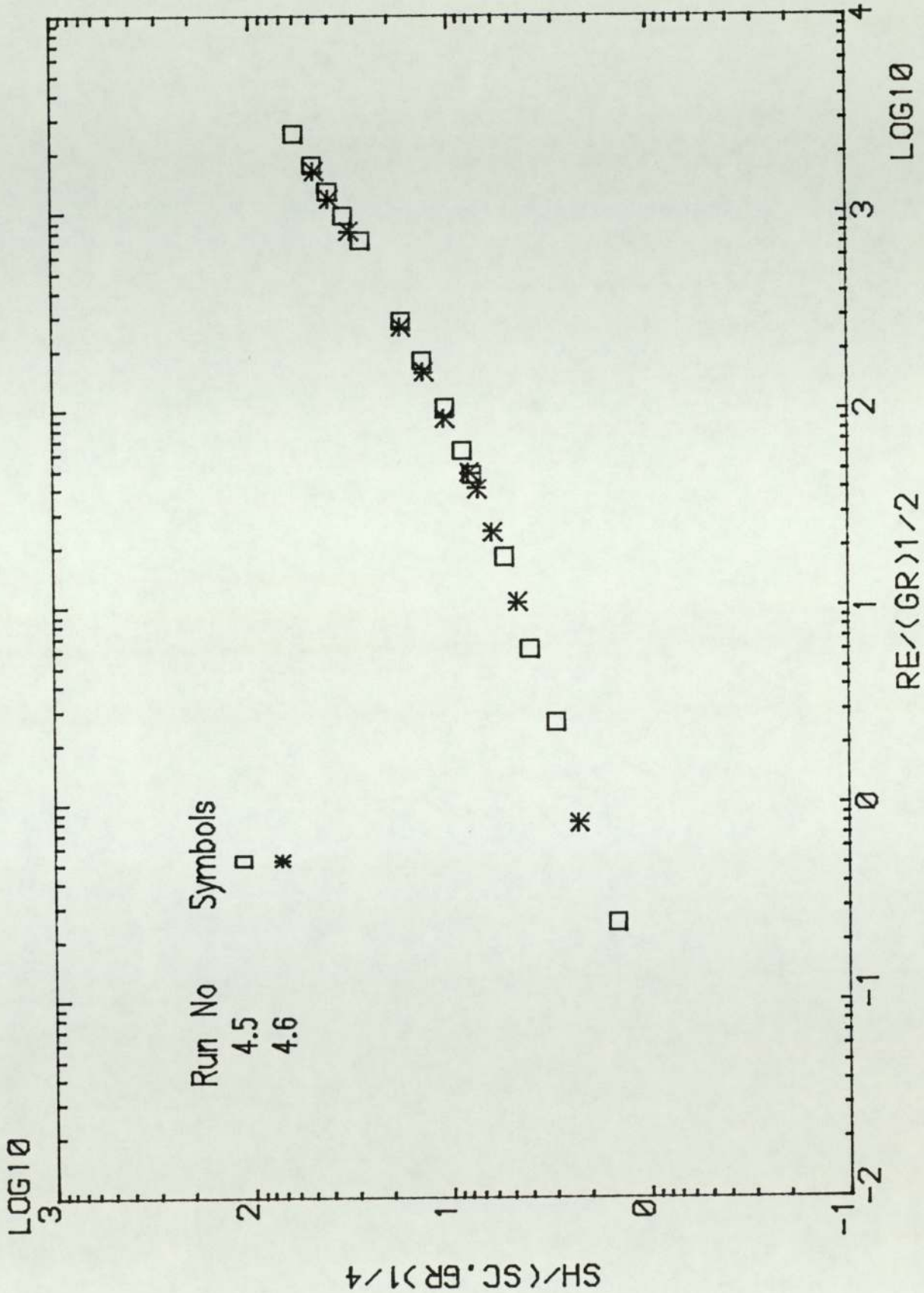

Fig. 9.9 Test for role of natural convection for Model 4

To illustrate the reproducibility of the results, the data from each model from the two runs forming the second set of runs are plotted in Figures 9.16–9.21. For convenience the Reynolds number range is divided into values below and above 1000. The data from Run 5 are linked by lines, those from Run 6 are not.

Figures 9.16–9.18 show how individual mass transfer coefficients vary with row number for Reynolds number less than 1000. It is clear that for all three inclined tube banks the transfer coefficients of the first and the last tube rows are significantly lower than that of a tube row in the interior of the tube bank. In addition, a relatively constant mass transfer coefficient holds in the interior of the tube bank. The depression in transfer coefficients of first and twelfth row increases as Reynolds number increases, but the depression seems to be weaker as the angle of inclination increases for all Reynolds numbers less than 1000.

The variation of transfer coefficient at Reynolds numbers greater than 1000 are shown in Figures 9.19, 9.20 and 9.21. It can be seen that the entrance effect over the first few rows is different from the cases for Reynolds number less than 1000.

The inclined tube bank with a yaw angle of 70^{o} shows an increase in transfer coefficient over the first four rows, but one which remains nearly constant after the fourth row until the eleventh row. The last row, the 12th row, shows a significant depression with respect to the interior rows (Fig. 9.19). Again it is seen that as the Reynolds number increases the first few rows show a lower transfer coefficient.

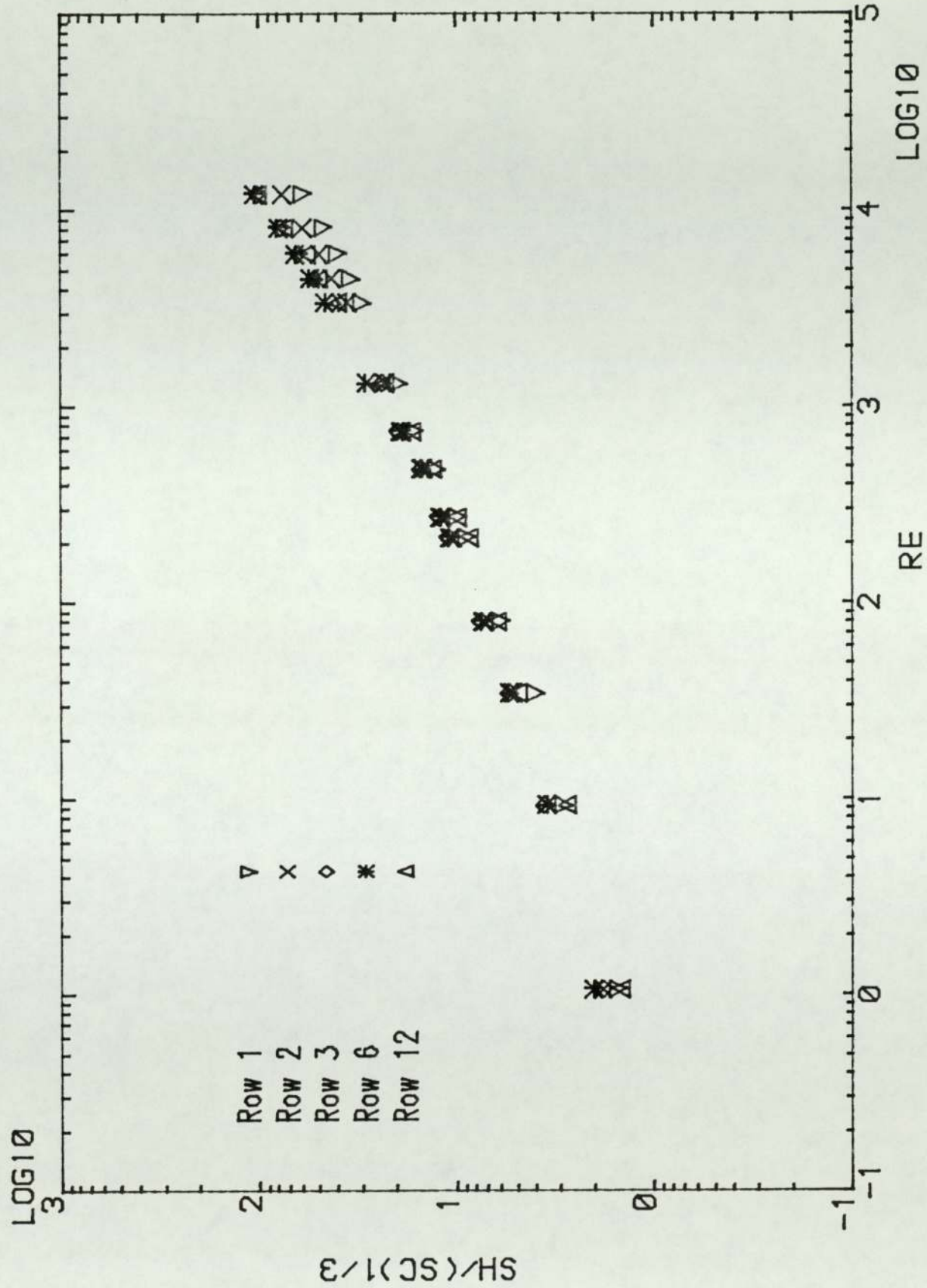

Fig. 9.10 Row-by-Row variation of transfer coefficients For Model 2

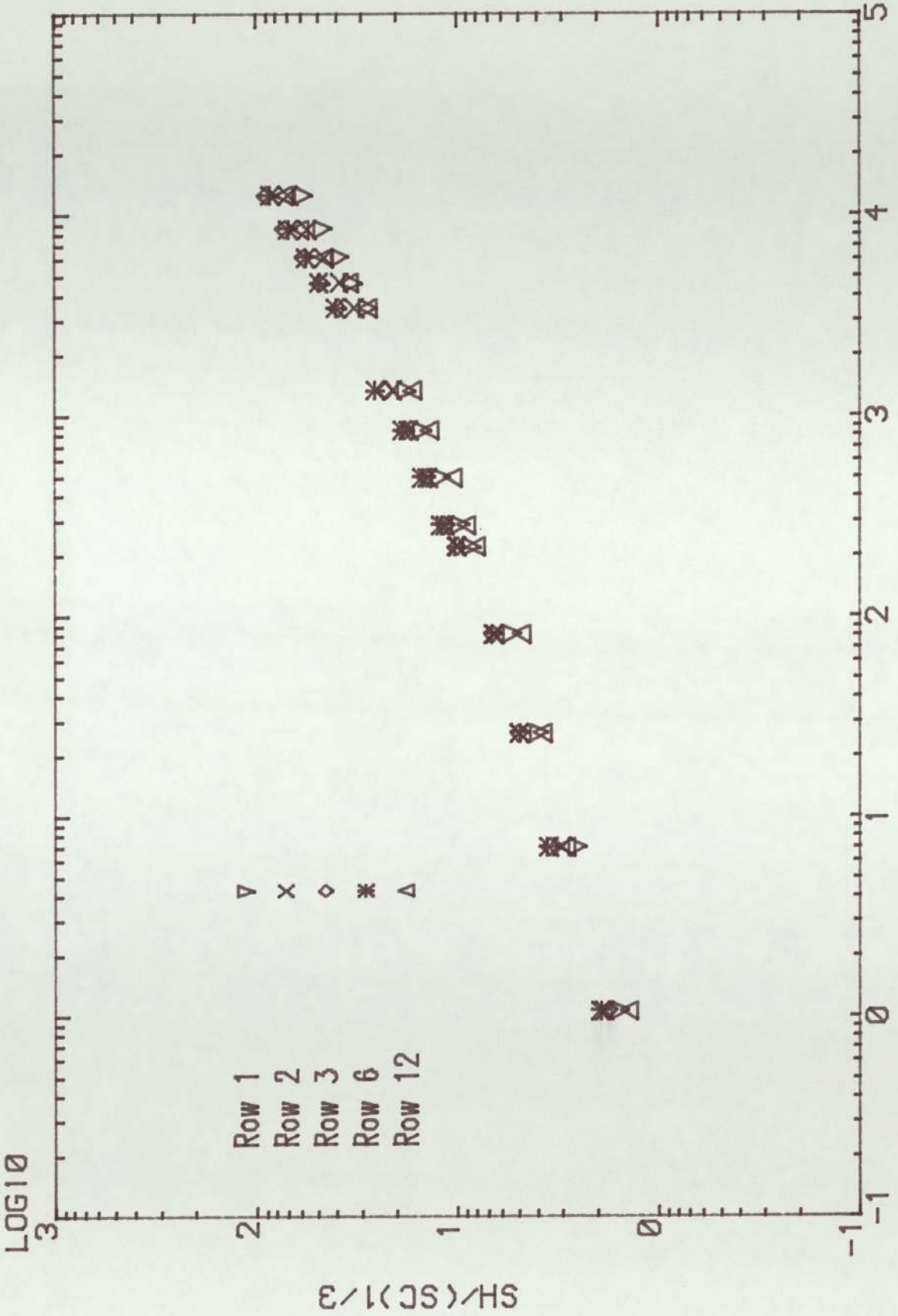

Fig. 9.11 Row-by-Row variation of transfer coefficients For Model 3

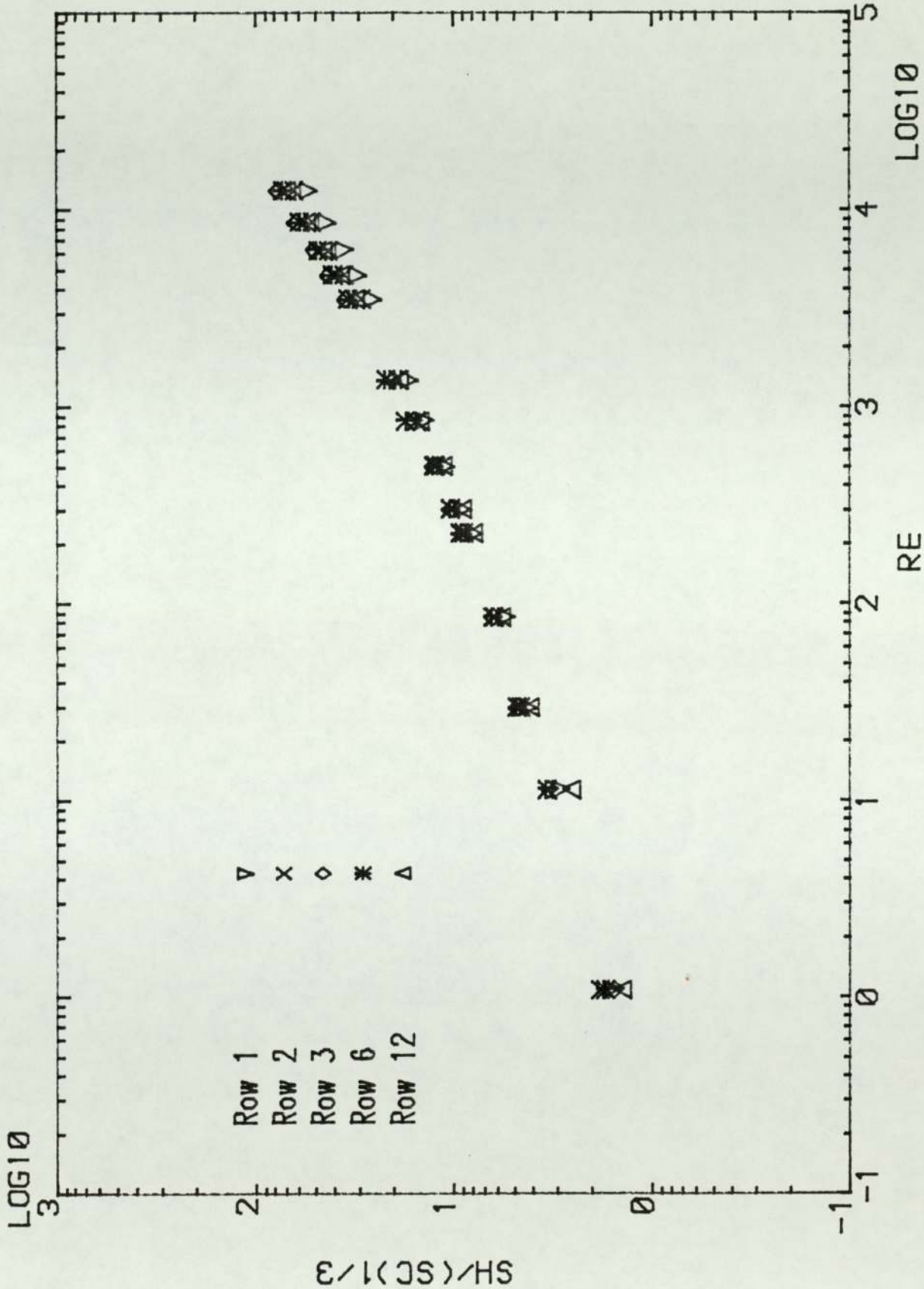

Fig. 9.12 Row-by-Row variation of transfer coefficients For Model 4

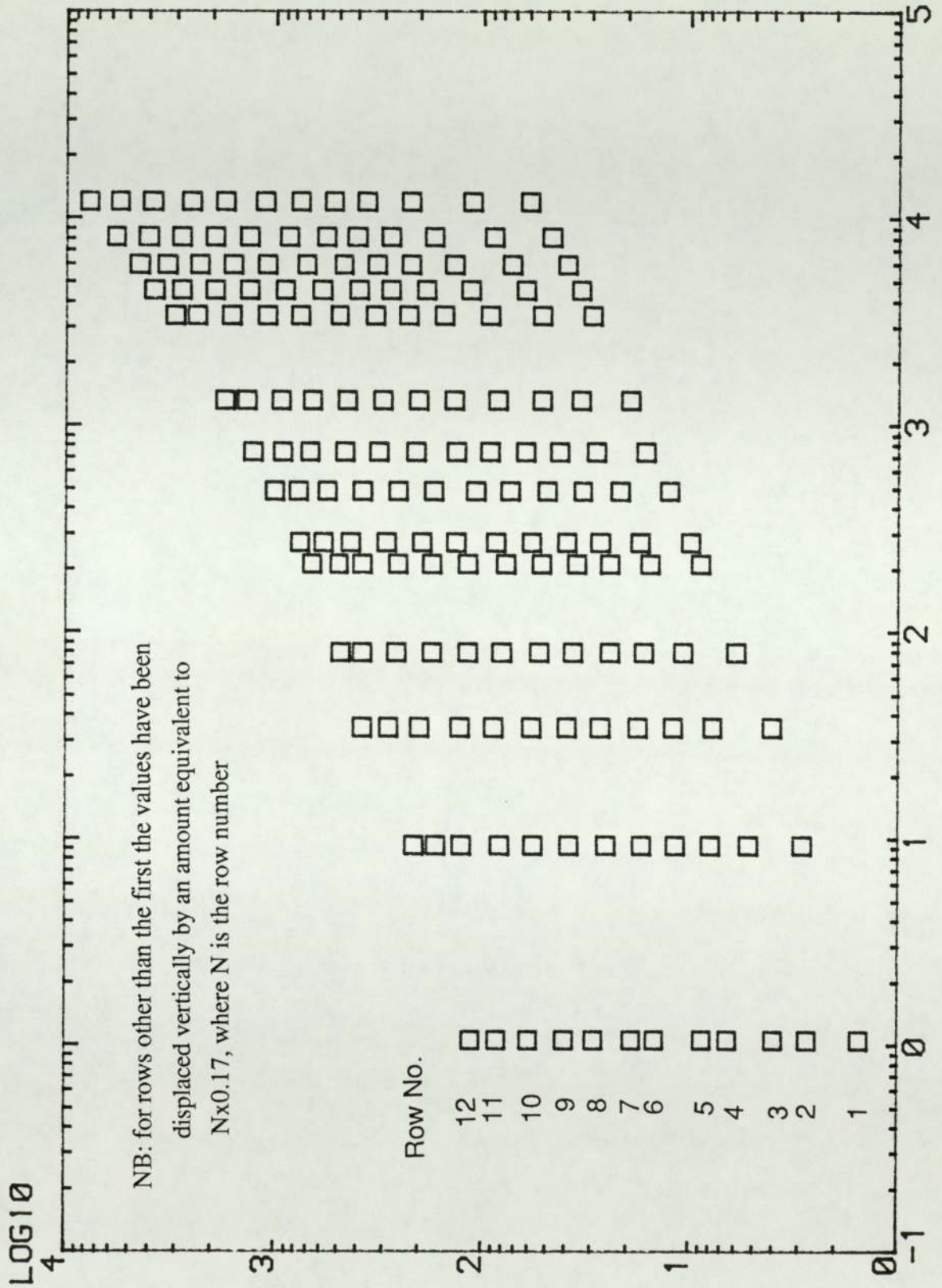

Fig. 9.13 Schematic representation of row-by-row variations by successive displacement of Sh/(Sc)1/3 values for Model 2

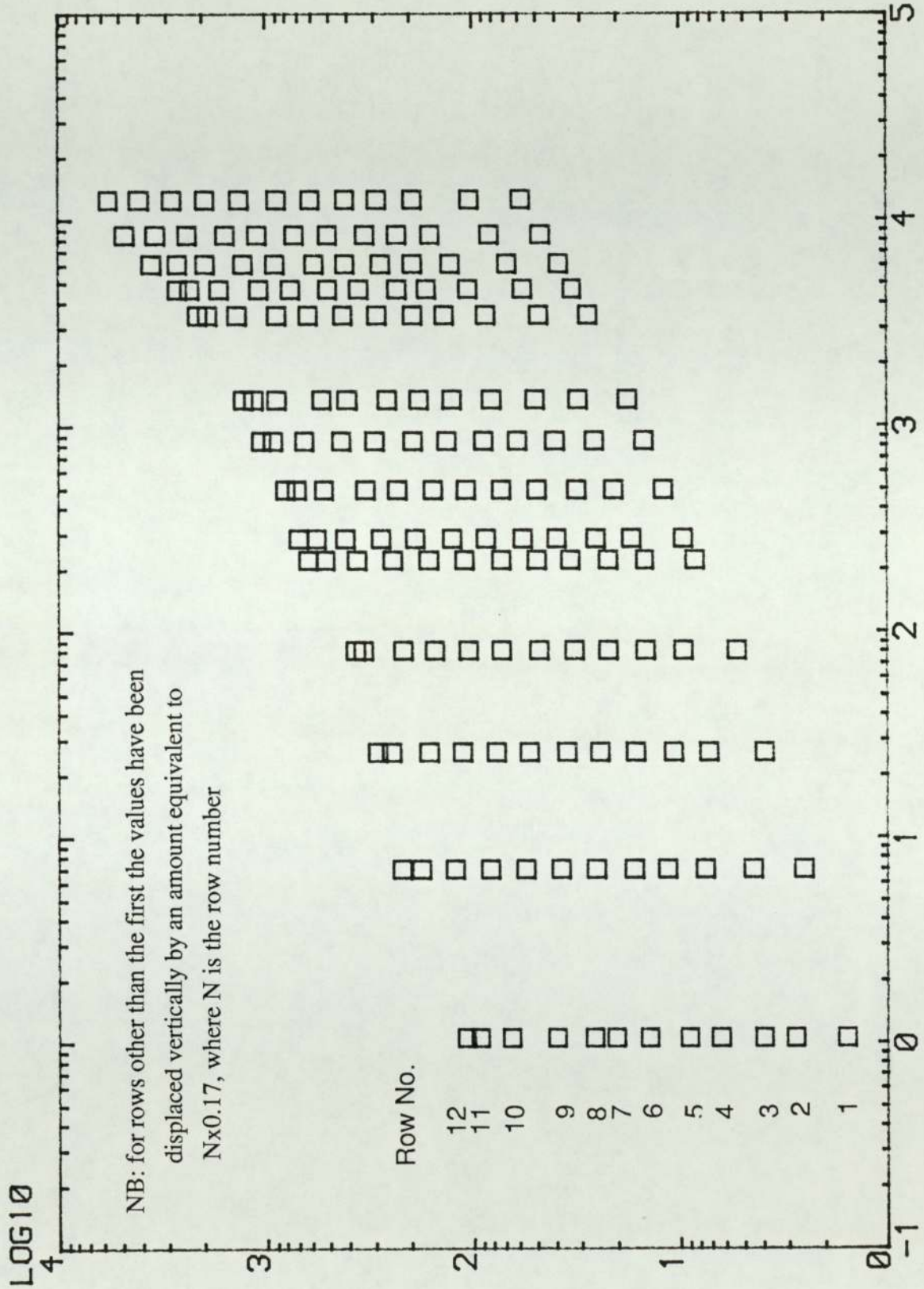

Fig. 9.14 Schematic representation of row-by-row variations by successive displacement of Sh/(Sc)1/3 values for Model 3

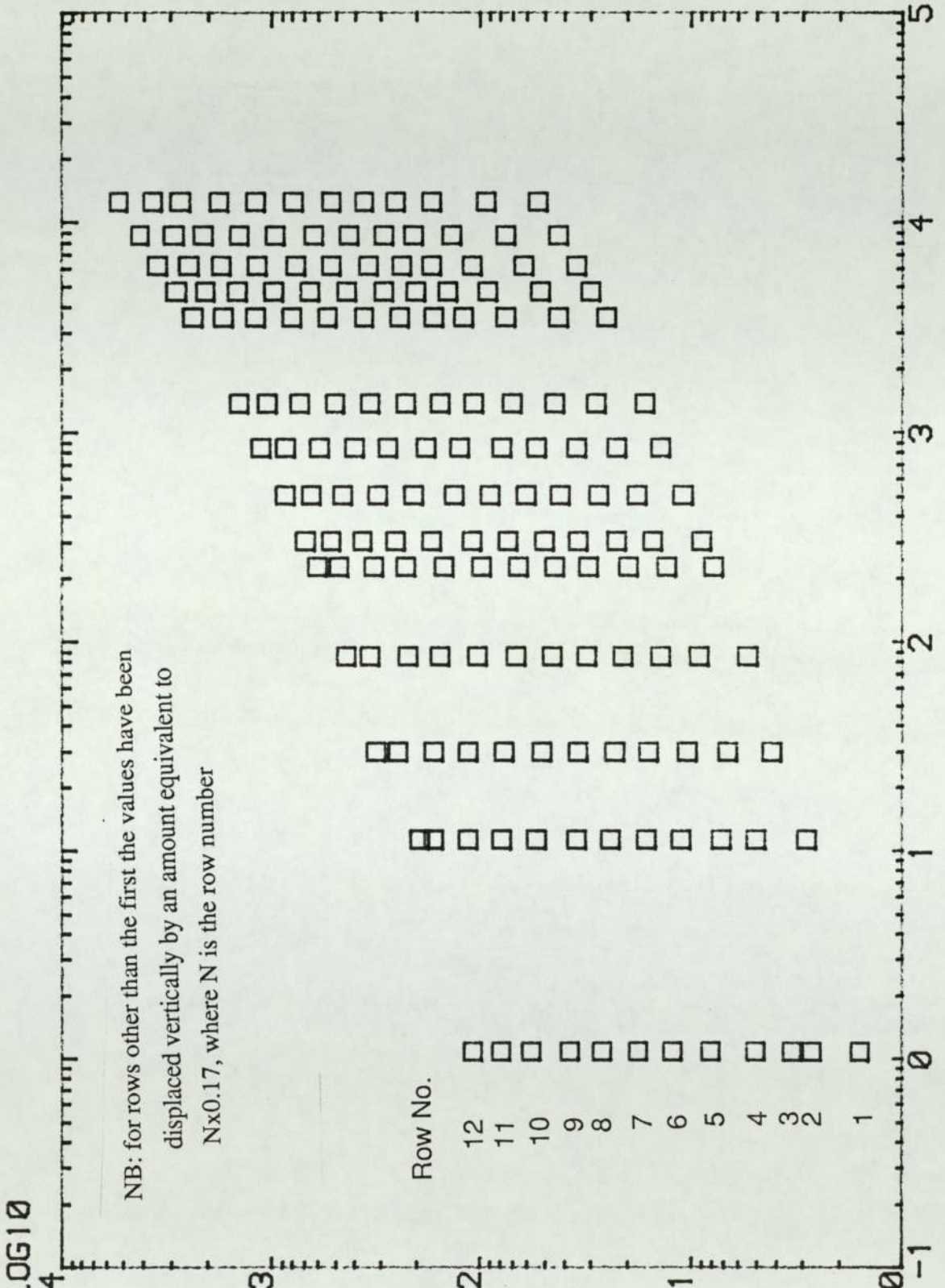

Fig. 9.15 Schematic representation of row-by-row variations by successive displacement of Sh/(Sc)1/3 values for Model 4

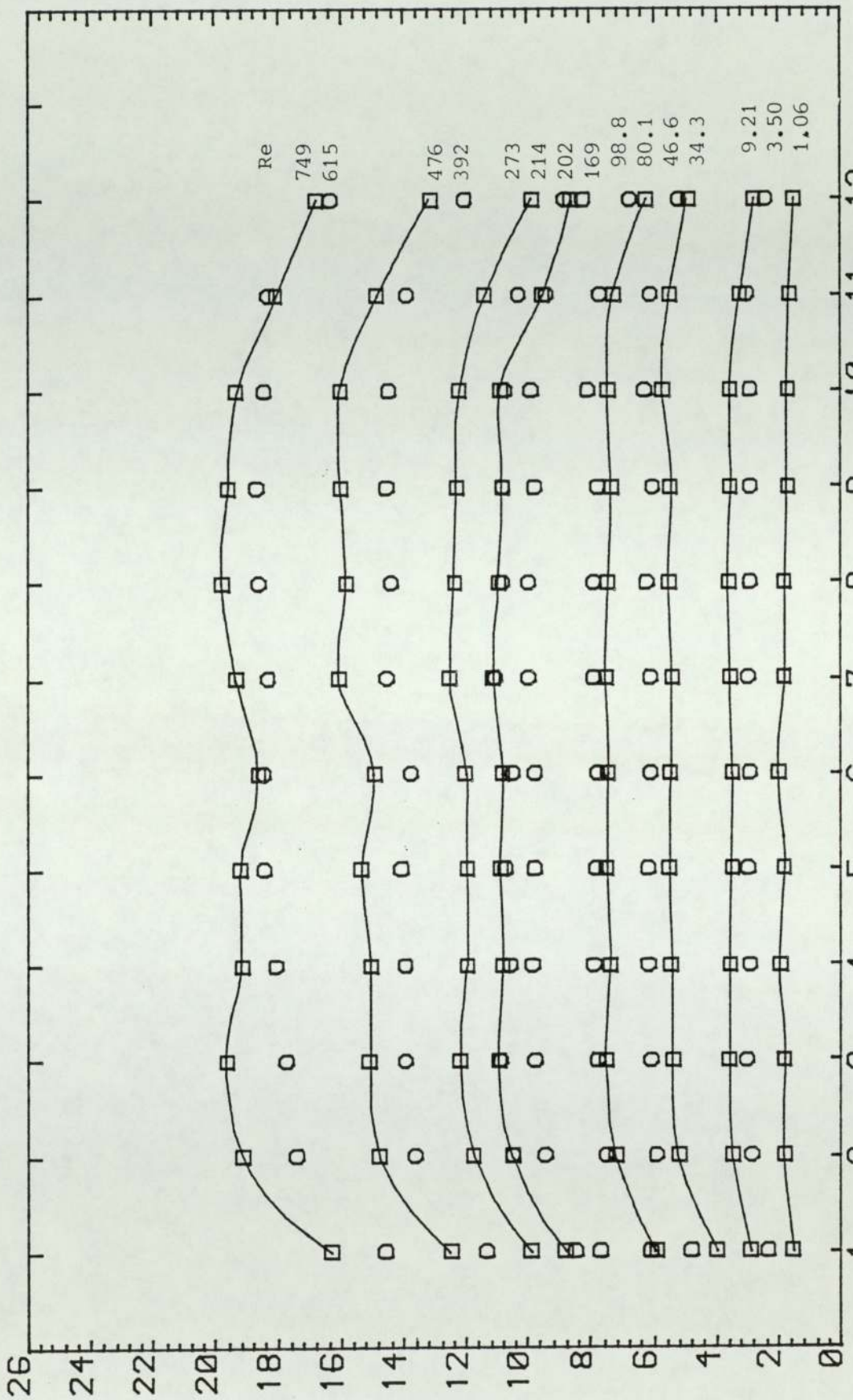

Fig. 9.16 Row-by-row variation of transfer rate for Model 2 1.0<Re<1000

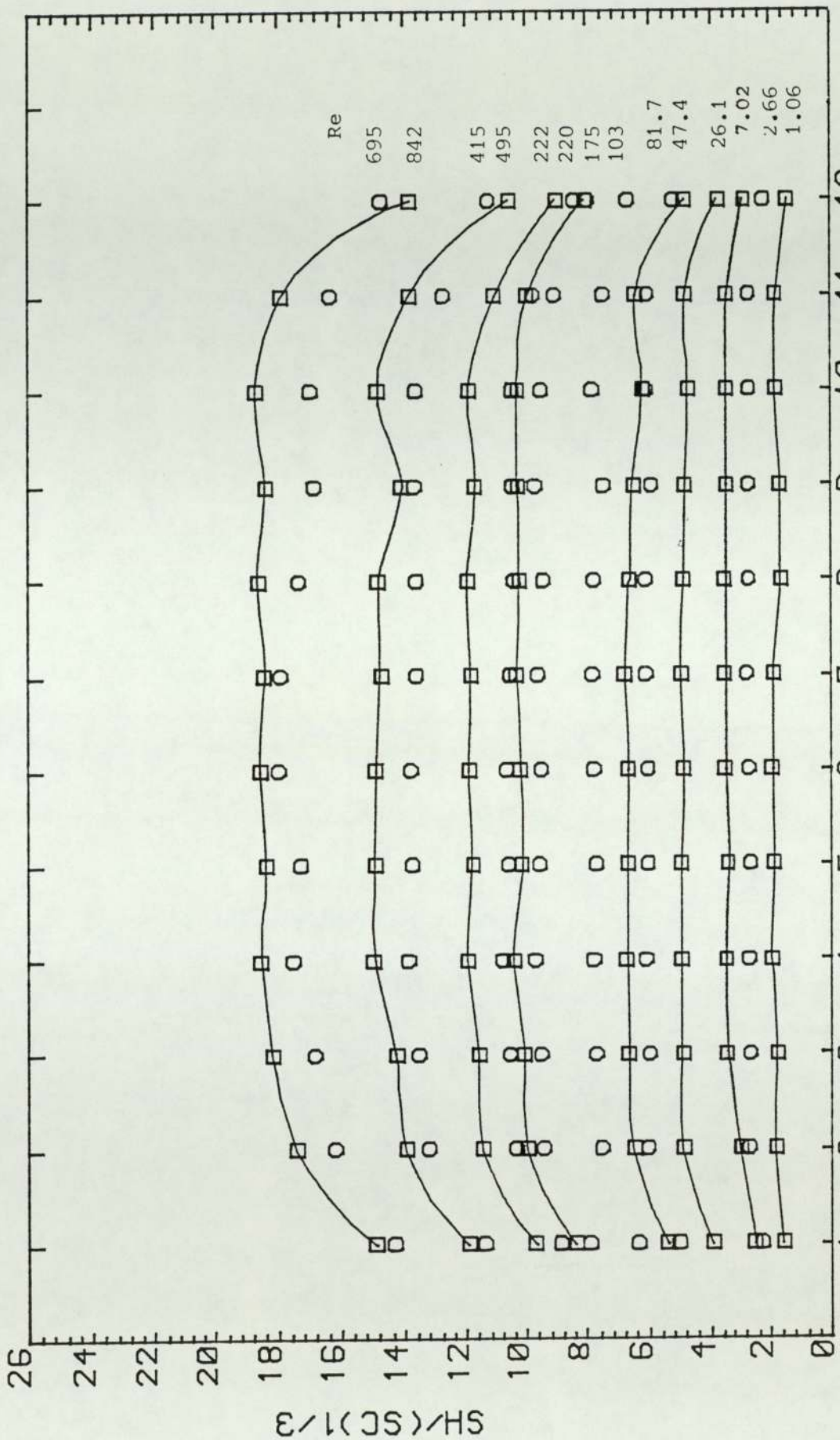

Fig. 9.17 Row-by-row variation of transfer rate for Model 3 1.0<Re<1000

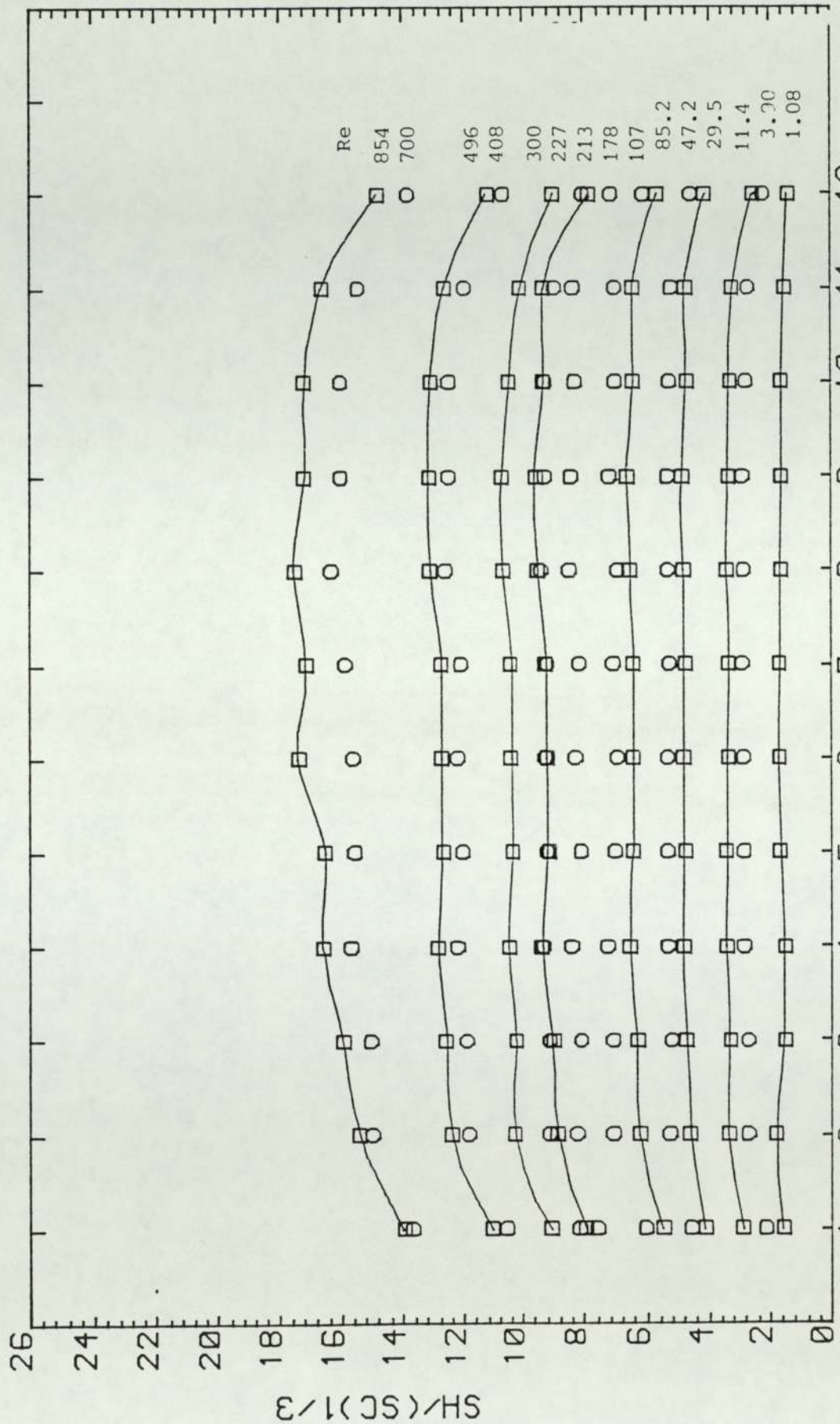

Fig. 9.18 Row-by-row variation of transfer rate for Model 4 1.0<Re<1000

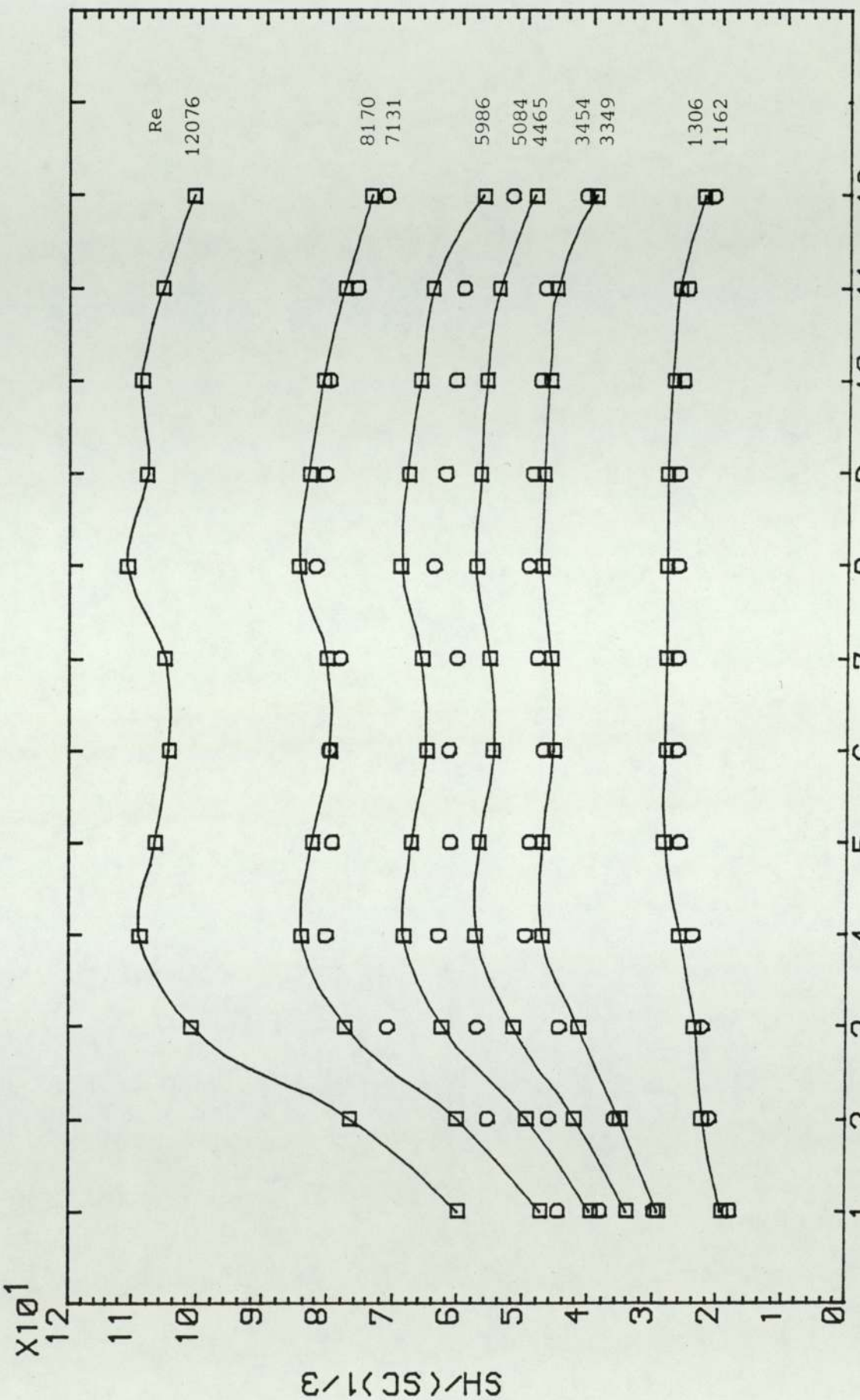

Fig. 9.19 Row-by-row variation of transfer rate for Model 2 1000<Re<10 600

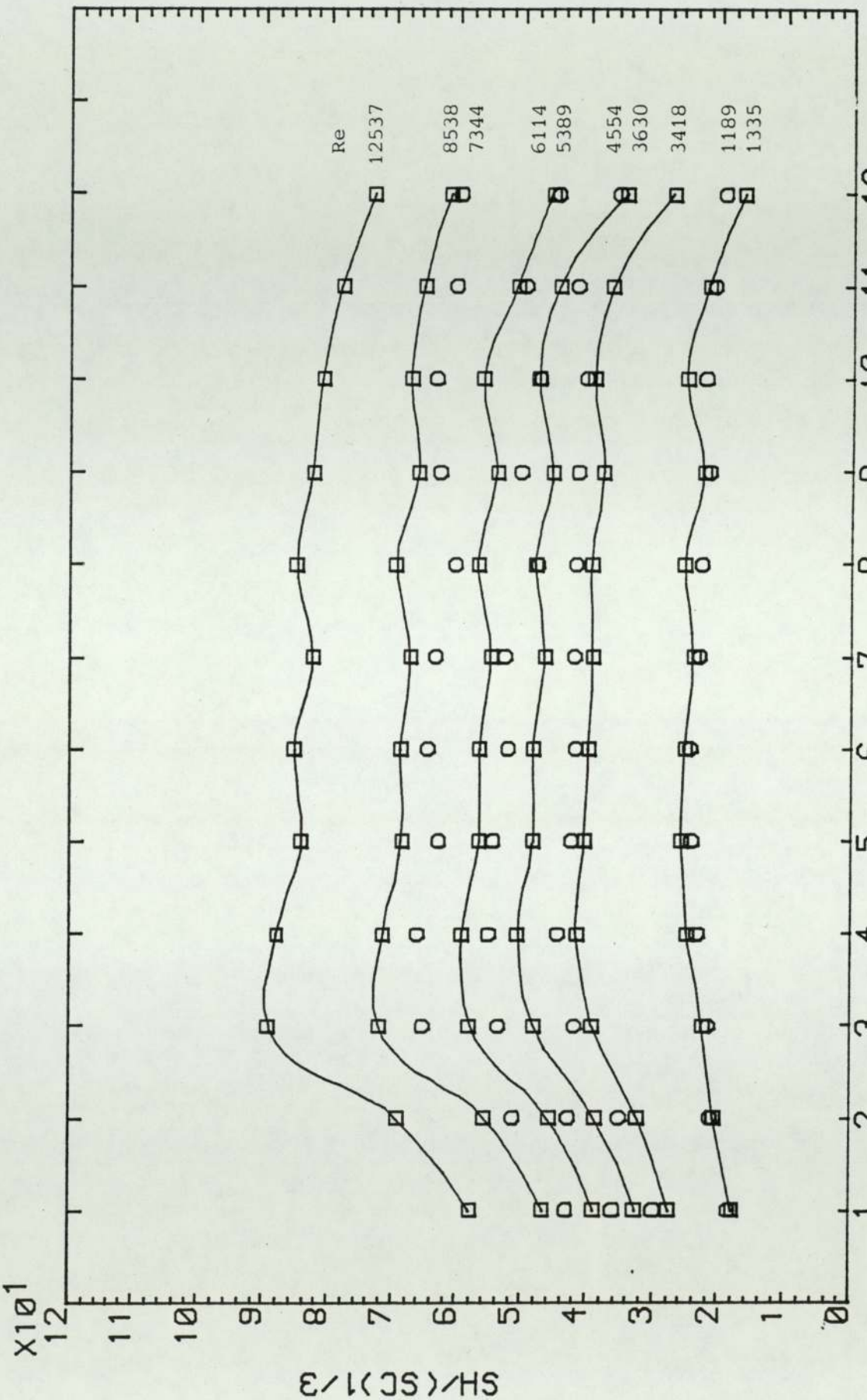

Fig. 9.20 Row-by-row variation of transfer rate for Model 3 1000<Re<10 600

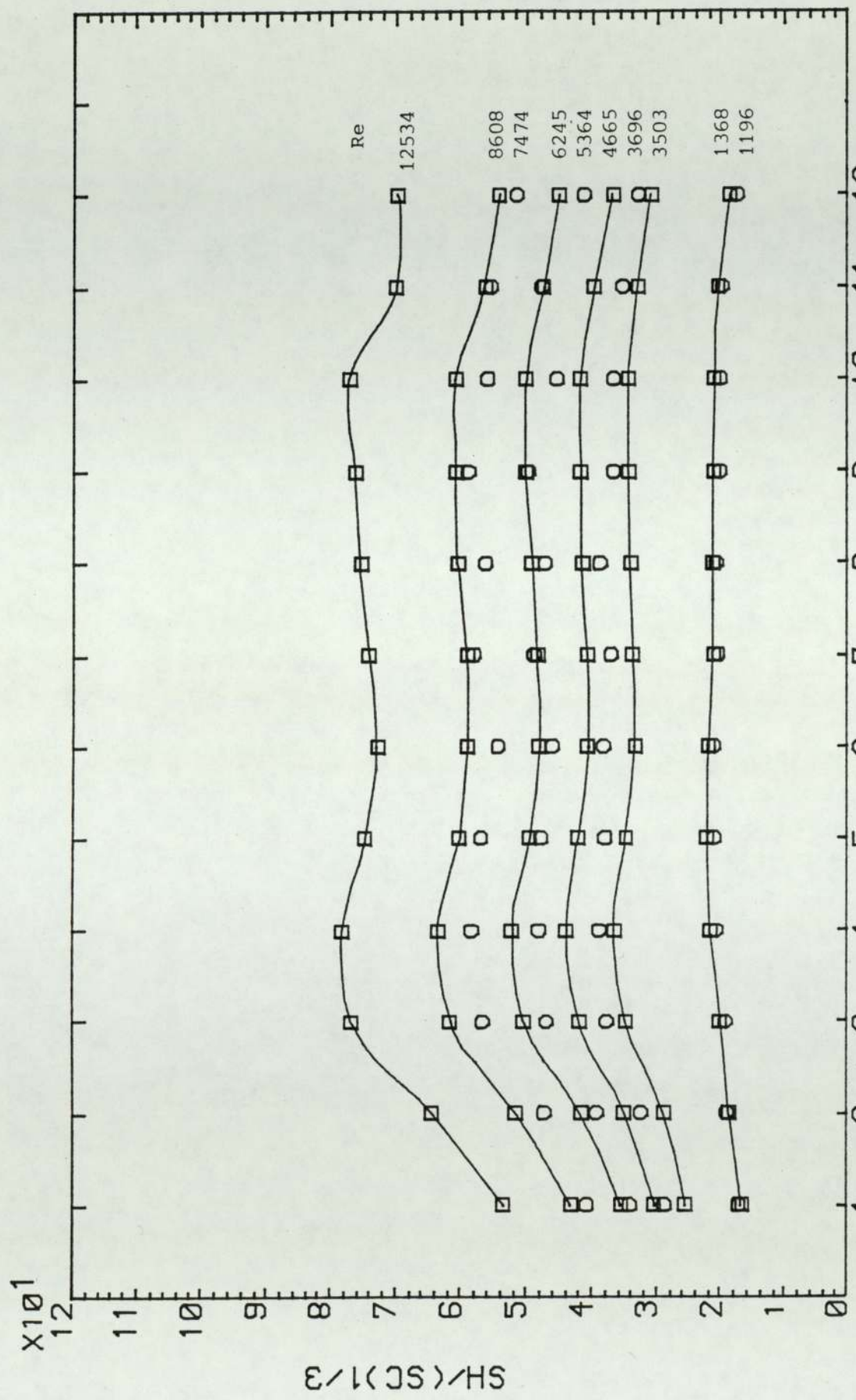

Fig. 9.21 Row-by-row variation of transfer rate for Model 4 1000<Re<10 600

The results of the third model ($\varphi = 57.5^{o}$) for Reynolds number greater than 1000 are shown in Figure 9.20. There is an increase over the first three rows and a depression in the 11th and 12th rows. Figure 9.21 shows the results for $\varphi = 45^{o}$, for this model the entrance and exit effects are nearly identical to those of the third model, but the increase in the first three rows of this model is lower than that for the third model, and the depression of the 12th row is not as acute as in the third model.

It is also interesting to note the variation of entrance and exit effects with Reynolds number. As Reynolds number increases the ratio of the $Sh/Sc^{1/3}$ group of the first few rows to those of interior rows increases over the Reynolds number range studied. This also happens for the last row which shows lower ratios of the transfer coefficient to the mean values for higher Reynolds number.

9.3.6 PRESSURE DROP ACROSS INCLINED TUBE BANKS

Two runs were carried out for each inclined tube bank. The pressure drops from two runs for each bank are plotted in the form of the dimensionless friction factor f $= 2\Delta P \rho g_c / 4G_{max}{}^2 N'$ against Reynolds number in Figures 9.22, 9.23 and 9.24 for Models 2, 3 and 4 respectively.

The maximum mass flow velocity is based on the projected minimum flow area, which is the same as the minimum flow area in the ideal normal tube bank, i.e. the projection of the free flow area to the horizontal plane.

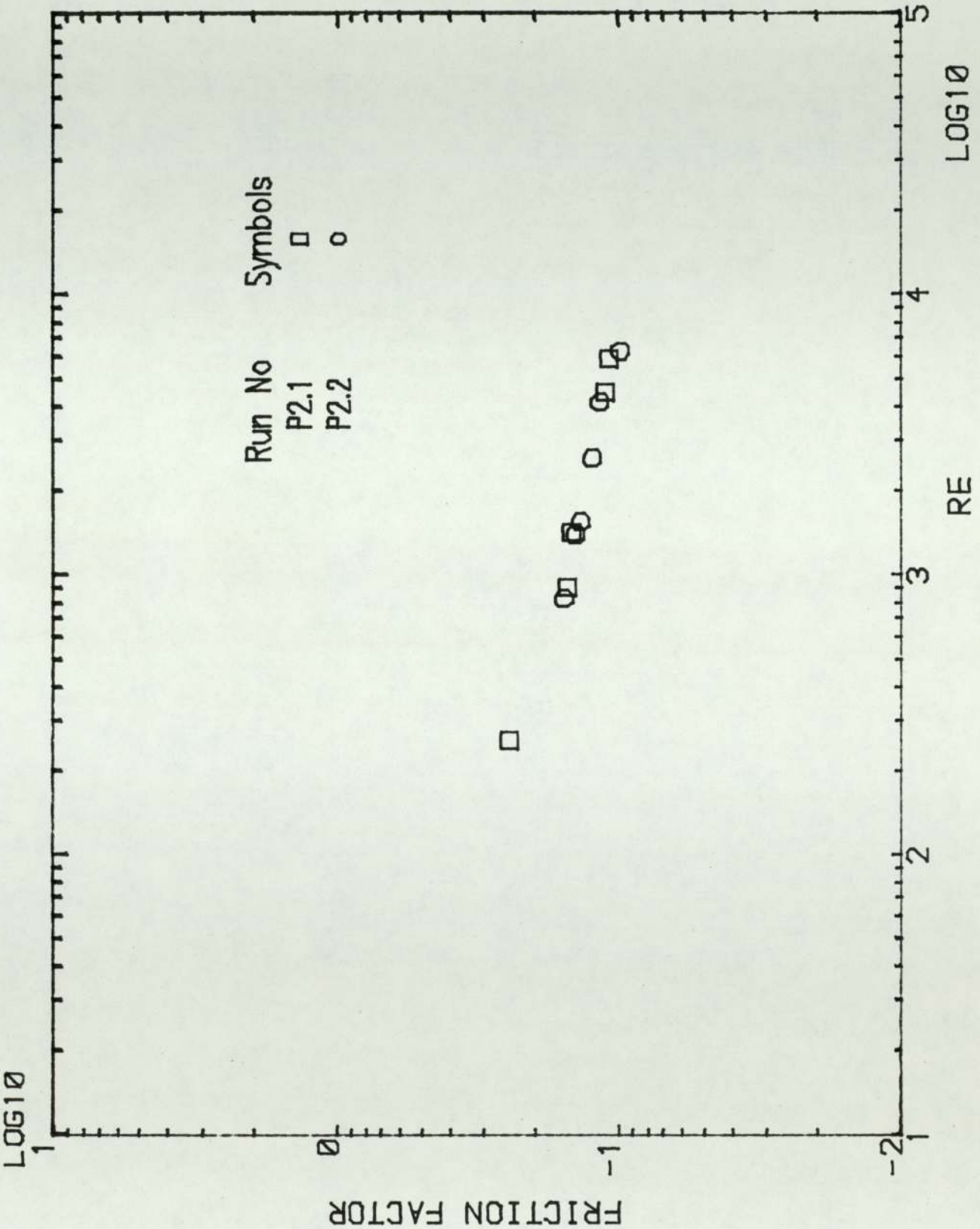

Fig. 9.22 Pressure drop results From Model 2

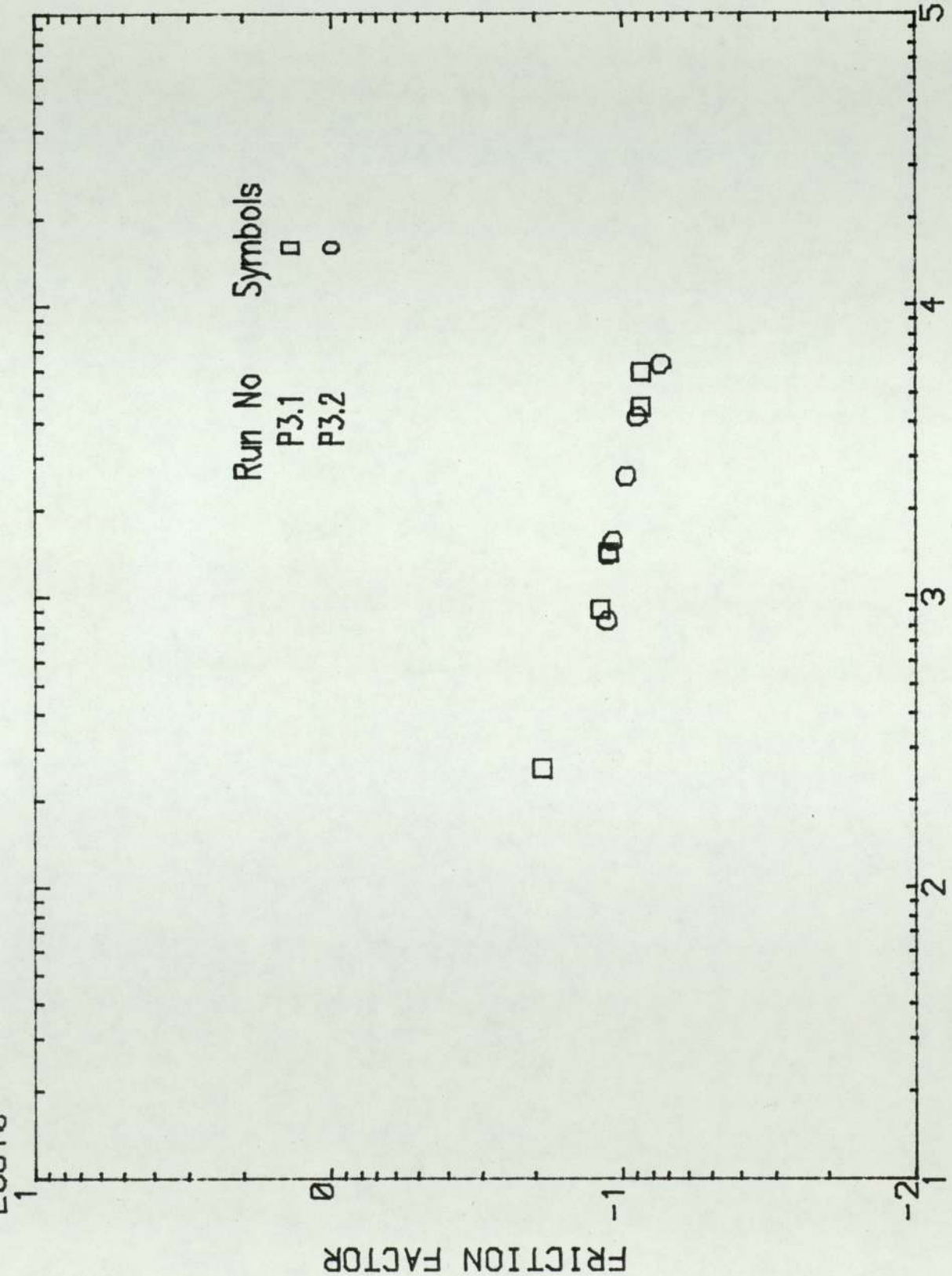

Fig. 9.23 Pressure drop results From Model 3

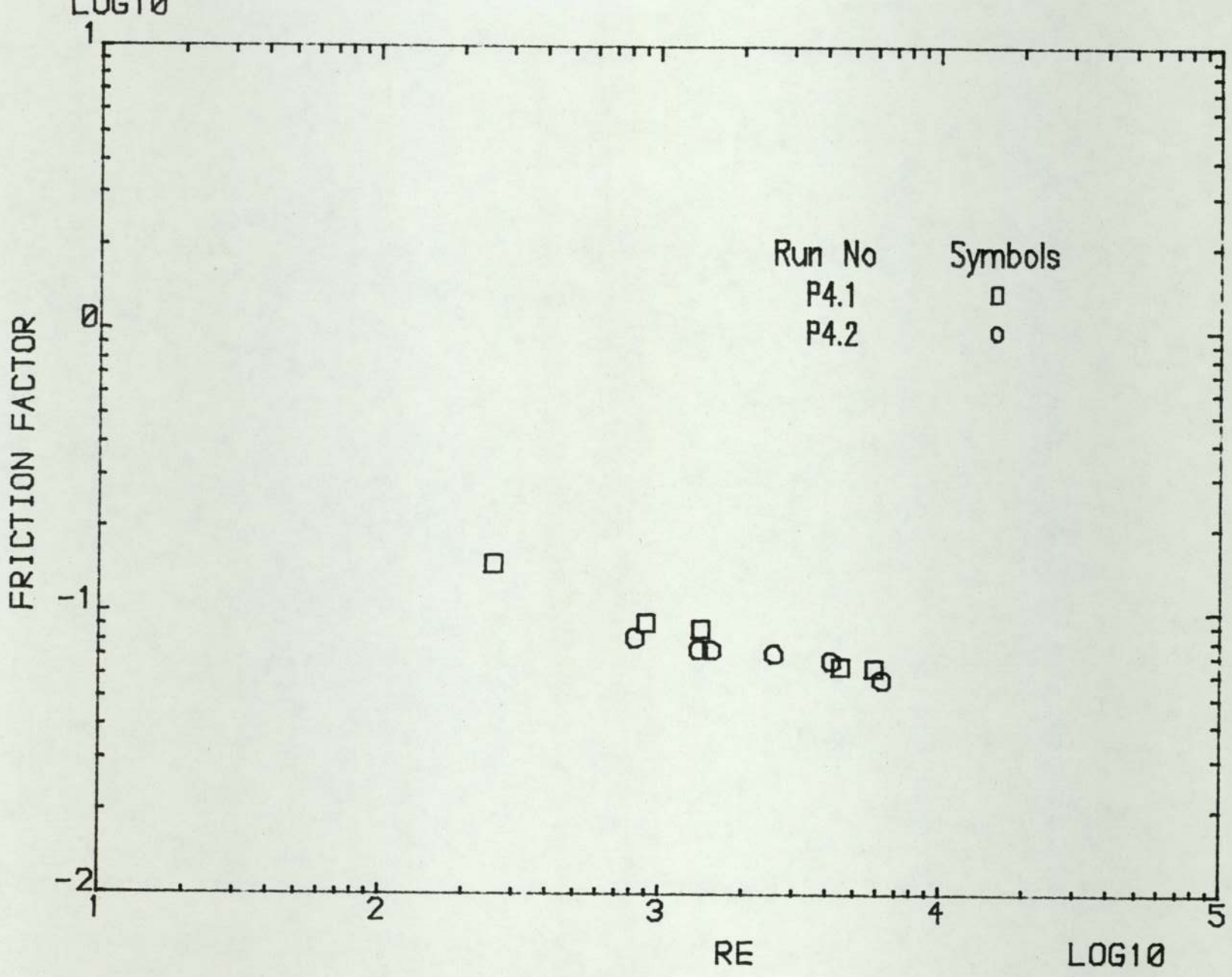

Fig. 9.24 Pressure drop results From Model 4

9.3.6.1 COMPARISON OF PRESSURE DROP FOR INCLINED TUBE BANKS WITH THE IDEAL NORMAL TUBE BANK

As discussed in Chapter 6 due to limitations in the pressure measuring equipment, the pressure drops were measured only across the Reynolds number range from 200 to 6300 for all four models; the comparison is therefore limited to this range, and is shown in Figures 9.25–9.27. It can be seen that compared on this basis the results of the three inclined tube banks showed a marked deviation with respect to the normal tube bundle data.

The pressure drop of inclined tube banks indicated values of 86±2% for Model 2 ($\varphi=70^{o}$), 68±2% for Model 3 ($\varphi=57.5^{o}$) and 50±2% for Model 4 ($\varphi=45^{o}$) with respect to the pressure drop for the ideal normal tube bank.

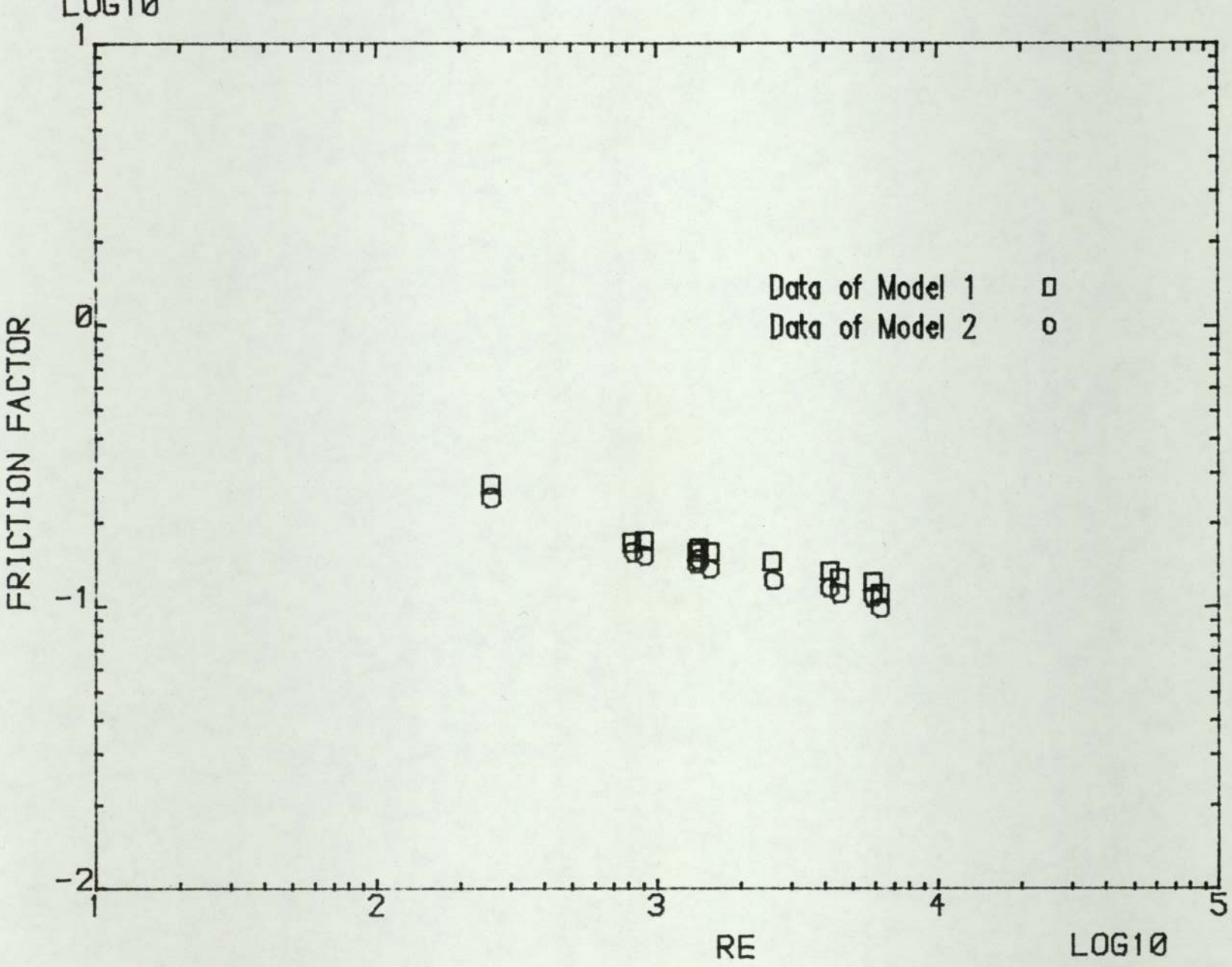

Fig. 9.25 Comparison of pressure drop data from Model 2 with those from Model 1

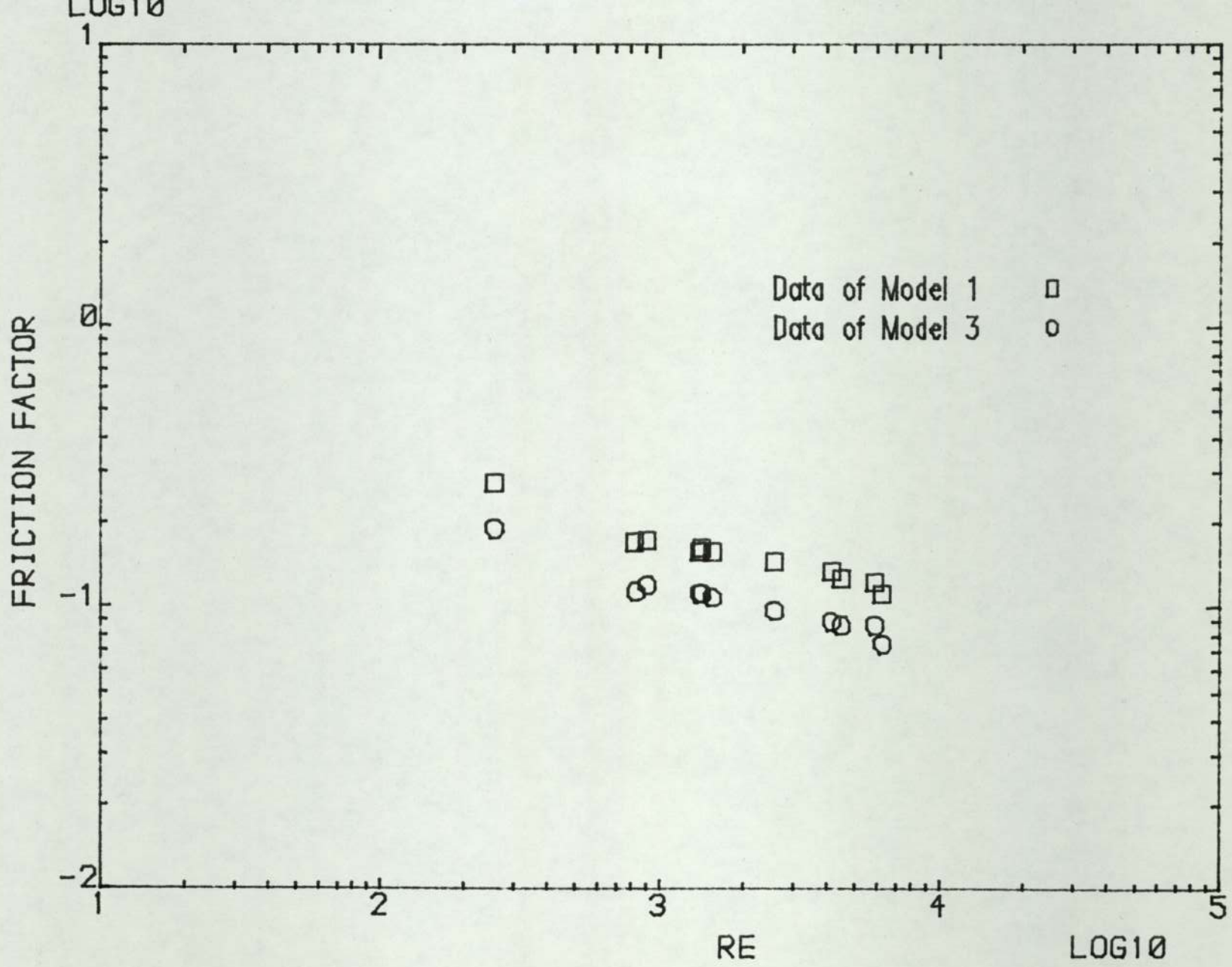

Fig. 9.26 Comparison of pressure drop data From Model 3 with those From Model 1

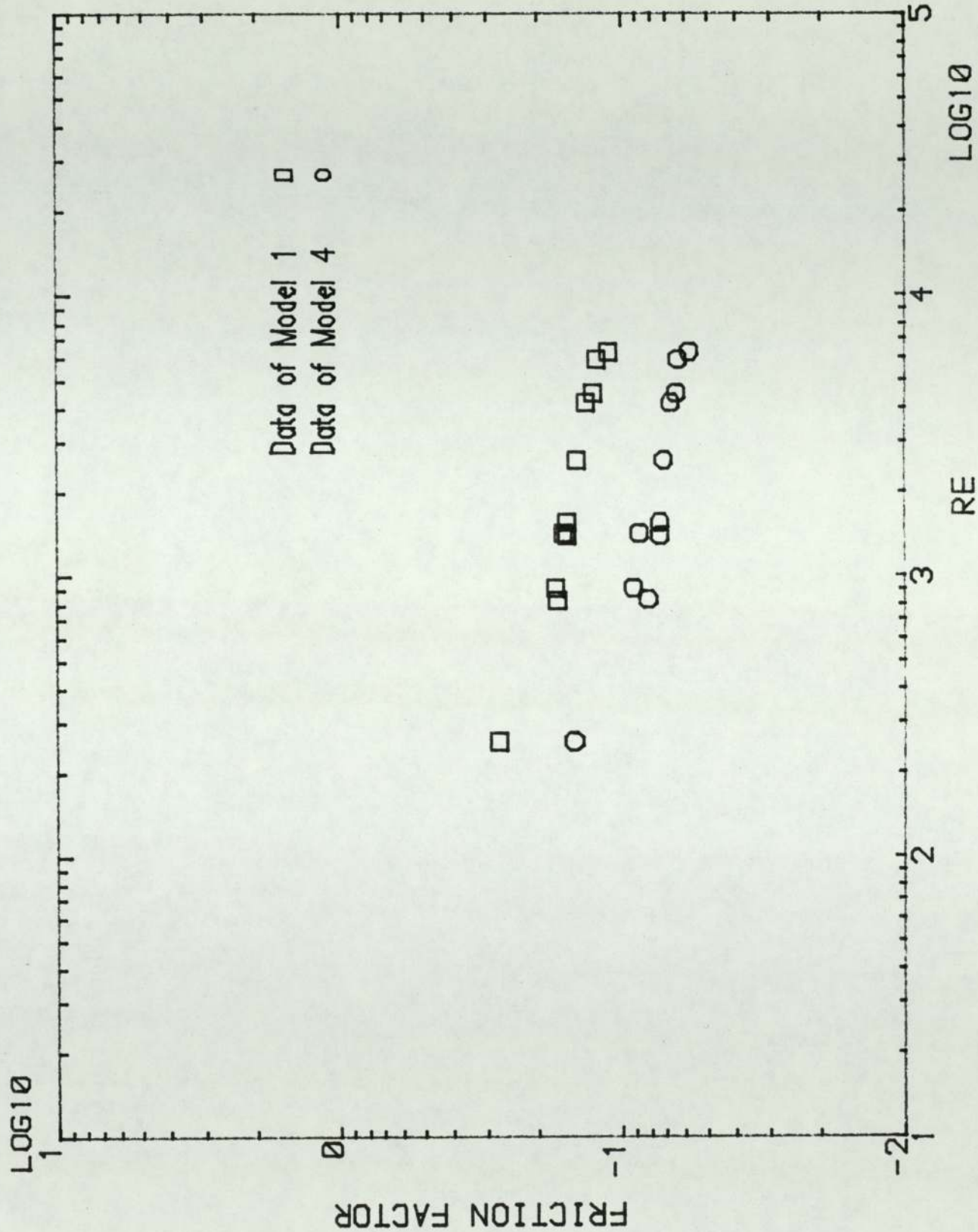

Fig. 9.27 Comparison of pressure drop data From Model 4 with those From Model 1

9.4 CONCLUSIONS

The following conclusions can be drawn from this work.

1. The investigation of transfer coefficients for the inclined tube bank shows the following.

(i) The transfer coefficients from Models 1 and 2 at Reynolds number less than 200 and transfer coefficients from Models 1 and 3 at Re<50 are virtually the same and hence a single curve can be used to show the correlation of the results from these three models at Re<50, whereas the results from Model 4 are 10% lower as compared to those of the normal tube bank. Therfore as the yaw angle decreases the effect of inclination on transfer coefficient appears at lower Reynolds numbers.

(ii) For the Reynolds number range 200–1300, the differences between transfer coefficients increase up to 5, 16 and 25% as Reynolds number increases for Models 2, 3 and 4 respectively, but the gradient of the curves are different and decrease with lower yaw angle.

(iii) The differences between inclined and normal tube bank results remain constant for the range 3000<Re<12 600. The transfer coefficient values, i.e. $Sh/Sc^{1/3}$, decreased by roughly 5% for Model 2 ($\varphi=70^{o}$), 21% for Model 3 ($\varphi=57.5^{o}$) and 30% for Model 4 ($\varphi=45^{o}$).

2. The role of natural convection in inclined tube banks has been investigated

using the method of analysis of Mandelbaum et al. [1973]. It was found that natural convection plays no significant role at the lowest Reynolds numbers considered in this work.

3. The entrance and exit effects of inclined tube banks have been studied and the following conclusions are drawn.

(i) In the range $1.0<Re<1000$ the first and twelfth (i.e. last row) rows of Models 2, 3 and 4 show significantly lower transfer coefficients to those for a tube row in the interior of the tube bank, and the interior rows exhibit nearly constant values of transfer coefficient, to within $\pm 2\%$.

(ii) For Reynolds number greater than 1000 up to 12 600 the entrance effects differ from the cases where $Re<1000$. Model 2 with a yaw angle of 70^{o} showed an increase in transfer coefficient over the first four rows whereas Models 3 and 4 gave an elevation in transfer coefficient over the first three rows. The last row showed a decrease for all models.

ii) The increase in transfer coefficient for first few rows depends on both Reynolds number and yaw angle. As Reynolds number increases the depression in transfer coefficient is lower with respect to the interior transfer coefficients, and with lower yaw angle the slope of the transfer coefficient variation for first few rows shows a lower value.

iv) The exit effect is nearly the same for the complete range of Reynolds number measured, there being a considerable decrease for the 11th and 12th rows.

4. The pressure drops for the three inclined tube bundles were compared to those of the ideal normal tube bank in the range 200<Re<6300 using a friction factor versus Reynolds number plot. In the investigated region the pressure drop at a yaw angle of 70^{o} decreased by roughly 14%, at $\varphi=57.5^{o}$ by 32% and at $\varphi=45^{o}$ by 50 per cent.

CHAPTER TEN

CORRELATION OF TRANSFER COEFFICIENT AND PRESSURE DROP DATA

In the following sections the influence of the yaw angle on the average transfer coefficients and pressure drops are discussed together with the correlation of the experimental results.

10.1 INFLUENCE OF INCLINATION ON TRANSFER COEFFICIENT AND PRESSURE DROP

The average transfer coefficients, in the form of $Sh/Sc^{1/3}$, of the four models are plotted in Figure 10.1 and cover the range of Reynolds number 1.0 to 12 600.

As already noted, the results from the normal tube bank ($\varphi=90^{o}$) and Model 2 ($\varphi=70^{o}$) are very close to each other in the range of $1.0<Re<200$ whereas the Model 3 ($\varphi=57.5^{o}$) starts to deviate from Re=50 and the Model 4 ($\varphi=45^{o}$) indicates a 10% lower magnitude in transfer coefficient to the corresponding value of ideal normal tube bank at the lowest value of Reynolds number measured, i.e. 1.0. It can be seen that as the yaw angle decreases the deviation or decrease in transfer coefficient starts at a lower Re.

From the deviation point, which was at Re = 200 for Model 2, at Re = 50 for Model 3 and at Re = 1.0 for Model 4, the transfer coefficients of the three inclined tube banks diverge and differences increase as the yaw angle decreases up to a Reynolds

number of 1300.

In the range of 3000<Re<12 600 the difference between the transfer coefficients remains constant, i.e. is independent of Reynolds number variation. In this region the transfer coefficients show a decrease by roughly 5% at a yaw angle of 70^{o}, 21% at $\varphi=57.5^{o}$ and 30% at $\varphi=45^{o}$ compared with those of the normal tube bank ($\varphi=90^{o}$). This can be seen more clearly from the replotted data in Figure 10.2.

The effect of yaw angle is seen more clearly in Figure 10.3, where the transfer coefficients are plotted against yaw angle at constant Reynolds number. Figure 10.4 shows the variation of $(Sh/Sc^{1/3})_{ratio}$ (the ratio of the average value of $Sh/Sc^{1/3}$ for each model to the corresponding value for the normal tube bank) for the range 3000<Re<12 600.

The friction factor, f, of the four models are plotted in Figure 10.5 for the range 200<Re<6300. It can be seen that the influence of yaw angle on pressure drop is greater than on the transfer coefficient, i.e. the differences between the pressure drops for inclined tube banks and those for the normal tube bank are greater. The ratio of the friction factor of inclined tube banks with yaw angles of 70^{o}, 57.5^{o} and 45^{o} show values of 86±2%, 68±2% and 50±2% with respect to those of the ideal normal tube bank. The ratio of friction factors for the four models against yaw angle are shown in Figure 10.6.

The above comparisons show an important behaviour characteristic of inclined tube banks. The influence of yaw angle on the pressure drop is greater than on the mass and hence heat transfer.

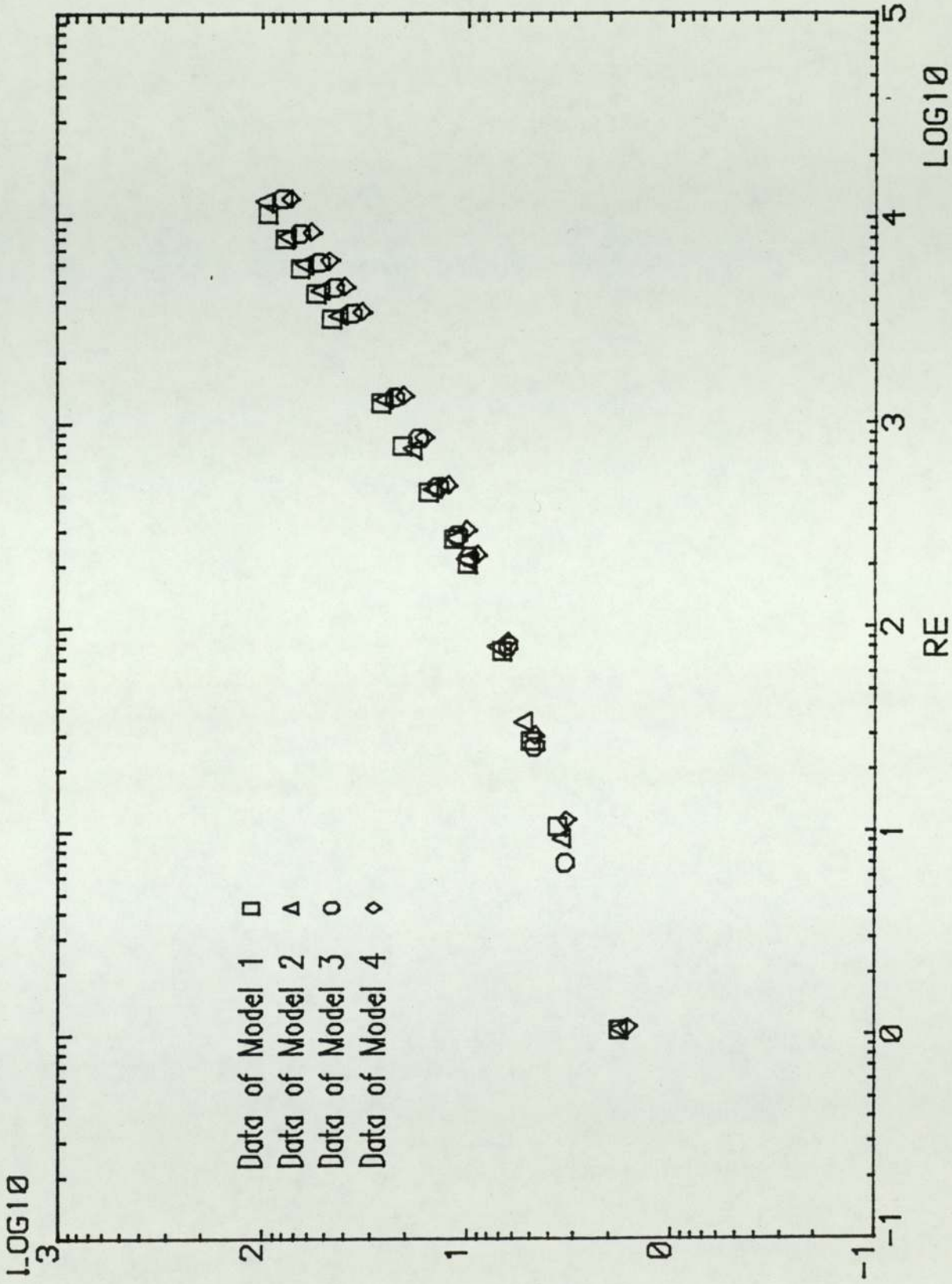

Fig. 10.1 Comparison of transfer coefficient results From the Four Models

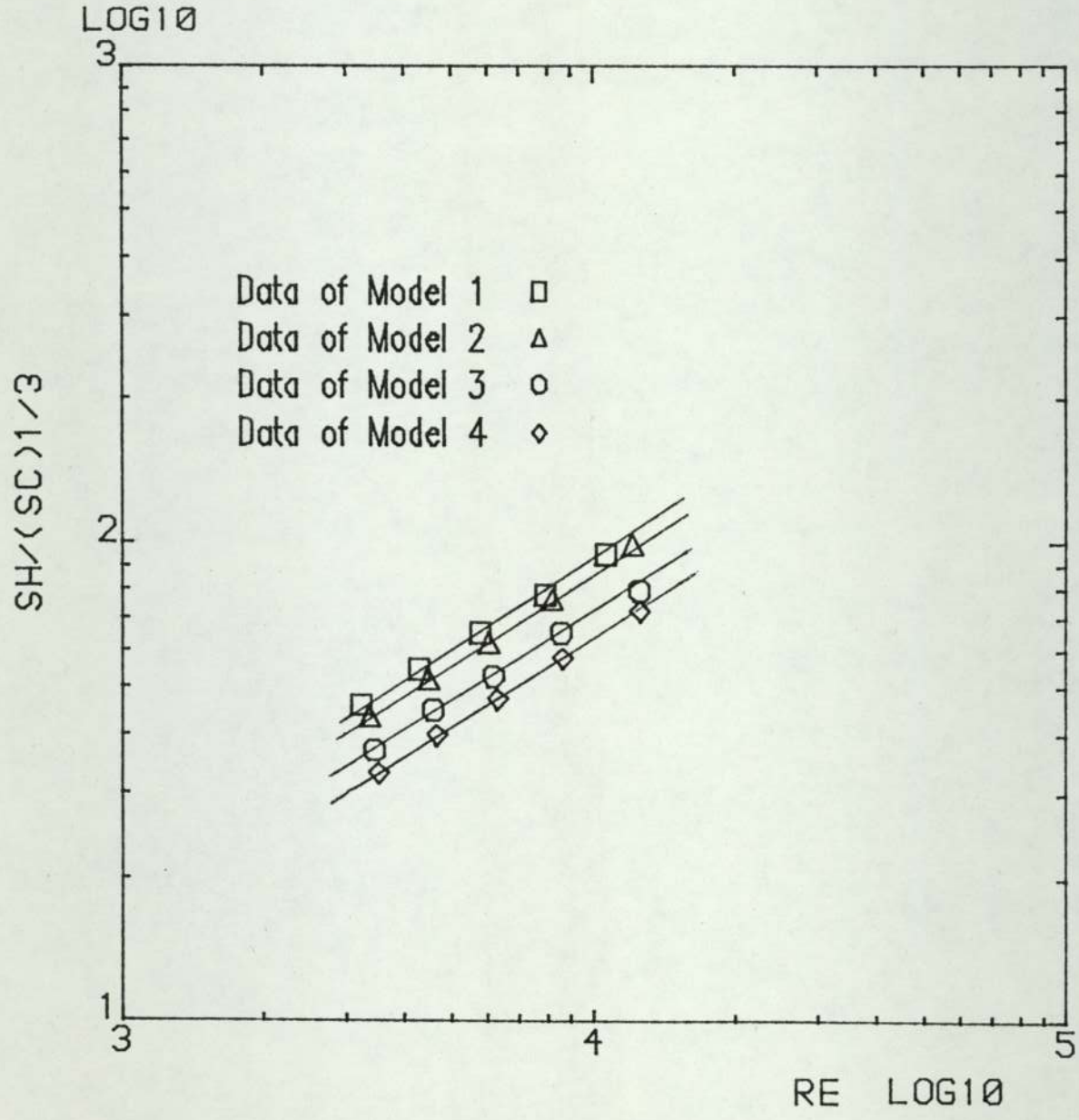

Fig. 10.2 Comparison of results from the Four Models 3000<Re<12 600

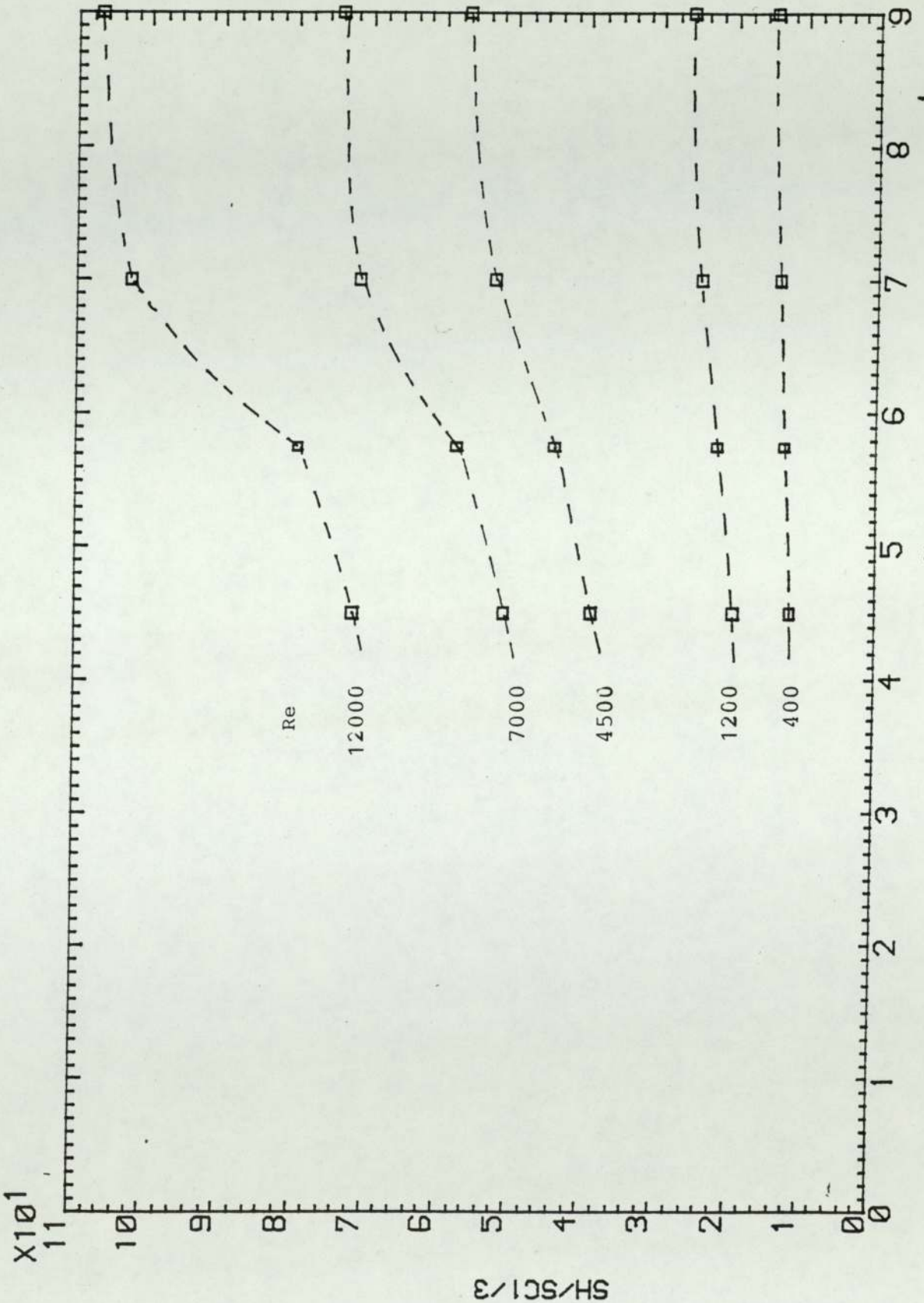

Fig. 10.3 Transfer coefficients From the Four Models at constant Re

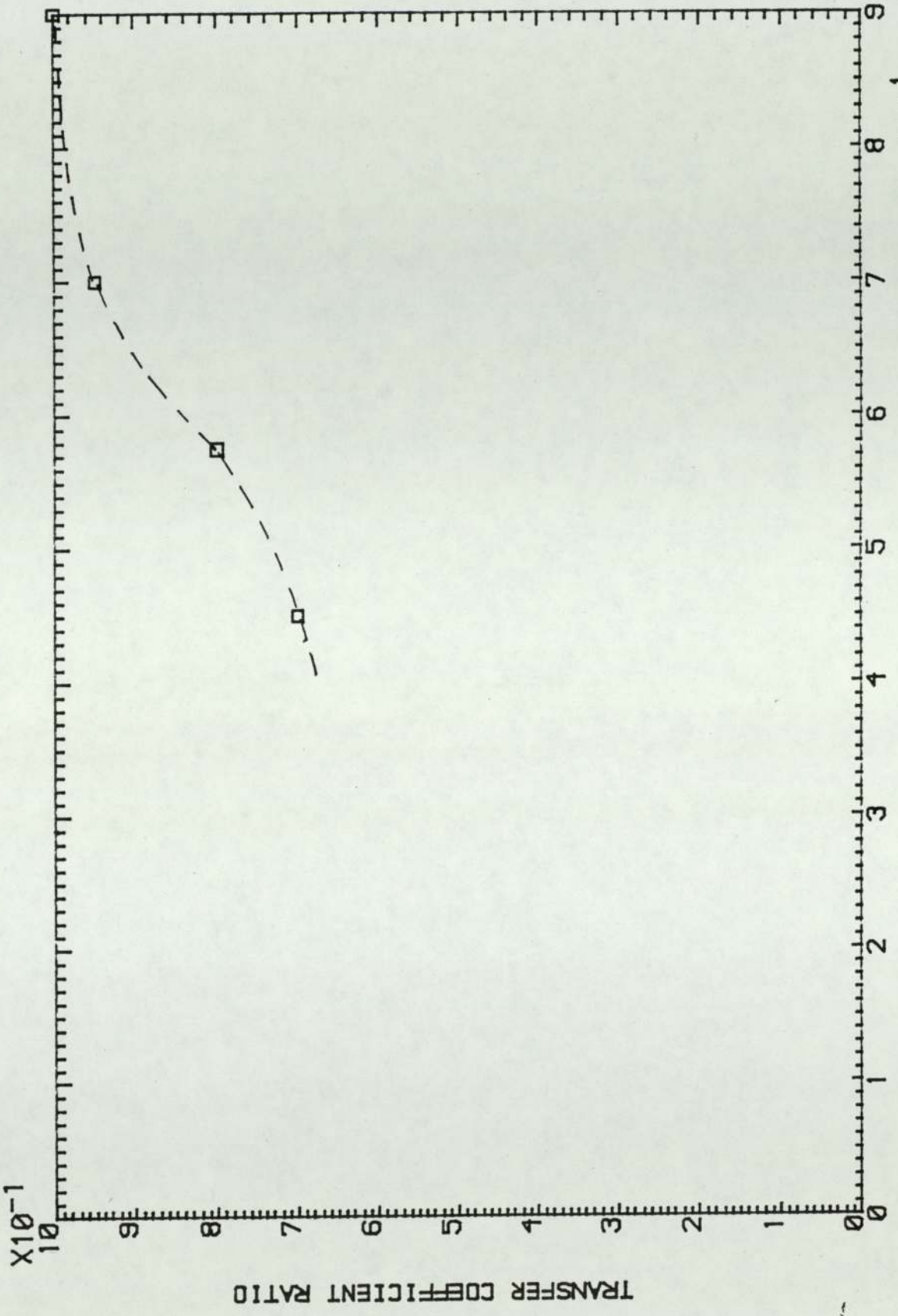

Fig. 10.4 Variation of transfer coefficients with inclination to flow

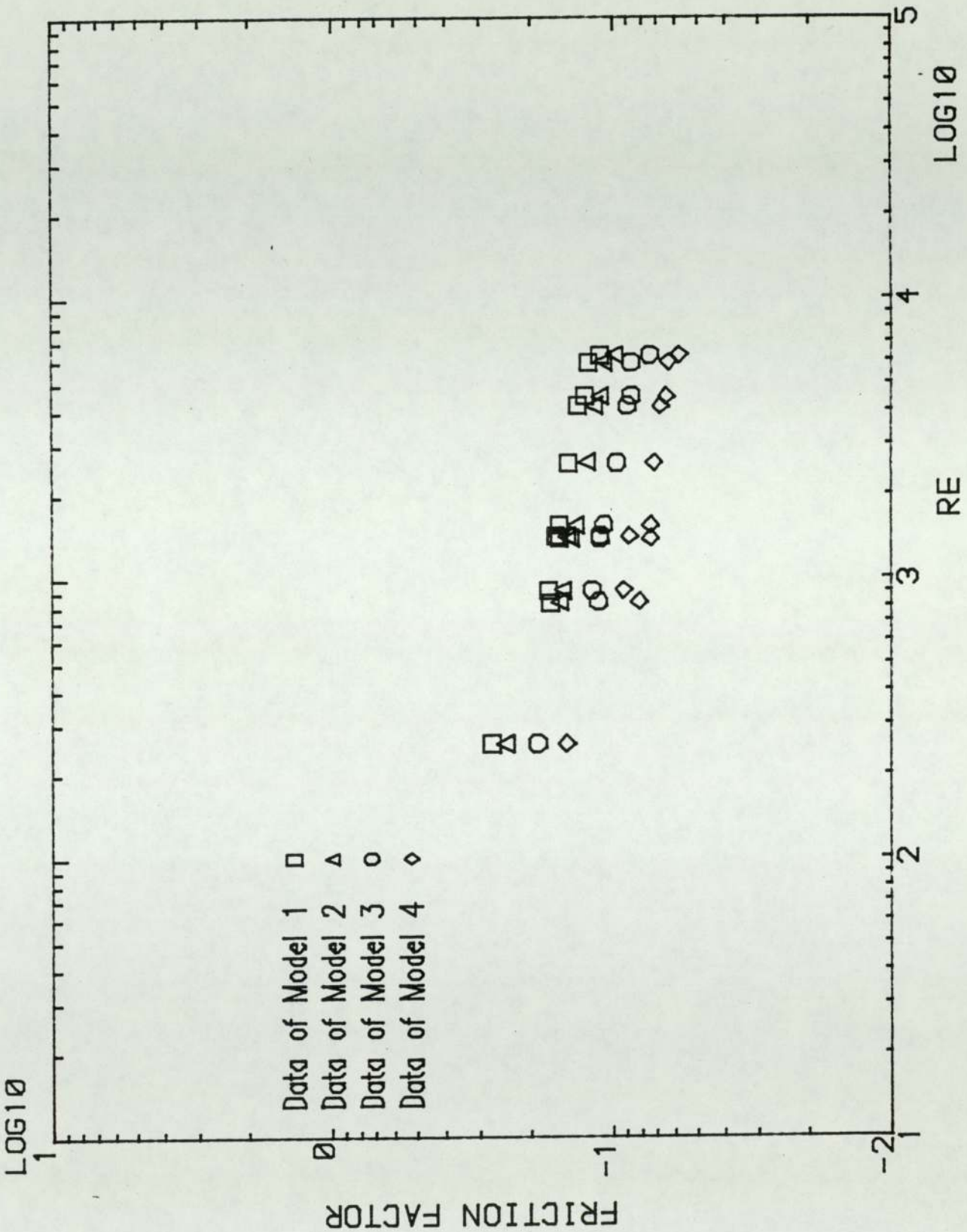

Fig. 10.5 Comparison of pressure drop results from the four models

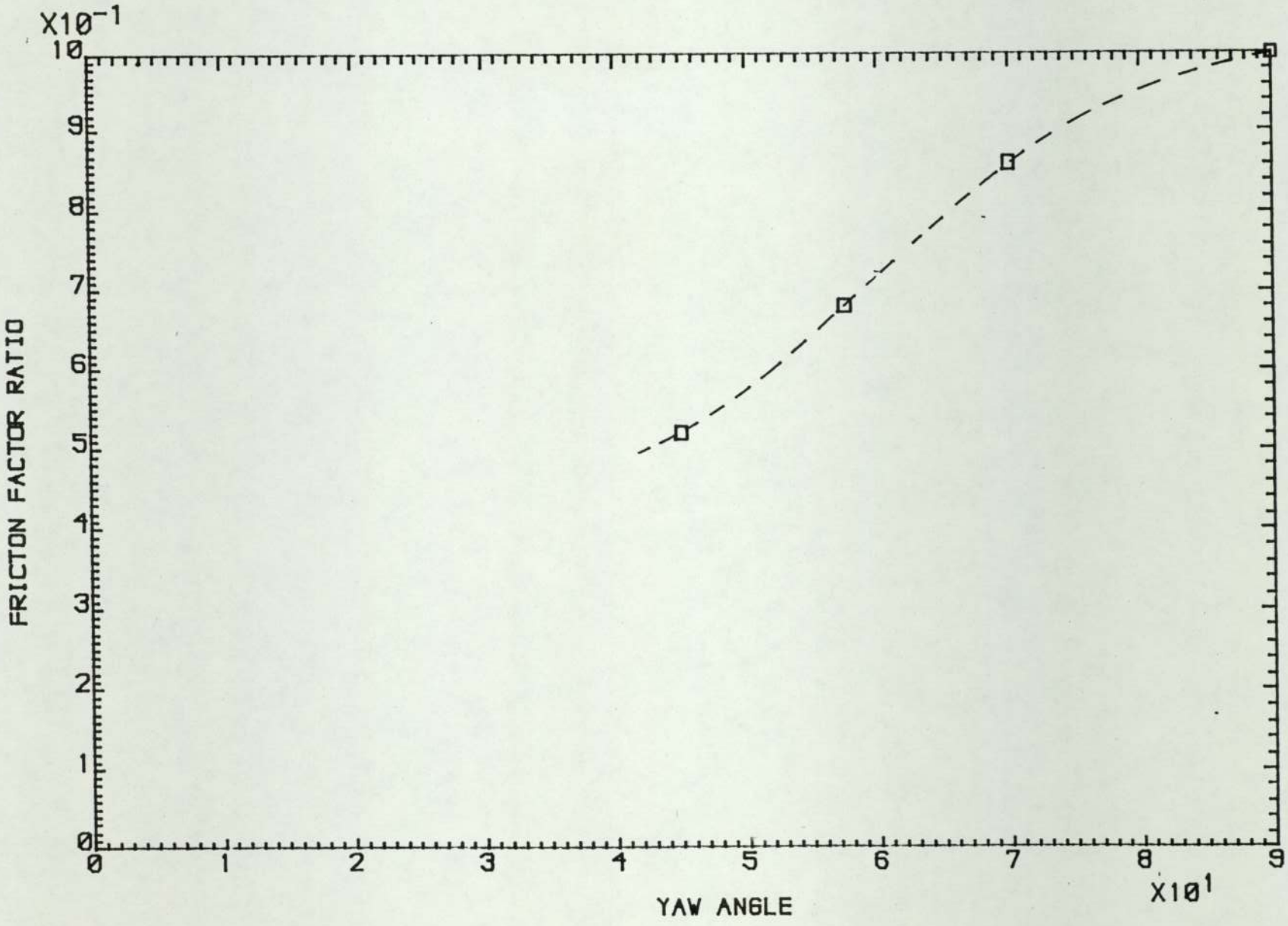

Fig. 10.6 Variation of pressure drops with inclination to Flow

10.2 COMPARISON OF TRANSFER COEFFICIENT RESULTS WITH PREVIOUS WORK

The transfer coefficient ratios of this work are compared with the theoretical work of Butterworth [1978] and the inclination factor of ESDU [1973] in Figures 10.7 and 10.8 respectively. Butterworth [1978] derived the following equation to provide a heat transfer coefficient for the source/sink term in the differential heat balance equation over a portion of the bundle.

$$(h/h_t)^n = \cos^2\phi + (h_a/h_t)^n \sin^2\phi \qquad [10.1]$$

where h_t = heat transfer coefficient for transverse flow

h_a = heat transfer coefficient for axial flow

n = index for power–law relationship between heat transfer coefficient and the viscous dissipation rates

ϕ = inclination angle

h_a/h_t was given the value of 0.2, this being the ratio of literature axial to transverse heat transfer coefficients used by Butterworth [1978]. The relationship was treated as Reynolds number independent by Butterworth [1978], since the Ornatski [1940] data showed a uniform effect of inclination angle across the Reynolds number range investigated. As shown in Figure 10.7 the data of this work are in fair agreement with a value of n = 2, whereas Butterworth obtained a best agreement for values of n of 3 and 4.

The ESDU factor clearly does not agree with the experimental results of this work, although lying close to the n = 3 curve of Butterworth (see Fig. 10.8).

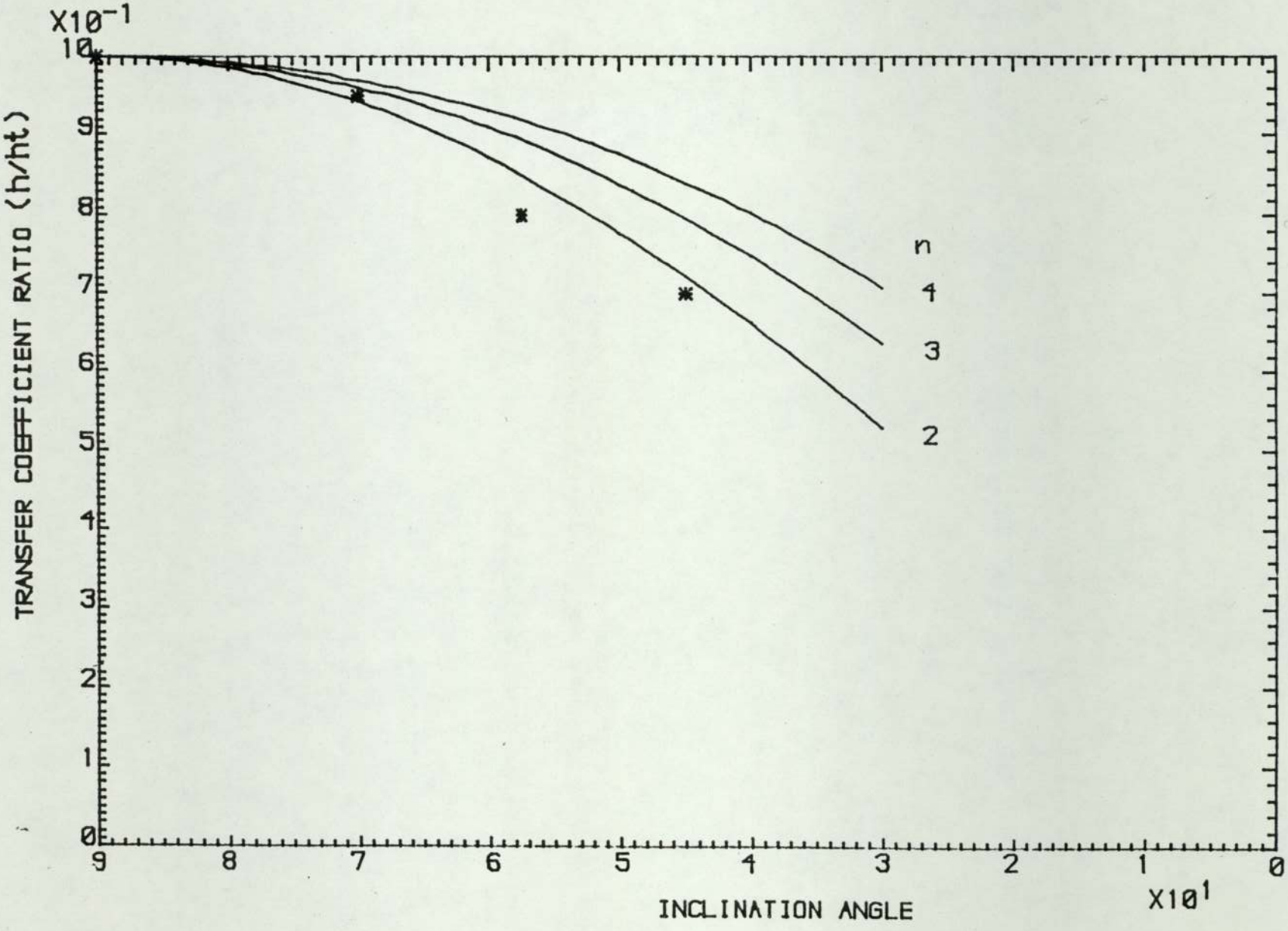

Fig. 10.7 Comparison of transfer coefficient results with Butterworth theory

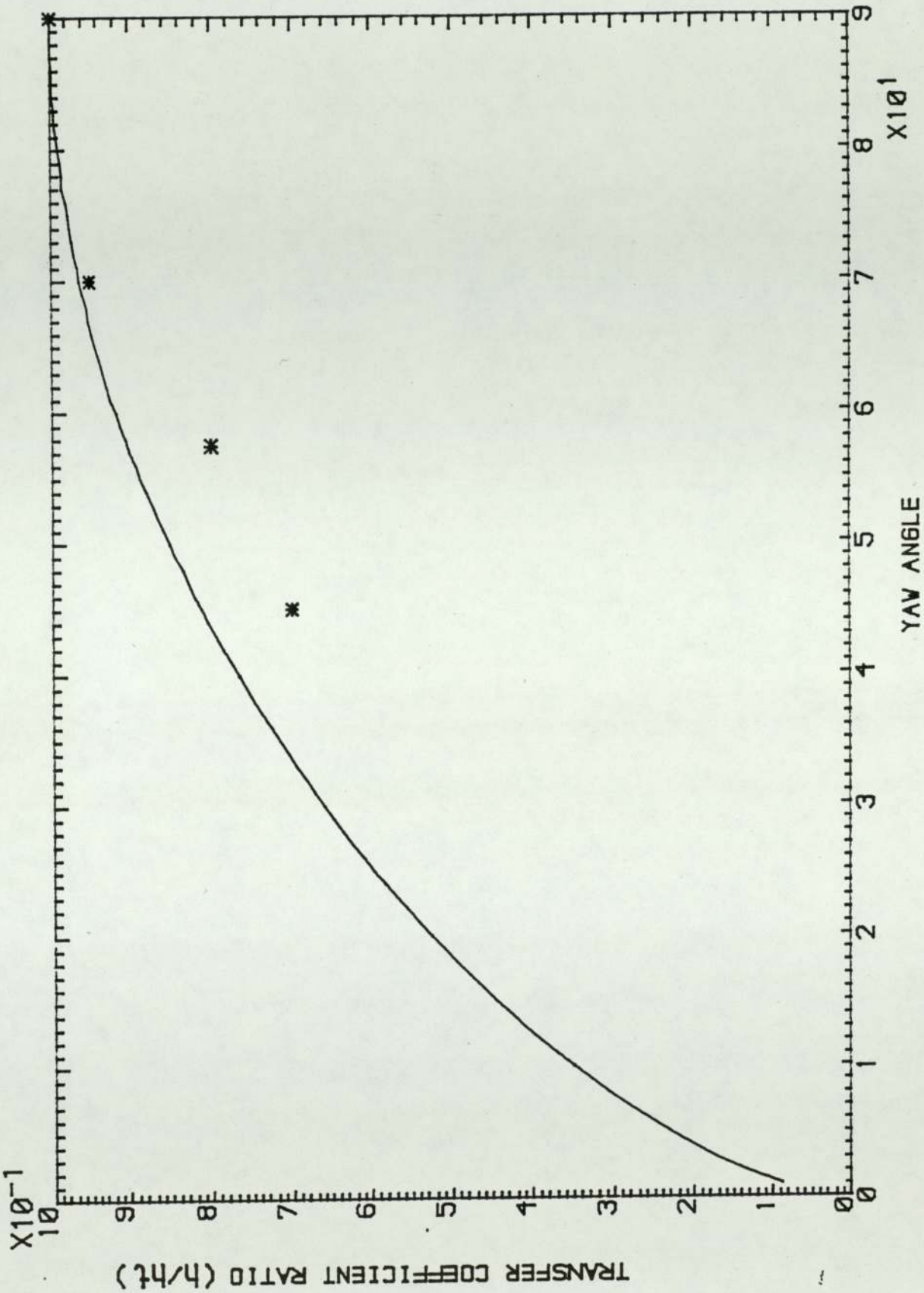

Fig. 10.8 Comparison of transfer coefficient results with ESDU Factor

10.3 CORRELATION OF TRANSFER COEFFICIENT DATA

In this section an attempt is made to correlate the data from the four models against the yaw angle. As discussed before, the differences between the transfer coefficients for inclined tube banks and those of the normal tube bank are constant in the range $3000<Re<12\ 600$. The results in this region are correlated here as the $(Sh/Sc^{1/3})_{ratio}$ against the yaw angle.

No correlation method exists in the literature, the one presented here is based on no theoretical basis but is chosen to have the correct mathematical form to represent the extremes of the data.

Antonopoulos [1984 and 1985] showed that for yaw angles close to 90^{o}, the transfer ratio of coefficients remained close to 1, hence any correlating curve has to be asymptotic at this point. Similarly, at φ close to zero, the limiting case should give the axial flow values, so the curve has to be asymptotic here also. A suitable mathematical function is the hyperbolic tangent and the relationship below is a form of this.

$$T_i/T_n = \{\tanh[S(\varphi - \varphi')\pi/180] + 1\}\{T_c - T_a\}/2 + T_a \qquad [10.2]$$

where $$\tanh[S(\varphi - \varphi')\pi/180] = \frac{e^{S(\varphi - \varphi')\pi/180} - e^{-S(\varphi - \varphi')\pi/180}}{e^{S(\varphi - \varphi')\pi/180} + e^{-S(\varphi - \varphi')\pi/180}}$$

T_a= axial flow value of $(Sh/Sc^{1/3})_{ratio}$

T_c= cross flow value of $(Sh/Sc^{1/3})_{ratio}$

T_i= inclined transfer coefficient $Sh/Sc^{1/3}$

T_n= normal transfer coefficient $Sh/Sc^{1/3}$

S = fitting parameter 1

φ = yaw angle

φ'= fitting parameter 2, values of S and φ' are varied to give the best fit

The value of T_c is 1 and the value of T_a was chosen to be 0.2 (Butterworth [1978]), since this is the ratio of the pure axial to the pure cross flow coefficient.

To find the best correlation fitting the data, a computer programme was used to change the value of φ' between 35^o and 55^o and the value of S between 1 and 5. The best fit is given by values of $\varphi'=40^o$ and S=2.5 therefore

$$T_i/T_n = \{\tanh[2.5(\varphi - 40)\pi/180] + 1\}\{1 - 0.2\}/2 + 0.2 \qquad [10.3]$$

or $$T_i/T_n = 0.4\{\tanh[2.5(\varphi - 40)\pi/180] + 1\} + 0.2 \qquad [10.4]$$

The above correlation and data are plotted in Figure 10.9. The agreement is reasonable and enables prediction to be attempted for yaw angles between 45^o and 0^o, angles outside the range measured experimentally in this work.

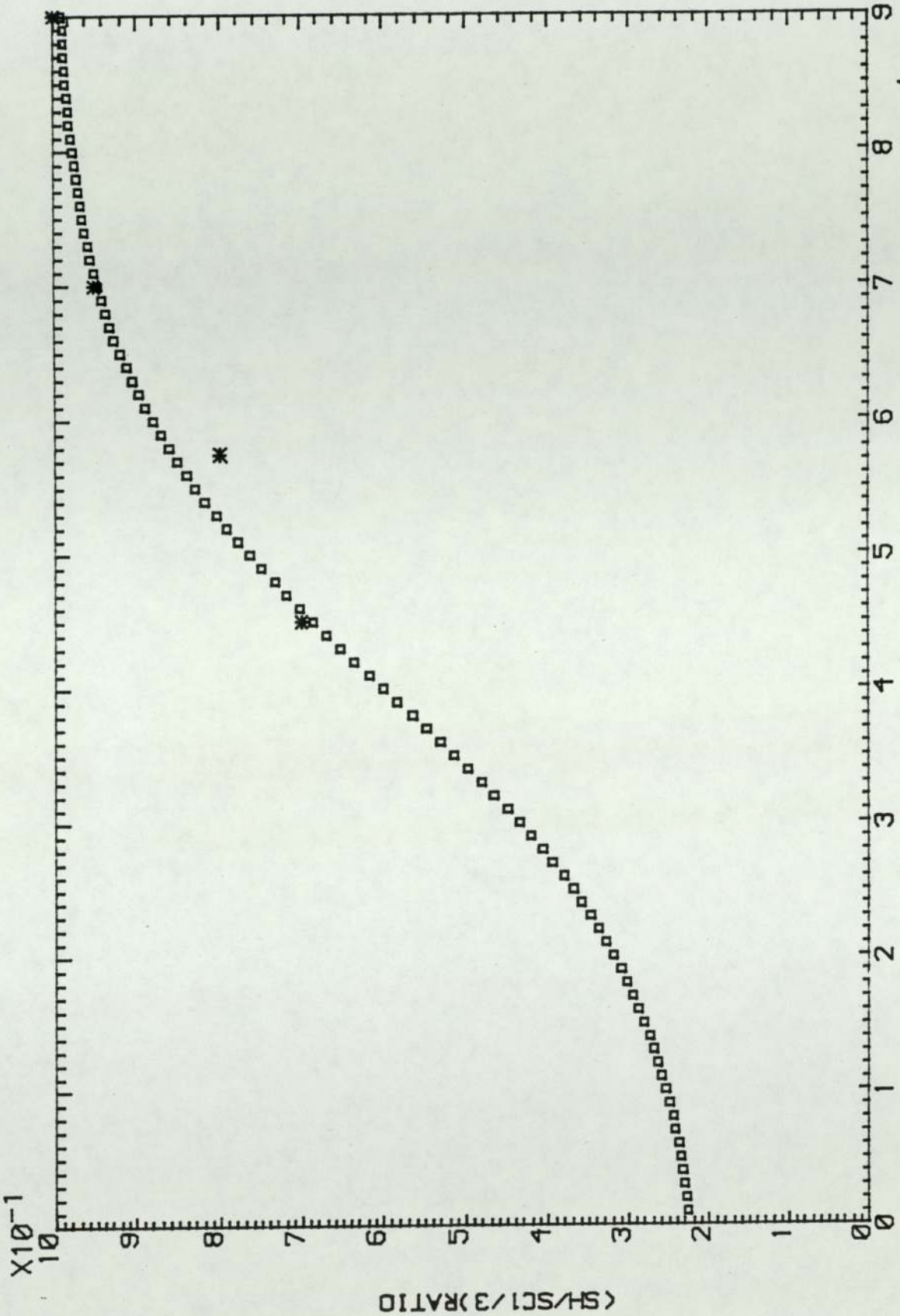

Fig. 10.9 Correlation of ratio of Sh/(Sc)1/3 values for inclined flow against yaw angle

10.4 CORRELATION OF PRESSURE DROP DATA

Comparison of friction factors from inclined tube banks with those from normal tube banks shows that the differences are constant in the range 200<Re<6300. In this section the ratio of the friction factors for inclined tube bank to those of the ideal normal tube bank are correlated against variation in the yaw angle.

As noted above, Antonopoulos [1984] has shown that pressure drop coefficients for inclined tube banks tend asymptotically to those for pure axial and pure transverse flows respectively. Any correlation has then to be asymptotic in the same way, a condition we have already seen to hold for the correlation of transfer coefficients, therefore the previous used equation [10.2] is rewritten in the following form

$$F_i/F_n = \{\tanh[S(\varphi - \varphi')\pi/180] + 1\}\{F_c - F_a\}/2 + F_a \qquad [10.5]$$

where F_a= ratio of axial friction factor to corresponding transverse value

F_c= friction factor ratio at pure cross flow = 1

F_i= inclined friction factor

F_n= normal friction factor

S = fitting parameter 1

φ = yaw angle

φ'= fitting parameter 2, values of S and φ' are varied to give the best fit

The value of F_c was chosen to be 0.18 (Antonopoulos [1984]) which is the ratio of the pure axial to the pure transverse flow friction factor.

The same procedure was used as in the correlation of transfer coefficient data and the best fit is given by the following equation.

$$F_i/F_n = 0.41\{\tanh[3.0(\varphi - 50)\pi/180] + 1\} + 0.18 \qquad [10.6]$$

In Figure 10.10 the above correlation and the pressure drop data are plotted. As shown the agreement is quite good and hence predictions can be attempted for $0^o<\varphi<45^o$, yaw angles outside the range for which measurements were made.

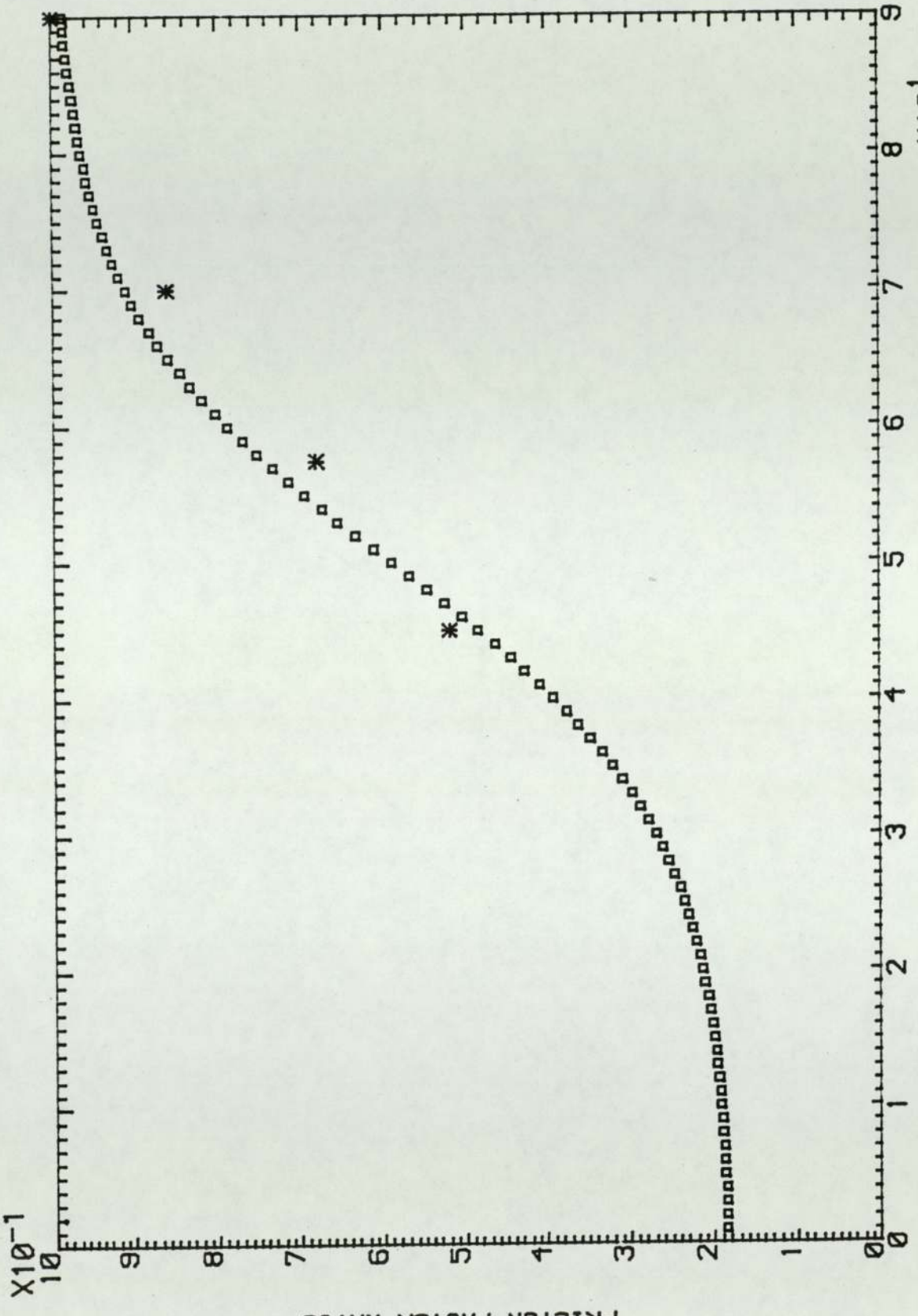

Fig. 10.10 Correlation of ratio of Frictain Factor values for inclined flow against yaw angle

CHAPTER ELEVEN

GENERAL DISCUSSION AND CONCLUSIONS

The following overall conclusions are drawn from the investigations using an electrochemical technique on the performance of ideal normal and inclined tube bank arrangements.

11.1 ELECTROCHEMICAL TECHNIQUE

During the first set of experiments two main problems existed.

First, a current of 1.3 A was needed to activate the complete tube bundle simultaneously, but the maximum current following through the system was about 0.33 A which was not sufficient for the required activation process. Therefore the activation process had to be done row–by–row and hence a long period of time was necessary.

Second, obtaining the plateaux was problematic especially at high flow rates, and this reduced the accuracy of the first set of experimental results at high Reynolds number.

These two main problems were solved in the second set of experiments by placing the anodes and activation anode closer to the cathodes (tube banks), by improving the pretreatment of the cathodes and by using a longer activation process period, with the following results.

1. The current following through the system went up to about 1.1 A since the distance between the cathodes and activation anode was shorter. The overall activation process was reduced in time by carrying out the activation process for every six rows simultaneously. The ohmic resistance of the current flow path had been reduced by moving the anode closer.

2. The limiting current plateaux in the second set of experiments were more pronounced and obtained easily, hence better and more accurate results were obtained. This was achieved by better cleaning of the surface area of the cathodes by rinsing them in 10% HCl solution, and by using a longer period for the activation process (20 minutes). The decreased distance between anodes and cathodes was also a major factor.

11.2 IDEAL NORMAL TUBE BANK

The transfer coefficients in and pressure drops across normal tube banks with P/D ratio of 1.25 have been studied in the range $1.0<Re<11\ 000$, and the following conclusions drawn.

1. The comparison of transfer coefficients and pressure drop data with previous data obtained in direct heat transfer work by Bergelin and co–workers showed a good agreement, striking in view of the difference in scale of the models used.

2. It was found that natural convection has no role at low Reynolds number, by using the method of analysis of Mandelbaum et al. [1973]. Comparison of the results of heat and mass transfer at low Reynolds number showed $Nu/Pr^{1/3}$ and $Sh/Sc^{1/3}$ to

behave in the same way, confirming that natural convection does not contribute to either heat transfer or mass transfer in ideal normal tube banks at the conditions considered in this work.

3. The variation of transfer coefficients of individual rows, thus giving the entrance and exit effects on transfer coefficients, have been studied and the following conclusions are made.

i) The transfer coefficients for the first three row increase, this is due to the turbulence created by the first few rows of the tube bank and hence increasing the heat and mass transfer on the internal rows.

ii) The entrance effect on the transfer coefficients of the first few rows was shown to be greater at higher Reynolds numbers, i.e. the first and second rows show a lower relative mass and hence heat transfer at higher Reynolds number. This decrease was from 85% to 58% for the first row and from 99% to 78% for the second row in the range of Reynolds number studied, i.e. $1.0<Re<11\,000$. At higher Reynolds numbers, the turbulence created by the first few rows of the tube bank is greater.

iii) The transfer coefficients of interior rows, i.e. after the third row, become stable to within ±2% until the 11th row for Reynolds number less than 1000. There is a slight decrease in transfer coefficient for the 11th row at Reynolds number greater than 1000.

iv) The exit effect on the transfer coefficient of the 12th row (i.e. the last row) showed that the variation of transfer coefficient is independent of Reynolds number for

this work. The last row showed a decrease of about 15% for all Reynolds numbers investigated. The 11th row gave a slight decrease at high Reynolds number.

11.3 INCLINED TUBE BANKS

Three inclined tube banks with yaw angles of 70^{o}, 57.5^{o} and 45^{o}, with a staggered tube arrangement have been investigated. The following conclusions may be drawn.

1. The variation with Reynolds number of the average transfer coefficients of inclined tube banks have been studied and the results were compared with those for normal tube banks and show the following.

i) The deviation of the transfer coefficients of inclined tube banks from those of nomal tube banks starts at lower Reynolds number as the yaw angle increases. This happens for Model 2 ($\varphi=70^{o}$) at Re=200, Model 3 ($\varphi=57.5^{o}$) at Re=50 and Model 4 ($\varphi=45^{o}$) at the lowest Reynolds number measured i.e. 1.0 with a low deviation 10%. Therefore as the yaw angle decreases the effect of inclination on transfer coefficient appears at a lower Reynolds number.

ii) The behaviour of three inclined tube banks in the range $200<Re<1300$ is similar, i.e. the differences between the transfer coefficients of inclined tube banks and those of the normal tube bank increases with different slopes up to 5, 16 and 25% as Reynolds number increases for Models 2, 3 and 4 respectively.

iii) The comparison of $Sh/Sc^{1/3}$ for inclined tube banks with those of the normal tube bank shows a constant difference for the range $3000<Re<12\,600$. In this region the transfer coefficients of the inclined tube banks shows a decrease of roughly 5% at a yaw angle of 70^{o}, 21% at a yaw angle of 57.5^{o} and 30% at a yaw angle of 45^{o}, compared with those for the ideal normal tube bank ($\varphi=90^{o}$).

2. The investigation of the role of natural convection for inclined tube banks using the Mandelbaum et al. [1973] technique show the same features as for the normal tube bank, i.e. there is no natural convection contribution at low Reynolds numbers over the range of values studied.

3. The row–by–row variation giving the entrance and exit effects on transfer coefficients has been considered and the following conclusions made.

i) The first and twelfth (i.e. the last row) of all three inclined tube banks have significantly lower values of transfer coefficient from those of a tube row in the interior of the tube bank in the range $1.0<Re<1000$. The interior rows show nearly stable values of transfer coefficient to within ±2%.

ii) The entrance effects differ for Reynolds number greater than 1000. The elevation appears over the first four rows of the second model ($\varphi=70^{o}$) and over the first three rows for Models 3 and 4.

iii) The increase in transfer coefficient of the first few rows depend upon both Reynolds number and yaw angle. The differences between the transfer coefficients of

first few rows and those of the interior rows increase with increasing Reynolds number. The gradient of the transfer coefficient plots show lower values with lower yaw angle.

iv) The exit effect on transfer coefficients is nearly similar for the complete range of Reynolds number investigated and the last row shows a considerable depression.

4. The overall pressure drops across inclined tube banks were measured for Reynolds numbers from 200 to 6300, and compared in the form of a friction factor against Reynolds number plot with those of the normal tube bank. In the investigated region the pressure drops of Models 2, 3 and 4 show decreases of 14%, 32% and 50% compared with results from the normal tube bank.

5. From the points mentioned above it is concluded that the decrease in pressure drop for the inclined tube banks is greater than for mass and hence heat transfer depression, i.e. the effect of flow inclination is higher on pressure drop than on mass and hence heat transfer.

The complex role of tube bank geometry is obvious in process equipment for the chemical and nuclear industries as already discussed. The results obtained in this thesis will aid future analysis of such situations.

An example of this is that the approach of Butterworth [1978] is clearly inadequate. As noted before, transfer coefficients for inclined tube banks are, for laminar flow the same except for $\varphi = 45^{o}$, for which they are 10% lower. Through the transition zone they diverge, and in fully developed turbulent flow the variations become constant. When plotted as a function of inclination in the turbulent region, the

dependence on yaw angle is not as Butterwoth [1978], using a porous body model, supposed, nor is it that proposed by ESDU [1973].

We have seen that Antonopoulos [1984 and 1985] predicted heat transfer in inclined tube banks under conditions of turbulent fully–developed flow, but at Reynolds number above those reached in this work, so that direct comparison is not possible. But his plots of heat transfer and fluid flow show that the results are asymptotic to those for pure cross flow and for pure axial flow, a result confirmed here.

Recent extensions of the porous body approach, (e.g. Zijl and Bruijn [1983]) unlike Butterworth, do not assume isentropic behaviour but allow for different resistances to flow along the principal axes of the tube bank being modelled. While these models have been used to give predictions for complete exchangers, including shell–and–tube heat exchangers, they have not been rigorously tested, and the data obtained here provide such a series of tests.

It is, however, well beyond the scope of this thesis to do this and this task remains a challenge for future work.

NOMENCLATURE

SYMBOL		UNITS
A_{min}	Minimum cross-flow area	m^2
A	Constant (Equation 5.1)	
A_s	Surface area of tube	m^2
B	Constant (Equation 5.11)	
C	Constant (Equation 2.15)	
C_f	Constant (Equation 2.53)	
C_h	Constant (Equation 2.25)	
C_i	Concentration of species i	$kmol/m^3$
Cp	Specific heat evaluated at bulk Temperature	J/kg K
C_b	Bulk ferricyanide ion concentration	$kmol/m^3$
C_s	Ferricyanide ion concentration at cathode surface	$kmol/m^3$
D	Tube outside diameter	m
D_h	Hydraulic diameter (Equation 2.24)	m
D_v	Diffusion coefficient	m^2/s
D_v	Volumetric equivalent diameter	m
D'_v	Modified volumetric diameter	m
D_c	Tube clearance ($P_t - D$)	m
D_i	Diffusion coefficient of species i	m^2/s
ε_D	Eddy diffusivity of mass	
ε_ϕ	Eddy diffusivity of electrostatic potential	
e_{ij}	Rate of strain tensor	m^2/s

SYMBOL		UNITS
f, f_G	Friction factor defined by Grimison	
f_{KL}	Friction factor defined by Kays and London	
f_{CG}	Friction factor defined by Chilton and Generaus	
F	Faraday's constant	C/kmol
F_A	Actual flow rate at any selected reading	m^3/s
F_n	Factor (Equation 2.29)	
F_T	Theoretical capacity	m^3/s
g	Acceleration due to gravity	m/s^2
g_c	Conversion factor	
G	Shell–side mass velocity	kg/m^2s
G_{max}	Mass velocity based on minimum free area	kg/m^2s
h	Heat transfer coefficient	W/m^2K
I	Electrical current density	A/m^2
I_L	Limiting (or diffusion) current	A
k	Thermal conductivity	W/m K
K_1	Rotameter constant	
K_2	Rotameter constant	
k_m	Mass transfer coefficient	m/s
N	Number of tube rows in cross flow zone	
N'	Number of major restrictions encountered in flow through the tube bank	
N_A	Rate of mass transfer	$kmol/m^2s$
NL	Number of tube transverse rows	
n	Number of electrons exchanged in a given electrode process	

SYMBOL		UNITS
P	Tube pitch	m
P_d	Diagonal pitch	m
P_l	Longitudinal pitch	m
P_t	Transverse pitch	m
ΔP	Overall pressure drop	N/m^2
Q	Shell-side fluid volumetric flow rate	m^3/s
R	Universal gas constant	8.314 J/mol K
S	Surface area of rows	m^2
S_e	Outside surface area of even row	m^2
S_i	Outside surface area of a tube	m^2
S_l	Longitudinal pitch to diameter ratio	m
S_o	Outside surface area of odd rows	m^2
S_p	Perimeter of tube across the minor axis	m
S_t	Transverse pitch to diameter ratio	m
T	Temperature of fluid	K
t	Time	s
V	Velocity of fluid	m/s
V_{max}	Maximum velocity based on the minimum free area	m/s
V_s	Superficial velocity	m/s
y	Distance from electrode	m
w	Weight of stainless steel float	kg

GREEK		UNITS
α	Densification coefficient	$m^3/kmol$
β	Densification coefficient	$m^3/kmol$
γ_i	Ionic mobility of species i	
γ_{ij}	Kronecker delta	
∇	Operator $\partial/\partial x + \partial/\partial y + \partial/\partial y$	
∇^2	Laplacian operator $\partial^2/\partial x^2 + \partial^2/\partial y^2 + \partial^2/\partial y^2$	
η	Kinematic viscosity, μ/ρ	m^2/s
μ	Fluid viscosity evaluated at bulk temperature	$N\ s/m^2$
μ_w	Fluid viscosity at wall temperature	$N\ s/m^2$
ψ	Applied potential	
φ	Angle between fluid flow and tube bank	degrees
φ'	Fitting parameter 2 of equation [10.2]	
ϕ	Inclination angle	
ρ	Fluid density evaluated at bulk temperature	kg/m^3
σ	Density of stainless steel float material	kg/m^3
τ	Shear stress	N/m^2

DIMENSIONLESS GROUPS

j_m	Mass transfer j-factor,	$(k_m/V)Sc^{2/3}$
j_h	Heat transfer j-factor	$(h/C_p\rho V)Pr^{2/3}$
Gr	Grashof number	$g\alpha\Delta CD^3/\eta^2$

Nu	Nusselt number	hD/k
Nu_h	Nusselt number based on hydraulic diameter	hD_h/k
Pr	Prandtl number	$C_p\mu/k$
Re	Reynolds number	$\rho VD/\mu$
Re_a	Axial Reynolds number	$\rho V_a D/\mu$
Re_c	Transverse Reynolds number	$\rho V_c D/\mu$
Re_h	Reynolds number based on hydraulic diameter	$\rho V D_h/\mu$
Re_v	Reynolds number based on volumetric equivalent diameter	$\rho V D_v/\mu$
Re'_v	Reynolds number based on modified volumetric equivalent diameter	$\rho V D'_v/\mu$
Sc	Schmidt number	$\mu/\rho D_v$
Sh	Sherwood number	$k_m D/D_v$
Sh_{av}	Average Sherwood number for whole tube banks	
$Sh/Sc^{1/3}$	Mass transfer dimensionless group for each row	
$(Sh/Sc^{1/3})_{av}$	Average $Sh/Sc^{1/3}$ for whole tube bank	
$(Sh/Sc^{1/3})_{mean}$	Mean $Sh/Sc^{1/3}$ for rows 5-10	
$(Sh/Sc^{1/3})_{rel}$	Relative $Sh/Sc^{1/3}$ of each row with respect to the $(Sh/Sc^{1/3})_{mean}$	
$Re/Gr^{1/2}$	Dimensionless parameter to test for natural convection effects	
$Sh/(ScGr)^{1/4}$	Dimensionless parameter to test for natural convection effects	
St	Stanton number	$h/C_p\rho V$

BIBLIOGRAPHY

Achenbach E
The Effect of Surface Roughness on the Heat Transfer from a Circular Cylinder to the Cross Flow of Air
Int. J. Heat Mass Transfer 20 359–369 [1977]

Aggarwal JK and Talbot L
Electrochemical Measurements of Mass Transfer in Semi–Cylindrical Hollows
Int. J. Heat Mass Transfer 22 61–75 [1979]

Agar JN
Diffusion and Convection at Electrodes
Disc. Faraday Soc. 1 26 [1947]

Antonopoulos KA
The Simulation of Turbulent Tube Bank Flow
Proc. of International 84 Athens Conference for Modelling and Simulation
AMSE France [1984]

Antonopoulos KA
Heat Transfer in Tube Banks under Conditions of Turbulent Inclined Flow
Int. J. Heat Mass Transfer 28(9) 1645–1656 [1985]

Bazan JC and Arvia AJ
Ionic Mass Transfer in Flowing Solutions, Electrochemical Reactions under Ionic Mass Transfer Rate Control on Cylindrical Electrodes
Electrochim. Acta 9 667–684 [1964]

Bazan JC and Arvia AJ
The Diffusion of Ferri- and Ferrocyanide Ions in Aqueous Solutions of Sodium Hydroxide
Electrochim. Acta 10 1025–1032 [1965]

Bell KJ
Exchanger Design Based on the Delaware Research Programme
Petrol. Engr. 32 (11) C26 and C409 [1960]

Bell KJ
Final Report of the Co-operative Research Programme on Shell and Tube Heat Exchanger
University of Delaware Engineering Experimental Station
Bulletin No.5 [1963]

Bergelin OP, Davis ES and Hull HL
A Study of Three Tube Arrangements in Unbaffled Tubular Heat Exchangers
Trans. ASME 72 369–374 [1949]

Bergelin OP, Brown GA, Hull HL and Sullivan FW
Heat Transfer and Fluid Friction during Viscous Flow across Banks of Tubes III-A Study of Tube Spacing and Tube Size
Trans. ASME 72 882–888 [1950]

Bergelin OP, Brown GA and Doberstein SC
Part IV – Heat Transfer and Fluid Friction during Flow across Banks of Tubes
Trans. ASME 79 953 [1952]

Bergelin OP, Brown GA and Colburn AP
Part V – A Study of a Cylindrical Baffled Exchanger without Internal Leakage
Trans. ASME 74 841–850 [1950]

Bergelin OP, Bell KJ and Leighton MD
Part VI – Heat Transfer and Fluid Friction during Flow
Across Banks of Tubes : The Effect of Internal Leakage
Trans. ASME 84 53–60 [1958]

Bergelin OP, Bell KJ and Leighton MD
Part VII – By–Passing Between Tube Bundle and Shell, Heat Transfer
Chicago, Chem. Engng Progress Symp. Series, No. 29 55 45–58 [1959]

Bergelin OP, Sullivan KW
Heat Transfer and Fluid Friction in a Shell and Tube Heat Exchanger with a Single Baffle
Chicago, Chem. Engng Progress Symp. Series 52 (18) 85–94 [1950]

Bergelin OP , Colburn AP and Hull HL
Heat Transfer and Pressure Drop during Viscous Flow across Unbaffled Tube Banks
University of Delaware Engineering Experiment Station
Bulletin No. 2 [1950]

Bergelin OP, Leighton MD, Lafferty WL and Pigford RL
Heat Transfer and Pressure Drop during Viscous and Turbulent Flow across Baffled and Unbaffled Tube Banks
Bulletin No.4 [1957]

Berger FP and Ziai Anne
Optimisation of Experimental Conditions for Electrochemical Mass Transfer Measurements
Chem. Eng. Res. Des. 61 377–382 [1983]

Berger FP and Hau K-F. F.-L
Mass Transfer in Turbulent Pipe Flow Measured by the Electrochemical method
Int. J. Heat Mass Transfer 20 1185–1194 [1977]

Bohm U
The specific Densification Coefficient for a Ternary Electrolyte
Anales Asoc. Quim. Argentina, 58, 127–131 [1970]

Boucher DF and Lapple CE
Pressure Drop Across Tube Banks, a Critical Comparison of Available Data and of Proposed Methods of Correlation
Chem. Engng Progress 44 117–134 [1948]

Brauer H
Heat and Flow Investigations on Finned Tube Banks subject to Transverse Flow
Chem. Ing. Tech. 33 (5) 327–335 [1961]

Brauer M
Tests on Cross Flow Heat Exchangers Tubes of Different Shapes
Engrs. Digest, XXII No. 11, 83–87 and No. 12, 85 [1961]

Butterworth D
A Model for Heat Transfer during Three-Dimensional Flow in Tube Bundles
Paper HX–6, 6th. International Heat Transfer Conference, Tornoto 219–224 [1978]

Butterworth D
The Development of a Model for Three–Dimensional Flow in Tube Bundles
Int. J. Heat Mass Transfer 21 253–256 [1977]

Butterworth D
The Correlation of Cross-Flow Pressure Drop Data by Means of the Permeability Concept
UKAEA Report AERE R9435, HTFS RS300 [1979]

Chilton TH and Colburn AD
Mass Transfer (Absorption) Coefficients
Ind. Engng. Chem. 26 1183–1187 [1934]

Chilton TH and Genereaux RP
Trans. AIChE. 29 161–173 [1933]

Colburn AP
A Method of Correlating Forced Convection Heat Transfer Data and a Comparison with Fluid Friction
Trans. AIChE 29 174–210 [1933]

Costello J
Ph.D Thesis, University of Aston [1969]

Coulson JM and Richarson JF
Chemical Engineering Vol. 1 3rd Ed. [1985]

Dobry R and Finn KN
Mass Transfer to a Cylinder at Low Reynolds Numbers
Ind. Engng Chem. 48 1540–1543 [1956]

Dwyer OE, Sheehan TV, and Schomer RT
Heat Transfer for Cross Flow of Water through a Tube Bank at Reynolds Numbers up to a Million, Part 1
Paper No. 54–F–19 ASME meeting, New York [1954]

Dwyer OE, Sheehan TV and Weisman J
Heat Transfer for Cross Flow of Water through a Tube Bank at Reynolds Numbers up to a Million, Part 2
Paper No. 54–F–20 ASME meeting, New York [1954]

Dwyer OE, Sheehan TV, Weisman J and Horn FL
Cross Flow of Water through a Tube Bank at Reynolds Numbers up to a Million
Ind. Engng Chem. 48 1836–1846 [1956]

Edwards A and Furber BN
Proc. Inst. Mech. Engrs. (London) 170 941 [1950]
Eisenberg M, Tobias CW and Wilke CR
Correlation of Limiting Currents under Free Convection Conditions
J. Electrochem. Soc. 100 513–523 [1953]

Eisenberg M, Tobias CW and Wilke CR
Ionic Mass Transfer and Concentration Polarisation of Rotating Electrodes
J. Electrochem. Soc. 101 306 [1954]

Eisenberg M, Tobias CW and Wilke CR
Selected Physical Properties of Ternary Electrolytes Employed in Ionic Mass Transfer Studies
J. Electrochem. Soc. 103 413–416 [1956]

Engineering Science Data Unit (ESDU)
Convective Heat Transfer during Cross Flow of Fluid over Plain Tube Banks
Item No. 73031 [1973]

Engineering Science Data Unit (ESDU)
Pressure Loss during Cross Flow of Fluids with Heat Transfer over Plain Tube Banks without Baffles
Item No. 74040 [1974]

Fairchild HN and Welch CP
Paper No. 61–WA–250, Presented at ASME Ann. Mtg [1961]

Fenech EJ and Tobias CW
Mass Transfer by Free Convection at Horizontal Electrodes
Electrochim. Acta 2 311–325 [1960]

Fouad MG and Gouda AT
Natural Convection Mass Transfer at Vertical Electrodes
Electrochim. Acta 9 1071–1076 [1964]

Fouad MG and Ibl N
Natural Convection Mass Transfer at Vertical Electrodes under Turbulent Flow Conditions
Electrochim. Acta 3 233–243 [1960]

Gosman AD, Run WM, Runchal AK, Spalding DB and Wolfstein MW
Heat and Mass Transfer in Recirculating Flows
Academic Press, London [1969]

Gram AJ, Mackey CC and Monroe ES
Convection Heat Transfer and Pressure Drop of Air Flowing across In-Line Banks, Part II
Trans. ASME Vol. 80 25–35 [1958]

Grassmann PP
Application of Electrolytic Method – I. Advantages and Disadvantages, Mass Transfer between a Falling Film and the Wall
Int. J. Heat Mass Transfer 22 795–798 [1979]

Grassmann P, Ibl N and Trub J
Elektrochemische Messungen von Stoffubergangszahlen
Chem. Ing. Techn. 33 529–533 [1961]

Griffiths E and Awebery JH
Heat Transfer between Metal Pipes and a Stream of Air
Proc. Instn. Mech. Engrs. 39 125 [1933]

Grimison ED
Correlation and Utilisation of New Data on Flow Resistance and Heat Transfer for Cross Flow of Gases Over Tube Banks
Trans. ASME 59 (7) 583–594 [1937]

Hammeke K, Heinecke E and Scholz F
Heat Transfer and Pressure Drop Measurements in Smooth Tube Bundles with Transverse Flow, especially at High Reynolds Numbers
Int. J. Heat Mass Transfer, Vol. 10, pp. 427–446 [1967]

Hegge Zijnen, van der BG
Heat Transfer from Horizontal Cylinders to a Turbulent Air Flow
Appl. Sci. Res. 7(A)205–223 [1958]

Hicks RE and Mandersloot WGB
Chem. Engng Sci. 23 1201 [1968]

Hilpert R
Forschung a.d. Geb. d. Ingenieurwes, 4 215 [1933]

Hinze JO
Turbulence
McGraw Hill, New York [1954]

Hubbard DW and Lightfoot EN
Correlation of Heat and Mass Transfer Data for High Schmidt and Reynolds Numbers
Ind. Engng Chem. Fundam 5 370–379 [1966]

Huge EC
Experimental Investigation of Effects of Equipment Size on Convection Heat Transfer and Flow Resistance in Cross Flow of Gases Over Tube Banks
Trans. ASME 59 (7) 573–581 [1937]

Ibl N
Chimica 9 135-141 [1955]

Jakob M
Heat Transfer and Flow Resistance in Cross Flow of Gases over Tube Banks
Trans. ASME 60 384 [1938]

Jenkins JD
Private Communication [1983]

Jenkins JD, Mackley NV and Gay B
The Influence of Property Number in Forced Convection Heat and Mass Transfer Correlations Letters Heat Mass Transfer 3 105–110 [1976]

Jolls KR and Hanratty TJ
Use of Electrochemical Techniques to Study Mass Transfer Rate and Local Skin Friction to a Sphere in a Dumped Bed
AIChE J. 15 (2) 199–205 [1969]

Jones CE and Monroe ES
Convection Heat Transfer and Pressure Drop of Air Flowing across In–Line Banks, Part I
Trans. ASME 80 18–24, [1958]

Kays WM and London AL
Compact Heat Exchangers
McGraw Hill [1964]

Kays WM, London AL and Lo RK
Heat Transfer and Friction Characteristics of Gas Flow Normal to Tube Banks –The Use of a Transient – Test Technique
Trans. ASME 76 387–396 [1954]

Kazakevitch FP
Effect of the Angle of Incidence of a Gas Stream on the Heat Transfer from a Circular Cylinder
Zh. Tekh. Fiz. 24 1341–1347 [1954]

King DH and Smith JW
Can. J. Chem. Engng 45 329 [1967]

Knudsen JG and Katz DL
Fluid Dynamics and Heat Transfer
McGraw Hill [1958]

Kolthoff IM and Lingane JJ
Polarography Vol. 1
New York Interscience Publishers [1941]

Kolthoff IM and Pearson P
Stability of Potassium Ferrocyanide Solutions
Ind. Eng. Chem. (Anal) 3 381 [1931]

Kraabel JS , Mckillop AA and Baughn JW
Heat Transfer to Air from a Yawed Cylinder
Int. J. Heat Mass Transfer 25 409–418 [1982]

Landolt H, Bornstein R, Eucken Arnold and Hellwege KH
Zahlenwerte und Funktionen aus Physik, Chemie, Astronomie, Geophysik und Techik
Vol II Part 5 P. 316–317, 92 and Part 1 P. 861–863 [1950]

Launder BE and Spalding DB
Mathematical Models of Turbulence
Academic Press, London [1972]

Levich VG
Disc. Faraday Soc. 1 37 [1947]

Lin CS, Denton EB, Gaskill HS and Putnam GL
Diffusion Controlled Electrode Reactions
Ind. Engng Chem. 43 2136–2143 [1951]

Lucas DM
Prediction of the Performance of Rapid Heating Furnaces using Physical and Mathematical Modelling Tecniques
Ph.D Thesis University of Aston [1971]

Lucas DM and Davies RM
Mass Transfer Modelling Techniques in the Prediction of Convective Heat Transfer Coefficients in Industrial Heating Processes
Paper Presented at 4th International Heat Transfer, Conference, Versailles [1970]

Lucas DM and Davies RM
Evaluation of Local and Average Convective Heat Transfer Coefficients in a Furnace Using an Electrolytic Mass Transfer Model
J. Inst. Fuel 31 3137 [1975]

Lyon RN
Chem. Engng Progr. 47 75 [1951]

Mackley NV
Local Shell-Side Coefficients in Shell and Tube Heat Exchangers – The Use of a Mass Transfer Technique
Ph.D Thesis University of Aston [1973]

Mandelbaum JA and Bohm U
Mass Transfer in Packed Beds at Low Reynolds Numbers
Chem. Engng Sci. 28 569–576 [1973]

Masliyah JH
Viscous Flow Across Banks of Circular and Elliptical Cylinders, Momentum and Heat Transfer
Can. J. Chem. Engng 51 550–555[1973]

McAdams WH
Heat Transmission
3rd Edition, McGraw Hill [1954]

Mizushina T
The Electrochemical Method in Transport Phenomena
Adv. Heat Transfer 7 87–161 [1971]

Mizushina T, Ogino F, Oka J and Fukuda H
Turbulent Heat and Mass Transfer between Wall and Fluid Streams of Large Prandtl and Schmidt Numbers
Int. J. Heat Mass Transfer 14 1705–1716 [1971]

Nibber SPS
Shell-Side Transfer in Shell and Tube Heat Exchangers
Ph.D Thesis University of Aston [1981]

Omohundro GA, Bergelin OP and Colburn AP
Heat Transfer and Fluid Friction during Viscous Flow Across Banks of Tubes
Trans. ASME 71 27–34 [1949]

Ornatski AP
Heat Transfer in Tube Banks with Differing Angles of Attack of Gas in Cross–flow
Sovetskoe Kultoturbostroenie, 2 48–52 [1940]

Pascal P
Noureau Traite De Chemie Minerale [1956–64]
Vol. II

Patrick MA, Pembery JGA and Wragg AA
Simulation of Heat Transfer in a Partially Blocked Nine Pin Sub–Channel Using Electrochemical Mass Transfer Techniques
Inst. Chem. Eng. Symp. Ser., 96 879–892 [1984]

Patrick MA and Wragg AA
Modelling of Free Convection in Heat Transfer Using Electrochemical Mass Transfer Techniques
Inst. Chem. Eng. Symp. Ser., 94 45–55 [1985]

Pierson OL
Experimental Investigation of the Influence of Tube Arrangement on Convection Heat Transfer and Flow Resistance in Cross Flow of Gases over Tube Banks
Trans. ASME 59 (7) 563–572 [1937]

Polhausen E
Theoretical Equation for Heat Transfer in the Flow of a Fluid Parallel to Plane Surfaces
Z. angew. Math. Mech. 1 252 [1921]

Prandtl L
Physik Z. 29 487 [1928]

Prandtl L and Tietjens OG
Applied Hydro– and Aeromechanics
McGraw–Hill Book Co. [1934]

Prowse JN
Local Heat Trasnfer Coefficients in a Baffled Shell and Tube Heat Exchanger – End Compartment Study
Ph.D Thesis University of Aston [1977]

Reynolds O
Proc. Manchester Lit. Phil. Soc. 14 7 [1874]

Ross TK and Wragg AA
Electrochemical Mass Transfer Studies in Annuli
Electrochim. Acta 10 1093–1106 [1965]

Rotameter Manufacturing Company
Calibration Data for Metric Series Rotameters
330 Purley Way, Croydon, Surrey

Schutz F
Effect of Number of Rows of Tubes on Pressure Drop and Heat Transfer at High Reynolds Number
Chem. –Ing. Tech. 40 988 [1968]

Schutz G
Natural Convection Mass Transfer Measurements on Spheres and Horizontal Cylinders by an Electrochemical Method
Int. J. Heat Mass Transfer 6 873–879 [1963]

Seban RA and Shimazaki TT
Heat Transfer to a Fluid Flowing Turbulently in a Smooth Pipe with Wall at Constant Temperature
Trans. ASME 73 803–809 [1951]

Shaw PV, Reiss LP and Hanratty TJ
Rates of Turbulent Transfer to a Pipe Wall in the Mass Transfer Entry Region
AIChE J. 9 362 [1963]

Sherwood TK
Trans. AIChE 36 817 [1940]

Sieder EN and Tate GE
Heat Transfer and Pressure Drop of Liquids in Tubes
Ind. Engng Chem. 23 1429–1434 [1936]

Smith AFJ and Wragg AA
An Electrochemical Study of Mass Transfer in Free Convection at Vertical Arrays of Horizontal Cylinders
J. Appl. Electrochem. 4 219–228 [1974]

Snyder NW
Heat Transfer in Air from a Single Tube in a Staggered Tube Bank
Chem. Engng Prog. Symp. Ser.,(5), 49, 11–20 [1953]

Standards of Tubular Exchanger Manufacturers Association
6th Ed. TEMA New York [1978]

Stasiulevicius K et al.
Thermophysical Studies of a Group of Smooth Tube in a Tranverse Flow of Compressed Air
Liet T.S.R Mokelu Akad, Darbai B.4 69–75 [1963]

Stasiulevicius K and Samoska PS
Heat Transfer in Groups of Smooth Tubes
Liet T.S.R Mokelu Akad, Darbai B.4 77–91 [1963]

Sutey AM and Knudsen G
Effect of Dissolved Oxygen on Redox Method for Measurement of Mass Transfer Coefficients
Ind. Engng Chem. Fundam. 6(1) 132 [1967]

Tagg DJ, Patrick MA and Wragg AA
Heat and Mass Transfer Downsteam of Abrupt Nozzle Expansions in Turbulent Flow
Trans. IChemE 57 176–181 [1979]

Taylor GI
Great Britain Advisory Comm. Aeronaut
Report Memo 2272 [1916]

Thoma H
Hochleistungkessel, Julius Springer Berlin, [1921]

Thomson AS, Scott AW, Mck Laird A and Holden HS
Variation in Heat Transfer Rate Around Tubes in Cross Flow
Inst. Mech. Engrs – ASME Proc. General Discussion on Heat Transfer, London, 177 [1951]

Tinker T
Shell–Side Characteristics of Shell and Tube Heat Exchangers, Part I (Analysis for Shell and Tube Exchangers),
General Discussion on Heat Transfer
Inst. Mech. Engrs, London, 89–96 [1951]

Tsederberg NV
Thermal Conductivity of Gases and Liquids p. 231 [1965]

Thorpe JF and Whitely MA
Dictionary of Applied Chemistry
4th Ed. P. 260–262 and 856–859 [1937]

Ulsamer J
Forschung a.d. Geb. d. Ingenieurwes, 3 94 [1932]

Vogtlander PH and Bakker CP
An Experimental Study of Mass Transfer from a Liquid Flow to Wires and Gauzes
Chem. Engng Sci. 18 583–589 [1963]

Walker ATS and Wragg AA
Mass Transfer in Fluidized Bed Electrochemical Reactors
Electrochem. Acta 25(3) 323–330 [1980]

Wallis RP
Photographic Study of Fluid Flow between Banks of Tubes
Engineering 148 423–427 [1939]

Wagner CJ
The Role of Natural Convection in Electrolytic Processes
J. Electrochem. Soc. 95(4) 161-173 [1949]

Washburn Edward W
International Critical Tables of Numerical Data, Physics, Chemistry and Technology
Vol. 5 p 115 [1929]

Weast Robert C
Handbook of Chemistry and Physics
Ed. 1983-1984 p F36-38, F5, D223, D261, B140

Weismam J
Effect of Void Volume and Prandtl Modulus on Heat Transfer in Tube Banks and Packed Beds
AIChE J. 342–348 [1955]

Welch CP and Fairchild HN
Individual Row Heat Transfer in a Cross Flow In–Line Tube Bank
Trans. ASME J. Heat Transfer 143–148 [1964]

Whitaker S
Forced Convection Heat Transfer Correlations for Flow in Pipes, past Flat Plates, Single Cylinders, Single Spheres, and for Flow in Packed Beds and Tube Bundles
AIChE J. 18 (2) 361–371 [1972]

Whitaker S
Elementary Heat Transfer Analysis
Pergaman Press Inc. [1976]

Wilke CR, Tobias CW and Eisenberg M
Free Convection Mass Transfer at Vertical Plates
Chem. Engng Prog. 49 663–674 [1953]

Williams TA
A Mass Transfer Study of Local Transfer Coefficients on the Shell Side of a Cylindrical Shell and Tube Heat Exchanger Fitted with Segmental Baffles
Ph.D Thesis University of Manchester [1962]

Williams FP and Griskey RG
Mass Transfer from Cylinders at Various Orientations to Flowing Gas Streams
Can. J. Chem. Engng 53 500–504 [1975]

Wragg AA
Application of the Limiting Diffusion Current Technique in Chemical Engineering
The Chemical Engineer 39–44, 49 [1977]

Wragg AA and Ross TK
Diffusivity and Ionic Mass Transfer in the Cupric Sulphate System
Electrochim. Acta 13 2192–2194 [1968]

Wragg AA, Serafimidis P and Einarsson A
Mass Transfer between a Falling Liquid Film and a Plane Vertical Surface
Int. J. Heat Mass Transfer 11 1287–1292 [1968]

Zijl W and Bruijn HD
Continuum Equations for the Prediction of Shell–Side Flow and Temperature Patterns in Heat Exchanger
Int. J. Heat Mass Trans. 25(3) 411–424 [1983]

Zukauskas A
Heat Transfer from Tubes in Cross Flow
Adv. Heat Transfer 8 93–160 [1972]

Zukauskas A, Makarevicius VJ and Slanciauskas A
Heat Transfer in Banks of Tubes in Cross Flow of Fluid
Mintis, Vinius [1968]

Zukauskas A, Samoshka PS, Makaryavichyus VI, Shlanchyauskas AA and Zhyugzhda II
Heat Transfer and Pressure Drop for Closely Spaced Tube Banks in Water Flows
Int. Chem. Engng 8 388–392 [1968]

APPENDIX 1

PREPARATION OF ELECTRODES

The electrode surfaces need cleaning for two reasons. The first is to remove any oxide film. Secondly, most previous users of the ferri– and ferrocyanide redox couple (e.g. Eisenberg et al. [1956], Sutey and Knudsen [1967], Mackley [1973] and Berger et al. [1983]) have found that chemical polarisation was an occasional problem unless the electrode surfaces were treated prior to operation.

Some workers such as Hubbard and Lightfoot [1966] and Aggarwal and Talbot [1979] found that the activation process was not necessry. Berger et al. [1983] found that the error (i.e. the difference in value of I_L) caused by omitting the activation step at the lowest value of Reynolds number, $4x10^4$, was 2–3% and become around 9–10% at the highest value of Reynolds number, $4x10^5$, they concluded that the reason why Aggarwal and Talbot [1979] and also Hubbard et al. [1966], found the activation was unnecessary was that in their experiments the Reynolds numbers were less than $3x10^4$.

Eisenberg et al. [1954] performed an investigation into the chemical polarisation in the ferri– and ferrocyanide redox reaction at rotating electrodes and recommended cathodic activation of the electrodes. This consisted of a hydrogen discharge treatment on the cathodes using a current density of 0.2 mA/mm^2 in 5% sodium hydroxide solution for 12–15 min. They found that with freshly prepared solutions under the exclusion of light and with cathodically treated nickel electrodes the chemical polarisation was relatively small. Sutey and Knudsen [1967] also used the cathodic activation

recommended by Eisenberg et al. [1954].

Mackley [1973] extended Eisenberg's procedure for the pre–treatment of the nickel anode and cathodes. He found that satisfactory results were obtained by polishing the electrode surfaces with a fine emery paper. An activation process was then performed by evolving hydrogen at the electrode surface. The current density used for this cathode activation was 0.1 mA/mm^2 for 4–5 minutes. The procedure of Mackley [1973] was used by Prowse [1977] and Nibber [1981].

Berger et al. [1983] used the cathodic activation method of Eisenberg, but before cathodic activation they buffed the electrode surfaces (which were already polished) with fine emery paper and washed with a decreasing agent, carbon tetrachloride.

In the present study an activation current density of 0.1 mA/mm^2, after Mackley [1973], was used. Satisfactory results were obtained by carrying out the activation process for 20 minutes. Due to the construction of the models, polishing the electrode surfaces with emery cloth was impossible, therefore the nickel tube bundles (cathodes) were first rinsed in 10% hydrochloric acid solution, and then in distilled water before the models were replaced in the flow circuit.

APPENDIX 2

ASSEMBLY OF THE EXCHANGER MODELS

Because each model was assembled in the same way, only the assembly of the normal tube bank model is described.

The nickel tubes were rinsed in 1,1,1,–trichloroethane, then these tubes were filled with a low melting point solder (Wood's metals m.p. 70^{o}C) by means of Pasteur pipettes. Nichrome wires were inserted in the solder to act as conductors. In order to keep the solder in its liquid state, the test tube containing it was placed in a beaker of boiling water. While filling these tubes hot air was blown over the work area to prevent early solidification.

The two walls upon which the tubes were mounted were placed in a polystyrene section in order to avoid misalignment and provide perfect parallels. The filled tubes were then inserted into the 3 mm thick and 31.8 mm width walls which had been previously drilled according to the designed dimensions. Twelve perspex half tube sections were fixed to the walls in line with the tubes in alternative rows in order to provide an ideal tube bank.

Once the tubes were placed in their positions the unfilled gap at either end of the tubes were filled by "Araldite". Two identical perspex sheets 26 mm width and 2 mm thick were used to form a rectangular duct which had the following internal dimensions, 20 x 31.8 x 130 mm.

All of the wires from the tubes were insulated by PTFE sleeves. The sixty-six wires were then bundled together and taken out through the gap provided between the flanges. Two identical perspex sections 12 mm width and 2 mm thick were joined together onto this wall providing a triangular duct through which the bundle of wires passed. Any remaining gap in the duct was filled by "Araldite".

The top of this rectangular tube bank was glued to a flange with a thickness of 10 mm. Another flange providing a gap for wires to go through, and two holes for passing the pressure tapping, was sandwiched between this flange and an upper flange. The upper and lower flanges were attached together by four equi-spaced screws.

Two 50 mm long perspex pipes with internal diameters of 6.3 mm were glued to the back of the channel section.

The whole assembly was placed in the flow circuit and held by two flanges.

APPENDIX 3

CALIBRATION OF ROTAMETERS

Five variable area rotameters were used. The first was a glass float GPE MeteRate, which was used for low flow rates. The remaining were Metric 7S, 14S, 24S and 47S sizes Rotameters with stainless steel floats.

In order to increase the accuracy of the results, error in the flow rate had to be reduced. This required calibration of the flowmeters with electrolyte as the flowing media.

Previous users of the electrochemical technique at Aston University and AEE Winfrith used water for the calibration runs and applied the resulting curve for determining the electrolyte flow. The physical properties, especially viscosity, of the two fluids would effect the accuracy of the flow rate. A better technique was needed to increase the accuracy of the flowmeters.

The following procedure was used to calibrate the rotameters with electrolyte as the flowing medium.

A3.1 CALIBRATION OF METERATE ROTAMETER

After finishing the experimental runs a direct calibration using the electrolyte solution was used to calibrate the GPE MeteRate rotameter. By passing the electrolyte

fluid through the rotameter the various flow rates were measured by measuring cylinders, and the actual readings corresponding to these flows were taken from the tube graduation. A table of the tube graduation readings and the actual flow rate measurements is shown in Table A.1, and a calibration graph provided in Figure A.1.

Table A.1

The tube graduation readings and the actual flow rate measurements of the MeteRate rotameter

Scale reading	Flowrate dm^3/min	Scale reading	Flowrate dm^3/min
0.30	1.50	6.70	22.00
0.70	2.00	7.25	24.50
0.80	2.20	7.70	25.00
1.05	2.26	8.58	29.80
1.45	2.70	8.60	30.50
1.80	2.90	9.05	31.80
2.20	3.40	9.18	33.10
2.40	4.00	9.48	34.00
2.90	5.00	9.60	36.80
3.20	5.60	10.50	40.00
3.51	6.16	11.05	43.00
3.82	6.60	11.90	47.00
4.05	7.60	12.20	49.00
4.20	8.32	12.95	52.00
4.39	8.60	13.10	54.30
5.00	11.50	14.00	57.00
5.50	14.75	14.45	61.20
5.80	16.75	14.60	61.70
6.00	17.00	15.50	69.00

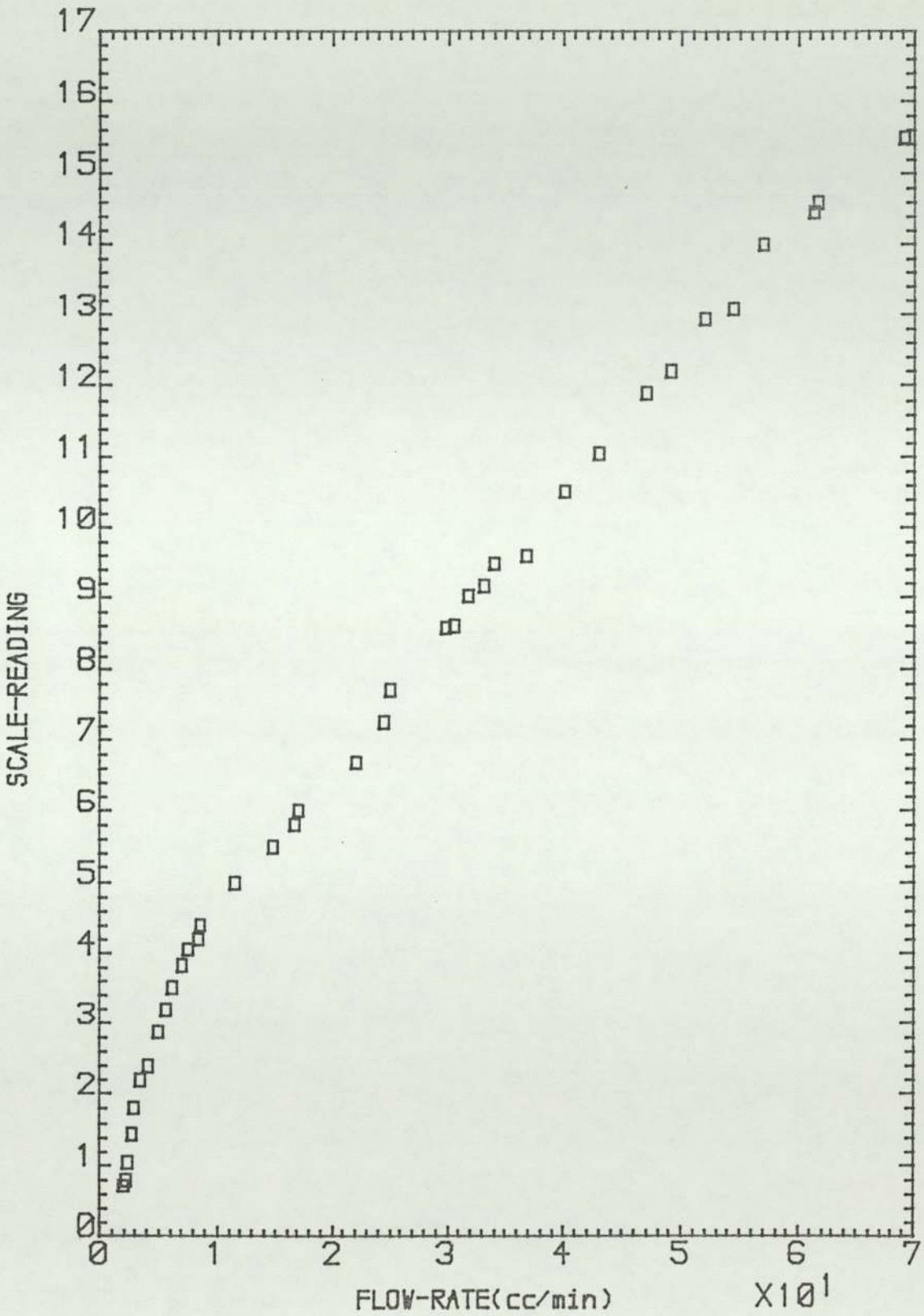

Fig. A.1 Calibration curve of Rotameter G.P.E MeteRate

By using a computer program a polynomial equation through these points was found to be

$$Q = 2.2521 - 0.71168xSR + 0.46714xSR^2 + 4.45395x10^{-2}xSR^3 - 7.40079x10^{-3}xSR^4 + 2.53441x10^{-4}xSR^5 \quad [A.1]$$

where Q is the actual flow rate and SR the scale reading.

Equation A.1 is used in the main computer program to represent the actual flow rate, for calculating the parameters described in Section 8.1.

A3.2 CALIBRATION OF ROTAMETERS SIZES 7S, 14S, 24S AND 47S

For the very high flowrates the direct calibration was hazardous. Therefore Rotameters 7S, 14S, 24S and 47S were calibrated indirectly using the Rotameter Manufacturing Company techniques, since Nibber [1981] had found that the viscosity correction method in these techniques gave virtually the same calibration as the direct method. This is also confirmed below. In the following the indirect calibration method for Rotameters 7S, 14S, 24S and 47S is given.

The Rotameter Manufacturing Company Calibration techniques were used to generate calibration curves for the four flowmeters with the electrolyte physical properties at different temperatures namely 20^{o}C, 25^{o}C and 30^{o}C. The two equations of interest are

$$I = \log \{K_1 \eta [\sigma\rho / w(\sigma - \rho)]^{1/2} x 10^4\} \qquad [A.2]$$

$$F_T = K_2 [w(\sigma - \rho)/\sigma\rho]^{1/2} \qquad [A.3]$$

where w = weight of float in gm,

σ = mean density of float in gm/cm^3,

ρ = density of fluid at working temperature and pressure in gm/cm^3,

η = kinematic viscosity of fluid at working conditions in Stokes, and

K_1, K_2= instrument constants which vary with size of rotameter.

A3.2.1 CALIBRATION OF ROTAMETER SIZE 7S

From the chart for size 7S Figure [A.2], the variables of equation A.2 and A.3 are

$K_1 = 0.147$ $\qquad$ $K_2 = 0.679$

w = float weight = 2.48 gms $\qquad$ σ = float density = 7.96 gm/cc

At $T = 20^oC$ the physical properties of the electrolyte are

$\rho = 1.0419$ gm/cc $\qquad$ $\mu = 0.01233$ P

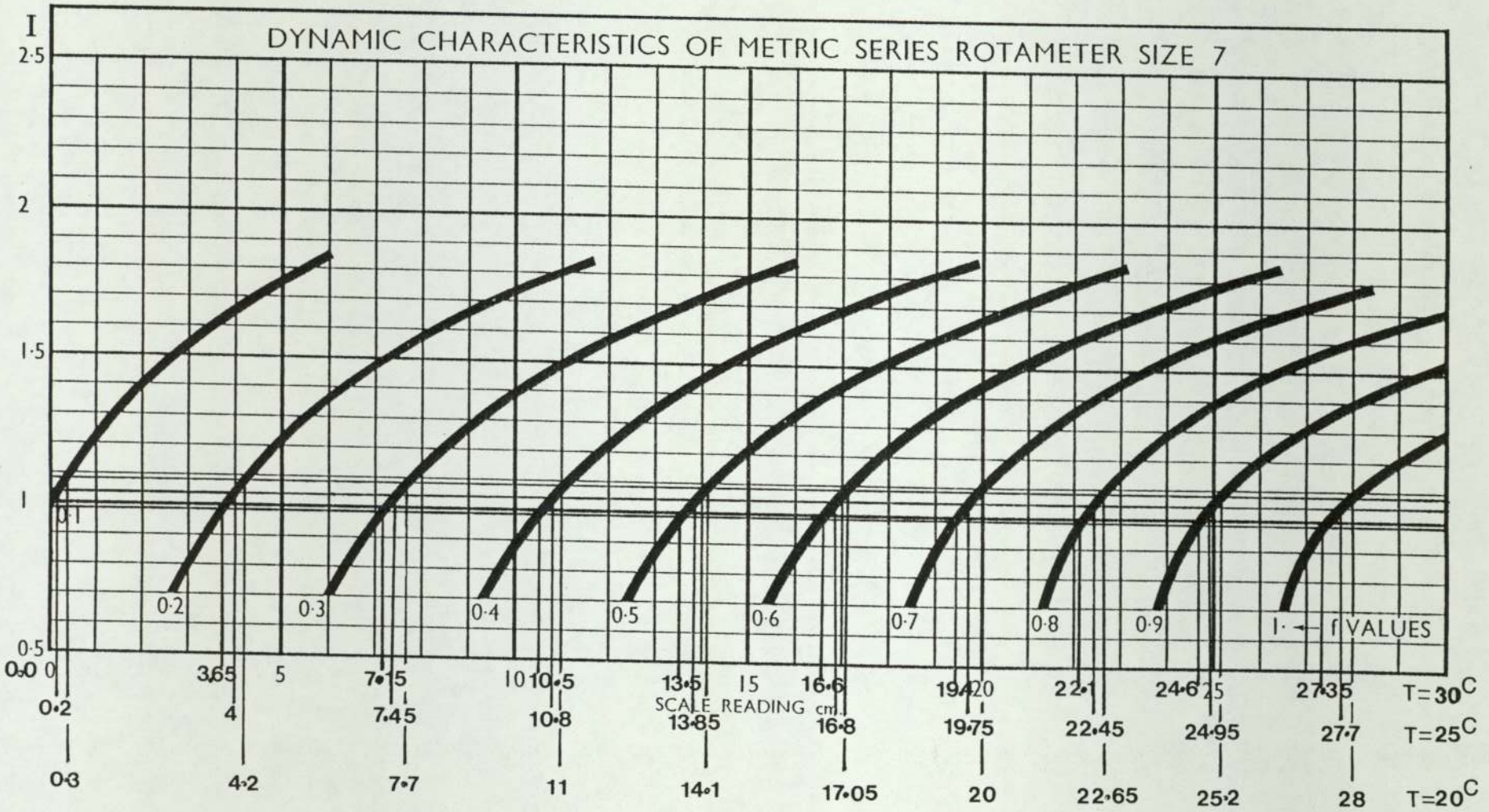

Instrument Constants

$K_1 = 0{\cdot}147$

$K_2 = 0{\cdot}679$

Fig. A.2

Using the formulae of [A.2] and [A.3] we get

$$I = \log\{\ 0.147 \times \frac{0.01233}{1.0419} \times \left[\frac{7.96 \times 1.0419}{2.48(7.96 - 1.0419)}\right]^{1/2} \times 10^4\ \}$$

$$I = 1.082$$

$$F_T = 0.679\ \left[\frac{2.48(7.96 - 1.0419)}{7.96 \times 1.0419}\right]^{1/2}$$

$$F_T = 0.976\ dm^3/min$$

Using the equations [A.2] and [A.3] and physical properties of the electrolyte at T = 25°C and T = 30°C we get:

T = 25°C	I = 1.036874	F_T = 0.977 dm^3/min
T = 30°C	I = 0.9852	F_T = 0.978 dm^3/min

From the characteristic curve (Figure A.2) the scale readings which correspond to plotted values of f at the calculated value I were determined. The values of $F = F_T x\ f$ were obtained. The values of F and the scale reading at temperatures 20°C, 25°C and 30°C are tabulated in Table A.2. The calibration curve of rotameter 7S is plotted in Figure A.3.

Table A.2

Deduced calibration table rotameter size 7S, using electrolyte as flow medium

f	T = 20°C		T = 25°C		T = 30°C	
	Scale Reading	$F = F_T x f$	Scale Reading	$F = F_T x f$	Scale Reading	$F = F_T x f$
0.1	0.30	0.097	0.20	0.097	0.00	0.097
0.2	4.20	0.195	4.00	0.195	3.65	0.195
0.3	7.70	0.293	7.45	0.293	7.10	0.293
0.4	11.00	0.390	10.80	0.391	10.50	0.391
0.5	14.10	0.488	13.85	0.488	13.50	0.489
0.6	17.05	0.586	16.80	0.586	16.60	0.586
0.7	20.00	0.683	19.75	0.684	19.40	0.684
0.8	22.65	0.781	22.45	0.782	22.10	0.782
0.9	25.20	0.878	24.95	0.879	24.60	0.880
1.0	28.00	0.976	27.75	0.977	27.35	0.978

The polynomial equation of those points were found by using a computer program to be

$$Q = 9.03681 \times 10^{-2} + 2.52775 \times 10^{-2} \times SR + 2.45638 \times 10^{-4} \times SR^2 \qquad [A.4]$$

Equation A.4 was utilized in the main computer programme to find the actual flow rate.

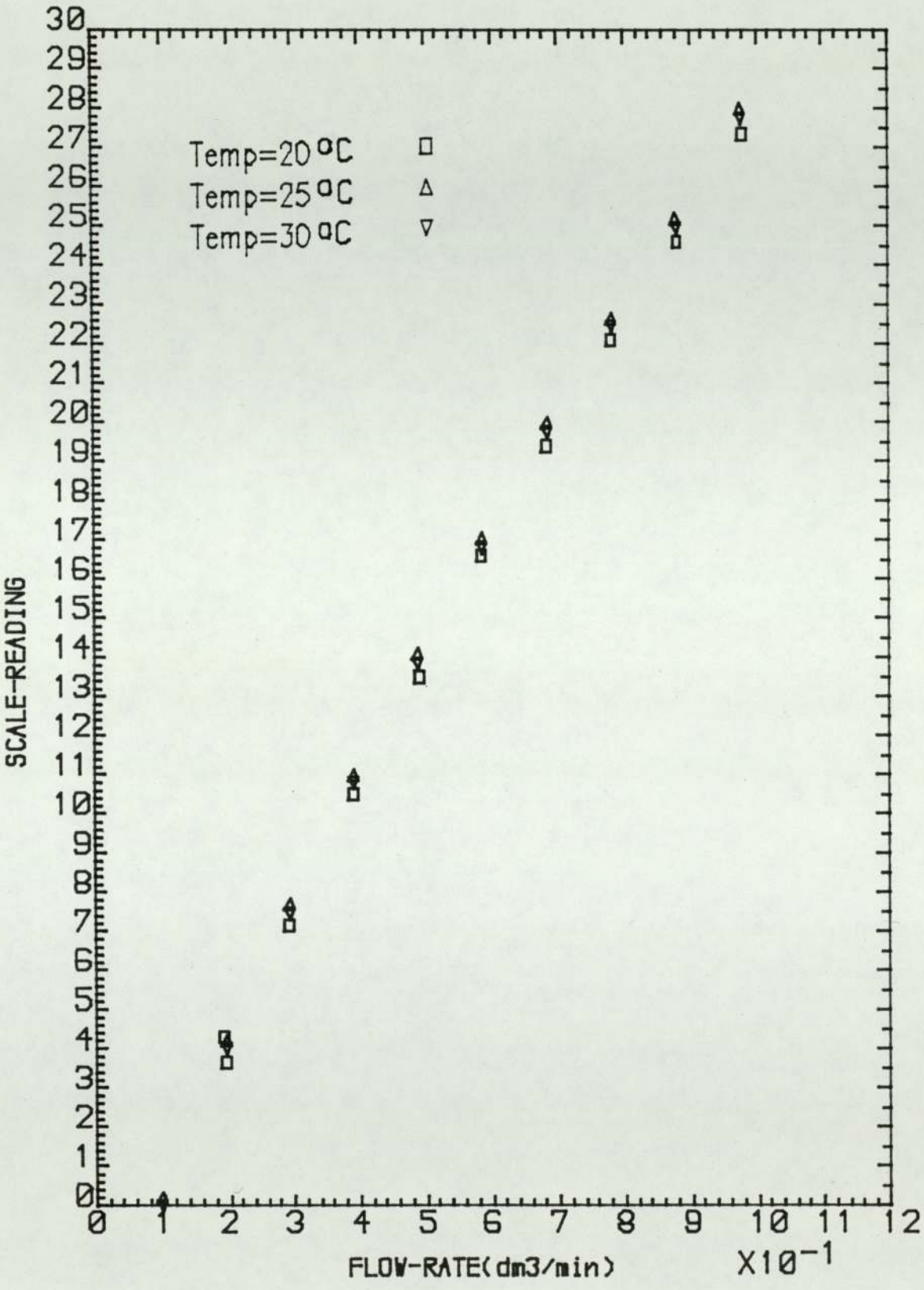

Fig. A.3 Calibration curve of Rotameter 7S

After finishing the experiments, a direct calibration was carried out on rotameter size 7S, similar to that for calibration of the GPE Rotameter (see above). The scale reading in cm and the actual flow rate measured in cm^3/min are set out in Table A.3. The comparison of the results of this direct calibration with the method of the Rotameter handbook is given in Figure A.4. It can be seen that the agreement is good and therefore confirms the method of the Rotameter Manufacturing Company used here.

Table A.3

The tube graduation readings and the actual flow rate measurements

Scale reading	Flowrate cm^3/min
24.0	835
22.5	810
16.9	585
16.4	568
10.3	375
10.1	360
9.2	340
9.0	330
3.75	204
4.5	196
4.3	190

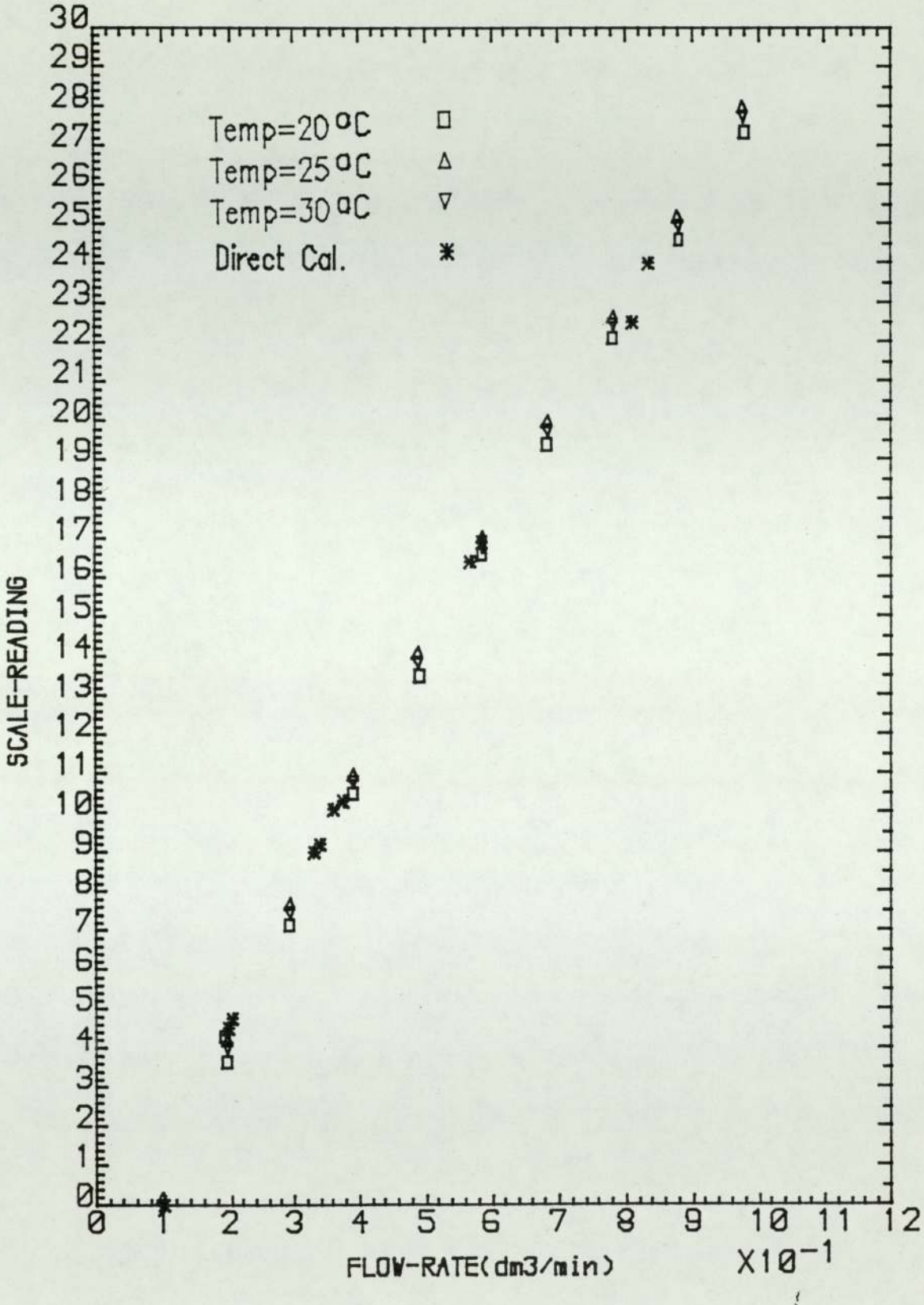

Fig. A.4 Comparison of two calibration methods

A3.2.2 CALIBRATION OF ROTAMETER SIZE 14S

The variables for rotameter size 14S are

$K_1 = 0.379$ $K_2 = 1.316$ $w = 16.5$ gms $\sigma = 7.96$ g/cc

The values of I and F_T at diffrent temperature were calculated using the equations A.2 and A.3.

At	T = 20°C	$\rho = 1.0419$ gm/cc	$\mu = 0.01233$ poises
		I = 1.082	$F_T = 4.882$ dm^3/min
At	T = 25°C	$\rho = 1.0402$ gm/cc	$\mu = 0.01109$ poises
		I = 1.037	$F_T = 4.887$ dm^3/min
At	T = 30°C	$\rho = 1.0385$ gm/cc	$\mu = 0.00984$ poises
		I = 0.985	$F_T = 4.891$ dm^3/min

From Figure A.5 the co–ordinate I and F_T were used with the empirical corrections provided to produce the calibration curve. The values of F and scale reading at temperature 20°C, 25°C and 30°C are shown in Table A.4. The calibration curve of Rotameter size 14S is plotted in Figure A.6.

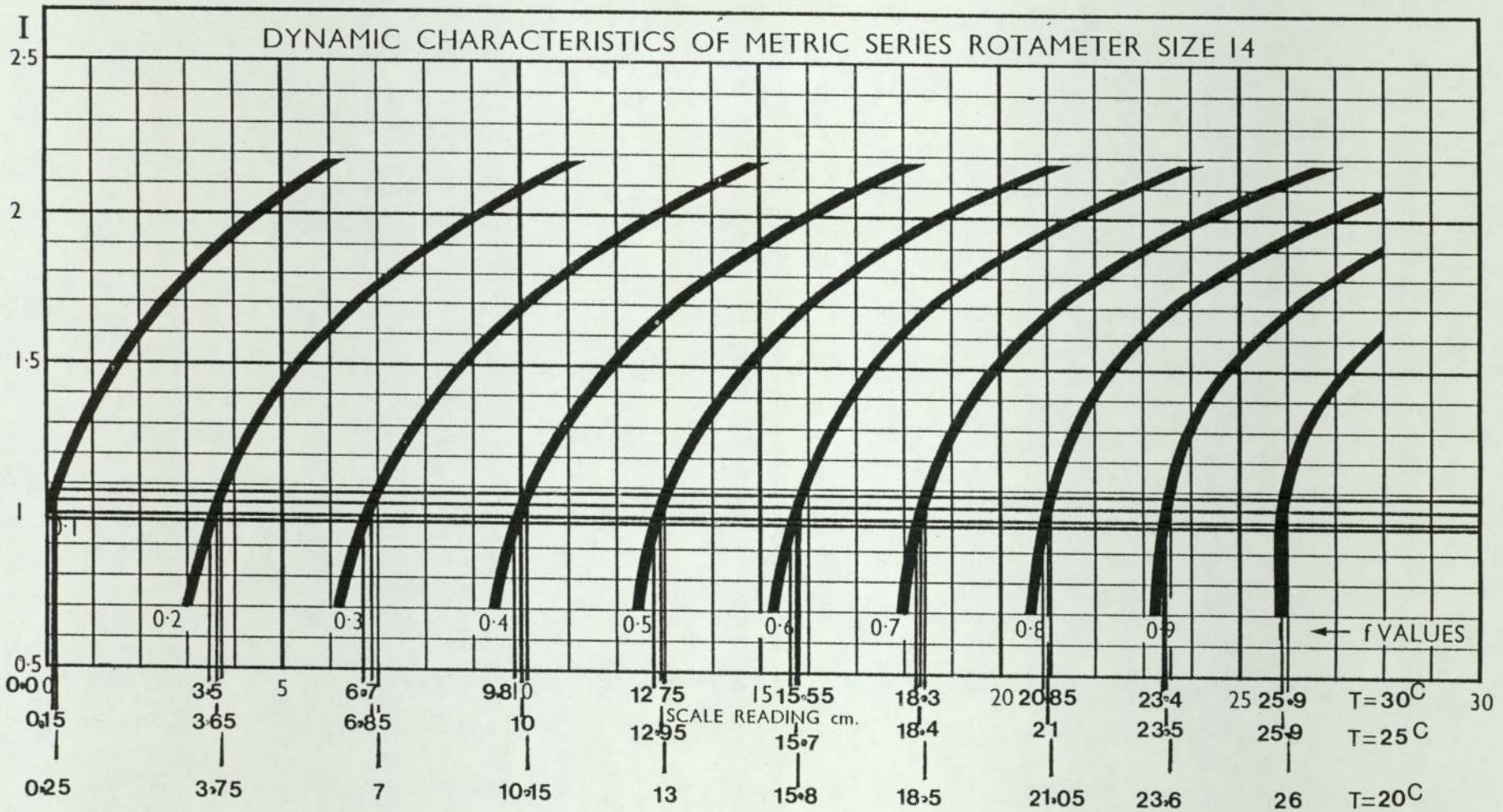

Instrument Constants

$K_1 = 0{\cdot}379$
$K_2 = 1{\cdot}316$

Fig. A.5

METRIC 14

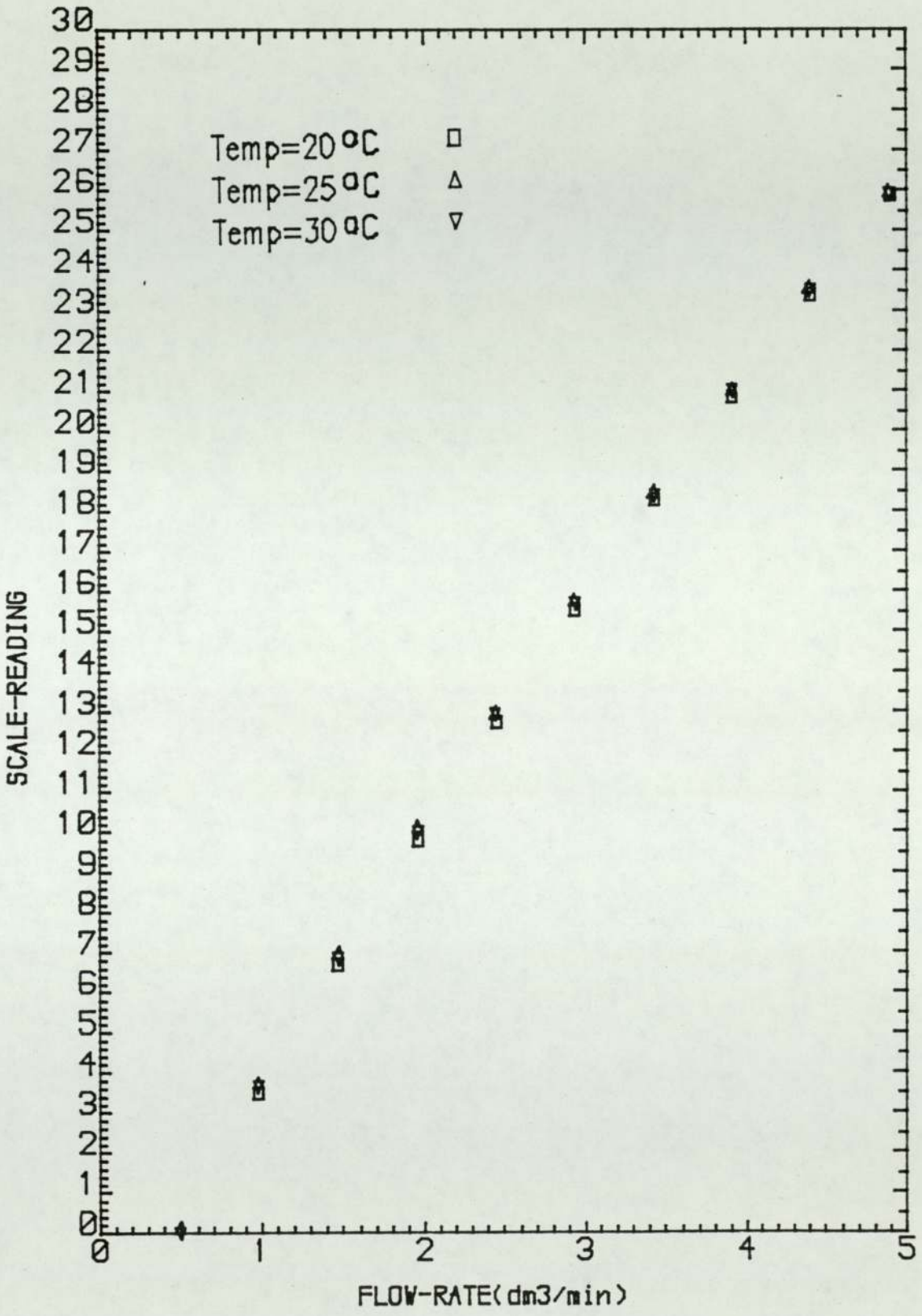

Fig. A.6 Calibration curve of Rotameter 14S

Table A.4

Deduced calibration table rotameter size 14S, using electrolyte as flow medium

f	T = 20°C		T = 25°C		T = 30°C	
	Scale Reading	$F = F_T x f$	Scale Reading	$F = F_T x f$	Scale Reading	$F = F_T x f$
0.1	0.25	0.4882	0.15	0.4887	0.00	0.4891
0.2	3.75	0.9764	3.65	0.9774	3.50	0.9782
0.3	7.00	1.4646	6.85	1.4661	6.70	1.4673
0.4	10.15	1.9528	10.00	1.9548	9.85	1.9564
0.5	13.00	2.4410	12.95	2.4435	12.80	2.4455
0.6	15.80	2.9292	15.70	2.9322	15.55	2.9346
0.7	18.50	3.4174	18.40	3.4209	18.30	3.4237
0.8	21.05	3.9056	21.00	3.9096	20.85	3.9128
0.9	23.60	4.3938	23.50	4.3983	23.40	4.4019
1.0	26.00	4.882	25.90	4.8870	25.9	4.8910

The polynomial equation of those points was found to be

$$Q = 0.46824 + 0.13533xSR + 1.3602x10^{-3}xSR^2 \qquad [A.5]$$

A3.2.3 CALIBRATION OF ROTAMETER SIZE 24S

The variables for rotameter size 24S are

$K_1 = 0.865$ $K_2 = 2.314$ $w = 85.5$ gms $\sigma = 7.96$ g/cc

Using the same calculation as above at different temperatures (see Fig. A.7):

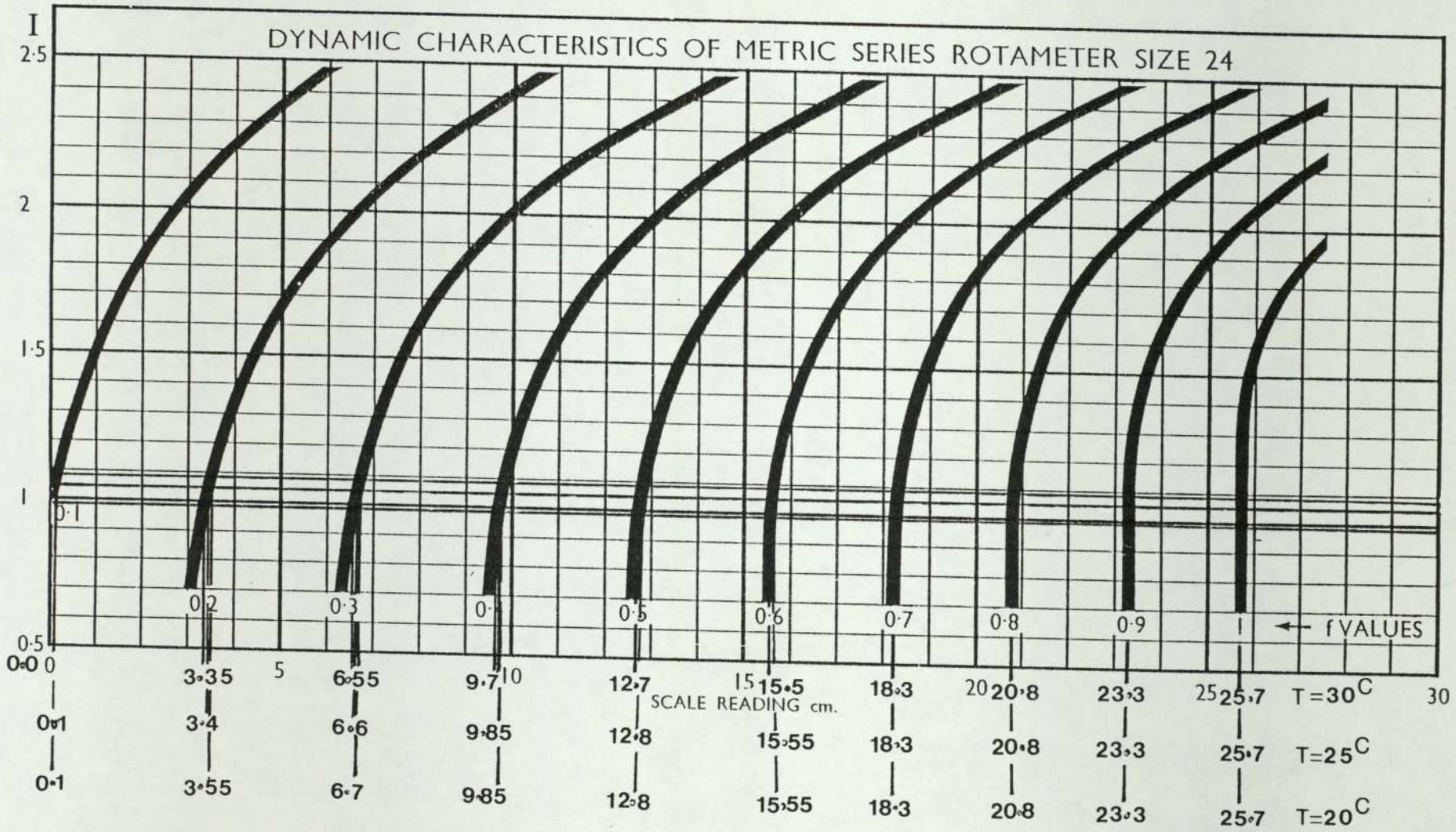

Instrument Constants

$K_1 = 0{\cdot}865$

$K_2 = 2{\cdot}314$

Fig. A.7

At T = 20°C ρ = 1.0419 gm/cc μ = 0.01233 poises

I = 1.0835 F_T = 19.542 dm^3/min

At T = 25°C ρ = 1.0402 gm/cc μ = 0.01109 poises

I = 1.0378 F_T = 19.560 dm^3/min

At T = 30°C ρ = 1.0385 gm/cc μ = 0.00984 poises

I = 0.9860 F_T = 19.579 dm^3/min

The values of F and scale reading for size 24S are shown in Table A.2 at temperatures 20°C, 25°C and 30°C, and the calibration curve is plotted in Figure A.8.

Table A.5

Deduced calibration table rotameter size 24S, using electrolyte as flow medium

f	T = 20°C		T = 25°C		T = 30°C	
	Scale Reading	$F = F_T xf$	Scale Reading	$F = F_T xf$	Scale Reading	$F = F_T xf$
0.1	0.10	1.954	0.10	1.956	0.00	1.958
0.2	3.55	3.908	3.40	3.912	3.35	3.916
0.3	6.70	5.862	6.60	5.868	6.55	5.874
0.4	9.85	7.817	9.85	7.824	9.70	7.832
0.5	12.80	9.771	12.80	9.780	12.70	9.789
0.6	15.55	11.725	15.55	11.736	15.50	11.747
0.7	18.30	13.679	18.30	13.692	18.30	13.705
0.8	20.80	15.634	20.80	15.648	20.80	15.663
0.9	23.30	17.588	23.30	17.600	23.30	17.621
1.0	25.70	19.542	25.70	19.560	25.70	19.579

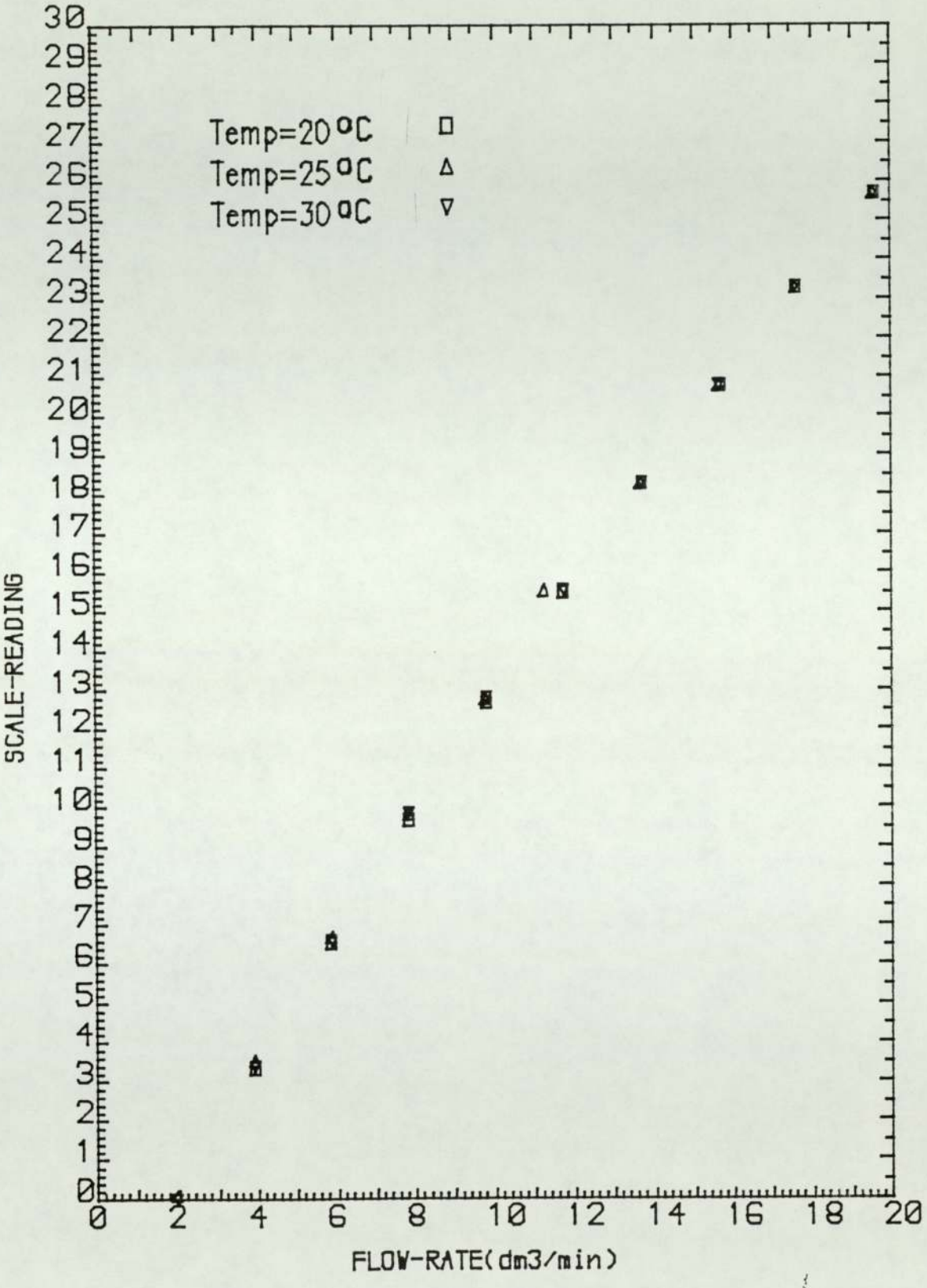

Fig. A.8 Calibration curve of Rotameter 21S

The polynomial equation of these points is

$$Q = 1.957 + 0.56449xSR + 3.15593x10^{-3}xSR^2 \qquad [A.6]$$

A3.2.4 CALIBRATION OF ROTAMETER SIZE 47S

The variables for rotameter size 24S are

$K_1 = 02.30$ $K_2 = 4.355$ $w = 603$ gms $\sigma = 7.96$ g/cc

Using the same calculation as above at different temperatures (see Fig. A.9)

At	$T = 20^oC$	$\rho = 1.0419$ gm/cc	$\mu = 0.01233$ poises
		$I = 1.084$	$F_T = 97.22$ dm^3/min
At	$T = 25^oC$	$\rho = 1.0402$ gm/cc	$\mu = 0.01109$ poises
		$I = 1.038$	$F_T = 97.76$ dm^3/min
At	$T = 30^oC$	$\rho = 1.0385$ gm/cc	$\mu = 0.00984$ poises
		$I = 0.986$	$F_T = 97.85$ dm^3/min

As can be seen in Figure A.8 the scale readings at temperature between 20^oC to 30^oC are very close and nearly the same, therefore the values of F and scale reading at temperature = 25^oC were obtained and tabulated in Table A.6. The calibration curve at this temperature is plotted in Figure A.10.

Table A.6

Deduced calibration table rotameter size 47S, using electrolyte as flow medium

f	Scale Reading	$F = F_T x f$
0.1	0.10	9.72
0.2	3.40	19.44
0.3	6.65	29.16
0.4	9.70	38.89
0.5	12.50	48.61
0.6	15.40	58.33
0.7	18.15	68.05
0.8	20.80	77.78
0.9	23.20	87.50
1.0	25.60	97.22

The polynomial equation of these points is

$$Q = 9.1788 + 2.9224xSR + 1.2696x10^{-2}xSR^2 + 2.88779x10^{-4}xSR^3 \qquad [A.7]$$

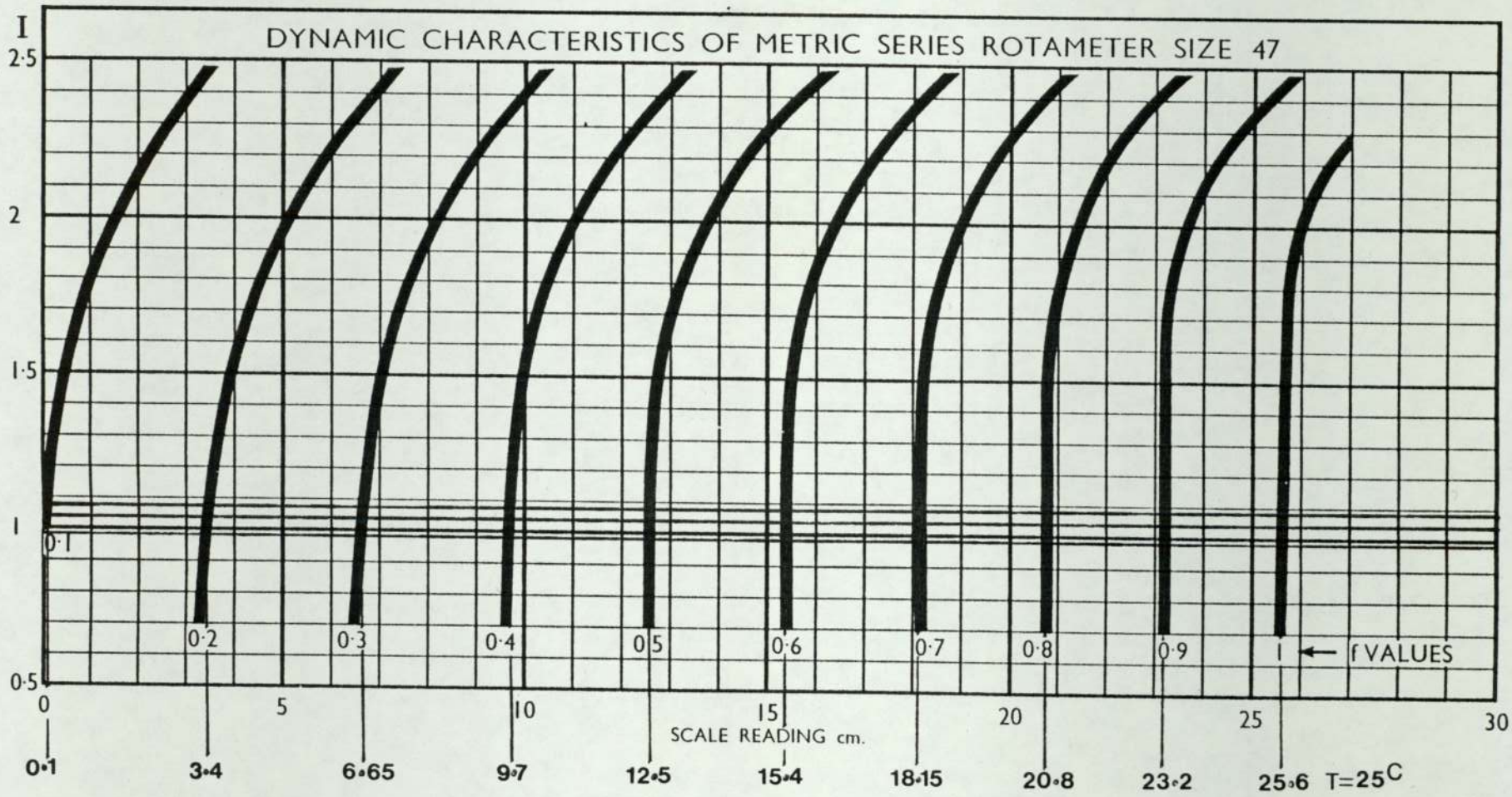

Instrument Constants

$K_1 = 2{\cdot}30$
$K_2 = 4{\cdot}355$

Fig. A.9

METRIC 47

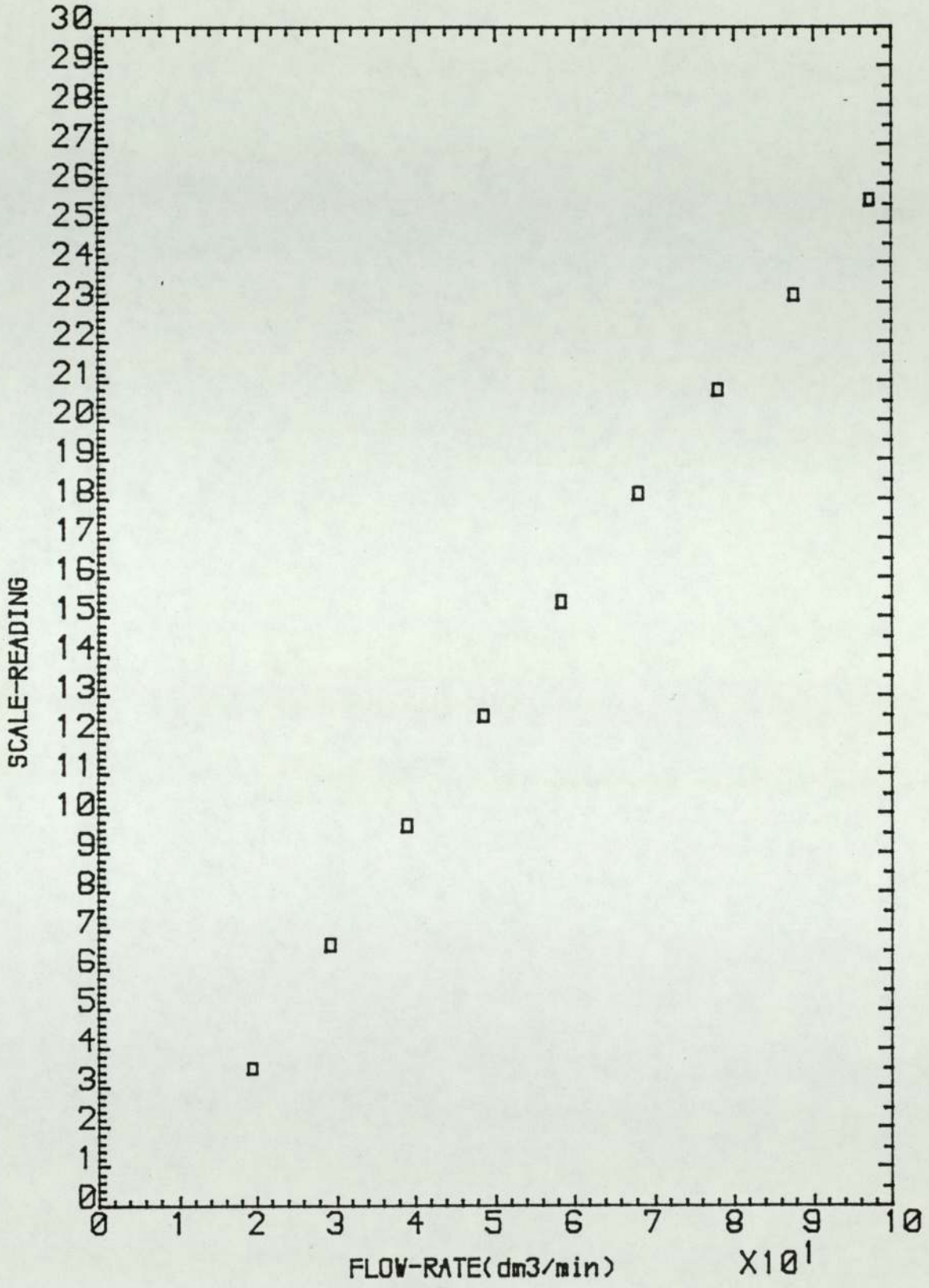

Fig. A.10 Calibration curve of Rotameter 47S Temp=25°C

APPENDIX 4

PREPARATION OF ELECTROLYTE SOLUTION

The electrolyte comprised a molar aqueous solution of sodium hydroxide and a 0.01 equimolar mixture of potassium ferrocyanide and potassium ferricyanide. The volume of solution needed was approximately 70 litres. The following procedure was adopted in making up this solution.

All valves except DV2, VV1, NV1, and NV2 in Figure 5.1 were opened. Nitrogen was then introduced into the system through DV1, and displaced gas vented through VV2 on the top of the rig at the highest point on the pipe. After a short time (about 5-10 minutes), when most of the air had been expelled, VV2 and DV1 were closed.

Then all the valves were closed except NV1, VV1, and V6. Through VV1, 70 litres of tap water were poured into the storage tank. The oxygen was then displaced from the water by bubbling nitrogen by way of NV1. The deoxygenation process was typically carried out for about 48 hours, for twenty hours of these the water was circulated through the by–pass line V6 by the pump. The clip valve on the by–pass line was squeezed to create cavitation and this helped to remove any dissolved oxygen.

Approximately 10 litres of deoxygenated water were then withdrawn from the storage tank via DV2 and a suitable amount of sodium hydroxide pellets were

dissolved in about eight litres of this water. The solution was poured back into the storage tank, through VV1 to give an overall concentration of 1 mol/litre of sodium hydroxide. Circulating the liquid ensured homogeneity. Samples were taken and titrated against molar acid indicator phenophethalein to check the alkali concentration.

The activation process as illustrated in Section 6.5 was then carried out for approximately 2 hours for each model. After the activation process an appropriate weight of potassium ferrocyanide and potassium ferricyanide were added in the remaining two litres of the deoxygenated water which had been removed from the system before. The solution was returned through VV1 to the storage tank, to give an overall concentration of 0.01 mol/litre. The electrolyte solution in the storage tank was circulated through the by–pass line and samples were taken to be titrated. The titration technique used to measure the concentration of ferricyanide is described in Appendix 5.

During both transfers a steady purge of nitrogen was maintained in the rig and the circulating pump was on to promote mixing.

The electrolyte solution was forced to fill the pipe work between the exchanger model and the storage tank by partially closing V7, and it was allowed to circulate at high flowrate (about 25 dm^3/min) through the system for about 20 minutes to make sure that the electrolyte is homogenous.

Finally VV1 was closed and the nitrogen supply to the rig switched off. The rig was now in an operational condition.

APPENDIX 5

FERRICYANIDE ION CONCENTRATION DETERMINATION

The concentration of the ferricyanide ion in the electrolyte was determined by iodometric titration with thiosulphate. The procedure was as follows.

1. Take exactly 10 mls of potassium ferricyanide solution.
2. Add approximately 10 mls of 5% zinc sulphate solution.
3. Add approximately 10 mls of 0.025N potassium iodide sol.
4. Add exactly 10 mls of 0.02N sodium thiosuiphate solution.
5. Add approximately 10 mls of 4N sulphuric acid.
6. Titrate against 0.01N iodine solution with starch as indicator. The end point is light blue.

The calculation is as follows:

$$X = 0.01/0.02X_i \qquad [A.8]$$

where: X = amount of excess thiosulphate added

X_i = amount of iodine solution added

Hence $(10 - X)\ 0.02 = 10N_f$

where N_f = normality of ferricyanide in solution

APPENDIX 6

COMPARISON OF PHYSICAL PROPERTIES WITH MACKLEY'S POLYNOMINAL FORMULAE

The physical properties of the electrolyte at 20^{o}C are

$\mu = 0.001233$ kg/m s $\qquad \rho = 1041.9$ kg/m^3

$C_p = 3.9723$ kJ/kg K $\qquad k = 6.123416 \times 10^{-4}$ kJ/m s K

Diffusion coefficients are obtained from the Stokes–Einstein equation

$$\frac{D_v \mu}{T} = \text{constant} \qquad [A.9]$$

where D_v= diffusion coefficient m^2/s

μ = dynamic viscosity N s/m

T = temperature K

For the diffusion coefficient for the ferricyanide ion in the electrolye solution the value of the constant was found to be 2.5×10^{-15} N m/K.

therefore $$D_v = \frac{2.5\text{x}10^{-15}\text{x}293}{0.001233} = 5.9408\text{x}10^{-10} \ \text{m}^2/\text{s}$$

The Schmidt number, Sc, Prandt number, Pr, and kinematic viscosity, η, of the electrolyte, using the above physical properties are calculated to be

$$Sc = \frac{\mu}{\rho D_v} = \frac{0.001233}{1041.9\text{x}5.9408\text{x}10^{-10}} = 1992.01$$

$$Pr = \frac{C_p\mu}{k} = \frac{3.9723\text{x}0.001233}{6.123416\text{x}10^{-4}} = 7.9985$$

$$\eta = \frac{\mu}{\rho} = \frac{0.001233}{1041.9} = 1.18341\text{x}10^{-6} \ \text{m}^2/\text{s}$$

And using the interpolation formula of Mackley [1973] at T = 20°C

$$Sc = 0.595\text{x}10^4 - 0.319\text{x}10^3\text{x}T + 0.790\text{x}10\text{x}T^2 - 0.983\text{x}10^{-1}\text{x}T^3 + 0.496\text{x}10^{-3}\text{x}T^4$$

$$Sc = 2022.96$$

$$Pr = 0.144\text{x}10^2 - 0.443\text{x}T + 0.701\text{x}10^{-2}\text{x}T^2 - 0.450\text{x}10^{-4}\text{x}T^3$$

Pr =7.9840

$$\eta = 0.205x10^{-5} - 0.598x10^{-7}xT + 0.943x10^{-9}xT^2 - 0.608x10^{-11}xT^3$$

$$\eta = 1.1825x10^{-6}\ m^2/s$$

The same procedure was carried out at T = 25°C and T = 30°C and the results are tabulated in Table A.7.

Table A.7

Comparison of physical properties with Mackley polynomial formula

	T	Sc	Δ%*	Pr	Δ%	η(m^2/s)	Δ%
This work		1992.01		7.9985		$1.183x10^{-6}$	
	20°C		1.54		1.18		0.07
Mackley		2022.96		7.9840		$1.182x10^{-6}$	
This work		1587.05		7.1323		$1.0661x10^{-6}$	
	25°C		−1.06		1.80		1.58
Mackley		1570.31		7.003		$1.0444x10^{-6}$	
This work		1230.83		6.2711		$9.4752x10^{-7}$	
	30°C		0.55		1.07		0.74
Mackley		1237.66		6.2040		$9.4054x10^{-7}$	

*Δ% – Percent deviation between polynomial value and literature value.

Therefore from the above comparison it can be seen that the discrepency is low and it is reasonable to use the interpolation formulae of Mackley [1973].

APPENDIX 7

METHODS OF CALCULATION

A7.1 TRANSFER COEFFICIENT CALCULATION

The calculations for run 1.7, reading 4, were chosen to illustrate the methods of obtaining the transfer coefficient.

1-Temperature of electrolyte circuit T (^{o}C)

The temperature reading by the thermometer was 22.45^{o}C. From the temperature calibration curve the actual temperature was found to be 22.89^{o}C.

Therefore T = 22.89^{o}C

2-Volumetric flow rate Q (m^3/s)

Scale reading from rotameter 7S was 4.0. The volumetric flow rate was calculated from the polynomial equation A.4, i.e.

$$Q = 9.03681 \times 10^{-2} + 2.52775 \times 10^{-2} \times SR + 2.45638 \times 10^{-4} \times SR^2 \qquad [A.10]$$

where SR is scale reading. Therefore the value of Q is found to be 0.1195 dm^3/min

or $Q = 3.25 \times 10^{-6}$ m^3/s

3-Surface area of rows S (m^2)

S_1 = Surface area of one tube

$S_1 = 0.003 \times 3.14 \times 0.02 = 1.884 \times 10^{-4}$ m^2

S_o = Surface area of odd rows

$S_o = 5 \times 1.884 \times 10^{-4} = 9.42 \times 10^{-4}$ m^2

S_e = Surface area of even rows

$S_e = 6 \times 1.884 \times 10^{-4} = 1.1304 \times 10^{-3}$ m^2

4-Kinematic viscosity η (m^2/s)

The kinematic viscosity is defined by $\eta = \mu/\rho$, using the Mackley formula

$$\eta = 0.205 \times 10^{-5} - 0.598 \times 10^{-7} \times T + 0.943 \times 10^{-9} \times T^2 - 0.608 \times 10^{-11} \times T^3$$

Therefore

$\eta = 1.1 \times 10^{-6}$ m^2/s

5-Limiting current I_L (A)

Limiting currents for each of twelve rows were read by an digital ammeter and are tabulated in Table A.8.

Table A.8

Limiting currents of twelve rows, Run No. 1.7 Reading 4

Row	1	2	3	4	5	6
Current (A)	0.00890	0.01250	0.01130	0.01300	0.01110	0.01350
Row	7	8	9	10	11	12
Current (A)	0.01140	0.01370	0.01180	0.01345	0.01160	0.01130

6-Minimum flow area A (m^2) (see Fig. 8.1)

$$A = 0.75x10^{-3}x0.02x12 = 1.8x10^{-4}\ m^2$$

7-Velocity of flow V (m/s)

$$V = \frac{Q}{A} = \frac{3.25x10^{-6}}{1.8x10^{-4}} = 1.8x10^{-2}\ m/s$$

8-Ferricyanide ion concentration C_b (mol/m^3)

The ferricyanide ion concentration was 8.9 mol/m^3 determined using a titration method (A5)

9-Schmidt number $$Sc = \frac{\eta}{D_v}$$

Using the Mackley formula

$$Sc = 0.595x10^{4} - 0.319x10^{3}xT + 0.79x10xT^{2} - 0.982x10^{-1}xT^{3} + 0.496x10^{-3}xT^{4}$$

$$Sc = 1748.07$$

10-Sherwood number

$$Sh = \frac{k_m D}{D_v}$$

where k_m = mass transfer coefficient I_L/FC_bS m/s

D_v = diffusivity = Sc/η m^2/s

Therefore

$$Sh = \frac{I_L ScD}{FC_b S\eta}$$

the Sherwood number for row 4 is

$$Sh = \frac{0.013x1748.07x0.003}{9.487x10^{4}x8.9x1.1304x10^{-3}x1.1x10^{-6}}$$

$$Sh = 63.61$$

For row 5 it is

$$Sh = \frac{0.0111x1748.07x0.003}{9.487x10^{4}x8.9x9.42x10^{-4}x1.1x10^{-6}}$$

$$Sh = 65.18$$

11-Mass transfer dimensionless group $Sh/Sc^{1/3}$

The mass transfer dimensionless group $Sh/Sc^{1/3}$ was calculated for each run individually. The average, mean and relative of $Sh/Sc^{1/3}$ for the tube banks were obtained for each run by equations A.11, A12 and A.13.

$$(Sh/Sc^{1/3})_{av} = \frac{\Sigma_1{}^{z}(Sh/Sc^{1/3})_z}{12} \qquad [A.11]$$

$$(Sh/Sc^{1/3})_{mean} = \frac{\Sigma_5{}^{10}(Sh/Sc^{1/3})_z}{6} \qquad [A.12]$$

$$(Sh/Sc^{1/3})_{rel} = \frac{(Sh/Sc^{1/3})_z}{(Sh/Sc^{1/3})_{mean}} \qquad [A.13]$$

where Z is the row number.

A7.2 REYNOLDS NUMBER CALCULATION

$$Re = \frac{VD}{\eta} = \frac{1.8x10^{-2}x0.003}{1.1x10^{-6}} = 49.19$$

A7.3 NATURAL CONVECTION PARAMETERS CALCULATION

The Grashof number for natural convection mass transfer is given by

$$Gr = \frac{g\alpha C_b D^3}{\eta^2}$$

where g = acceleration of gravity $9.81\ m/s^2$

α = densification coefficient $10.2x10^{-6}\ m^3/mol$

The value of densification coefficient for the electrochemical system used in this work was taken as that reported by Bohm [1970].

Therefore

$$Gr = \frac{9.81x10.2x10^{-6}x8.9x(0.003)^3}{(1.1x10^{-6})^2} = 19.75$$

The correlation of $Sh/(ScGr)^{0.25}$ and $Re/Gr^{0.5}$ for each run were calculated to investigate the role of natural convection.

Sample of the output of the calculations by the computer for run 1.7 reading 4 is shown in Table A.9.

A7.4 FRICTION FACTOR CALCULATION

Run P1.1 reading 1 was chosen to illustrate the calculation of the friction factor. The friction factor was defined as

$$f = \frac{2\Delta P \rho g_c}{4G^2_{max} N'}$$

where g_c = conversion factor = 1

N' = number of major restrictions = 11

ρ = density of water = 1000 kg/m^3

G_{max} = mass velocity = $\rho V = \rho Q/A$

Scale reading from Rotameter 7S was 9.55. Therefore the value of Q was found to be 6.08×10^{-3} dm^3/min

or $Q = 6.08 \times 10^{-6}$ m^3/s

therefore

$$G_{max} = 1000 \times 6.08 \times 10^{-6} / 1.8 \times 10^{-4} = 33.77 \text{ kg/m}^2\text{s}$$

Pressure drop across tube banks was measured in millimeter water and was 1.8 mm. Therefore in N/m^2 it is

$$\Delta P = 1.8/0.101981 \quad \text{N/m}^2$$

Therefore

$$f = \frac{2x1.8/0.101981x1000x1}{2x(33.77)^2x11} = 0.7042$$

RUN NUMBER = 1.7

READING = 4

T = 22.85 Cb = 8.90 SR = 4.00

Q = 0.000003257 U = 0.018093 KV = 0.00000110

Sc = 1748.07 Re = 49.19 Gr = 19.75

ROW NUMBER	LIMITING CURRENT	Sh	(Sh)av	Sh/Sc1/3	(Sh/Sc1/3)av	(Sh/Sc1/3)mean	(Sh/Sc1/3)rel
1	0.00890	52.26	63.92	4.34	5.31	5.54	0.78
2	0.01250	61.16	63.92	5.08	5.31	5.54	0.92
3	0.01130	66.35	63.92	5.51	5.31	5.54	0.99
4	0.01300	63.61	63.92	5.28	5.31	5.54	0.95
5	0.01110	65.18	63.92	5.41	5.31	5.54	0.98
6	0.01350	66.06	63.92	5.48	5.31	5.54	0.99
7	0.01140	66.94	63.92	5.56	5.31	5.54	1.00
8	0.01370	67.03	63.92	5.56	5.31	5.54	1.00
9	0.01180	69.29	63.92	5.75	5.31	5.54	1.04
10	0.01345	65.81	63.92	5.46	5.31	5.54	0.99
11	0.01160	68.11	63.92	5.65	5.31	5.54	1.02
12	0.01130	55.29	63.92	4.59	5.31	5.54	0.83

Sh/(ScGr)1/4 = 4.69 Re/Gr1/2 = 11.07

Table A.9

Table A.10
Data from first set of experiments for Model 1

Run Number 1.1 Cb=9.15

RN	T	SR	Limiting Current I 1	2	3	4	5	6	7	8	9	10	11	12
1	25.10	0.90	0.0023	0.0032	0.0030	0.0035	0.0028	0.0034	0.0028	0.0035	0.0029	0.0034	0.0024	0.0029
2	25.09	2.70	0.0030	0.0044	0.0039	0.0045	0.0037	0.0045	0.0038	0.0045	0.0039	0.0045	0.0037	0.0037
3	25.08	8.00	0.0049	0.0075	0.0066	0.0077	0.0066	0.0079	0.0066	0.0079	0.0069	0.0079	0.0067	0.0062
4	24.84	5.30	0.0098	0.0141	0.0126	0.0145	0.0124	0.0149	0.0125	0.0151	0.0131	0.0151	0.0128	0.0129
5	25.19	22.00	0.0161	0.0187	0.0186	0.0188	0.0184	0.0197	0.0189	0.0199	0.0192	0.0205	0.0198	0.0203
6	25.54	1.40	0.0259	0.0351	0.0355	0.0394	0.0356	0.0443	0.0388	0.0458	0.0404	0.0462	0.0391	0.0410
7	25.22	15.00	0.0592	0.0691	0.0795	0.0902	0.0740	0.0945	0.0838	0.1040	0.0886	0.1040	0.0848	0.0930

Run Number 1.2 Cb=9.15

RN	T	SR	Limiting Current I 1	2	3	4	5	6	7	8	9	10	11	12
1	25.14	1.50	0.0026	0.0040	0.0033	0.0039	0.0032	0.0039	0.0033	0.0041	0.0035	0.0041	0.0032	0.0043
2	25.16	4.20	0.0035	0.0054	0.0047	0.0055	0.0047	0.0056	0.0047	0.0056	0.0048	0.0056	0.0047	0.0053
3	25.32	1.65	0.0083	0.0120	0.0108	0.0124	0.0106	0.0128	0.0108	0.0131	0.0113	0.0134	0.0112	0.0113
4	25.22	14.80	0.0145	0.0199	0.0181	0.0202	0.0174	0.0212	0.0178	0.0212	0.0184	0.0217	0.0181	0.0193
5	25.44	28.80	0.0174	0.0239	0.0225	0.0247	0.0215	0.0265	0.0225	0.0269	0.0239	0.0275	0.0229	0.0230
6	25.74	9.65	0.0579	0.0607	0.0655	0.0756	0.0645	0.0802	0.0705	0.0860	0.0745	0.0870	0.0725	0.0780
7	25.44	24.95	0.0609	0.0860	0.1040	0.1116	0.0940	0.1177	0.1091	0.1233	0.1140	0.1256	0.1103	0.1222

Run Number 1.3 Cb=9.05

RN	T	SR	Limiting Current I 1	2	3	4	5	6	7	8	9	10	11	12
1	25.14	4.20	0.0035	0.0054	0.0046	0.0055	0.0045	0.0055	0.0046	0.0056	0.0048	0.0056	0.0046	0.0055
2	25.19	7.50	0.0049	0.0075	0.0066	0.0077	0.0065	0.0078	0.0066	0.0079	0.0068	0.0079	0.0067	0.0070
3	25.07	0.30	0.0070	0.0105	0.0093	0.0108	0.0092	0.0111	0.0093	0.0112	0.0096	0.0112	0.0094	0.0087
4	25.14	9.95	0.0119	0.0166	0.0151	0.0171	0.0147	0.0178	0.0150	0.0180	0.0158	0.0182	0.0155	0.0162
5	24.94	27.95	0.0180	0.0244	0.0226	0.0249	0.0216	0.0267	0.0227	0.0272	0.0241	0.0275	0.0231	0.0238
6	25.36	6.50	0.0390	0.0508	0.0570	0.0626	0.0535	0.0662	0.0590	0.0693	0.0621	0.0704	0.0597	0.0639
7	25.35	25.15	0.0899	0.0931	0.1030	0.1127	0.0957	0.1186	0.1083	0.1292	0.1135	0.1305	0.1091	0.1210

continue ...

continued

Run Number 1.4 Cb=9.05

RN	T	SR	Limiting Current I											
			1	2	3	4	5	6	7	8	9	10	11	12
1	25.14	1.50	0.0027	0.0039	0.0034	0.0040	0.0034	0.0041	0.0034	0.0041	0.0035	0.0041	0.0032	0.0043
2	25.07	6.10	0.0044	0.0067	0.0058	0.0068	0.0058	0.0069	0.0058	0.0069	0.0060	0.0069	0.0059	0.0056
3	24.08	10.05	0.0055	0.0083	0.0073	0.0085	0.0073	0.0087	0.0072	0.0087	0.0075	0.0087	0.0073	0.0069
4	24.96	4.00	0.0089	0.0130	0.0117	0.0136	0.0115	0.0139	0.0115	0.0141	0.0122	0.0140	0.0120	0.0117
5	24.89	10.80	0.0118	0.0164	0.0150	0.0169	0.0147	0.0177	0.0149	0.0180	0.0157	0.0181	0.0154	0.0160
6	24.56	17.35	0.0139	0.0193	0.0178	0.0197	0.0170	0.0210	0.0176	0.0211	0.0187	0.0215	0.0181	0.0188
7	25.34	12.00	0.0536	0.0620	0.0701	0.0803	0.0679	0.0839	0.0755	0.0892	0.0795	0.0906	0.0768	0.0830

Run Number 1.5 Cb=9.05

RN	T	SR	Limiting Current I											
			1	2	3	4	5	6	7	8	9	10	11	12
1	25.07	3.50	0.0033	0.0048	0.0042	0.0048	0.0042	0.0049	0.0042	0.0049	0.0043	0.0050	0.0042	0.0040
2	25.09	9.40	0.0054	0.0081	0.0072	0.0083	0.0071	0.0085	0.0071	0.0085	0.0073	0.0085	0.0072	0.0067
3	24.89	10.60	0.0118	0.0163	0.0150	0.0169	0.0146	0.0176	0.0147	0.0179	0.0156	0.0180	0.0153	0.0159
4	25.35	21.90	0.0165	0.0225	0.0209	0.0230	0.0198	0.0244	0.0208	0.0249	0.0216	0.0252	0.0213	0.0230
5	25.38	19.85	0.0783	0.0812	0.0904	0.1000	0.0839	0.1052	0.0953	0.1152	0.1002	0.1151	0.0959	0.1054
6	25.74	24.00	0.0804	0.0845	0.0982	0.1071	0.0889	0.1128	0.1042	0.1202	0.1095	0.1221	0.1044	0.1155

Run Number 1.6 Cb=9.05

RN	T	SR	Limiting Current I											
			1	2	3	4	5	6	7	8	9	10	11	12
1	25.12	0.90	0.0024	0.0034	0.0030	0.0035	0.0029	0.0035	0.0030	0.0035	0.0031	0.0035	0.0029	0.0031
2	25.22	7.50	0.0049	0.0075	0.0066	0.0078	0.0066	0.0079	0.0066	0.0080	0.0068	0.0080	0.0068	0.0071
3	25.09	12.90	0.0061	0.0091	0.0081	0.0094	0.0080	0.0096	0.0080	0.0096	0.0083	0.0096	0.0082	0.0076
4	24.96	4.20	0.0091	0.0132	0.0119	0.0137	0.0117	0.0141	0.0117	0.0142	0.0133	0.0142	0.0120	0.0118
5	25.24	16.90	0.0148	0.0203	0.0186	0.0207	0.0177	0.0216	0.0184	0.0220	0.0196	0.0224	0.0191	0.0200
6	25.66	10.95	0.0514	0.0584	0.0668	0.0756	0.0641	0.0805	0.0718	0.0834	0.0758	0.0849	0.0725	0.0780

continue ...

continued

Run Number 1.7 Cb=8.9

RN	T	SR	Limiting Current I 1	2	3	4	5	6	7	8	9	10	11	12
1	23.06	1.00	0.0024	0.0034	0.0030	0.0035	0.0030	0.0034	0.0030	0.0034	0.0029	0.0035	0.0032	0.0043
2	22.74	4.90	0.0036	0.0055	0.0048	0.0057	0.0048	0.0059	0.0049	0.0058	0.0049	0.0056	0.0049	0.0049
3	23.72	13.50	0.0063	0.0091	0.0081	0.0094	0.0080	0.0096	0.0081	0.0096	0.0084	0.0095	0.0081	0.0076
4	22.85	4.00	0.0089	0.0125	0.0113	0.0130	0.0111	0.0135	0.0114	0.0137	0.0118	0.0134	0.0116	0.0113
5	23.44	14.15	0.0125	0.0163	0.0154	0.0169	0.0151	0.0178	0.0155	0.0182	0.0164	0.0183	0.0159	0.0163
6	23.61	23.80	0.0157	0.0210	0.0197	0.0215	0.0187	0.0229	0.0197	0.0236	0.0209	0.0237	0.0200	0.0206
7	23.84	28.85	0.0170	0.0224	0.0211	0.0231	0.0202	0.0247	0.0213	0.0255	0.0227	0.0255	0.0216	0.0222
8	24.08	2.00	0.0256	0.0331	0.0335	0.0375	0.0343	0.0440	0.0380	0.0458	0.0396	0.0457	0.0379	0.0403
9	24.14	7.32	0.0368	0.0466	0.0520	0.0594	0.0515	0.0623	0.0572	0.0680	0.0605	0.0688	0.0579	0.0622
10	24.17	13.30	0.0496	0.0581	0.0678	0.0755	0.0640	0.0802	0.0734	0.0847	0.0774	0.0861	0.0735	0.0807
11	24.14	17.30	0.0642	0.0676	0.0776	0.0857	0.0720	0.0914	0.0833	0.1004	0.0877	0.1010	0.0834	0.0921

Run Number 1.8 Cb=8.9

RN	T	SR	Limiting Current I 1	2	3	4	5	6	7	8	9	10	11	12
1	23.70	0.50	0.0021	0.0030	0.0025	0.0030	0.0024	0.0030	0.0025	0.0030	0.0025	0.0030	0.0023	0.0035
2	23.78	2.10	0.0028	0.0040	0.0035	0.0041	0.0035	0.0042	0.0035	0.0042	0.0036	0.0042	0.0036	0.0051
3	23.92	15.00	0.0065	0.0094	0.0084	0.0097	0.0083	0.0101	0.0083	0.0101	0.0087	0.0103	0.0087	0.0089
4	23.94	0.74	0.0075	0.0108	0.0096	0.0112	0.0095	0.0115	0.0095	0.0116	0.0099	0.0118	0.0099	0.0101
5	23.96	10.00	0.0113	0.0153	0.0142	0.0159	0.0139	0.0167	0.0143	0.0173	0.0151	0.0176	0.0150	0.0161
6	24.08	25.55	0.0165	0.0219	0.0208	0.0229	0.0198	0.0247	0.0209	0.0252	0.0220	0.0255	0.0213	0.0233
7	24.15	4.09	0.0306	0.0394	0.0417	0.0473	0.0427	0.0510	0.0467	0.0525	0.0490	0.0535	0.0471	0.0500
8	24.17	23.10	0.0726	0.0758	0.0883	0.0963	0.0803	0.1027	0.0950	0.1108	0.1002	0.1123	0.0947	0.1054

Table A.11
Data from first set of experiments for Model 2

Run Number 2.1 Cb=10.0

RN	T	SR	Limiting Current I											
			1	2	3	4	5	6	7	8	9	10	11	12
1	23.05	4.00	0.0046	0.0048	0.0057	0.0048	0.0058	0.0047	0.0058	0.0048	0.0057	0.0049	0.0058	0.0040
2	22.35	9.50	0.0073	0.0075	0.0090	0.0078	0.0094	0.0073	0.0093	0.0076	0.0092	0.0080	0.0094	0.0060
3	26.30	0.50	0.0106	0.0107	0.0126	0.0112	0.0133	0.0102	0.0132	0.0106	0.0131	0.0114	0.0134	0.0082
4	24.10	10.00	0.0157	0.0151	0.0178	0.0162	0.0195	0.0143	0.0191	0.0150	0.0187	0.0165	0.0196	0.0128
5	25.40	21.00	0.0203	0.0194	0.0231	0.0214	0.0255	0.0185	0.0255	0.0198	0.0250	0.0224	0.0263	0.0167
6	26.30	3.00	0.0228	0.0215	0.0251	0.0234	0.0279	0.0203	0.0279	0.0213	0.0272	0.0244	0.0283	0.0180
7	27.15	10.00	0.0341	0.0315	0.0351	0.0344	0.0406	0.0320	0.0420	0.0334	0.0416	0.0372	0.0430	0.0333
8	27.15	22.00	0.0453	0.0408	0.0445	0.0472	0.0600	0.0415	0.0587	0.0450	0.0572	0.0528	0.0624	0.0416
9	25.05	8.00	0.0531	0.0471	0.0544	0.0600	0.0732	0.0461	0.0690	0.0523	0.0682	0.0645	0.0776	0.0446
10	23.40	27.00	0.0887	0.0812	0.0948	0.1019	0.1070	0.0802	0.1061	0.0962	0.1076	0.1040	0.1081	0.0826

Run Number 2.2 Cb=9.82

RN	T	SR	Limiting Current I											
			1	2	3	4	5	6	7	8	9	10	11	12
1	19.20	15.00	0.0084	0.0084	0.0102	0.0091	0.0107	0.0083	0.0107	0.0087	0.0107	0.0094	0.0109	0.0070
2	19.05	2.00	0.0105	0.0105	0.0125	0.0112	0.0132	0.0102	0.0132	0.0106	0.0130	0.0116	0.0137	0.0084
3	26.80	16.00	0.0209	0.0204	0.0231	0.0213	0.0246	0.0188	0.0248	0.0198	0.0241	0.0218	0.0217	0.0165
4	26.80	29.00	0.0261	0.0251	0.0277	0.0262	0.0308	0.0246	0.0305	0.0252	0.0297	0.0275	0.0310	0.0251
5	25.80	7.00	0.0307	0.0282	0.0313	0.0297	0.0355	0.0260	0.0360	0.0275	0.0349	0.0322	0.0375	0.0260
6	25.70	15.00	0.0383	0.0346	0.0371	0.0373	0.0453	0.0324	0.0474	0.0362	0.0510	0.0427	0.0502	0.0383
7	25.25	5.00	0.0465	0.0413	0.0458	0.0492	0.0619	0.0404	0.0600	0.0441	0.0580	0.0541	0.0655	0.0392
8	25.10	14.00	0.0652	0.0589	0.0705	0.0805	0.0938	0.0561	0.0880	0.0670	0.0880	0.0852	0.1057	0.0590
9	25.15	27.20	0.0880	0.0822	0.0967	0.1077	0.1262	0.0744	0.1175	0.0922	0.1180	0.1143	0.1382	0.0832

continue ...

continued

Run Number 2.3 Cb=9.74

RN	T	SR	Limiting Current I											
			1	2	3	4	5	6	7	8	9	10	11	12
1	23.10	6.00	0.0059	0.0056	0.0069	0.0047	0.0057	0.0047	0.0050	0.0042	0.0059	0.0051	0.0060	0.0039
2	22.90	12.00	0.0085	0.0085	0.0105	0.0093	0.0111	0.0089	0.0108	0.0086	0.0108	0.0096	0.0114	0.0075
3	24.50	0.30	0.0108	0.0107	0.0126	0.0114	0.0133	0.0106	0.0133	0.0106	0.0128	0.0116	0.0135	0.0088
4	24.60	8.00	0.0156	0.0153	0.0176	0.0159	0.0190	0.0146	0.0191	0.0151	0.0185	0.0167	0.0196	0.0134
5	24.60	23.00	0.0227	0.0218	0.0246	0.0233	0.0275	0.0202	0.0274	0.0208	0.0265	0.0238	0.0277	0.0187
6	25.35	5.00	0.0279	0.0262	0.0292	0.0275	0.0326	0.0233	0.0332	0.0250	0.0320	0.0292	0.0340	0.0218
7	26.20	18.00	0.0424	0.0384	0.0414	0.0415	0.0514	0.0362	0.0540	0.0405	0.0524	0.0480	0.0581	0.0349
8	26.15	3.50	0.0446	0.0401	0.0433	0.0443	0.0562	0.0381	0.0570	0.0427	0.0564	0.0515	0.0621	0.0369
9	26.50	10.00	0.0604	0.0536	0.0611	0.0692	0.0828	0.0503	0.0787	0.0585	0.0789	0.0735	0.0814	0.0530
10	26.75	23.00	0.0843	0.0778	0.0880	0.0984	0.1166	0.0727	0.1093	0.0912	0.1108	0.1061	0.1177	0.0753

Run Number 2.4 Cb=9.51

RN	T	SR	Limiting Current I											
			1	2	3	4	5	6	7	8	9	10	11	12
1	19.35	8.00	0.0066	0.0069	0.0078	0.0068	0.0077	0.0057	0.0074	0.0061	0.0069	0.0060	0.0060	0.0051
2	19.50	14.50	0.0072	0.0073	0.0093	0.0080	0.0091	0.0066	0.0085	0.0073	0.0088	0.0077	0.0092	0.0064
3	25.50	1.00	0.0100	0.0090	0.0112	0.0101	0.0131	0.0098	0.0126	0.0099	0.0122	0.0096	0.0136	0.0085
4	24.55	5.00	0.0133	0.0128	0.0151	0.0132	0.0156	0.0117	0.0152	0.0123	0.0156	0.0137	0.0163	0.0112
5	24.80	29.00	0.0246	0.0223	0.0254	0.0238	0.0282	0.0202	0.0282	0.0218	0.0287	0.0261	0.0303	0.0197
6	26.65	8.30	0.0312	0.0278	0.0313	0.0301	0.0358	0.0270	0.0363	0.0292	0.0374	0.0334	0.0389	0.0273
7	25.60	27.10	0.0463	0.0414	0.0455	0.0498	0.0622	0.0410	0.0596	0.0445	0.0592	0.0553	0.0664	0.0403
8	25.45	12.20	0.0620	0.0550	0.0627	0.0706	0.0832	0.0515	0.0798	0.0601	0.0794	0.0755	0.0929	0.0541
9	25.20	26.70	0.0862	0.0835	0.0888	0.0979	0.1124	0.0807	0.1093	0.0872	0.1097	0.1048	0.1256	0.0843

Table A.12
Data from first set of experiments for Model 3

Run Number 3.1 Cb=10.0

RN	T	SR	Limiting Current I 1	2	3	4	5	6	7	8	9	10	11	12
1	22.80	4.00	0.0058	0.0057	0.0066	0.0057	0.0066	0.0056	0.0067	0.0056	0.0066	0.0056	0.0061	0.0047
2	22.15	9.50	0.0082	0.0083	0.0101	0.0084	0.0102	0.0085	0.0103	0.0085	0.0099	0.0084	0.0100	0.0067
3	25.80	0.50	0.0117	0.0118	0.0144	0.0121	0.0147	0.0123	0.0148	0.0122	0.0141	0.0120	0.0143	0.0092
4	24.20	10.00	0.0173	0.0169	0.0203	0.0175	0.0208	0.0178	0.0203	0.0176	0.0184	0.0176	0.0201	0.0147
5	25.20	21.00	0.0226	0.0220	0.0252	0.0227	0.0259	0.0232	0.0262	0.0192	0.0237	0.0236	0.0250	0.0195
6	25.90	3.00	0.0252	0.0246	0.0292	0.0255	0.0301	0.0259	0.0305	0.0210	0.0264	0.0262	0.0286	0.0213
7	27.00	10.00	0.0359	0.0346	0.0412	0.0357	0.0431	0.0368	0.0448	0.0371	0.0400	0.0376	0.0418	0.0323
8	26.75	22.00	0.0464	0.0441	0.0526	0.0486	0.0561	0.0521	0.0560	0.0490	0.0504	0.0495	0.0525	0.0438
9	24.00	8.00	0.0540	0.0526	0.0660	0.0580	0.0723	0.0558	0.0725	0.0530	0.0550	0.0533	0.0555	0.0524
10	23.00	27.00	0.0863	0.0851	0.1019	0.0960	0.1041	0.0960	0.1057	0.0932	0.1000	0.0970	0.1036	0.0920

Run Number 3.2 Cb=9.82

RN	T	SR	Limiting Current I 1	2	3	4	5	6	7	8	9	10	11	12
1	19.35	15.00	0.0088	0.0089	0.0108	0.0092	0.0109	0.0094	0.0111	0.0059	0.0102	0.0072	0.0109	0.0071
2	19.35	2.00	0.0112	0.0112	0.0133	0.0115	0.0137	0.0117	0.0139	0.0073	0.0127	0.0091	0.0133	0.0088
3	26.60	16.00	0.0213	0.0208	0.0226	0.0213	0.0229	0.0216	0.0233	0.0179	0.0221	0.0178	0.0213	0.0186
4	26.35	29.00	0.0282	0.0275	0.0326	0.0279	0.0331	0.0279	0.0336	0.0275	0.0315	0.0232	0.0320	0.0240
5	25.75	7.00	0.0312	0.0305	0.0360	0.0310	0.0368	0.0316	0.0378	0.0311	0.0340	0.0256	0.0362	0.0270
6	25.55	15.00	0.0392	0.0379	0.0454	0.0394	0.0480	0.0424	0.0509	0.0416	0.0450	0.0347	0.0476	0.0365
7	25.05	5.00	0.0477	0.0445	0.0591	0.0513	0.0638	0.0558	0.0640	0.0528	0.0582	0.0407	0.0616	0.0452
8	25.40	14.00	0.0625	0.0607	0.0852	0.0700	0.0897	0.0754	0.0927	0.0815	0.0825	0.0603	0.0901	0.0683
9	24.75	27.20	0.0853	0.0838	0.1092	0.0962	0.1055	0.0920	0.1193	0.0921	0.0967	0.0754	0.1174	0.0935

continue ...

continued

Run Number 3.3 Cb=9.74

RN	T	SR	Limiting Current I 1	2	3	4	5	6	7	8	9	10	11	12
1	22.50	6.00	0.0053	0.0051	0.0070	0.0057	0.0076	0.0058	0.0078	0.0059	0.0075	0.0049	0.0069	0.0037
2	22.90	12.00	0.0093	0.0094	0.0112	0.0095	0.0113	0.0096	0.0116	0.0095	0.0111	0.0074	0.0115	0.0077
3	24.20	0.30	0.0112	0.0114	0.0134	0.0115	0.0136	0.0116	0.0139	0.0117	0.0136	0.0094	0.0137	0.0093
4	24.30	8.00	0.0162	0.0161	0.0189	0.0161	0.0194	0.0172	0.0210	0.0172	0.0201	0.0136	0.0204	0.0145
5	24.65	23.00	0.0245	0.0236	0.0274	0.0234	0.0282	0.0242	0.0292	0.0241	0.0277	0.0195	0.0279	0.0202
6	24.95	5.00	0.0302	0.0299	0.0326	0.0271	0.0332	0.0285	0.0345	0.0280	0.0322	0.0236	0.0324	0.0243
7	26.00	18.00	0.0422	0.0415	0.0474	0.0412	0.0510	0.0456	0.0560	0.0474	0.0532	0.0345	0.0515	0.0376
8	26.10	3.50	0.0443	0.0427	0.0493	0.0418	0.0560	0.0465	0.0572	0.0443	0.0540	0.0354	0.0532	0.0405
9	26.60	10.00	0.0586	0.0558	0.0671	0.0562	0.0734	0.0621	0.0745	0.0603	0.0726	0.0496	0.0775	0.0598
10	26.70	23.00	0.0844	0.0845	0.0965	0.0869	0.1017	0.0945	0.1084	0.0905	0.1066	0.0922	0.1082	0.0847

Run Number 3.4 Cb=9.51

RN	T	SR	Limiting Current I 1	2	3	4	5	6	7	8	9	10	11	12
1	19.30	8.00	0.0065	0.0067	0.0082	0.0070	0.0081	0.0066	0.0083	0.0068	0.0074	0.0055	0.0082	0.0056
2	19.55	14.50	0.0084	0.0088	0.0105	0.0088	0.0107	0.0089	0.0106	0.0087	0.0097	0.0057	0.0107	0.0070
3	24.90	1.00	0.0119	0.0121	0.0145	0.0122	0.0148	0.0122	0.0142	0.0116	0.0121	0.0092	0.0133	0.0092
4	24.25	5.00	0.0141	0.0143	0.0172	0.0144	0.0174	0.0144	0.0174	0.0142	0.0150	0.0113	0.0163	0.0117
5	24.75	19.00	0.0248	0.0242	0.0284	0.0244	0.0292	0.0249	0.0300	0.0237	0.0247	0.0202	0.0283	0.0211
6	26.10	8.30	0.0312	0.0305	0.0360	0.0308	0.0373	0.0317	0.0387	0.0311	0.0320	0.0276	0.0370	0.0288
7	25.55	27.10	0.0480	0.0467	0.0533	0.0484	0.0600	0.0511	0.0607	0.0470	0.0516	0.0461	0.0578	0.0453
8	25.40	12.20	0.0607	0.0599	0.0691	0.0636	0.0733	0.0593	0.0759	0.0507	0.0683	0.0530	0.0746	0.0595
9	25.15	26.70	0.0848	0.0850	0.0947	0.0854	0.0992	0.0880	0.1047	0.0791	0.0996	0.0840	0.1042	0.0840

Table A. 13
Data from first set of experiments for Model 4

Run Number 4. 1 Cb=10. 0

RN	T	SR	Limiting Current I 1	2	3	4	5	6	7	8	9	10	11	12
1	22. 50	4. 00	0. 0058	0. 0060	0. 0066	0. 0057	0. 0068	0. 0057	0. 0066	0. 0058	0. 0069	0. 0057	0. 0066	0. 0050
2	22. 00	9. 50	0. 0089	0. 0090	0. 0107	0. 0092	0. 0110	0. 0091	0. 0109	0. 0093	0. 0111	0. 0091	0. 0109	0. 0074
3	25. 10	0. 50	0. 0133	0. 0132	0. 0162	0. 0136	0. 0164	0. 0136	0. 0163	0. 0138	0. 0166	0. 0136	0. 0163	0. 0108
4	24. 45	10. 00	0. 0191	0. 0188	0. 0207	0. 0189	0. 0211	0. 0188	0. 0214	0. 0190	0. 0216	0. 0189	0. 0216	0. 0163
5	24. 90	21. 00	0. 0256	0. 0244	0. 0283	0. 0257	0. 0288	0. 0259	0. 0292	0. 0264	0. 0294	0. 0255	0. 0294	0. 0222
6	26. 15	3. 00	0. 0284	0. 0271	0. 0327	0. 0280	0. 0333	0. 0281	0. 0335	0. 0285	0. 0340	0. 0284	0. 0338	0. 0260
7	26. 65	10. 00	0. 0402	0. 0372	0. 0454	0. 0386	0. 0461	0. 0389	0. 0465	0. 0400	0. 0476	0. 0401	0. 0476	0. 0360
8	25. 90	22. 00	0. 0484	0. 0454	0. 0560	0. 0495	0. 0585	0. 0520	0. 0592	0. 0510	0. 0592	0. 0504	0. 0590	0. 0461
9	23. 70	8. 00	0. 0560	0. 0541	0. 0693	0. 0623	0. 0717	0. 0620	0. 0716	0. 0609	0. 0723	0. 0615	0. 0724	0. 0585
10	22. 80	27. 00	0. 0820	0. 0812	0. 0911	0. 0881	0. 0924	0. 0893	0. 0936	0. 0900	0. 0945	0. 0911	0. 0952	0. 0800

Run Number 4. 2 Cb=9. 82

RN	T	SR	Limiting Current I 1	2	3	4	5	6	7	8	9	10	11	12
1	19. 10	15. 00	0. 0093	0. 0094	0. 0115	0. 0101	0. 0114	0. 0098	0. 0118	0. 0099	0. 0119	0. 0099	0. 0117	0. 0080
2	19. 15	2. 00	0. 0116	0. 0116	0. 0124	0. 0117	0. 0126	0. 0116	0. 0124	0. 0117	0. 0126	0. 0116	0. 0127	0. 0095
3	26. 65	16. 00	0. 0235	0. 0230	0. 0276	0. 0238	0. 0285	0. 0238	0. 0284	0. 0241	0. 0287	0. 0239	0. 0285	0. 0211
4	26. 00	29. 00	0. 0297	0. 0285	0. 0346	0. 0297	0. 0352	0. 0294	0. 0351	0. 0297	0. 0357	0. 0294	0. 0348	0. 0260
5	25. 60	7. 00	0. 0328	0. 0314	0. 0380	0. 0331	0. 0309	0. 0332	0. 0390	0. 0335	0. 0395	0. 0331	0. 0389	0. 0291
6	25. 25	15. 00	0. 0403	0. 0391	0. 0477	0. 0410	0. 0488	0. 0424	0. 0504	0. 0430	0. 0510	0. 0427	0. 0502	0. 0383
7	25. 05	5. 00	0. 0498	0. 0488	0. 0634	0. 0516	0. 0695	0. 0577	0. 0679	0. 0559	0. 0676	0. 0536	0. 0643	0. 0504
8	25. 10	14. 00	0. 0645	0. 0625	0. 0911	0. 0752	0. 0952	0. 0732	0. 0926	0. 0778	0. 0950	0. 0751	0. 0903	0. 0723
9	24. 50	27. 20	0. 0841	0. 0834	0. 1125	0. 0915	0. 1167	0. 0906	0. 1147	0. 0923	0. 1182	0. 0968	0. 1209	0. 0981

continue ...

continued

Run Number 4.3 Cb=9.74

RN	T	SR	Limiting Current I 1	2	3	4	5	6	7	8	9	10	11	12
1	22.10	6.00	0.0075	0.0074	0.0090	0.0074	0.0085	0.0073	0.0083	0.0074	0.0096	0.0074	0.0094	0.0056
2	23.00	12.00	0.0106	0.0106	0.0126	0.0108	0.0130	0.0107	0.0127	0.0110	0.0130	0.0107	0.0129	0.0092
3	23.90	0.30	0.0130	0.0129	0.0151	0.0131	0.0155	0.0130	0.0154	0.0131	0.0157	0.0128	0.0153	0.0106
4	25.00	8.00	0.0191	0.0190	0.0225	0.0191	0.0230	0.0191	0.0229	0.0192	0.0233	0.0192	0.0230	0.0168
5	25.15	23.00	0.0262	0.0250	0.0300	0.0255	0.0311	0.0253	0.0318	0.0262	0.0320	0.0260	0.0319	0.0229
6	25.10	5.00	0.0345	0.0338	0.0374	0.0338	0.0380	0.0345	0.0382	0.0352	0.0392	0.0360	0.0389	0.0264
7	25.75	18.00	0.0460	0.0439	0.0528	0.0440	0.0544	0.0452	0.0562	0.0462	0.0573	0.0464	0.0541	0.0408
8	26.20	3.50	0.0482	0.0458	0.0560	0.0480	0.0581	0.0505	0.0596	0.0494	0.0587	0.0491	0.0586	0.0462
9	26.60	10.00	0.0624	0.0597	0.0803	0.0631	0.0800	0.0643	0.0801	0.0641	0.0813	0.0645	0.0798	0.0637
10	26.70	23.00	0.0859	0.0845	0.1067	0.0840	0.1056	0.0873	0.1082	0.0863	0.1101	0.0870	0.1080	0.0843

Run Number 4.4 Cb=9.51

RN	T	SR	Limiting Current I 1	2	3	4	5	6	7	8	9	10	11	12
1	19.40	2.50	0.0072	0.0071	0.0084	0.0073	0.0088	0.0072	0.0087	0.0074	0.0088	0.0072	0.0087	0.0064
2	19.40	8.00	0.0081	0.0083	0.0097	0.0084	0.0102	0.0082	0.0097	0.0084	0.0099	0.0082	0.0097	0.0069
3	19.70	14.50	0.0105	0.0104	0.0120	0.0104	0.0125	0.0103	0.0123	0.0106	0.0126	0.0103	0.0124	0.0084
4	24.60	1.00	0.0137	0.0136	0.0160	0.0137	0.0164	0.0137	0.0164	0.0140	0.0166	0.0137	0.0164	0.0112
5	24.40	5.00	0.0163	0.0163	0.0197	0.0167	0.0202	0.0166	0.0201	0.0169	0.0203	0.0166	0.0199	0.0140
6	25.25	19.00	0.0276	0.0266	0.0323	0.0273	0.0326	0.0273	0.0330	0.0279	0.0336	0.0277	0.0329	0.0252
7	26.05	8.30	0.0341	0.0323	0.0391	0.0330	0.0396	0.0332	0.0412	0.0339	0.0407	0.0335	0.0041	0.0313
8	25.50	27.10	0.0481	0.0462	0.0575	0.0495	0.0599	0.0512	0.0603	0.0501	0.0604	0.0500	0.0603	0.0480
9	25.35	12.20	0.0621	0.0584	0.0735	0.0633	0.0793	0.0639	0.0808	0.0638	0.0817	0.0642	0.0804	0.0641

Table A.14
Data from second set of experiments for Model 1

Run Number 1.9 Cb=10.1

RN	T	SR	Limiting Current I											
			1	2	3	4	5	6	7	8	9	10	11	12
1	16.74	2.95	0.0034	0.0048	0.0041	0.0048	0.0040	0.0048	0.0041	0.0048	0.0039	0.0047	0.0040	0.0039
2	16.66	12.20	0.0070	0.0098	0.0086	0.0100	0.0083	0.0099	0.0085	0.0099	0.0080	0.0095	0.0080	0.0073
3	19.20	1.20	0.0094	0.0131	0.0115	0.0134	0.0115	0.0134	0.0115	0.0136	0.0115	0.0133	0.0113	0.0121
4	19.35	8.70	0.0132	0.0181	0.0159	0.0189	0.0159	0.0189	0.0161	0.0189	0.0161	0.0192	0.0160	0.0171
5	19.44	25.20	0.0204	0.0271	0.0240	0.0277	0.0233	0.0281	0.0241	0.0281	0.0238	0.0282	0.0222	0.0243
6	19.37	5.00	0.0232	0.0305	0.0276	0.0318	0.0270	0.0323	0.0277	0.0323	0.0275	0.0322	0.0271	0.0282
7	19.38	10.20	0.0293	0.0388	0.0355	0.0420	0.0363	0.0435	0.0378	0.0435	0.0373	0.0437	0.0368	0.0372
8	19.25	18.00	0.0373	0.0494	0.0467	0.0570	0.0501	0.0600	0.0514	0.0593	0.0499	0.0581	0.0481	0.0492
9	20.06	28.00	0.0462	0.0615	0.0611	0.0771	0.0651	0.0778	0.0650	0.0779	0.0649	0.0759	0.0632	0.0655
10	20.25	1.50	0.0717	0.1020	0.1100	0.1364	0.1120	0.1326	0.1112	0.1329	0.1105	0.1298	0.1070	0.1120
11	20.42	3.00	0.0840	0.1230	0.1342	0.1623	0.1337	0.1590	0.1340	0.1593	0.1320	0.1550	0.1280	0.1360
12	20.56	5.00	0.0978	0.1470	0.1613	0.1900	0.1583	0.1910	0.1580	0.1900	0.1570	0.1844	0.1460	0.1590
13	20.78	7.80	0.1170	0.1800	0.1990	0.2390	0.1950	0.2310	0.1920	0.2300	0.1900	0.2220	0.1770	0.1930
14	21.20	11.20	0.1370	0.2200	0.2410	0.2910	0.2390	0.2790	0.2410	0.2810	0.2320	0.2720	0.2140	0.2370

Run Number 1.10 Cb=9.94

RN	T	SR	Limiting Current I											
			1	2	3	4	5	6	7	8	9	10	11	12
1	20.09	5.80	0.0057	0.0081	0.0071	0.0083	0.0070	0.0081	0.0070	0.0082	0.0067	0.0080	0.0066	0.0062
2	17.75	4.30	0.0110	0.0150	0.0131	0.0156	0.0131	0.0154	0.0132	0.0155	0.0130	0.0156	0.0127	0.0135
3	17.78	12.20	0.0143	0.0195	0.0171	0.0201	0.0169	0.0202	0.0171	0.0202	0.0169	0.0202	0.0167	0.0184
4	17.77	21.00	0.0179	0.0240	0.0213	0.0249	0.0210	0.0247	0.0212	0.0248	0.0211	0.0250	0.0208	0.0229
5	17.78	3.00	0.0199	0.0266	0.0234	0.0270	0.0229	0.0275	0.0237	0.0273	0.0235	0.0279	0.0228	0.0250
6	17.78	8.35	0.0268	0.0351	0.0319	0.0366	0.0320	0.0374	0.0331	0.0382	0.0326	0.0382	0.0321	0.0336
7	18.25	15.30	0.0346	0.0443	0.0412	0.0492	0.0435	0.0522	0.0450	0.0520	0.0438	0.0508	0.0427	0.0438
8	18.45	26.30	0.0442	0.0576	0.0565	0.0702	0.0615	0.0717	0.0620	0.0715	0.0596	0.0700	0.0586	0.0605
9	18.65	2.00	0.0748	0.1040	0.1122	0.1388	0.1150	0.1336	0.1160	0.1350	0.1120	0.1320	0.1090	0.1150
10	18.80	4.20	0.0900	0.1310	0.1440	0.1740	0.1460	0.1680	0.1450	0.1690	0.1400	0.1620	0.1340	0.1440
11	19.00	7.00	0.1080	0.1630	0.1780	0.2150	0.1790	0.2080	0.1780	0.2100	0.1760	0.2020	0.1620	0.1770

Table A.16
Data from second set of experiments for Model 3

Run Number 3.5 Cb=10.1

RN	T	SR	Limiting Current I											
			1	2	3	4	5	6	7	8	9	10	11	12
1	18.05	2.90	0.0050	0.0049	0.0056	0.0052	0.0059	0.0051	0.0060	0.0043	0.0053	0.0049	0.0057	0.0037
2	17.92	8.80	0.0080	0.0079	0.0109	0.0092	0.0108	0.0093	0.0112	0.0093	0.0111	0.0092	0.0109	0.0075
3	22.10	0.60	0.0130	0.0135	0.0162	0.0136	0.0163	0.0134	0.0164	0.0134	0.0159	0.0130	0.0159	0.0103
4	22.11	8.75	0.0178	0.0179	0.0220	0.0185	0.0221	0.0183	0.0224	0.0182	0.0215	0.0170	0.0212	0.0132
5	22.07	25.45	0.0276	0.0274	0.0332	0.0286	0.0334	0.0280	0.0340	0.0281	0.0339	0.0283	0.0328	0.0221
6	21.08	5.00	0.0316	0.0311	0.0378	0.0325	0.0384	0.0324	0.0386	0.0325	0.0381	0.0323	0.0360	0.0245
7	22.03	10.30	0.0392	0.0383	0.0470	0.0410	0.0491	0.0408	0.0485	0.0406	0.0463	0.0407	0.0455	0.0290
8	22.40	18.20	0.0492	0.0479	0.0601	0.0510	0.0607	0.0511	0.0608	0.0513	0.0607	0.0515	0.0590	0.0380
9	22.67	28.00	0.0596	0.0576	0.0750	0.0692	0.0860	0.0701	0.0802	0.0703	0.0752	0.0701	0.0730	0.0460
10	22.80	1.50	0.0917	0.0893	0.1300	0.1150	0.1340	0.1100	0.1300	0.1090	0.1250	0.1080	0.1210	0.0760
11	22.90	3.00	0.1085	0.1070	0.1600	0.1400	0.1605	0.1340	0.1550	0.1330	0.1510	0.1320	0.1480	0.0950
12	23.10	5.00	0.1290	0.1270	0.1930	0.1640	0.1880	0.1570	0.1830	0.1580	0.1800	0.1560	0.1700	0.1270
13	23.15	8.05	0.1550	0.1545	0.2400	0.1980	0.2280	0.1910	0.2240	0.1930	0.2200	0.1870	0.2175	0.1700
14	23.30	12.80	0.1930	0.1920	0.2970	0.2440	0.2800	0.2370	0.2750	0.2360	0.2750	0.2250	0.2600	0.2030

Run Number 3.6 Cb=9.94

RN	T	SR	Limiting Current I											
			1	2	3	4	5	6	7	8	9	10	11	12
1	25.20	4.50	0.0077	0.0075	0.0088	0.0075	0.0089	0.0076	0.0093	0.0075	0.0091	0.0075	0.0090	0.0061
2	20.18	4.20	0.0159	0.0160	0.0191	0.0162	0.0192	0.0160	0.0195	0.0162	0.0189	0.0163	0.0193	0.0138
3	20.10	12.32	0.0203	0.0200	0.0245	0.0207	0.0246	0.0207	0.0250	0.0206	0.0238	0.0208	0.0238	0.0177
4	20.10	21.40	0.0252	0.0250	0.0303	0.0257	0.0305	0.0252	0.0306	0.0251	0.0308	0.0252	0.0288	0.0211
5	20.08	3.40	0.0283	0.0274	0.0335	0.0286	0.0337	0.0282	0.0336	0.0276	0.0332	0.0278	0.0311	0.0223
6	20.04	8.80	0.0362	0.0350	0.0430	0.0368	0.0437	0.0366	0.0432	0.0360	0.0435	0.0361	0.0405	0.0298
7	20.40	15.70	0.0456	0.0430	0.0536	0.0465	0.0550	0.0478	0.0571	0.0461	0.0536	0.0451	0.0520	0.0390
8	20.83	26.25	0.0590	0.0572	0.0700	0.0624	0.0780	0.0658	0.0745	0.0612	0.0695	0.0600	0.0675	0.0522
9	21.00	2.00	0.0960	0.0935	0.1343	0.1190	0.1360	0.1120	0.1353	0.1120	0.1337	0.1080	0.1340	0.0950
10	21.14	4.40	0.1150	0.1140	0.1720	0.1480	0.1750	0.1400	0.1700	0.1280	0.1620	0.1270	0.1600	0.1200
11	21.20	7.00	0.1380	0.1370	0.2100	0.1770	0.2020	0.1730	0.2040	0.1620	0.2020	0.1700	0.1940	0.1600

Table A.15
Data from second set of experiments for Model 2

Run Number 2.5 Cb=10.1

RN	T	SR	Limiting Current I											
			1	2	3	4	5	6	7	8	9	10	11	12
1	18.18	2.90	0.0044	0.0043	0.0051	0.0047	0.0051	0.0048	0.0051	0.0043	0.0049	0.0041	0.0047	0.0035
2	18.25	10.65	0.0082	0.0083	0.0103	0.0085	0.0100	0.0083	0.0102	0.0086	0.0101	0.0085	0.0092	0.0066
3	21.11	2.00	0.0117	0.0128	0.0159	0.0133	0.0162	0.0133	0.0159	0.0136	0.0160	0.0140	0.0161	0.0120
4	21.12	8.80	0.0174	0.0176	0.0221	0.0180	0.0220	0.0182	0.0221	0.0181	0.0215	0.0183	0.0213	0.0152
5	21.05	25.40	0.0257	0.0256	0.0320	0.0263	0.0318	0.0263	0.0325	0.0267	0.0316	0.0265	0.0278	0.0210
6	20.93	4.70	0.0289	0.0286	0.0356	0.0291	0.0350	0.0292	0.0366	0.0301	0.0359	0.0297	0.0332	0.0240
7	21.40	10.00	0.0366	0.0361	0.0443	0.0368	0.0450	0.0365	0.0472	0.0387	0.0470	0.0391	0.0435	0.0321
8	21.52	16.50	0.0479	0.0468	0.0578	0.0469	0.0564	0.0456	0.0568	0.0485	0.0575	0.0473	0.0530	0.0410
9	21.76	28.00	0.0571	0.0554	0.0698	0.0642	0.0838	0.0695	0.0828	0.0691	0.0830	0.0672	0.0780	0.0560
10	21.95	1.50	0.0864	0.0863	0.1230	0.1164	0.1392	0.1120	0.1360	0.1169	0.1390	0.1140	0.1340	0.0970
11	22.08	3.00	0.1005	0.1035	0.1530	0.1416	0.1680	0.1350	0.1640	0.1420	0.1680	0.1380	0.1600	0.1200
12	22.21	5.00	0.1170	0.1220	0.1850	0.1690	0.1990	0.1602	0.1950	0.1700	0.2010	0.1630	0.1900	0.1400
13	22.30	7.80	0.1400	0.1485	0.2290	0.2080	0.2440	0.1970	0.2380	0.2090	0.2460	0.2000	0.2300	0.1820
14	22.60	12.50	0.1780	0.1890	0.3000	0.2700	0.3170	0.2590	0.3130	0.2750	0.3210	0.2700	0.3140	0.2500

Run Number 2.6 Cb=9.94

RN	T	SR	Limiting Current I											
			1	2	3	4	5	6	7	8	9	10	11	12
1	25.80	5.20	0.0070	0.0072	0.0091	0.0073	0.0090	0.0074	0.0090	0.0074	0.0088	0.0074	0.0091	0.0061
2	18.90	4.30	0.0136	0.0140	0.0172	0.0145	0.0175	0.0144	0.0173	0.0148	0.0171	0.0148	0.0173	0.0123
3	18.90	12.10	0.0173	0.0177	0.0220	0.0186	0.0221	0.0183	0.0224	0.0186	0.0219	0.0191	0.0218	0.0159
4	18.90	21.25	0.0217	0.0222	0.0275	0.0231	0.0276	0.0229	0.0280	0.0234	0.0276	0.0233	0.0265	0.0193
5	18.85	3.00	0.0240	0.0246	0.0307	0.0248	0.0302	0.0246	0.0312	0.0254	0.0304	0.0252	0.0290	0.0207
6	18.90	8.50	0.0319	0.0320	0.0393	0.0327	0.0396	0.0323	0.0409	0.0338	0.0410	0.0340	0.0391	0.0282
7	19.30	14.20	0.0412	0.0410	0.0501	0.0426	0.0522	0.0435	0.0517	0.0439	0.0529	0.0435	0.0517	0.0385
8	19.65	26.40	0.0513	0.0507	0.0642	0.0570	0.0744	0.0625	0.0754	0.0630	0.0753	0.0610	0.0715	0.0509
9	19.80	1.90	0.0843	0.0853	0.1270	0.1180	0.1400	0.1118	0.1370	0.1175	0.1390	0.1135	0.1340	0.0970
10	19.90	4.20	0.1080	0.1090	0.1630	0.1500	0.1750	0.1460	0.1720	0.1520	0.1770	0.1440	0.1700	0.1240
11	20.00	7.00	0.1270	0.1320	0.2020	0.1910	0.2260	0.1900	0.2230	0.1950	0.2300	0.1900	0.2160	0.1700

Table A.17
Data from second set of experiments for Model 4

Run Number 4.5 Cb=10.1

RN	T	SR	Limiting Current I											
			1	2	3	4	5	6	7	8	9	10	11	12
1	19.88	2.85	0.0061	0.0058	0.0059	0.0049	0.0065	0.0055	0.0065	0.0053	0.0062	0.0052	0.0059	0.0045
2	19.90	12.20	0.0112	0.0108	0.0127	0.0110	0.0131	0.0108	0.0128	0.0110	0.0130	0.0106	0.0124	0.0081
3	23.30	1.00	0.0165	0.0153	0.0189	0.0161	0.0191	0.0160	0.0190	0.0161	0.0195	0.0157	0.0190	0.0136
4	23.30	8.90	0.0219	0.0207	0.0252	0.0217	0.0256	0.0213	0.0255	0.0217	0.0264	0.0213	0.0257	0.0188
5	23.28	25.40	0.0317	0.0294	0.0359	0.0310	0.0364	0.0305	0.0367	0.0315	0.0381	0.0308	0.0370	0.0260
6	23.22	5.00	0.0360	0.0340	0.0406	0.0347	0.0410	0.0344	0.0413	0.0354	0.0426	0.0346	0.0400	0.0297
7	23.12	10.00	0.0438	0.0410	0.0499	0.0424	0.0503	0.0420	0.0504	0.0433	0.0520	0.0432	0.0500	0.0370
8	23.42	18.00	0.0556	0.0511	0.0634	0.0550	0.0657	0.0575	0.0680	0.0580	0.0682	0.0568	0.0660	0.0490
9	23.70	28.00	0.0670	0.0628	0.0804	0.0724	0.0890	0.0730	0.0845	0.0709	0.0846	0.0700	0.0820	0.0620
10	23.85	1.50	0.1018	0.0963	0.1390	0.1220	0.1390	0.1113	0.1352	0.1140	0.1380	0.1150	0.1320	0.1030
11	23.92	3.00	0.1209	0.1164	0.1680	0.1462	0.1682	0.1351	0.1630	0.1390	0.1670	0.1395	0.1590	0.1230
12	24.00	5.00	0.1420	0.1390	0.2020	0.1740	0.1980	0.1600	0.1940	0.1640	0.2010	0.1670	0.1900	0.1500
13	24.10	7.90	0.1730	0.1720	0.2470	0.2120	0.2410	0.1970	0.2370	0.2020	0.2440	0.2030	0.2260	0.1810
14	24.18	12.50	0.2140	0.2150	0.3080	0.2610	0.2990	0.2430	0.2970	0.2520	0.3060	0.2580	0.2800	0.2330

Run Number 4.6 Cb=9.94

RN	T	SR	Limiting Current I											
			1	2	3	4	5	6	7	8	9	10	11	12
1	24.60	5.60	0.0086	0.0091	0.0108	0.0093	0.0112	0.0095	0.0115	0.0095	0.0116	0.0091	0.0108	0.0073
2	21.10	4.00	0.0176	0.0168	0.0200	0.0171	0.0205	0.0171	0.0202	0.0171	0.0206	0.0169	0.0201	0.0146
3	21.03	12.60	0.0233	0.0225	0.0270	0.0231	0.0268	0.0222	0.0270	0.0221	0.0275	0.0223	0.0268	0.0194
4	20.95	21.30	0.0291	0.0262	0.0310	0.0268	0.0311	0.0264	0.0313	0.0270	0.0323	0.0265	0.0319	0.0227
5	20.94	3.00	0.0313	0.0290	0.0348	0.0297	0.0352	0.0294	0.0351	0.0299	0.0355	0.0295	0.0342	0.0256
6	20.86	8.40	0.0402	0.0376	0.0454	0.0389	0.0459	0.0388	0.0462	0.0400	0.0476	0.0396	0.0456	0.0339
7	21.20	15.50	0.0524	0.0478	0.0577	0.0500	0.0595	0.0498	0.0608	0.0520	0.0612	0.0511	0.0592	0.0441
8	21.50	26.00	0.0670	0.0610	0.0742	0.0670	0.0812	0.0681	0.0785	0.0672	0.0782	0.0650	0.0767	0.0562
9	21.74	2.00	0.1115	0.1040	0.1452	0.1250	0.1461	0.1231	0.1433	0.1253	0.1420	0.1180	0.1360	0.1060
10	21.80	4.25	0.1320	0.1260	0.1810	0.1540	0.1840	0.1480	0.1890	0.1520	0.1920	0.1460	0.1840	0.1330
11	21.92	7.00	0.1570	0.1520	0.2190	0.1880	0.2200	0.1750	0.2240	0.1810	0.2280	0.1800	0.2140	0.1660

Table A.18
Individual row transfer coefficients from first set of experiments for Model 1

Run Number 1.1 Sh/Sc1/3

RN	Re	1	2	3	4	5	6	7	8	9	10	11	12
1	0.54	1.09	1.24	1.39	1.35	1.30	1.31	1.30	1.35	1.34	1.31	1.11	1.12
2	1.13	1.39	1.70	1.81	1.74	1.72	1.74	1.76	1.74	1.81	1.74	1.72	1.43
3	7.23	2.27	2.90	3.06	2.98	3.06	3.05	3.06	3.05	3.20	3.05	3.11	2.40
4	60.99	4.56	5.46	5.86	5.62	5.76	5.77	5.81	5.85	6.09	5.85	5.95	5.00
5	203.48	7.46	7.22	8.62	7.26	8.52	7.60	8.76	7.68	8.89	7.91	9.17	7.84
6	737.94	11.93	13.50	16.39	15.16	16.43	17.04	17.91	17.62	18.65	17.77	18.05	15.77
7	3016.65	27.42	26.67	36.82	34.81	34.27	36.47	38.81	40.14	41.03	40.14	39.27	35.89

Run Number 1.2 Sh/Sc1/3

RN	Re	1	2	3	4	5	6	7	8	9	10	11	12
1	0.62	1.21	1.54	1.53	1.53	1.48	1.51	1.53	1.58	1.62	1.58	1.48	1.66
2	2.35	1.62	2.09	2.18	2.12	2.18	2.16	2.18	2.16	2.22	2.16	2.18	2.05
3	35.40	3.84	4.63	5.00	4.78	4.90	4.93	5.00	5.05	5.23	5.17	5.18	4.36
4	137.88	6.72	7.68	8.38	7.80	8.06	8.18	8.24	8.18	8.52	8.37	8.38	7.45
5	273.29	8.04	9.22	10.42	9.53	9.91	10.19	10.37	10.38	11.07	10.57	10.56	8.86
6	2087.06	26.68	23.31	30.18	29.03	29.72	30.79	32.48	33.02	34.32	33.40	33.40	29.95
7	5065.97	28.14	33.12	48.06	42.98	43.44	45.32	50.42	47.48	52.68	48.37	50.97	47.06

Run Number 1.3 Sh/Sc1/3

RN	Re	1	2	3	4	5	6	7	8	9	10	11	12
1	2.35	1.64	2.11	2.16	2.15	2.11	2.15	2.16	2.19	2.25	2.19	2.16	2.15
2	6.53	2.29	2.93	3.09	3.01	3.04	3.04	3.09	3.08	3.18	3.08	3.14	2.73
3	25.98	3.28	4.10	4.36	4.22	4.31	4.34	4.36	4.38	4.50	4.38	4.41	3.40
4	97.25	5.58	6.48	7.08	6.68	6.89	6.95	7.03	7.03	7.40	7.11	7.26	6.33
5	261.37	8.45	9.55	10.61	9.74	10.14	10.45	10.66	10.64	11.32	10.76	10.85	9.31
6	1541.62	18.24	19.79	26.65	24.39	25.02	25.79	27.59	27.00	29.04	27.43	27.91	24.90
7	5100.26	42.04	36.28	48.17	43.92	44.75	46.22	50.64	50.35	53.08	50.85	51.02	47.15

continue ...

continued

Run Number 1.4 Sh/Sc1/3

RN	Re	1	2	3	4	5	6	7	8	9	10	11	12
1	0.62	1.27	1.52	1.59	1.58	1.59	1.60	1.59	1.60	1.64	1.60	1.50	1.68
2	4.59	2.06	2.62	2.72	2.66	2.72	2.70	2.72	2.70	2.81	2.70	2.77	2.19
3	9.84	2.60	3.28	3.46	3.35	3.46	3.43	3.41	3.43	3.55	3.43	3.46	2.72
4	51.68	4.18	5.09	5.49	5.32	5.40	5.44	5.40	5.54	5.70	5.48	5.63	4.58
5	103.51	5.54	6.42	7.05	6.64	6.91	6.95	7.00	7.07	7.38	7.09	7.23	6.27
6	157.98	6.55	7.58	8.41	7.76	8.01	8.23	8.32	8.29	8.81	8.42	8.53	7.38
7	2478.33	25.07	24.16	32.78	31.29	31.75	32.70	35.31	34.76	37.18	35.31	35.92	32.35

Run Number 1.5 Sh/Sc1/3

RN	Re	1	2	3	4	5	6	7	8	9	10	11	12
1	1.70	1.55	1.88	1.97	1.88	1.97	1.91	1.97	1.91	2.02	1.95	1.97	1.56
2	9.19	2.53	3.16	3.38	3.24	3.33	3.32	3.33	3.32	3.42	3.32	3.38	2.62
3	101.90	5.54	6.40	7.02	6.62	6.86	6.91	6.91	7.01	7.33	7.05	7.19	6.22
4	203.26	7.72	8.77	9.77	8.96	9.26	9.51	9.73	9.70	10.10	9.82	9.96	8.96
5	3973.07	36.60	31.63	42.26	38.96	39.22	40.98	44.55	44.88	46.84	44.84	44.83	41.06
6	4888.83	37.45	32.80	45.74	41.57	41.41	43.79	48.54	46.66	51.01	47.40	48.63	44.84

Run Number 1.6 Sh/Sc1/3

RN	Re	1	2	3	4	5	6	7	8	9	10	11	12
1	0.54	1.12	1.33	1.41	1.37	1.36	1.37	1.41	1.37	1.45	1.37	1.36	1.21
2	6.54	2.29	2.93	3.09	3.04	3.09	3.08	3.09	3.12	3.18	3.12	3.18	2.77
3	13.80	2.86	3.56	3.80	3.67	3.75	3.75	3.75	3.75	3.89	3.75	3.84	2.97
4	53.12	4.27	5.16	5.59	5.36	5.49	5.52	5.49	5.57	6.27	5.55	5.63	4.62
5	156.43	6.93	7.92	8.71	8.08	8.29	8.43	8.64	8.58	9.18	8.74	8.94	7.80
6	2309.94	24.39	23.07	31.67	29.87	30.39	31.80	34.06	32.95	35.93	33.54	34.37	30.81

continue ...

continued

Run Number 1.7 Sh/Sc1/3

RN	Re	1	2	3	4	5	6	7	8	9	10	11	12
1	0.52	1.17	1.40	1.46	1.42	1.46	1.38	1.46	1.40	1.41	1.44	1.56	1.74
2	2.93	1.76	2.24	2.34	2.32	2.37	2.40	2.39	2.38	2.39	2.28	2.39	2.01
3	14.18	3.04	3.66	3.91	3.79	3.87	3.87	3.91	3.87	4.06	3.83	3.91	3.06
4	49.19	4.34	5.08	5.51	5.28	5.41	5.48	5.56	5.56	5.75	5.46	5.65	4.59
5	126.94	6.03	6.58	7.46	6.84	7.29	7.19	7.49	7.37	7.95	7.41	7.73	6.60
6	213.02	7.62	8.47	9.51	8.65	9.07	9.23	9.51	9.51	10.11	9.53	9.65	8.32
7	263.90	8.23	8.99	10.16	9.29	9.75	9.96	10.28	10.24	10.98	10.28	10.40	8.93
8	803.10	12.33	13.30	16.16	15.05	16.52	17.66	18.30	18.38	19.09	18.34	18.25	16.17
9	1630.18	17.71	18.69	25.02	23.82	24.78	24.98	27.50	27.27	29.11	27.61	27.86	24.94
10	2639.83	23.86	23.29	32.62	30.27	30.79	32.15	35.31	33.98	37.26	34.52	35.36	32.35
11	3368.60	30.92	27.11	37.34	34.37	34.65	36.67	40.11	40.26	42.23	40.50	40.14	36.94

Run Number 1.8 Sh/Sc1/3

RN	Re	1	2	3	4	5	6	7	8	9	10	11	12
1	0.52	1.02	1.21	1.21	1.21	1.18	1.21	1.21	1.21	1.21	1.21	1.11	1.43
2	0.80	1.35	1.63	1.69	1.67	1.69	1.69	1.69	1.69	1.74	1.69	1.74	2.05
3	16.73	3.13	3.78	4.05	3.90	4.03	4.04	4.03	4.08	4.20	4.14	4.20	3.58
4	28.21	3.62	4.32	4.63	4.50	4.58	4.62	4.58	4.66	4.77	4.72	4.77	4.06
5	95.02	5.45	6.15	6.85	6.41	6.70	6.71	6.89	6.93	7.28	7.09	7.21	6.49
6	232.34	7.95	8.81	9.99	9.19	9.53	9.89	10.06	10.13	10.59	10.25	10.28	9.33
7	1122.02	14.75	15.80	20.07	18.97	20.55	20.47	22.47	21.07	23.58	21.47	22.66	20.05
8	4525.69	34.95	30.39	42.50	38.63	38.63	41.17	45.73	44.40	48.21	45.02	45.56	42.26

Table A.19
Individual row transfer coefficients from first set of experiments for Model 2

Run Number 2.1 Sh/Sc1/3

RN	Re	1	2	3	4	5	6	7	8	9	10	11	12
1	2.05	1.56	1.95	1.93	1.95	1.97	1.91	1.98	1.95	1.93	1.99	1.97	1.63
2	8.75	2.49	3.07	3.07	3.20	3.21	2.99	3.19	3.13	3.14	3.28	3.21	2.46
3	28.10	3.48	4.22	4.14	4.41	4.37	4.02	4.33	4.18	4.30	4.49	4.40	3.23
4	95.33	5.27	6.08	5.97	6.52	6.54	5.76	6.41	6.04	6.27	6.64	6.58	5.15
5	194.88	6.72	7.71	7.65	8.51	8.46	7.35	8.46	7.87	8.28	8.88	8.71	6.64
6	241.67	7.49	8.47	8.24	9.22	9.16	8.00	9.16	8.39	8.93	9.59	9.29	7.09
7	543.86	11.10	12.31	11.44	13.46	13.22	12.52	13.67	13.05	13.54	14.53	14.00	13.01
8	1140.17	14.76	15.96	14.49	18.44	19.55	16.21	19.11	17.58	18.62	20.63	20.31	16.25
9	1777.14	17.65	18.79	18.08	23.93	24.33	18.39	22.93	20.86	22.67	25.73	25.79	17.79
10	5277.31	29.97	32.92	32.03	41.31	36.15	32.52	35.85	39.00	36.35	42.17	36.52	33.49

Run Number 2.2 Sh/Sc1/3

RN	Re	1	2	3	4	5	6	7	8	9	10	11	12
1	14.92	3.01	3.61	3.66	3.92	3.84	3.57	3.84	3.74	3.84	4.04	3.91	3.01
2	32.55	3.77	4.52	4.49	4.85	4.74	4.40	4.74	4.57	4.67	5.00	4.92	3.62
3	153.74	6.94	8.14	7.68	8.52	8.18	7.52	8.27	7.90	8.02	8.70	7.22	6.61
4	283.94	8.68	10.00	9.20	10.46	10.23	9.82	10.15	10.08	9.90	10.96	10.31	10.02
5	399.56	10.31	11.37	10.52	11.97	11.93	10.48	12.10	11.09	11.73	12.98	12.60	10.48
6	754.26	12.88	13.96	12.49	15.05	15.23	13.08	15.94	14.61	17.15	17.23	16.88	15.46
7	1295.43	15.71	16.74	15.47	19.94	20.91	16.38	20.27	17.88	19.59	21.93	22.13	15.89
8	2824.19	22.06	23.91	23.85	32.68	31.73	22.77	29.77	27.20	29.77	34.59	35.76	23.95
9	5542.22	29.76	33.35	32.70	43.70	42.67	30.19	39.73	37.41	39.90	46.38	46.73	33.76

continue ...

continued

Run Number 2.3 Sh/Sc1/3

RN	Re	1	2	3	4	5	6	7	8	9	10	11	12
1	4.25	2.05	2.34	2.40	1.96	1.98	1.96	1.74	1.77	2.05	2.13	2.09	1.65
2	11.98	2.98	3.56	3.66	3.89	3.87	3.72	3.78	3.62	3.75	4.02	3.97	3.14
3	25.64	3.71	4.41	4.32	4.69	4.56	4.36	4.56	4.36	4.39	4.78	4.63	3.62
4	80.86	5.35	6.29	6.03	6.54	6.51	6.01	6.55	6.21	6.34	6.87	6.72	5.51
5	210.27	7.76	8.97	8.43	9.58	9.43	8.31	9.39	8.56	9.07	9.79	9.48	7.67
6	314.57	9.49	10.70	9.94	11.23	11.09	9.51	11.30	10.21	10.89	11.92	11.57	8.90
7	909.88	14.31	15.55	13.97	16.80	17.34	14.66	18.22	16.40	17.68	19.43	19.60	14.13
8	1079.75	15.06	16.24	14.62	17.94	18.97	15.43	19.24	17.30	19.04	20.86	20.96	14.95
9	2184.73	20.32	21.64	20.55	27.93	27.85	20.30	26.47	23.62	26.54	29.67	27.38	21.39
10	4776.83	28.29	31.33	29.53	39.62	39.13	29.27	36.68	36.72	37.18	42.72	39.50	30.32

Run Number 2.4 Sh/Sc1/3

RN	Re	1	2	3	4	5	6	7	8	9	10	11	12
1	6.30	2.46	3.06	2.88	3.02	2.87	2.53	2.74	2.71	2.55	2.66	2.24	2.26
2	14.20	2.66	3.23	3.43	3.54	3.36	2.92	3.14	3.23	3.25	3.41	3.40	2.84
3	31.03	3.48	3.76	3.90	4.22	4.56	4.09	4.40	4.13	4.25	4.01	4.73	3.55
4	58.39	4.67	5.40	5.30	5.56	5.48	4.93	5.34	5.18	5.48	5.75	5.73	4.72
5	271.40	8.62	9.38	8.90	10.01	9.88	8.47	9.88	9.17	10.06	10.97	10.62	8.30
6	463.03	10.73	11.48	10.79	12.43	12.32	11.15	12.49	12.05	12.87	13.79	13.38	11.27
7	1377.98	16.09	17.27	15.82	20.77	21.62	17.10	20.72	18.56	20.58	23.07	23.08	16.81
8	2520.24	21.58	22.98	21.83	29.49	28.96	21.51	27.78	25.11	27.64	31.54	32.34	22.60
9	5433.33	30.08	34.97	30.99	41.00	39.23	33.80	38.14	36.52	38.28	43.89	43.83	35.30

Table A.20
Individual row transfer coefficients from first set of experiments for Model 3

Run Number 3.1 Sh/Sc1/3

RN	Re	1	2	3	4	5	6	7	8	9	10	11	12
1	2.04	1.77	2.09	2.01	2.09	2.01	2.05	2.04	2.05	2.01	2.05	1.86	1.72
2	8.71	2.52	3.06	3.10	3.09	3.13	3.13	3.16	3.13	3.04	3.09	3.07	2.47
3	27.78	3.46	4.19	4.26	4.30	4.35	4.37	4.37	4.34	4.18	4.26	4.23	3.27
4	95.55	5.20	6.10	6.11	6.32	6.26	6.43	6.11	6.35	5.55	6.37	6.05	5.31
5	194.00	6.73	7.86	7.51	8.11	7.72	8.29	7.80	6.86	7.06	8.44	7.45	6.97
6	239.51	7.45	8.73	8.64	9.05	8.89	9.19	9.02	7.45	7.81	9.30	8.46	7.56
7	542.06	10.51	12.17	12.06	12.54	12.61	12.92	13.11	13.03	11.72	13.20	12.23	11.34
8	1130.13	13.61	15.52	15.44	17.11	16.46	18.34	16.43	17.25	14.78	17.44	15.39	15.42
9	1734.54	16.28	19.03	19.90	20.98	21.79	20.18	21.85	19.17	16.58	19.28	16.73	18.95
10	5227.65	26.27	31.09	31.02	35.07	31.69	35.07	32.18	34.05	30.44	35.44	31.54	33.61

Run Number 3.2 Sh/Sc1/3

RN	Re	1	2	3	4	5	6	7	8	9	10	11	12
1	14.98	2.84	3.43	3.47	3.57	3.50	3.64	3.57	2.28	3.28	2.78	3.50	2.74
2	32.80	3.60	4.32	4.29	4.43	4.39	4.51	4.47	2.82	4.08	3.51	4.27	3.39
3	153.06	6.37	7.47	6.76	7.65	6.85	7.74	6.97	6.43	6.61	6.39	6.37	6.68
4	281.11	8.47	9.88	9.78	10.04	9.93	10.04	10.09	9.90	9.45	8.35	9.60	8.64
5	399.11	9.43	11.04	10.86	11.20	11.10	11.44	11.40	11.26	10.27	9.29	10.92	9.79
6	751.70	11.85	13.75	13.72	14.29	14.51	15.38	15.39	15.09	13.60	12.59	14.39	13.24
7	1289.52	14.49	16.22	17.95	18.70	19.38	20.34	19.44	19.25	17.68	14.84	18.71	16.48
8	2843.59	18.92	22.05	25.79	25.43	27.16	27.39	28.06	29.61	24.98	21.91	27.28	24.81
9	5491.60	25.99	30.64	33.27	35.17	32.15	33.64	36.35	33.67	29.46	27.57	35.77	34.19

continue ...

continued

Run Number 3.3 Sh/Sc1/3

RN	Re	1	2	3	4	5	6	7	8	9	10	11	12
1	4.19	1.66	1.92	2.20	2.15	2.39	2.21	2.47	2.22	2.36	1.85	2.17	1.39
2	11.98	2.91	3.53	3.52	3.57	3.55	3.60	3.63	3.59	3.47	2.78	3.60	2.89
3	25.46	3.46	4.23	4.14	4.26	4.20	4.30	4.29	4.34	4.20	3.48	4.23	3.45
4	80.31	5.00	5.96	5.83	5.98	5.99	6.37	6.48	6.37	6.20	5.04	6.29	5.37
5	210.51	7.53	8.71	8.43	8.65	8.67	8.93	8.98	8.89	8.52	7.20	8.58	7.45
6	311.71	9.26	11.00	9.99	9.97	10.18	10.49	10.58	10.30	9.87	8.68	9.93	8.94
7	905.80	12.80	15.11	14.38	15.00	15.47	16.60	16.99	17.26	16.14	12.56	15.63	13.69
8	1078.53	13.43	15.53	14.94	15.20	16.97	16.91	17.34	16.11	16.37	12.88	16.13	14.73
9	2189.60	17.68	20.20	20.24	20.34	22.14	22.48	22.47	21.83	21.90	17.95	23.38	21.64
10	4771.53	25.43	30.55	29.08	31.42	30.64	34.17	32.66	32.72	32.12	33.34	32.60	30.63

Run Number 3.4 Sh/Sc1/3

RN	Re	1	2	3	4	5	6	7	8	9	10	11	12
1	6.29	2.16	2.67	2.72	2.79	2.71	2.65	2.76	2.71	2.46	2.19	2.72	2.23
2	14.22	2.78	3.50	3.48	3.50	3.54	3.54	3.51	3.46	3.23	2.27	3.54	2.78
3	30.61	3.74	4.56	4.56	4.60	4.65	4.58	4.46	4.37	3.80	3.47	4.18	3.47
4	57.99	4.46	5.43	5.44	5.46	5.50	5.48	5.50	5.39	4.74	4.29	5.15	4.44
5	173.53	7.80	9.14	8.94	9.21	9.20	9.40	9.44	8.95	7.77	7.63	8.90	7.99
6	457.37	9.69	11.34	11.18	11.47	11.58	11.81	12.01	11.59	9.93	10.28	11.49	10.73
7	1376.42	14.98	17.49	16.64	18.13	18.73	19.14	18.95	17.60	16.11	17.27	18.04	16.97
8	2517.38	18.98	22.47	21.60	23.86	22.91	22.25	23.73	19.02	21.35	19.88	23.32	22.32
9	5427.13	26.57	31.96	29.68	32.12	31.09	33.09	32.81	29.75	31.21	31.59	32.65	31.59

Table A.21
Individual row transfer coefficients from first set of experiments for Model 4

Run Number 4.1 Sh/Sc1/3

RN	Re	1	2	3	4	5	6	7	8	9	10	11	12
1	2.02	1.50	1.85	1.69	1.77	1.74	1.75	1.69	1.79	1.77	1.75	1.69	1.54
2	8.68	2.29	2.78	2.76	2.85	2.84	2.81	2.81	2.88	2.86	2.81	2.81	2.29
3	27.35	3.32	3.96	4.05	4.08	4.10	4.08	4.07	4.14	4.15	4.08	4.07	3.24
4	96.11	4.81	5.68	5.21	5.71	5.31	5.68	5.38	5.74	5.43	5.71	5.43	4.92
5	192.67	6.41	7.35	7.09	7.73	7.20	7.79	7.31	7.94	7.36	7.66	7.36	6.66
6	240.86	7.03	8.05	8.10	8.33	8.24	8.34	8.29	8.48	8.42	8.45	8.37	7.70
7	537.87	9.91	10.99	11.19	11.40	11.35	11.49	11.45	11.82	11.73	11.85	11.72	10.64
8	1108.83	12.00	13.51	13.89	14.73	14.51	15.48	14.68	15.18	14.70	15.00	14.63	13.72
9	1722.42	14.20	16.46	17.57	18.95	18.17	18.86	18.15	18.52	18.33	18.71	18.35	17.79
10	5202.88	20.97	24.92	23.30	27.04	23.63	27.41	23.94	27.62	24.17	27.96	24.35	24.55

Run Number 4.2 Sh/Sc1/3

RN	Re	1	2	3	4	5	6	7	8	9	10	11	12
1	14.88	2.51	3.05	3.11	3.26	3.08	3.18	3.19	3.21	3.21	3.21	3.16	2.59
2	32.63	3.13	3.76	3.35	3.79	3.40	3.76	3.35	3.79	3.40	3.77	3.43	3.08
3	153.23	5.89	6.92	6.92	7.16	7.14	7.16	7.12	7.24	7.20	7.19	7.14	6.33
4	278.91	7.48	8.63	8.73	9.01	8.89	8.90	8.87	8.99	9.01	8.90	8.78	7.87
5	397.76	8.31	9.56	9.64	10.06	7.82	10.09	9.89	10.18	10.02	10.08	9.85	8.85
6	746.58	10.24	11.93	12.13	12.51	12.40	12.93	12.80	13.13	12.96	13.02	12.76	11.68
7	1289.52	12.68	14.92	16.15	15.77	17.70	17.64	17.29	17.09	17.22	16.38	16.38	15.40
8	2824.19	16.42	19.09	23.19	22.97	24.24	22.36	23.57	23.77	24.18	22.94	22.99	22.09
9	5460.02	21.54	25.63	28.81	28.12	29.89	27.84	29.37	28.36	30.27	29.75	30.96	30.15

continue ...

Run Number 4.3 Sh/Sc1/3

RN	Re	1	2	3	4	5	6	7	8	9	10	11	12
1	4.15	1.98	2.35	2.39	2.36	2.26	2.33	2.21	2.36	2.54	2.35	2.49	1.76
2	12.01	2.78	3.33	3.30	3.40	3.41	3.36	3.33	3.46	3.41	3.36	3.38	2.89
3	25.28	3.38	4.02	3.92	4.08	4.03	4.07	4.00	4.08	4.08	3.99	3.97	3.30
4	81.61	4.91	5.86	5.78	5.89	5.91	5.89	5.88	5.92	5.99	5.92	5.91	5.18
5	212.94	6.72	7.70	7.70	7.85	7.98	7.79	8.16	8.07	8.21	8.00	8.18	7.05
6	312.78	8.85	10.41	9.60	10.41	9.75	10.63	9.80	10.84	10.06	11.09	9.98	8.13
7	900.70	11.73	13.43	13.46	13.46	13.87	13.83	14.33	14.14	14.61	14.20	13.80	12.49
8	1080.96	12.24	13.95	14.22	14.62	14.75	15.39	15.13	15.05	14.90	14.96	14.88	14.08
9	2189.60	15.78	18.12	20.31	19.15	20.23	19.51	20.26	19.45	20.56	19.57	20.18	19.33
10	4771.53	21.70	25.62	26.96	25.47	26.68	26.47	27.34	26.16	27.82	26.38	27.28	25.56

Run Number 4.4 Sh/Sc1/3

RN	Re	1	2	3	4	5	6	7	8	9	10	11	12
1	0.88	2.00	2.37	2.34	2.44	2.46	2.40	2.43	2.47	2.46	2.40	2.42	2.14
2	6.31	2.25	2.77	2.70	2.80	2.84	2.74	2.70	2.82	2.75	2.75	2.70	2.30
3	14.28	2.91	3.46	3.33	3.46	3.47	3.43	3.41	3.53	3.49	3.43	3.44	2.81
4	30.40	3.62	4.31	4.23	4.34	4.33	4.34	4.33	4.44	4.40	4.33	4.33	3.55
5	58.19	4.31	5.18	5.21	5.32	5.36	5.29	5.31	5.38	5.37	5.29	5.27	4.45
6	175.53	7.24	8.38	8.48	8.60	8.56	8.58	8.66	8.79	8.83	8.72	8.64	7.94
7	456.85	8.88	10.09	10.18	10.31	10.31	10.37	10.73	10.59	10.61	10.48	1.06	9.78
8	1374.85	12.59	14.52	15.06	15.55	15.68	16.09	15.79	15.74	15.81	15.71	15.79	15.08
9	2514.51	16.28	18.38	19.27	19.92	20.79	20.11	21.19	20.08	21.42	20.20	21.08	20.17

Table A.22
Individual row transfer coefficients from second set of experiments for Model 1

Run Number 1.9 Sh/Sc1/3

RN	Re	1	2	3	4	5	6	7	8	9	10	11	12
1	1.05	1.55	1.84	1.87	1.82	1.82	1.82	1.87	1.82	1.80	1.79	1.82	1.48
2	10.47	3.17	3.73	3.92	3.80	3.81	3.78	3.88	3.76	3.65	3.61	3.65	2.78
3	27.87	4.18	4.86	5.12	4.97	5.10	4.99	5.12	5.05	5.12	4.93	5.03	4.49
4	76.01	5.87	6.72	7.09	7.00	7.07	7.00	7.14	7.02	7.14	7.11	7.11	6.33
5	204.62	9.06	10.03	10.66	10.25	10.35	10.40	10.68	10.40	10.57	10.44	9.86	8.99
6	272.60	10.29	11.30	12.27	11.78	12.00	11.96	12.31	11.96	12.22	11.93	12.05	10.45
7	460.30	13.02	14.37	15.78	15.56	16.13	16.11	16.80	16.11	16.58	16.18	16.35	13.78
8	771.15	16.60	18.32	20.78	21.14	22.29	22.25	22.87	21.99	22.21	21.55	21.40	18.24
9	1252.50	20.40	22.63	26.97	28.37	28.74	28.62	28.70	28.66	28.65	27.92	27.90	24.10
10	3212.54	31.60	37.46	48.47	50.09	49.35	48.69	49.00	48.80	48.69	47.67	47.15	41.13
11	4288.48	36.95	45.09	59.04	59.50	58.82	58.29	58.95	58.40	58.07	56.82	56.31	49.86
12	5750.50	42.97	53.82	70.86	69.56	69.54	69.93	69.41	69.56	68.97	67.51	64.14	58.21
13	7874.31	51.29	65.76	87.24	87.31	85.48	84.39	84.17	84.02	83.29	81.10	77.59	70.51
14	10623.06	59.81	80.04	105.21	105.87	104.34	101.50	105.21	102.23	101.28	98.96	93.43	86.22

Run Number 1.10 Sh/Sc1/3

RN	Re	1	2	3	4	5	6	7	8	9	10	11	12
1	3.72	2.56	3.05	3.16	3.10	3.14	3.05	3.14	3.06	3.00	3.01	2.96	2.32
2	45.19	5.05	5.73	6.01	5.96	6.01	5.89	6.06	5.93	5.96	5.96	5.83	5.16
3	96.68	6.56	7.45	7.87	7.68	7.73	7.72	7.87	7.72	7.73	7.72	7.66	7.03
4	161.98	8.21	9.17	9.77	9.52	9.63	9.44	9.75	9.48	9.70	9.56	9.54	8.75
5	196.89	9.13	10.19	10.76	10.34	10.50	10.49	10.85	10.43	10.78	10.66	10.46	9.56
6	376.04	12.29	13.42	14.65	14.01	14.68	14.29	15.18	14.60	14.95	14.60	14.72	12.86
7	642.27	15.80	16.85	18.81	18.72	19.86	19.86	20.55	19.78	20.00	19.33	19.50	16.66
8	1122.53	20.14	21.87	25.75	26.66	28.02	27.23	28.25	27.15	27.16	26.58	26.70	22.97
9	3423.54	34.02	39.42	51.03	52.61	52.30	50.63	52.76	51.17	50.94	50.03	49.57	43.59
10	4945.85	40.87	49.58	65.40	65.85	66.30	63.58	65.85	63.96	63.58	61.31	60.85	54.50
11	6954.47	48.95	61.57	80.68	81.21	81.13	78.56	80.68	79.32	79.77	76.30	73.43	66.86

Table A.23
Individual row transfer coefficients from second set of experiments for Model 2

Run Number 2.5 Sh/Sc1/3

RN	Re	1	2	3	4	5	6	7	8	9	10	11	12
1	1.06	1.55	1.84	1.80	1.99	1.80	2.03	1.80	1.82	1.73	1.73	1.65	1.48
2	9.21	2.89	3.50	3.62	3.59	3.52	3.50	3.59	3.63	3.55	3.59	3.24	2.79
3	34.26	4.00	5.26	5.44	5.46	5.54	5.48	5.44	5.58	5.47	5.75	5.51	4.93
4	80.13	5.95	7.23	7.56	7.39	7.53	7.47	7.56	7.45	7.36	7.51	7.29	6.24
5	214.75	8.80	10.52	10.96	10.81	10.89	10.81	11.13	10.97	10.82	10.89	9.52	8.63
6	272.64	9.91	11.76	12.20	11.97	12.00	12.01	12.55	12.38	12.31	12.22	11.38	9.87
7	475.93	12.49	14.78	15.11	15.07	15.35	14.94	16.10	15.85	16.04	16.03	14.84	13.16
8	748.95	16.32	19.14	19.70	19.18	19.22	18.65	19.36	19.83	19.60	19.34	18.06	16.77
9	1305.78	19.41	22.60	23.73	26.19	28.49	28.35	28.15	28.19	28.22	27.42	26.52	22.85
10	3348.80	29.32	35.14	41.74	47.40	47.24	45.61	46.15	47.60	47.17	46.42	45.47	39.50
11	4465.60	34.06	42.09	51.85	57.59	56.94	54.90	55.58	57.75	56.94	56.12	54.23	48.80
12	5986.05	39.60	49.55	62.62	68.64	67.36	65.07	66.00	69.05	68.03	66.21	64.31	56.86
13	8170.24	47.34	60.26	77.44	84.41	82.52	79.95	80.49	84.81	83.19	81.16	77.78	73.86
14	12076.39	60.02	76.47	101.15	109.24	106.88	104.79	105.54	111.27	108.23	109.24	105.87	101.15

Run Number 2.6 Sh/Sc1/3

RN	Re	1	2	3	4	5	6	7	8	9	10	11	12
1	3.50	2.32	2.87	3.02	2.91	3.00	2.95	2.99	2.95	2.92	2.95	3.02	2.43
2	46.53	4.83	5.97	6.11	6.18	6.22	6.14	6.15	6.29	6.08	6.31	6.13	5.24
3	98.76	6.16	7.55	7.82	7.93	7.85	7.80	7.96	7.93	7.78	8.14	7.75	6.78
4	168.74	7.71	9.46	9.77	9.85	9.81	9.76	9.97	9.98	9.81	9.93	9.41	8.23
5	202.32	8.53	10.49	10.91	10.58	10.73	10.49	11.09	10.83	10.81	10.75	10.31	8.83
6	392.32	11.33	13.64	13.96	13.94	14.07	13.77	14.53	14.41	14.57	14.50	13.89	12.02
7	614.98	14.58	17.41	17.73	18.09	18.47	18.47	18.30	18.64	18.72	18.47	18.30	16.35
8	1161.78	18.09	21.46	22.64	24.12	26.24	26.45	26.59	26.66	26.56	25.82	25.22	21.54
9	3454.33	29.69	36.05	44.73	49.87	49.30	47.25	48.25	49.66	48.95	47.97	47.19	40.99
10	5084.16	38.00	46.02	57.35	63.33	61.57	61.64	60.52	64.17	62.27	60.80	59.81	52.35
11	7130.66	44.64	55.68	71.00	80.56	79.44	80.14	78.38	82.25	80.84	80.14	75.92	71.70

Table A.24
Individual row transfer coefficients from second set of experiments for Model 3

Run Number 3.5 Sh/Sc1/3

RN	Re	1	2	3	4	5	6	7	8	9	10	11	12
1	1.06	1.58	1.86	1.77	1.97	1.87	1.94	1.90	1.64	1.69	1.86	1.80	1.42
2	7.02	2.53	3.00	3.47	3.52	3.42	3.55	3.55	3.54	3.52	3.50	3.47	2.87
3	26.12	3.95	4.93	4.93	4.96	4.96	4.89	4.99	4.89	4.84	4.74	4.84	3.76
4	81.71	5.41	6.53	6.69	6.75	6.72	6.68	6.81	6.64	6.54	6.20	6.45	4.82
5	220.60	8.40	10.00	10.10	10.44	10.16	10.22	10.34	10.26	10.31	10.33	9.98	8.07
6	284.39	9.71	11.46	11.61	11.98	11.80	11.94	11.86	11.98	11.70	11.91	11.06	9.03
7	495.32	11.93	13.99	14.30	14.97	14.94	14.90	14.76	14.83	14.09	14.86	13.85	10.59
8	842.31	14.92	17.43	18.22	18.56	18.41	18.59	18.44	18.67	18.41	18.74	17.89	13.83
9	1334.63	18.02	20.90	22.68	25.11	26.01	25.44	24.25	25.51	22.74	25.44	22.08	16.69
10	3417.68	27.70	32.36	39.26	41.68	40.47	39.87	39.26	39.50	37.75	39.14	36.54	27.54
11	4554.01	32.74	38.74	48.28	50.69	48.43	48.52	46.77	48.16	45.56	47.79	44.66	34.40
12	6114.44	38.85	45.89	58.12	59.26	56.61	56.73	55.11	57.09	54.20	56.37	51.19	45.89
13	8538.79	46.65	55.80	72.23	71.51	68.62	68.98	67.42	69.71	66.22	67.54	65.46	61.40
14	12536.86	58.00	69.24	89.26	88.00	84.15	85.47	82.65	85.11	82.65	81.14	78.14	73.21

Run Number 3.6 Sh/Sc1/3

RN	Re	1	2	3	4	5	6	7	8	9	10	11	12
1	2.66	2.31	2.70	2.65	2.70	2.67	2.73	2.79	2.72	2.74	2.70	2.70	2.19
2	47.39	5.01	6.05	6.00	6.14	6.05	6.05	6.16	6.12	5.95	6.16	6.08	5.21
3	103.39	6.40	7.56	7.72	7.83	7.75	7.83	7.88	7.79	7.50	7.85	7.50	6.69
4	175.15	7.94	9.45	9.55	9.72	9.61	9.53	9.64	9.49	9.71	9.53	9.08	7.98
5	222.20	8.92	10.36	10.56	10.82	10.62	10.67	10.59	10.44	10.47	10.52	9.80	8.44
6	414.89	11.42	13.24	13.56	13.93	13.78	13.85	13.62	13.62	13.72	13.66	12.77	11.28
7	694.69	14.33	16.21	16.84	17.53	17.28	18.02	17.94	17.38	16.84	17.01	16.34	14.71
8	1188.77	18.46	21.48	21.90	23.43	24.41	24.71	23.31	22.98	21.75	22.53	21.12	19.60
9	3629.86	29.99	35.05	41.95	44.61	42.48	41.98	42.27	41.98	41.77	40.49	41.86	35.61
10	5389.22	35.87	42.68	53.66	55.40	54.59	52.41	53.03	47.92	50.54	47.54	49.91	44.92
11	7344.49	43.02	51.26	65.47	66.22	62.98	64.72	63.60	60.61	62.98	63.60	60.48	59.86

Table A.25
Individual row transfer coefficients from second set of experiments for Model 4

Run Number 4.5 Sh/Sc1/3

RN	Re	1	2	3	4	5	6	7	8	9	10	11	12
1	1.08	1.59	1.81	1.54	1.53	1.69	1.72	1.69	1.66	1.62	1.63	1.54	1.41
2	11.37	2.92	3.38	3.31	3.44	3.41	3.38	3.34	3.44	3.39	3.33	3.23	2.53
3	29.49	4.16	4.63	4.76	4.87	4.81	4.84	4.79	4.87	4.91	4.75	4.79	4.11
4	85.19	5.52	6.26	6.35	6.56	6.45	6.44	6.43	6.56	6.65	6.44	6.48	5.68
5	226.58	7.99	8.89	9.05	9.38	9.17	9.22	9.25	9.53	9.60	9.31	9.32	7.86
6	299.40	9.08	10.29	10.24	10.50	10.34	10.41	10.41	10.71	10.74	10.47	10.09	8.99
7	495.99	11.06	12.42	12.60	12.84	12.70	12.72	12.72	13.12	13.13	13.09	12.62	11.21
8	853.54	13.99	15.43	15.96	16.61	16.53	17.37	17.11	17.52	17.16	17.15	16.61	14.80
9	1367.53	16.82	18.91	20.18	21.80	22.34	21.99	21.21	21.35	21.23	21.08	20.58	18.67
10	3503.38	25.51	28.96	34.83	36.69	34.83	33.47	33.88	34.28	34.58	34.58	33.08	30.97
11	4664.74	30.28	34.98	42.07	43.93	42.12	40.60	40.82	41.77	41.82	41.92	39.82	36.96
12	6245.12	35.53	41.74	50.55	52.25	49.55	48.04	48.54	49.24	50.30	50.15	47.54	45.04
13	8607.61	43.25	51.60	61.75	63.59	60.25	59.10	59.25	60.60	61.00	60.90	56.50	54.30
14	12534.38	53.45	64.44	76.93	78.23	74.68	72.84	74.19	75.53	76.43	77.33	69.94	69.84

Run Number 4.6 Sh/Sc1/3

RN	Re	1	2	3	4	5	6	7	8	9	10	11	12
1	3.90	2.17	2.76	2.73	2.84	2.83	2.88	2.91	2.88	2.93	2.78	2.73	2.23
2	47.16	4.61	5.27	5.23	5.37	5.36	5.37	5.29	5.37	5.39	5.29	5.26	4.58
3	107.91	6.09	7.07	7.07	7.26	7.02	6.98	7.07	6.94	7.20	7.01	7.02	6.10
4	178.00	7.63	8.24	8.12	8.43	8.15	8.30	8.20	8.49	8.46	8.33	8.36	7.14
5	213.11	8.20	9.12	9.12	9.34	9.22	9.25	9.20	9.40	9.30	9.28	8.96	8.05
6	408.13	10.54	11.83	11.91	12.24	12.04	12.21	12.12	12.59	12.48	12.46	11.96	10.67
7	699.87	13.70	14.99	15.08	15.68	15.55	15.62	15.89	16.31	16.00	16.03	15.47	13.83
8	1195.80	17.46	19.08	19.34	20.95	21.16	21.30	20.46	21.02	20.38	20.33	19.99	17.58
9	3695.82	28.99	32.45	37.75	39.00	37.99	38.41	37.26	39.09	36.92	36.82	35.36	33.07
10	5364.09	34.30	39.29	47.03	48.02	47.81	46.15	49.11	47.40	49.89	45.53	47.81	41.47
11	7473.93	40.75	47.34	56.84	58.55	57.10	54.50	58.14	56.37	59.18	56.06	55.54	51.70

Derived values from first set of experiments for Model 1

Run Number 1.1

RN	Re	(Sh)av	(Sh/Sc1/3)av	(Sh/Sc1/3)mean	Re/Gr1/2	Sh/(ScGr)1/4
1	0.54	14.72	1.27	1.32	0.11	1.07
2	1.13	19.62	1.69	1.75	0.24	1.43
3	7.23	34.04	2.93	3.08	1.52	2.48
4	60.99	65.63	5.63	5.86	12.92	4.79
5	203.48	93.60	8.08	8.23	42.76	6.83
6	737.94	188.41	16.35	17.57	153.84	13.76
7	3016.65	416.67	35.98	38.48	633.49	30.41

Run Number 1.2

RN	Re	(Sh)av	(Sh/Sc1/3)av	(Sh/Sc1/3)mean	Re/Gr1/2	Sh/(ScGr)1/4
1	0.62	17.64	1.52	1.55	0.13	1.29
2	2.35	24.44	2.11	2.18	0.49	1.78
3	35.40	55.95	4.84	5.05	7.42	4.08
4	137.88	92.62	8.00	8.26	28.96	6.76
5	273.29	114.55	9.93	10.41	57.10	8.36
6	2087.06	350.51	30.52	32.29	433.13	25.60
7	5065.97	517.39	44.84	47.95	1058.53	37.77

Run Number 1.3

RN	Re	(Sh)av	(Sh/Sc1/3)av	(Sh/Sc1/3)mean	Re/Gr1/2	Sh/(ScGr)1/4
1	2.35	24.54	2.12	2.17	0.50	1.80
2	6.53	34.49	2.98	3.09	1.38	2.52
3	25.98	48.42	4.17	4.38	5.50	3.54
4	97.25	79.06	6.82	7.07	20.57	5.79
5	261.37	118.75	10.21	10.66	55.55	8.69
6	1541.62	292.49	25.31	26.98	324.49	21.41
7	5100.26	543.62	47.04	49.31	1073.76	39.79

continue ...

Run Number 1.1

RN	Re	(Sh)av	(Sh/Sc1/3)av	(Sh/Sc1/3)mean	Re/Gr1/2	Sh/(ScGr)1/4
1	0.54	14.72	1.27	1.32	0.11	1.07
2	1.13	19.62	1.69	1.75	0.24	1.43
3	7.23	34.04	2.93	3.08	1.52	2.48
4	60.99	65.63	5.63	5.86	12.92	4.79
5	203.48	93.60	8.08	8.23	42.76	6.83
6	737.94	188.41	16.35	17.57	153.84	13.76
7	3016.65	416.67	35.98	38.48	633.49	30.41

Run Number 1.2

RN	Re	(Sh)av	(Sh/Sc1/3)av	(Sh/Sc1/3)mean	Re/Gr1/2	Sh/(ScGr)1/4
1	0.62	17.64	1.52	1.55	0.13	1.29
2	2.35	24.44	2.11	2.18	0.49	1.78
3	35.40	55.95	4.84	5.05	7.42	4.08
4	137.88	92.62	8.00	8.26	28.96	6.76
5	273.29	114.55	9.93	10.41	57.10	8.36
6	2087.06	350.51	30.52	32.29	433.13	25.60
7	5065.97	517.39	44.84	47.95	1058.53	37.77

Run Number 1.3

RN	Re	(Sh)av	(Sh/Sc1/3)av	(Sh/Sc1/3)mean	Re/Gr1/2	Sh/(ScGr)1/4
1	2.35	24.54	2.12	2.17	0.50	1.80
2	6.53	34.49	2.98	3.09	1.38	2.52
3	25.98	48.42	4.17	4.38	5.50	3.54
4	97.25	79.06	6.82	7.07	20.57	5.79
5	261.37	118.75	10.21	10.66	55.55	8.69
6	1541.62	292.49	25.31	26.98	324.49	21.41
7	5100.26	543.62	47.04	49.31	1073.76	39.79

continue ...

continued

Run Number 1.4.

RN	Re	(Sh)av	(Sh/Sc1/3)av	(Sh/Sc1/3)mean	Re/Gr1/2	Sh/(ScGr)1/4
1	0.62	18.14	1.56	1.60	0.13	1.33
2	4.59	30.34	2.61	2.72	0.97	2.22
3	9.84	38.93	3.30	3.45	2.13	2.85
4	51.68	61.29	5.27	5.49	10.98	4.49
5	103.51	79.11	6.79	7.06	22.02	5.79
6	157.98	93.95	8.02	8.35	33.87	6.87
7	2478.33	374.30	32.38	34.50	521.88	27.40

Run Number 1.5

RN	Re	(Sh)av	(Sh/Sc1/3)av	(Sh/Sc1/3)mean	Re/Gr1/2	Sh/(ScGr)1/4
1	1.70	21.81	1.88	1.96	0.36	1.60
2	9.19	37.09	3.20	3.34	1.95	2.71
3	101.90	78.65	6.75	7.01	21.68	5.75
4	203.26	108.12	9.36	9.69	42.79	7.91
5	3973.07	478.09	41.39	43.55	835.89	35.00
6	4888.83	507.04	44.15	46.47	1020.18	37.13

Run Number 1.6

RN	Re	(Sh)av	(Sh/Sc1/3)av	(Sh/Sc1/3)mean	Re/Gr1/2	Sh/(ScGr)1/4
1	0.54	15.58	1.34	1.39	0.11	1.14
2	6.54	34.74	3.00	3.12	1.38	2.54
3	13.80	41.92	3.61	3.77	2.92	3.07
4	53.12	62.54	5.38	5.65	11.28	4.58
5	156.43	96.69	8.35	8.64	33.02	7.08
6	2309.94	357.26	31.07	33.11	486.95	26.27

continue ...

continued

Run Number 1.7

RN	Re	(Sh)av	(Sh/Sc1/3)av	(Sh/Sc1/3)mean	Re/Gr1/2	Sh/(ScGr)1/4
1	0.52	17.29	1.44	1.42	0.12	1.27
2	2.93	27.42	2.27	2.37	0.66	2.01
3	14.18	44.30	3.73	3.90	3.13	3.25
4	49.19	63.92	5.31	5.54	11.07	4.69
5	126.94	85.43	7.16	7.45	28.17	6.27
6	213.02	108.22	9.10	9.49	47.08	7.94
7	263.90	116.00	9.79	10.25	58.01	8.52
8	803.10	196.22	16.63	18.05	175.56	14.41
9	1630.18	294.06	24.94	26.88	355.86	21.59
10	2639.83	374.88	31.81	34.00	575.86	27.53
11	3368.60	433.50	36.77	39.07	735.35	31.83

Run Number 1.8

RN	Re	(Sh)av	(Sh/Sc1/3)av	(Sh/Sc1/3)mean	Re/Gr1/2	Sh/(ScGr)1/4
1	0.52	14.26	1.20	1.20	0.11	1.05
2	0.80	20.09	1.69	1.70	0.18	1.47
3	16.73	46.49	3.93	4.08	3.67	3.41
4	28.21	53.07	4.49	4.66	6.19	3.90
5	95.02	78.98	6.68	6.93	20.83	5.80
6	232.34	114.09	9.67	10.08	50.79	8.38
7	1122.02	237.62	20.16	21.60	244.87	17.45
8	4525.69	488.48	41.45	43.86	987.24	35.87

Table A.27
Derived values from first set of experiments for Model 2

Run Number 2.1

RN	Re	(Sh)av	(Sh/Sc1/3)av	(Sh/Sc1/3)mean	Re/Gr1/2	Sh/(ScGr)1/4
1	2.05	22.74	1.89	1.96	0.43	1.62
2	8.75	36.89	3.04	3.16	1.88	2.63
3	28.10	47.00	4.13	4.28	5.51	3.36
4	95.33	72.00	6.10	6.28	19.65	5.14
5	194.88	91.66	7.94	8.22	38.99	6.54
6	241.67	97.70	8.59	8.87	47.37	6.98
7	543.86	145.80	12.99	13.42	104.62	10.43
8	1140.17	198.24	17.66	18.62	219.33	14.18
9	1777.14	248.67	21.41	22.48	358.38	17.75
10	5277.31	425.98	35.69	37.01	1105.79	30.37

Run Number 2.2

RN	Re	(Sh)av	(Sh/Sc1/3)av	(Sh/Sc1/3)mean	Re/Gr1/2	Sh/(ScGr)1/4
1	14.92	47.01	3.67	3.81	3.49	3.36
2	32.55	58.16	4.52	4.69	7.65	4.15
3	153.74	88.16	7.81	8.10	30.08	6.33
4	283.94	112.70	9.98	10.19	55.55	8.09
5	399.56	131.51	11.46	11.72	79.94	9.44
6	754.26	172.34	15.00	15.54	151.24	12.36
7	1295.43	214.96	18.57	19.49	262.42	15.42
8	2824.19	326.90	28.17	29.31	574.06	23.44
9	5542.22	440.88	38.02	39.38	1125.26	31.62

continue ...

continued

Run Number 2.3

RN	Re	(Sh)av	(Sh/Sc1/3)av	(Sh/Sc1/3)mean	Re/Gr1/2	Sh/(ScGr)1/4
1	4.25	24.12	2.01	1.94	0.91	1.73
2	11.98	44.09	3.66	3.79	2.57	3.16
3	25.64	51.18	4.37	4.50	5.31	3.68
4	80.86	73.06	6.24	6.41	16.70	5.25
5	210.27	103.78	8.87	9.09	43.41	7.45
6	314.57	122.06	10.56	10.82	63.84	8.77
7	909.88	188.15	16.51	17.29	181.13	13.53
8	1079.75	200.21	17.55	18.47	215.19	14.40
9	2184.73	277.61	24.47	25.74	432.02	19.97
10	4776.83	395.71	35.02	36.95	939.35	28.48

Run Number 2.4

RN	Re	(Sh)av	(Sh/Sc1/3)av	(Sh/Sc1/3)mean	Re/Gr1/2	Sh/(ScGr)1/4
1	6.30	34.08	2.66	2.67	1.49	2.45
2	14.20	40.84	3.20	3.22	3.36	2.94
3	31.03	47.14	4.09	4.24	6.35	3.41
4	58.39	62.01	5.30	5.36	12.22	4.48
5	271.40	111.03	9.52	9.74	56.45	8.02
6	463.03	136.48	12.06	12.44	92.35	9.88
7	1377.98	222.04	19.29	20.28	281.40	16.06
8	2520.24	301.31	26.11	27.09	516.42	21.79
9	5433.33	430.62	37.17	38.31	1119.70	31.13

Table A.28
Derived values from first set of experiments for Model 3

Run Number 3.1

RN	Re	(Sh)av	(Sh/Sc1/3)av	(Sh/Sc1/3)mean	Re/Gr1/2	Sh/(ScGr)1/4
1	2.04	23.87	1.98	2.04	0.43	1.70
2	8.71	36.57	3.00	3.12	1.88	2.60
3	27.78	47.41	4.13	4.31	5.51	3.39
4	95.55	70.81	6.01	6.18	19.65	5.05
5	194.00	87.67	7.57	7.70	38.99	6.26
6	239.51	96.95	8.46	8.61	47.37	6.93
7	542.06	138.25	12.29	12.77	104.62	9.89
8	1130.13	181.89	16.10	16.78	219.33	13.00
9	1734.54	227.21	19.23	19.81	358.38	16.20
10	5227.65	387.99	32.29	33.15	1105.79	27.65

Run Number 3.2

RN	Re	(Sh)av	(Sh/Sc1/3)av	(Sh/Sc1/3)mean	Re/Gr1/2	Sh/(ScGr)1/4
1	14.98	41.14	3.22	3.17	3.49	2.94
2	32.80	51.25	4.01	3.96	7.65	3.66
3	153.06	77.65	6.86	6.83	30.08	5.58
4	281.11	108.17	9.51	9.63	55.55	7.77
5	399.11	122.49	10.67	10.79	79.94	8.79
6	751.70	161.08	13.98	14.43	151.24	11.56
7	1289.52	206.62	17.79	18.49	262.42	14.82
8	2843.59	291.94	25.28	26.52	574.06	20.94
9	5491.60	377.24	32.32	32.14	1125.26	27.04

continue ...

continued

Run Number 3.3

RN	Re	(Sh)av	(Sh/Sc1/3)av	(Sh/Sc1/3)mean	Re/Gr1/2	Sh/(ScGr)1/4
1	4.19	25.23	2.08	2.25	0.91	1.81
2	11.98	40.76	3.39	3.44	2.57	2.92
3	25.46	47.68	4.05	4.14	5.31	3.42
4	80.31	69.45	5.91	6.07	16.70	4.99
5	210.51	97.95	8.38	8.53	43.41	7.04
6	311.71	115.55	9.93	10.02	63.84	8.30
7	905.80	173.10	15.14	15.84	181.13	12.45
8	1078.53	177.48	15.55	16.10	215.19	12.76
9	2189.60	238.05	21.02	21.46	432.02	17.13
10	4771.53	353.70	31.28	32.61	939.35	25.45

Run Number 3.4

RN	Re	(Sh)av	(Sh/Sc1/3)av	(Sh/Sc1/3)mean	Re/Gr1/2	Sh/(ScGr)1/4
1	6.29	32.81	2.56	2.58	1.49	2.36
2	14.22	41.56	3.26	3.26	3.36	2.99
3	30.61	48.93	4.20	4.22	6.35	3.54
4	57.99	60.10	5.11	5.15	12.22	4.34
5	173.53	101.50	8.70	8.73	36.13	7.34
6	457.37	126.63	11.09	11.20	92.35	9.16
7	1376.42	201.63	17.50	17.97	281.40	14.58
8	2517.38	251.81	21.81	21.52	516.42	18.21
9	5427.13	361.48	31.18	31.59	1119.70	26.13

Table A. 29
Derived values from first set of experiments for Model 4

Run Number 4. 1

RN	Re	(Sh)av	(Sh/Sc1/3)av	(Sh/Sc1/3)mean	Re/Gr1/2	Sh/(ScGr)1/4
1	2. 02	20. 75	1. 71	1. 75	0. 43	1. 48
2	8. 68	33. 40	2. 73	2. 84	1. 88	2. 38
3	27. 35	45. 79	3. 95	4. 10	5. 51	3. 27
4	96. 11	63. 53	5. 42	5. 54	19. 65	4. 53
5	192. 67	85. 24	7. 32	7. 54	38. 99	6. 08
6	240. 86	92. 97	8. 15	8. 37	47. 37	6. 64
7	537. 87	127. 80	11. 29	11. 61	104. 62	9. 14
8	1108. 83	164. 20	14. 34	14. 92	219. 33	11. 73
9	1722. 42	211. 84	17. 84	18. 46	358. 38	15. 10
10	5202. 88	301. 26	24. 99	25. 79	1105. 79	21. 47

Run Number 4. 2

RN	Re	(Sh)av	(Sh/Sc1/3)av	(Sh/Sc1/3)mean	Re/Gr1/2	Sh/(ScGr)1/4
1	14. 88	39. 34	3. 06	3. 18	3. 49	2. 81
2	32. 63	44. 93	3. 50	3. 58	7. 65	3. 21
3	153. 23	78. 66	6. 95	7. 17	30. 08	5. 65
4	278. 91	99. 17	8. 67	8. 93	55. 55	7. 12
5	397. 76	109. 68	9. 53	9. 68	79. 94	7. 87
6	746. 58	143. 25	12. 38	12. 88	151. 24	10. 27
7	1289. 52	188. 35	16. 22	17. 22	262. 42	13. 51
8	2824. 19	258. 98	22. 32	23. 51	574. 06	18. 57
9	5460. 02	332. 72	28. 39	29. 25	1125. 26	23. 85

continue ...

continued

Run Number 4.3

RN	Re	(Sh)av	(Sh/Sc1/3)av	(Sh/Sc1/3)mean	Re/Gr1/2	Sh/(ScGr)1/4
1	4.15	27.84	2.28	2.34	0.91	2.00
2	12.01	39.47	3.28	3.39	2.57	2.83
3	25.28	46.28	3.91	4.04	5.31	3.32
4	81.61	66.86	5.75	5.92	16.70	4.80
5	212.94	90.25	7.78	8.03	43.41	6.48
6	312.78	115.62	9.96	10.36	63.84	8.31
7	900.70	156.31	13.61	14.16	181.13	11.24
8	1080.96	165.43	14.51	15.03	215.19	11.90
9	2189.60	219.37	19.37	19.93	432.02	15.78
10	4771.53	295.31	26.12	26.81	939.35	21.25

Run Number 4.4

RN	Re	(Sh)av	(Sh/Sc1/3)av	(Sh/Sc1/3)mean	Re/Gr1/2	Sh/(ScGr)1/4
1	0.88	30.17	2.36	2.44	0.21	2.17
2	6.31	34.20	2.68	2.77	1.49	2.46
3	14.28	42.55	3.35	3.46	3.36	3.06
4	30.40	49.29	4.21	4.36	6.35	3.56
5	58.19	60.40	5.15	5.33	12.22	4.36
6	175.53	97.83	8.45	8.69	36.13	7.07
7	456.85	107.99	9.45	10.52	92.35	7.81
8	1374.85	176.21	15.28	15.80	281.40	12.74
9	2514.51	230.07	19.91	20.63	516.42	16.63

Table A.30
Derived values from second set of experiments for Model 1

Run Number 1.9

RN	Re	(Sh)av	(Sh/Sc1/3)av	(Sh/Sc1/3)mean	Re/Gr1/2	Sh/(ScGr)1/4
1	1.05	23.79	1.78	1.82	0.26	1.69
2	10.47	48.66	3.63	3.75	2.58	3.45
3	27.87	63.01	4.91	5.05	6.44	4.47
4	76.01	88.05	6.88	7.08	17.49	6.24
5	204.62	129.52	10.14	10.47	46.97	9.19
6	272.60	149.72	11.71	12.06	62.69	10.62
7	460.30	198.98	15.56	16.32	105.83	14.11
8	771.15	266.56	20.80	22.19	177.88	18.90
9	1252.50	338.66	26.80	28.55	283.12	24.03
10	3212.54	575.17	45.68	48.70	722.77	40.81
11	4288.48	686.50	54.68	58.23	960.80	48.72
12	5750.50	808.40	64.54	69.15	1283.91	57.37
13	7874.31	979.68	78.51	83.74	1748.60	69.54
14	10623.06	1181.15	95.34	102.25	2334.88	83.86

Run Number 1.10

RN	Re	(Sh)av	(Sh/Sc1/3)av	(Sh/Sc1/3)mean	Re/Gr1/2	Sh/(ScGr)1/4
1	3.72	37.40	2.96	3.07	0.85	2.66
2	45.19	76.24	5.80	5.97	10.91	5.42
3	96.68	99.41	7.56	7.75	23.33	7.07
4	161.98	123.31	9.38	9.59	39.10	8.77
5	196.89	136.01	10.34	10.62	47.52	9.68
6	376.04	186.54	14.19	14.72	90.76	13.27
7	642.27	245.27	18.81	19.90	153.16	17.45
8	1122.53	334.03	25.71	27.40	266.33	23.77
9	3423.54	623.72	48.17	51.30	808.15	44.40
10	4945.85	776.60	60.14	64.10	1163.09	55.28
11	6954.47	952.81	74.04	79.29	1627.21	67.83

Table A.31
Derived values from second set of experiments for Model 2

Run Number 2.5

RN	Re	(Sh)av	(Sh/Sc1/3)av	(Sh/Sc1/3)mean	Re/Gr1/2	Sh/(ScGr)1/4
1	1.06	23.06	1.77	1.82	0.25	1.63
2	9.21	44.57	3.42	3.56	2.18	3.16
3	34.26	66.04	5.32	5.55	7.55	4.69
4	80.13	89.46	7.21	7.48	17.65	6.35
5	214.75	129.09	10.39	10.92	47.37	9.16
6	272.64	145.78	11.71	12.24	60.32	10.35
7	475.93	184.96	14.98	15.72	104.10	13.13
8	748.95	231.19	18.76	19.33	163.34	16.42
9	1305.78	317.12	25.84	28.14	283.12	22.52
10	3348.80	528.76	43.23	46.70	722.77	37.56
11	4465.60	637.52	52.24	56.37	960.80	45.29
12	5986.05	754.29	61.94	66.95	1283.91	53.59
13	8170.24	925.29	76.10	82.02	1748.60	65.74
14	12076.39	1209.59	99.99	107.66	2566.12	85.96

Run Number 2.6

RN	Re	(Sh)av	(Sh/Sc1/3)av	(Sh/Sc1/3)mean	Re/Gr1/2	Sh/(ScGr)1/4
1	3.50	32.81	2.86	2.96	0.70	2.35
2	46.53	76.97	5.97	6.20	10.91	5.48
3	98.76	98.24	7.62	7.91	23.17	6.99
4	168.74	122.13	9.47	9.88	39.58	8.69
5	202.32	133.72	10.36	10.78	47.52	9.52
6	392.32	176.87	13.72	14.31	92.03	12.59
7	614.98	227.81	17.80	18.51	142.81	16.22
8	1161.78	308.99	24.28	26.39	267.44	22.00
9	3454.33	570.99	44.99	48.56	792.21	40.67
10	5084.16	726.19	57.32	61.83	1163.09	51.72
11	7130.66	928.19	73.39	80.20	1627.21	66.11

Table A.32
Derived values from second set of experiments for Model 3

Run Number 3.5

RN	Re	(Sh)av	(Sh/Sc1/3)av	(Sh/Sc1/3)mean	Re/Gr1/2	Sh/(ScGr)1/4
1	1.06	23.23	1.78	1.82	0.25	1.65
2	7.02	43.65	3.33	3.51	1.68	3.09
3	26.12	57.61	4.72	4.88	5.62	4.09
4	81.71	77.50	6.35	6.60	17.57	5.51
5	220.60	120.65	9.88	10.27	47.48	8.57
6	284.39	140.74	11.34	11.86	62.69	9.99
7	495.32	171.02	14.00	14.73	106.70	12.15
8	842.31	214.53	17.67	18.54	179.84	15.24
9	1334.63	276.78	22.91	24.90	283.12	19.67
10	3417.68	443.17	36.76	39.33	722.77	31.50
11	4554.01	536.33	44.56	47.54	960.80	38.12
12	6114.44	635.09	52.94	56.02	1283.91	45.15
13	8538.79	780.62	65.13	68.08	1790.85	55.50
14	12536.86	953.47	79.75	83.53	2620.08	67.79

Run Number 3.6

RN	Re	(Sh)av	(Sh/Sc1/3)av	(Sh/Sc1/3)mean	Re/Gr1/2	Sh/(ScGr)1/4
1	2.66	30.49	2.63	2.72	0.54	2.18
2	47.39	74.56	5.91	6.08	10.77	5.31
3	103.39	95.01	7.53	7.77	23.54	6.77
4	175.15	117.04	9.27	9.59	39.87	8.34
5	222.20	128.62	10.18	10.55	50.61	9.16
6	414.89	166.88	13.20	13.71	94.58	11.89
7	694.69	209.81	16.70	17.41	156.97	14.95
8	1188.77	276.03	22.14	23.28	265.77	19.67
9	3629.86	497.29	40.00	41.83	808.15	35.44
10	5389.22	608.15	49.04	51.00	1195.76	43.35
11	7344.49	748.27	60.40	63.08	1627.21	53.34

Table A.33
Derived values from second set of experiments for Model 4

Run Number 4.5

RN	Re	(Sh)av	(Sh/Sc1/3)av	(Sh/Sc1/3)mean	Re/Gr1/2	Sh/(ScGr)1/4
1	1.08	20.52	1.62	1.67	0.25	1.46
2	11.37	41.27	3.26	3.38	2.58	2.93
3	29.49	56.07	4.69	4.83	6.16	3.99
4	85.19	75.54	6.32	6.49	17.80	5.37
5	226.58	108.21	9.05	9.35	47.37	7.69
6	299.40	121.98	10.19	10.51	62.69	8.67
7	495.99	150.11	12.52	12.91	104.10	10.67
8	853.54	195.13	16.35	17.14	177.88	13.88
9	1367.53	243.61	20.51	21.53	283.12	17.33
10	3503.38	390.61	32.97	34.27	722.77	27.79
11	4664.74	470.44	39.76	41.51	960.80	33.47
12	6245.12	559.79	47.37	49.30	1283.91	39.82
13	8607.61	680.35	57.67	60.18	1765.49	48.40
14	12534.38	848.12	71.99	75.17	2566.12	60.35

Run Number 4.6

RN	Re	(Sh)av	(Sh/Sc1/3)av	(Sh/Sc1/3)mean	Re/Gr1/2	Sh/(ScGr)1/4
1	3.90	31.85	2.72	2.87	0.80	2.28
2	47.16	64.52	5.20	5.34	10.47	4.60
3	107.91	85.74	6.90	7.04	24.01	6.11
4	178.00	101.45	8.15	8.32	39.68	7.23
5	213.11	112.46	9.04	9.28	47.52	8.01
6	408.13	148.55	11.92	12.32	91.18	10.59
7	699.87	190.13	15.35	15.90	155.06	13.55
8	1195.80	245.52	19.92	20.77	263.01	17.50
9	3695.82	443.03	36.09	37.75	808.15	31.59
10	5364.09	555.70	45.32	47.65	1171.25	39.63
11	7473.93	664.97	54.34	56.89	1627.21	47.42

Table A.34
Pressure drop data for Model 1

SR	Q	P	Re	f
Run Number P1.1				
9.55	0.00000608	1.8	110.11	0.7042
21.40	0.00001276	3.5	231.09	0.3109
2.70	0.00001418	3.8	256.85	0.2732
15.90	0.00005029	30.1	911.13	0.1720
24.20	0.00007769	67.4	1407.39	0.1614
1.85	0.00024632	536.0	4462.31	0.1277
3.35	0.00032625	901.0	5910.36	0.1224
Run Number P1.2				
13.85	0.00004499	23.8	814.95	0.1700
23.85	0.00007668	64.2	1389.05	0.1578
5.30	0.00008511	78.3	1541.91	0.1562
10.72	0.00014283	206.0	2587.54	0.1459
17.30	0.00022674	477.0	4107.61	0.1341
26.30	0.00034776	945.0	6299.93	0.1129

Table A.35
Pressure drop data for Model 2

SR	Q	P	Re	f
Run Number P2.1				
2.70	0.00001418	3.4	256.85	0.2445
15.90	0.00005029	26.7	911.13	0.1526
24.20	0.00007769	61.8	1407.39	0.1480
1.85	0.00024632	471.0	4462.31	0.1122
3.35	0.00032625	805.0	5910.36	0.1093
Run Number P2.2				
13.85	0.00004528	22.4	820.23	0.1579
23.85	0.00007668	58.5	1389.05	0.1438
5.30	0.00008511	69.1	1541.91	0.1379
10.72	0.00014327	178.0	2595.45	0.1253
17.30	0.00022674	415.0	4107.61	0.1167
26.30	0.00034776	826.0	6299.93	0.0987

Table A.36
Pressure drop data for Model 3

SR	Q	P	Re	f
		Run Number P3.1		
2.70	0.00001418	2.6	256.85	0.1905
15.90	0.00005029	21.0	911.13	0.1200
24.20	0.00007769	46.7	1407.39	0.1118
1.85	0.00024632	360.0	4462.31	0.0858
3.35	0.00032625	641.0	5910.36	0.0870
		Run Number P3.2		
13.85	0.00004528	16.1	820.23	0.1135
23.85	0.00007668	45.9	1389.05	0.1128
5.30	0.00008511	54.2	1541.91	0.1081
10.72	0.00014294	138.0	2589.51	0.0976
17.30	0.00022674	317.0	4107.61	0.0897
26.30	0.00034776	624.0	6299.93	0.0746

Table A.37
Pressure drop data for Model 4

SR	Q	P	Re	f
		Run Number P4.1		
2.70	0.00001418	2.1	256.85	0.1488
15.90	0.00005029	16.1	911.13	0.0920
24.20	0.00007769	36.7	1407.39	0.0879
1.85	0.00024632	272.0	4462.31	0.0648
3.35	0.00032625	466.0	5910.36	0.0633
		Run Number P4.2		
13.85	0.00004528	11.5	820.23	0.0811
23.85	0.00007668	30.0	1389.05	0.0738
5.30	0.00008511	37.1	1541.91	0.0740
10.72	0.00014283	101.0	2587.54	0.0716
17.30	0.00022674	241.0	4107.61	0.0678
26.30	0.00034776	485.0	6299.93	0.0580